Interactions between the human milk oligosaccharide 2'-fucosyllactose and *Bifidobacterium* species influence colonization in complex gut communities

By

BRITTA E. HEISS
DISSERTATION

Submitted in partial satisfaction of the requirements for the degree of

DOCTOR OF PHILOSOPHY

in

Microbiology

in the

OFFICE OF GRADUATE STUDIES

of the

UNIVERSITY OF CALIFORNIA

DAVIS

Approved:

David A. Mills, Chair

Helen Raybould

Andreas Bäumler

Committee in Charge

2021

Dissertation Abstract

Bifidobacterium taxa are associated with the breastfed infant gut, namely, due to the bifidogenic nature of human milk's oligosaccharide fraction. This association provides a model of resource-driven microbial assemblies as human milk oligosaccharides (HMO) are accessible to microbes found in the infant gut but the infant cannot use HMO as a nutrient resource. The catabolism strategy (intracellular versus extracellular) and breadth of HMO structures utilized by a *Bifidobacterium* microbe impacts fitness and competitive nature in a microbial community. Previous work focused on profiling *Bifidobacterium* genetic diversity and *in vitro* metabolism of human milk oligosaccharides (HMO). **Chapter 1**, a mini-review, attempts to synthesize research, focusing on how functional capabilities provide a fitness advantage to certain *Bifidobacterium* species when applied to an infant gut. The **addendum** contains primary research on how *Bifidobacterium pseudocatenulatum* strains forage for fucosylated HMO.

The principal goal of this dissertation was to understand if a *Bifidobacterium* population could be enriched in a complex microbial community and if persistence could be achieved through introduction of an HMO nutrient resource, 2'-fucosyllactose (2'FL). **Chapter 2** introduces how supplementation of 2'FL provides a fitness advantage to a *Bifidobacterium pseudocatenulatum* strain possessing a fucosylated HMO gene cluster in a mouse model. Even when high colonization resistance was present, 2'FL, a privileged nutrient resource, facilitated persistence and ameliorated a DSS-induced colitis model.

Chapter 3 further characterizes the *Bifidobacterium pseudocatenulatum* persistence mouse model. Bifidobacterial metabolite products from 2'FL catabolism were found locally and systemically, although enrichment of those metabolites was dependent on high levels of *B. pseudocatenulatum* persisting in the mouse gut. This study also introduces the concept of mice categorized as responders and non-responders in this work.

Additional *Bifidobacterium* species were tested for persistence in a mouse model. These strains evaluated hypotheses surrounding catabolism strategies and the necessity of HMO utilization genes. In **Chapter 4** subjects were categorized as responder and non-responder depending on *Bifidobacterium* persistence success, which was varied. This variance could not be determined by the presence of any one

bacterial taxa at baseline. However, future studies could assess the functional capacity of the baseline microbiota to test if certain niches were open in mice categorized as responders.

This work furthers our understanding of *Bifidobacterium* strain-specific fitness differences in complex microbial communities. When choosing bacterial species with the objective of persistence or engraftment, researchers should first understand the molecular mechanisms for resource capture and catabolism, and the baseline microbial community's functional capabilities.

Acknowledgements

To my mentor and major professor, Dr. David Mills, thank you for your steadfast support throughout my graduate career. Specifically, Dave taught me the importance of crafting a clear research narrative and mentorship. Dave has advocated for me to pursue funding and career development opportunities, take part in an internship, and connected me with experts in the field. One of the greatest gifts Dave provided was the team of researchers he crafted. To my lab group members, thank you for your guidance, questions, and support during critical experiments. To my collaborators in the Foods for Health Institute and the Raybould and Slupsky labs, it was incredibly informative to work as a team to tackle these research objectives and provided me with new perspectives when evaluating results. I greatly appreciate your contributions to this research. I would like to express my gratitude to Dr. Helen Raybould and Dr. Andreas Baumler for serving on my dissertation committee and providing feedback on my projects.

Acknowledging the funding programs that supported me, thank you to the Animal Models of Infectious Disease NIH T32 training program and the Innovation Institute for Food and Health's Innovator fellowship. Both of these programs provided me with training I will apply to future research projects.

To the dedicated team of undergraduates who assisted me in the lab, Heather Romasko, Julia Wong, Dadne Lopez, and Brooke Neville – this work could not have been accomplished without your unwavering eagerness to extract DNA, grow bacterial cultures, and optimize qPCR conditions. Working side-by-side with you all was some of the most fun I had in lab, but also challenged me to explain research objectives and protocols. I wish you all success in your future endeavors.

I would like to highlight a few key people who mentored me by questioning my experimental design, proposing alternative hypotheses, editing manuscript and grant drafts, and even serving as incredibly overqualified aides at the lab bench. Dr. Maria Ximena Maldonado-Gomez, Dr. Diana Taft, Dr. Jennifer Hoeflinger, Dr. Ishita Shah, Dr. Saumya Wickramasinghe and more recently, Dr. Rebecca Duar, thank you for your unerring guidance. These incredible women trained me in the majority of my lab bench skills and provided critical insight on navigating project management, collaborations, statistical analysis, and a career post-graduation.

Lastly, my family has been incredibly supportive of my pursuit of higher education and career goals. Thank you to my parents, Maura and Drew, and my siblings, Dietrich, Siobhan, Gabrielle, and Gloria. Thank you for consistently providing constructive feedback on my presentations even when outside of your field of study or career. You are often my harshest (a.k.a., bluntest) but most constructive critics, which I value tremendously.

Table of Contents

Chapter 1

HMO catabolism capacities by *Bifidobacterium* species influences strain-specific fitness

Britta E. Heiss[1], Rebecca M Duar[2], David A. Mills[1]

Author Affiliations: [1]Department of Food Science and Technology, University of California Davis, Davis, CA, USA; [2]Evolve BioSystems, Inc., Davis CA, USA

In preparation for a 2021 Gut Microbiome mini-review.

1.1 Definitions

Colonization: When a species population has successfully occupied a habitat or territory, in a firm or permanent way.[1–3]

Exploitation competition: The indirect interaction between individuals as they compete for common resources (i.e. territory, prey, food), can result in competitive exclusion over time.[4]

Metabolic cross-feeding: An interaction between bacterial strains where molecules derived from one strain's metabolism are further metabolized by a second strain.[5]

Niche (Hutchinsonian niche): Environmental conditions and resources allowing a species to satisfy minimum requirements to maintain a viable population.[6]

Persistence: Replication of a microbe at an equal or greater rate than washout within a defined region as determined by the environmental conditions in the habitat, presence of additional species, and access to nutrient resources .[7,8]

Priority effects: The composition of a microbial community is influenced by the colonization arrival order of microbes, as an early arriver gains priority access to a growth-limiting nutrient.[9]

Resource partitioning: Trophic phenomenon whereby bacteria develop nutritional adaptations in order to co-exist by consuming different resources within the same habitat.

Substrate cross-feeding: Refers to the putative cooperative behavior in which one bacterial strain further metabolizes molecules produced by the metabolic actions of another strain.[5]

1.2 Abstract

The structuring of the microbial community by breast milk in the infant gut is an example of resource-driven microbiome assembly. Historically, when infants were breastfed, *Bifidobacterium* species were found to be enriched. A component of breastmilk, human milk oligosaccharides (HMO) are microbially accessible carbohydrates for the bacterial genus *Bifidobacterium,* which possess genes that encode transport systems and glycosyl hydrolases specific to the linkages found in these glycans. In the complex microbial community of the gut, HMO serve as a resource niche for *Bifidobacterium,* providing a growth advantage. However, possession of HMO catabolism genes among *Bifidobacterium* is not universal. Select *Bifidobacterium* species provide an example of how resource partitioning and metabolic flexibility enable co-existence of bacterial species; and how strains less efficient at accessing HMO as a resource can persist in infants. This functional discrepancy between *Bifidobacterium* species and strains influences persistence in probiotic feeding trials where strains capable of utilizing the full HMO array possess a competitive advantage. Recent metagenomic analysis has revealed deficiencies in HMO utilization genes within the infant gut, spurring questions related to the extinction of HMO utilizing *Bifidobacterium* in infant cohorts.

1.3 Introduction

Over the past century, researchers studied the impact of diet on infant gut microbial communities. Motivating this research was the need to address high mortality rates for formula-fed infants which were seven times higher than breastfed infants.[10] Observations described the microbiota of breastfed infants as being dominated by *Bifidobacterium* species[11,12] while formula fed infants were characterized by a more diverse community of microorganisms.[12,13] These original observations suggested human milk contained essential factors to promote the growth of *Bifidobacterium*.[14]

Human milk contains a multitude of bioactive factors, including lactoferrin, lysozyme, α-lactalbumin (as human α-lactalbumin made lethal to tumor cells [HAMLET]), fatty acids, peptides and free or conjugated glycans that inhibit or retard growth of segments of the developing infant gut microbiota and thus shape the trajectory of the gut microbiome. [15-17] Notably, some of these antimicrobial agents are biased in their activity and, by reducing populations of other microbial clades, function as possible bifidogenic factors.[18–22]

As early as 1954, the oligosaccharide fraction of human milk was directly identified as promoting *Bifidobacterium* growth.[14] Human milk oligosaccharides (HMO) comprise the third most abundant solid component of human milk and are structurally diverse, with over 200 identified structures.[23] Varying in composition, size, and charge, HMO have a degree of polymerization (DP) ≥ 3.[24] Consisting of a lactose core extended by galactose and N-acetylglucosamine (GlcNAc) monomers, HMO are often decorated by terminal fucose and sialic acids, all of which are connected by glycosidic linkages. Galactooligosaccharides (GOS), frucotoligosaccharides (FOS), and inulin are supplemented to infant formula as HMO alternatives, however, these are less complex molecules and do not possess fucosylatation or sialylation and exhibit a broader DP range.[25] Infants do not express the catabolic capability to use HMO directly as a nutrient.[26] HMO survive gastrointestinal transit, reaching the colon where they act as selective growth substrates for some bacteria, specifically, species of *Bifidobacterium*. When it comes to the capacity to catabolize HMO, *Bifidobacterium* can be categorized as strong, moderate, limited, or a non-HMO catabolizers. Such HMO

catabolism disparities are due to functional differences related to glycosyl hydrolase and transport system genes.[27,28] A strong HMO catabolizer and consumer, *Bifidobacterium longum* subsp. *infantis* (*B. infantis*) possesses a 43 kb genomic loci that encodes glycosyl hydrolases active on all four glycosidic linkages in HMO[29], a trait broadly conserved amongst subspecies.[30,31] Importantly, *B. infantis* efficiently catabolizes almost all HMO structures [32–34], preferentially consuming HMO with a DP ≥ 7 which are the most abundant molecules in pooled milk samples.[35] Another broad HMO catabolizer, *B. bifidum* possesses the capacity to degrade almost all HMO, however, contrary to *B. infantis*, *B. bifidum* deploys extracellular enzymes to hydrolyze HMO, leaving behind a significant portion of HMO components in the growth media, resulting in moderate HMO consumption.[33,36] Some isolates of *B. longum* subsp. *longum, B. pseudocatenulatum* and *B. kashiwanohense* strains are moderate consumers, fermenting a limited HMO set, although some strains have been reported with a broader HMO catabolism.[37–41] *B. breve* is a limited HMO catabolizer, with high strain-to-strain variability as it pertains to the HMO consumption and degradation.[38,39,42–44] *B. animalis* subsp. *lactis* and *B. adolescentis* are non HMO-catabolizers due the lack the genetic capacity to harvest HMO.[35,36,45] Additional *Bifidobacterium* strains possess capabilities to utilize host glycans, although they vary by species and strain as to the breadth of HMO used.[32,36,42] The ecological role of these species and strain-specific disparities in catabolizing HMO have yet to be fully elucidated. However, they may be a result of nutritional adaptations to provide niche differentiation that assists cohabitation of *Bifidobacterium* species/strains through resource partitioning in the infant gut.

1.4 Molecular strategies for HMO catabolism by *Bifidobacterium*

In addition to HMO specialization, two strategies for assimilating HMO structures have evolved within the *Bifidobacterium* genus.[28] The most prominent strategy is intracellular digestion of HMOs, where the oligosaccharides are internalized via specific transporters and intracellular glycosidases cleave the glycosidic linkages.[29] The clear majority of species inhabiting the breastfed infant gut employ this strategy, including *B. infantis, B. breve, B. longum, B. pseudocatenulatum,* and *B. kashiwanohense.*[28,38] The second strategy, present chiefly in *B. bifidum* strains, is extracellular digestion, reliant on membrane-associated extracellular glycosidases which liberate mono- and disaccharides from HMO for subsequent import and

degradation.[34] Some strains possess specific external glycosyl hydrolases enabling both strategies (*B. longum* JCM 1217).[28] But overall, *B. bifidum* is the prototype of extracellular catabolism among the infant-adapted bifidobacteria.

In addition to *Bifidobacterium,* many *Bacteroides* species have the enzymatic capacity to catabolize HMO [46] and can be prevalent in the early infant microbiota.[47] *Bacteroides* are considered glycan generalists as they encode between 100 to 300 carbohydrate-active enzymes which permit them to access an array of glycans, including intestinal mucin.[48] HMO and mucin glycans share core similarities, although HMO are less structurally complex and have a lower DP.[46] This structural overlap between HMO and mucin glycans results in *Bacteroides* upregulating mucin-related genes to metabolize HMO.[46] However, *Bacteroides* species do not specialize in metabolizing shorter HMO glycans, and are readily outcompeted by HMO catabolizing specialist, such as *B. infantis, in vivo.*[46] Some have proposed that the high efficiency internalization of HMO by *Bifidobacterium* using glycan-specific ABC transporters provide a competitive advantage compared to the glycan generalist *Bacteroides.*[48,49] Additional glycan generalists including *Roseburia* and *Eubacterium* are also able to harvest HMO glycans, although less efficiently than bifidobacterial HMO-specialists.[50]

As discussed earlier, *Bifidobacterium* taxa differ in which HMO structures they are capable of degrading and consuming.[41,42] Notably, an uneven distribution of carbohydrate-active enzymes exists between *B. longum* subsp. *longum* and *B. longum* subsp. *infantis.*[51] Evolutionary selection has favored the acquisition of HMO-metabolizing genes by *B. infantis* while *B. longum* appears better adapted for plant glycan utilization.[51] *B. bifidum* and *B. dentium* are capable of catabolizing mucin while other *Bifidobacterium* cannot.[24,52] *B. bifidum* possesses a higher number of carbohydrate-binding modules (CBM) than other *Bifidobacterium* which concentrate carbohydrates and increase efficiency of extracellular glycosyl hydrolases.[24] Katoh et al. proposed that *B. bifidum's* extracellular strategy and high CBM count represents an evolutionary adaptation to mucin *O*-glycans, distinct from other *Bifidobacterium.*[24] *B. bifidum's* adaptations to plant-derived polysaccharides appear to favor a more matured or weaned infant's microbiota, however, *B. bifidum* is capable of harvesting monomers from HMO and mucins alike. In fact,

the extracellular deployment of enzymes is the most common strategy for glycan foraging in the complex ecosystem of the gut.[48] Discrepancies between HMO assimilation and catabolism strategy provides differential fitness advantages to *Bifidobacterium* which may influence colonization success. For example, genes necessary for internal catabolism of fucosylated HMO are factors in *Bifidobacterium* colonization by enabling resource specialization and niche differentiation.[31,38] Future research is warranted to answer questions regarding the fitness and the competitive advantage associated with *Bifidobacterium* catabolism strategies and how that impacts the ecology of the infant gut.

1.5 Resource partitioning as an ecological strategy to persist in the infant gut

If two species' occupy identical niches, theoretically, they should not be able to co-exist according to the 'competitive exclusion' principle.[53] To subvert such exclusion, bacterial adaptations may favor resource partitioning (see glossary of terms).[54] Thus, bacteria undergo nutritional adaptations by specializing in the harvest of specific substrates, different than their competitors, thus permitting microbes to co-exist in the same habitat. Such a strategy may be enhancing the dominance of *Bifidobacterium* in the infant gut as strains specialize in catabolism of specific HMO structures, depleting the HMO nutrient niche, impeding colonization by other microbes.[55] The depletion of HMO structures and metabolites is also accomplished through cross-feeding relationships.

Resource partitioning is distinct from cross-feeding as it is driven by exploitation competition, the indirect interactions between microbes competing for HMO in the infant gastrointestinal tract. During cross-feeding, microbes are not competing for the same nutrient resource but molecules created by metabolism of a resource. While there are many forms of nutrient exchange between microbes, two cross-feeding varieties consist of a bacterial species using the molecules of another species' metabolism as a resource (metabolic cross-feeding) or molecules produced by the metabolic actions of another bacterium (substrate cross-feeding).[5,56] *Bifidobacterium* species harvesting partially degraded HMO or mucin monomers from neighboring *Bifidobacterium*[57,58] is an example of substrate cross-feeding (glossary of terms). This behavior has predominantly been identified in extracellularly catabolizing *Bifidobacterium* strains with little evidence of intracellularly catabolizing strains conducting any sharing of resources.[55]

Metabolic cross-feeding relationships have also been identified with non-HMO consumers.[55] *Bifidobacterium* HMO byproducts (fucose, acetate, GlcNAc, galactose) were identified as supporting growth of non-HMO catabolizing *Bifidobacterium,* resulting in maximized nutrient consumption. However, the ecological relevance of these metabolic cross-feeding relationships in maintaining bifidobacterial populations in the infant gut has yet to be determined.

Glycan generalists *Bacteroidaceae and* Clostridiales are also capable of participating in cross-feeding relationships with *Bifidobacterium* [59] or *E. coli.*[60] Importantly, some HMO cross feeding relationships where *E. coli* is the recipient have shown detrimental outcomes to the host[61] illustrating an important concern in such networks to promote growth of pathogens.[62] Current research has focused on *in vitro* cross-feeding experiments where the two communities are grown separately, however, experiments in fermentation engineered chemostats may be appropriate to model such competition and would provide insight into infant gut ecosystems.[63] Investigation of *Bifidobacterium* inter-bacterial relationships is required to differentiate between cross-feeding commensalism or competition-driven resource partitioning and how each relationship influences the infant microbiome assembly.

1.6 *Bifidobacteriaceae* prevalence in infants associated with HMO molecular mechanisms

Considering the molecular strategies for HMO catabolism *in Bifidobacterium* species, one can evaluate whether this influences the ecological progression of the developing, breastfed infant microbiota. Prior research established that carbohydrates not digested by the host but fermentable by the microbiota maintain commensal colonic populations.[64] Alternatively, when these carbohydrates are scarce and bacterial taxa are not efficiently transferred among hosts, microbes can become extinct in populations.[64] In breastfed infants, HMO are a significant portion of the microbially accessible carbohydrates (MAC) and provide a privileged metabolic niche to bacterial species with that cognate functional capacity. In infant stool samples with low *Bifidobacterium* abundance, the HMOs are excreted into the stool, while high *Bifidobacterium* is associated with reduced, or digested, fecal HMO.[65–67] Moreover, species-specific analysis found low HMO fecal measurements were associated with HMO-metabolizing *B. infantis* and *B. bifidum* but not the more plant glycan-associated *B. longum*.[68] Also, abundance of HMO transport genes

was negatively correlated to fecal glycan concentrations.[31] The negative correlation between fecal HMO concentrations and HMO specialist *Bifidobacterium* suggests HMO serve as a privileged nutrient promoting the colonization of *Bifidobacterium* within the infant gut.

The underlying mechanisms for seeding of *Bifidobacterium*, growth expansion, and predominance in the infant gut are still unclear. Contrary to the current dogma, reports have shown that despite being breastfed, a proportion of infants have very low, or even undetectable levels of *Bifidobacterium.*[69] When comparing bacterial taxonomy across broad geographic regions, *Bifidobacteriaceae* abundance is unevenly distributed.[70,71] First, when evaluating taxonomy, exclusively breastfed infants vary in the composition and prevalence of *Bifidobacterium* species. *B. infantis* may possess a competitive advantage when grown on HMO[46], however, it was detectable in only 8% of children <2 years of age, in one study.[72] In a traditional Old Order Mennonite community with longer breastfeeding durations, *B. infantis* was demonstrated to be more abundant in contrast to a nearby suburban community.[73] Disruptions to common inoculation routes (fecal-oral, vaginal birth) and environmental conditions such as population-level breastfeeding rates, sanitation practices, and antimicrobial administration could be reasons for lower *Bifidobacterium* colonization rates.[74] Second, functional analysis of infants from three countries revealed intracellular enzyme genes were associated with breastfed versus formula fed infants.[28] Despite similar relative abundances of *Bifidobacteriaceae* amongst the countries, the *Bifidobacterium* from Malawian and Venezuelan infants mainly employed an intracellular catabolism strategy while USA infants were associated with extracellular.[28] Evaluating both taxonomy and functional capacity, a metagenomic survey of US infants found that average *Bifidobacterium* relative abundance was lower than expected (~20%) with *B. infantis* not detected in a majority of the infants (97%).[75] Even when infants possessed high levels of *Bifidobacterium longum, Bifidobacterium breve, and Bifidobacterium bifidum,* HMO catabolism genes were undetected suggesting that the HMO utilization capacity was deficient in this infant population.[75]

Infant colonization by HMO consuming *Bifidobacterium* is important, perhaps pivotal, when considering infant health outcomes. *Bifidobacterium* colonization is associated with improved vaccine response[76], reduced atopic disease incidence and allergy[73,77], improved intestinal barrier function[78], reduced

carriage of virulence factors[79], and reduced abundance of antimicrobial resistance genes.[80,81] Several health advantages appear specific to the functional capacity for HMO utilization. Such advantages include decreased allergy risk[82], reduced rates of necrotizing enterocolitis in very low birthweight infants[83], and microbial metabolites promoting immunoregulation and reducing systemic inflammation.[84] Based on taxonomy analysis, positive health associations have been established when the infant microbiome was characterized by high *Bifidobacterium* relative abundance. More specifically, metagenomic analysis revealed that health outcomes are associated more specifically to HMO utilization capacity. As research advances from surveying taxonomic composition to considering microbial functional capabilities, we begin reevaluating the ecological relevance of *Bifidobacterium* species and advantages conferred to the infant host when nutrient resources are efficiently used.[85]

1.7 Improving colonization and persistence outcomes: applications of *Bifidobacterium* supplementation

In an attempt to improve health outcomes and HMO nutrient utilization efficiency, probiotic interventions have been evaluated for infants, most notably in premature infants. Probiotic efficacy concerns are pervasive as colonization of a supplemented microbe in a complex microbial community has been challenging to achieve.[86] However, selecting a microbe that gains a fitness advantage through a microbially accessible food resource increases colonization rates. Recently, Ojima et al. proposed that a combination of niche and relative fitness differences between an exogenous administered probiotic and the indigenous (host) baseline microbiota determine colonization outcomes.[1] This is exemplified in Maldonado-Gomez et al., where colonization of *B. longum* AH1206 was dependent on the underrepresentation of specific carbohydrate utilization genes in the baseline microbiota and reduced *B. longum* abundance.[2] Successful engraftment occurred when the invading strain's unique functional capacity was absent amongst indigenous microbes, filling a vacant niche.[2] Administration of a carbohydrate, in particular, can provide a fitness advantage to a supplemented microbe, resulting in microbial population growth that exceeds washout of the microbe.[87,88] However, providing a targeted fitness advantage requires knowledge of the metabolic capacity of the indigenous microbiota and strain-level understanding of the

administered bacterium. Such concepts should be applied when attempting to improve persistence or colonization outcomes for probiotics.

Infant feeding trials reveal how available HMO can provide a growth advantage to administered probiotic microorganisms. For example, HMO catabolism differences between *Bifidobacterium* species was tested by administering two *Bifidobacterium* probiotic strains, *B. longum* subsp. *infantis* (HMO specialist) or *B. animalis* subsp. *lactis* (non-HMO utilizing), to preterm infants. Among human milk-fed infants, *B. longum* was the dominant *Bifidobacterium* species present. *B. animalis* subsp. *lactis* was incapable of colonizing breastfed infants despite continued administration. With formula-fed infants, *B. lactis* was more prevalent but the abundance did not increase over time.[45] Thus, HMO provided a fitness advantage only to the species capable of catabolizing such structures, a case of HMO specialization providing a competitive advantage.

Considering the glycan specialization of *B. infantis* and the HMO utilization gene deficiency documented in USA infants, the capacity to colonize breastfed term infants was tested by providing the probiotic *B. infantis* EVC001.[66] *B. infantis* EVC001 persisted for at least 30 days after probiotic discontinuation increasing *Bifidobacteriaceae* relative abundance. *B. infantis* EVC001 was capable of surpassing the population growth of *B. longum* subsp. *longum* and *B. breve*, the predominant *Bifidobacterium* amongst control infants. *B. infantis* EVC001-fed infants had lower fecal HMO concentrations compared to controls, supporting the premise that HMO promote HMO utilizing *Bifidobacterium* and *B. infantis* is highly competitive in such an environment.[66] A follow up study found that probiotic administration within the first month and consistent breastfeeding supported the long-term persistence of *B. infantis* EVC001, up to one year postpartum.[89] While *B. infantis* is well-recognized as an efficient consumer of HMO[29,30], HMO gene clusters variants have been identified.[90] *B. infantis* strains possessing the full repertoire of HMO catabolism genes (H5-positive) have a fitness advantage over H5-negative strains both *in vitro* and in breastfed infants *in vivo* **(Figure 1.1a)**.[90] This fitness differentiation at the strain-level calls for further understanding of a strain's HMO functional capacity when attempting to integrate into a microbial community.

Clinical trials using HMO-catabolizing *Bifidobacterium* in human milk-fed infants suggest that HMO are associated with increased colonization, and yet it is difficult to disentangle the impact of HMO from the myriad of pro- and antimicrobial factors present in human milk. Further, founding microbes may possess a priority effect over any successive microbes attempting colonize.[9] Therefore, when *Bifidobacterium* taxa are the founding occupants of infant gastrointestinal tract, the founder hypothesis muddles conclusions regarding HMO directly facilitating *Bifidobacterium* colonization. However, a recent mouse study, demonstrated that a single HMO, 2'-fucosyllactose (2'FL), was able to promote a 5 log CFU enrichment of a cognate 2'FL-utilizing *B. pseudocatenulatum* strain within a healthy adult mouse. Provision of 2'FL facilitated a 2'FL-catabolizing *B. pseudocatenulatum* strain to compete effectively within a complex mouse gut ecosystem and persist with population growth that exceeded washout. This persistence continued for as long as 2'FL supplementation occurred. Upon 2'FL cessation, the *B. pseudocatenulatum* strain population quickly diminished suggesting the HMO was providing a means for the strain to persist in the competitive environment of the indigenous mouse microbiota. A *B. pseudocatenulatum* strain incapable of *in vitro* 2'FL growth, failed to persist in this mouse model, implying possession of specific HMO catabolism genes provides a growth advantage necessary for selective enrichment **(Figure 1b)**.[91] This proof of concept study demonstrates that HMO alone can drive high level persistence of a microbe within a gastrointestinal tract and provides a mechanistic basis for the elevated *B. infantis* colonization levels observed in breastfed infants in specific regions of the world[71,76,92] and clinical trials employing strong HMO-catabolizing *Bifidobacterium* probiotics.[45,66,93]

1.8 Implications of differential HMO-catabolizing capacity for strains used as probiotics

Bifidobacterium colonization of infants has been associated with a number of health benefits (described above). The health benefits conferred by probiotics have been examined *in vitro* and *in vivo* for years, with some conflicting results among clinical trials.[83,94] A key criticism of commercial probiotics is the lack of persistence or growth *in situ* and/or fail to reach a significant population size relative to the resident gastrointestinal microbiome to have a significant metabolic or mucosal impact.[95] For *Bifidobacterium* probiotics specifically, despite vast amounts of available data on the differential HMO

capacities between microbes, studies often do not consider this factor when choosing a strains for probiotic purposes.[94,96,97] Heiss et al. demonstrated that high level persistence of the 2FL-catabolizing *B. pseudocatenulatum* correlated with benefits to barrier function and reduced inflammation within a chemically-induced mouse model of colitis.[91] These results coincide with clinical trials in which persistence of the probiotic strain *B. infantis* EVC001 was significantly associated with reduced enteric inflammation and a tolerogenic immune tone.[84,98] Such results argue that breastfed infants benefit from a high level of bifidobacterial colonization and that selection of probiotic strains should consider HMO-catabolism capacity as a main factor driving both persistence and the associated health benefits.

1.9 Conclusion

While human milk provides a litany of health promoting bioactive agents, is clear HMO provide a selective enrichment of *Bifidobacterium* the breastfed infant gut. The nature of such an enrichment is also affected by resource partitioning capabilities, metabolic flexibility, and cooperative bacterial networks containing *Bifidobacterium.* However, metagenomic analysis has pinpointed an absence of HMO-metabolizing *Bifidobacterium* and thus the functional compacity to utilize these nutrients in US infants.[72,75] While on the rise, the current rate of exclusive breastfeeding through six months in the US is ~25%.[99] It is thus possible the lack of nutritional resources (i.e., HMO) over generations may have disproportionally affected populations of HMO-specialists. This could explain the low prevalence of *B. infantis* among US infants[72,73,75] while this subspecies continues to be prevalent and highly abundant in populations where breastfeeding rates are high.[71] Recovering the functional deficit to metabolize HMO would improve the energy transfer from mother to infant in addition to protecting against pathogens and develop immune regulation.[84] The ecological strategies for HMO-utilization outlined here may aid the design of strategies to promote health benefits by enriching *Bifidobacterium* in the infant gut. For example, differences in the ability to catabolize HMO could explain why supplementation with *B infantis* but not *B. breve* resulted in a significant reduction of necrotizing enterocolitis in the infant gut.[83,100] Further research is needed to determine how these HMO-consuming mechanisms influence the assembly and persistence of bifidobacterial populations in the infant gut.

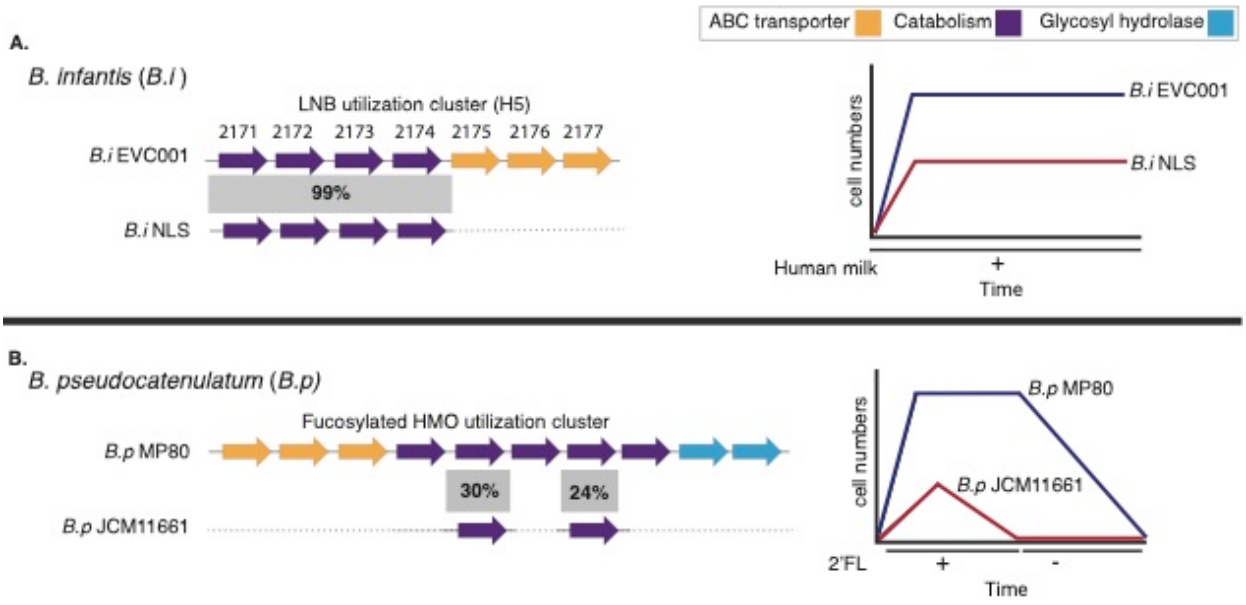

Figure 1.1. The reliance of HMO-specialists for (A) colonization and (B) persistence demonstrated using strains lacking genes to internalize HMO. (**A)** In competition, the strain *B. infantis* NLS lacking the LNB-ABC transporter, attains lower numbers in the gut of an exclusively breastfed infants when in competition with a the H5 positive strain EVC001, presumably due to competitive exclusion [90]. (**B)** Similarly, *B. pseudocatenulatum* MP80 successfully persisted in a mouse supplemented with 2'FL while *B. pseudocatenulatum* JCM11661 which is lacking fucosylated HMO utilization genes, fails to persist in a mouse consuming 2'FL. Together these experiments demonstrate that the ability of *Bifidobacterium* to colonize and persist is highly dependent on the ability to consume HMO.

1.10 References

1. Ojima MN, Yoshida K, Sakanaka M, Jiang L, Odamaki T, Katayama T. Ecological and molecular perspectives on responders and non-responders to probiotics and prebiotics. Curr Opin Biotechnol 2021; 73:108–20.
2. Maldonado-Gómez MX, Martínez I, Bottacini F, O'Callaghan A, Ventura M, van Sinderen D, Hillmann B, Vangay P, Knights D, Hutkins RW, et al. Stable Engraftment of Bifidobacterium longum AH1206 in the Human Gut Depends on Individualized Features of the Resident Microbiome. Cell Host Microbe 2016; 20:515–26.
3. Onofri S. Colonization (Biological). In: Gargaud M, Amils R, Quintanilla JC, Cleaves HJ, Irvine WM, Pinti DL, Viso M, editors. Encyclopedia of Astrobiology. Berlin, Heidelberg: Springer Berlin Heidelberg; 2011. page 326–8.
4. Lang J, Benbow E. Species Interactions and Competition. Nature Education Knowledge 2013; 4.
5. Smith NW, Shorten PR, Altermann E, Roy NC, McNabb WC. The Classification and Evolution of Bacterial Cross-Feeding. Front Ecol Evol 2019; 7.
6. Chase J, Leibold M. Ecological Niches: Linking Classical and Contemporary Approaches,. University of Chicago Press: 2003.
7. Bertuzzo E, Suweis S, Mari L, Maritan A, Rodríguez-Iturbe I, Rinaldo A. Spatial effects on species persistence and implications for biodiversity. Proc Natl Acad Sci USA 2011; 108:4346–51.
8. Walter J, Maldonado-Gómez MX, Martínez I. To engraft or not to engraft: an ecological framework for gut microbiome modulation with live microbes. Curr Opin Biotechnol 2018; 49:129–39.
9. Litvak Y, Baumler A. The founder hypothesis: A basis for microbiota resistance, diversity in taxa carriage, and colonization resistance against pathogens. PLoS Pathog 2019; 15.
10. Kunz C. Historical aspects of human milk oligosaccharides. Adv Nutr 2012; 3:430S–9S.
11. Tissier H. Repartitiondes microbes dans l'intestin du nourrisson. Annales de l'Institut Pasteur: journal de microbiologie 1905; :109–23.
12. Logan WR. The intestinal flora of infants and young children. J Pathol Bacteriol 1913; 18:527–51.
13. Snyder ML. The Normal Fecal Flora of Infants between Two Weeks and One Year of Age: I. Serial Studies. J Infect Dis 1940; 66:1–16.
14. Gyorgy P, Norris RF, Rose CS. Bifidus factor. I. A variant of Lactobacillus bifidus requiring a special growth factor. Arch Biochem Biophys 1954; 48:193–201.
15. Ballard O, Morrow AL. Human milk composition: nutrients and bioactive factors. Pediatr Clin North Am 2013; 60:49–74.
16. Hakansson AP, Roche-Hakansson H, Mossberg A-K, Svanborg C. Apoptosis-like death in bacteria induced by HAMLET, a human milk lipid-protein complex. PLoS One 2011; 6:e17717.
17. Welsh JK, May JT. Anti-infective properties of breast milk. J Pediatr 1979; 94:1–9.
18. Beverly RL, Woonnimani P, Scottoline BP, Lueangsakulthai J, Dallas DC. Peptides from the Intestinal Tract of Breast Milk-Fed Infants Have Antimicrobial and Bifidogenic Activity. Int J Mol Sci 2021; 22.
19. Schlievert PM, Kilgore SH, Seo KS, Leung DYM. Glycerol Monolaurate Contributes to the Antimicrobial and Anti-inflammatory Activity of Human Milk. Sci Rep 2019; 9:14550.

20. Minami J, Odamaki T, Hashikura N, Abe F, Xiao JZ. Lysozyme in breast milk is a selection factor for bifidobacterial colonisation in the infant intestine. Benef Microbes 2016; 7:53–60.
21. Oda H, Wakabayashi H, Yamauchi K, Abe F. Lactoferrin and bifidobacteria. Biometals 2014; 27:915–22.
22. Liepke C, Adermann K, Raida M, Mägert H-J, Forssmann W-G, Zucht H-D. Human milk provides peptides highly stimulating the growth of bifidobacteria. Eur J Biochem 2002; 269:712–8.
23. Ninonuevo MR, Park Y, Yin H, Zhang J, Ward RE, Clowers BH, German JB, Freeman SL, Killeen K, Grimm R, et al. A strategy for annotating the human milk glycome. J Agric Food Chem 2006; 54:7471–80.
24. Katoh T, Ojima MN, Sakanaka M, Ashida H, Gotoh A, Katayama T. Enzymatic Adaptation of Bifidobacterium bifidum to Host Glycans, Viewed from Glycoside Hydrolyases and Carbohydrate-Binding Modules. Microorganisms 2020; 8.
25. Bode L. Human milk oligosaccharides: every baby needs a sugar mama. Glycobiology 2012; 22:1147–62.
26. Gnoth MJ, Kunz C, Kinne-Saffran E, Rudloff S. Human milk oligosaccharides are minimally digested in vitro. J Nutr 2000; 130:3014–20.
27. Katayama T. Host-derived glycans serve as selected nutrients for the gut microbe: human milk oligosaccharides and bifidobacteria. Biosci Biotechnol Biochem 2016; 80:621–32.
28. Sakanaka M, Gotoh A, Yoshida K, Odamaki T, Koguchi H, Xiao J-Z, Kitaoka M, Katayama T. Varied Pathways of Infant Gut-Associated Bifidobacterium to Assimilate Human Milk Oligosaccharides: Prevalence of the Gene Set and Its Correlation with Bifidobacteria-Rich Microbiota Formation. Nutrients 2019; 12.
29. Sela DA, Chapman J, Adeuya A, Kim JH, Chen F, Whitehead TR, Lapidus A, Rokhsar DS, Lebrilla CB, German JB, et al. The genome sequence of Bifidobacterium longum subsp. infantis reveals adaptations for milk utilization within the infant microbiome. Proc Natl Acad Sci USA 2008; 105:18964–9.
30. LoCascio RG, Desai P, Sela DA, Weimer B, Mills DA. Broad conservation of milk utilization genes in Bifidobacterium longum subsp. infantis as revealed by comparative genomic hybridization. Appl Environ Microbiol 2010; 76:7373–81.
31. Sakanaka M, Hansen ME, Gotoh A, Katoh T, Yoshida K, Odamaki T, Yachi H, Sugiyama Y, Kurihara S, Hirose J, et al. Evolutionary adaptation in fucosyllactose uptake systems supports bifidobacteria-infant symbiosis. Sci Adv 2019; 5:eaaw7696.
32. Asakuma S, Hatakeyama E, Urashima T, Yoshida E, Katayama T, Yamamoto K, Kumagai H, Ashida H, Hirose J, Kitaoka M. Physiology of consumption of human milk oligosaccharides by infant gut-associated bifidobacteria. J Biol Chem 2011; 286:34583–92.
33. Gotoh A, Katoh T, Sakanaka M, Ling Y, Yamada C, Asakuma S, Urashima T, Tomabechi Y, Katayama-Ikegami A, Kurihara S, et al. Sharing of human milk oligosaccharides degradants within bifidobacterial communities in faecal cultures supplemented with Bifidobacterium bifidum. Sci Rep 2018; 8:13958.
34. Garrido D, Ruiz-Moyano S, Lemay DG, Sela DA, German JB, Mills DA. Comparative transcriptomics reveals key differences in the response to milk oligosaccharides of infant gut-associated bifidobacteria. Sci Rep 2015; 5:13517.
35. LoCascio RG, Ninonuevo MR, Freeman SL, Sela DA, Grimm R, Lebrilla CB, Mills DA,

German JB. Glycoprofiling of bifidobacterial consumption of human milk oligosaccharides demonstrates strain specific, preferential consumption of small chain glycans secreted in early human lactation. J Agric Food Chem 2007; 55:8914–9.
36. Ward RE, Niñonuevo M, Mills DA, Lebrilla CB, German JB. In vitro fermentability of human milk oligosaccharides by several strains of bifidobacteria. Mol Nutr Food Res 2007; 51:1398–405.
37. Bunesova V, Lacroix C, Schwab C. Fucosyllactose and L-fucose utilization of infant Bifidobacterium longum and Bifidobacterium kashiwanohense. BMC Microbiol 2016; 16:248.
38. Matsuki T, Yahagi K, Mori H, Matsumoto H, Hara T, Tajima S, Ogawa E, Kodama H, Yamamoto K, Yamada T, et al. A key genetic factor for fucosyllactose utilization affects infant gut microbiota development. Nat Commun 2016; 7:11939.
39. Xiao J, Takahashi S, Nishimoto M, Odamaki T, Yaeshima T, Iwatsuki K, Kitaoka M. Distribution of in vitro fermentation ability of lacto-N-biose I, a major building block of human milk oligosaccharides, in bifidobacterial strains. Appl Environ Microbiol 2010; 76:54–9.
40. Shani G, Hoeflinger J, Heiss B, Masarweh C, Larke J, Jensen N, Wickramasinghe S, Davis J, Goonatilleke E, El-Hawiet A, et al. Fucosylated human milkoligosaccharide foraging within the species Bifidobacterium pseudocatenulatum is driven by glycosyl hydrolase content and specificity. 2021;
41. Garrido D, Ruiz-Moyano S, Kirmiz N, Davis JC, Totten SM, Lemay DG, Ugalde JA, German JB, Lebrilla CB, Mills DA. A novel gene cluster allows preferential utilization of fucosylated milk oligosaccharides in Bifidobacterium longum subsp. longum SC596. Sci Rep 2016; 6:35045.
42. Ruiz-Moyano S, Totten SM, Garrido DA, Smilowitz JT, German JB, Lebrilla CB, Mills DA. Variation in consumption of human milk oligosaccharides by infant gut-associated strains of Bifidobacterium breve. Appl Environ Microbiol 2013; 79:6040–9.
43. James K, Motherway MO, Bottacini F, van Sinderen D. Bifidobacterium breve UCC2003 metabolises the human milk oligosaccharides lacto-N-tetraose and lacto-N-neo-tetraose through overlapping, yet distinct pathways. Sci Rep 2016; 6:38560.
44. Strum JS, Kim J, Wu S, De Leoz MLA, Peacock K, Grimm R, German JB, Mills DA, Lebrilla CB. Identification and accurate quantitation of biological oligosaccharide mixtures. Anal Chem 2012; 84:7793–801.
45. Underwood MA, Kalanetra KM, Bokulich NA, Lewis ZT, Mirmiran M, Tancredi DJ, Mills DA. A comparison of two probiotic strains of bifidobacteria in premature infants. J Pediatr 2013; 163:1585–1591.e9.
46. Marcobal A, Barboza M, Sonnenburg ED, Pudlo N, Martens EC, Desai P, Lebrilla CB, Weimer BC, Mills DA, German JB, et al. Bacteroides in the infant gut consume milk oligosaccharides via mucus-utilization pathways. Cell Host Microbe 2011; 10:507–14.
47. Mitchell CM, Mazzoni C, Hogstrom L, Bryant A, Bergerat A, Cher A, Pochan S, Herman P, Carrigan M, Sharp K, et al. Delivery mode affects stability of early infant gut microbiota. Cell Rep Med 2020; 1:100156.
48. Briggs JA, Grondin JM, Brumer H. Communal living: glycan utilization by the human gut microbiota. Environ Microbiol 2021; 23:15–35.
49. Ejby M, Fredslund F, Andersen JM, Vujičić Žagar A, Henriksen JR, Andersen TL, Svensson B, Slotboom DJ, Abou Hachem M. An ATP Binding Cassette Transporter

Mediates the Uptake of α-(1,6)-Linked Dietary Oligosaccharides in Bifidobacterium and Correlates with Competitive Growth on These Substrates. J Biol Chem 2016; 291:20220–31.
50. Pichler MJ, Yamada C, Shuoker B, Alvarez-Silva C, Gotoh A, Leth ML, Schoof E, Katoh T, Sakanaka M, Katayama T, et al. Butyrate producing colonic Clostridiales metabolise human milk oligosaccharides and cross feed on mucin via conserved pathways. Nat Commun 2020; 11:3285.
51. Tarracchini C, Milani C, Lugli GA, Mancabelli L, Fontana F, Alessandri G, Longhi G, Anzalone R, Viappiani A, Turroni F, et al. Phylogenomic disentangling of the Bifidobacterium longum subsp. infantis taxon. Microb Genom 2021; 7.
52. Engevik MA, Danhof HA, Hall A, Engevik KA, Horvath TD, Haidacher SJ, Hoch KM, Endres BT, Bajaj M, Garey KW, et al. The metabolic profile of Bifidobacterium dentium reflects its status as a human gut commensal. BMC Microbiol 2021; 21:154.
53. Hardin G. The Competitive Exclusion Principle. Science 1960; 131:1292–7.
54. Tannock GW, Wilson CM, Loach D, Cook GM, Eason J, O'Toole PW, Holtrop G, Lawley B. Resource partitioning in relation to cohabitation of Lactobacillus species in the mouse forestomach. ISME J 2012; 6:927–38.
55. Lawson MAE, O'Neill IJ, Kujawska M, Gowrinadh Javvadi S, Wijeyesekera A, Flegg Z, Chalklen L, Hall LJ. Breast milk-derived human milk oligosaccharides promote Bifidobacterium interactions within a single ecosystem. ISME J 2020; 14:635–48.
56. Seth EC, Taga ME. Nutrient cross-feeding in the microbial world. Front Microbiol 2014; 5:350.
57. Egan M, Motherway MO, Kilcoyne M, Kane M, Joshi L, Ventura M, van Sinderen D. Cross-feeding by Bifidobacterium breve UCC2003 during co-cultivation with Bifidobacterium bifidum PRL2010 in a mucin-based medium. BMC Microbiol 2014; 14:282.
58. Turroni F, Özcan E, Milani C, Mancabelli L, Viappiani A, van Sinderen D, Sela DA, Ventura M. Glycan cross-feeding activities between bifidobacteria under in vitro conditions. Front Microbiol 2015; 6:1030.
59. De Vuyst L, Leroy F. Cross-feeding between bifidobacteria and butyrate-producing colon bacteria explains bifdobacterial competitiveness, butyrate production, and gas production. Int J Food Microbiol 2011; 149:73–80.
60. Charbonneau MR, O'Donnell D, Blanton LV, Totten SM, Davis JCC, Barratt MJ, Cheng J, Guruge J, Talcott M, Bain JR, et al. Sialylated Milk Oligosaccharides Promote Microbiota-Dependent Growth in Models of Infant Undernutrition. Cell 2016; 164:859–71.
61. Huang Y-L, Chassard C, Hausmann M, von Itzstein M, Hennet T. Sialic acid catabolism drives intestinal inflammation and microbial dysbiosis in mice. Nat Commun 2015; 6:8141.
62. Ng KM, Ferreyra JA, Higginbottom SK, Lynch JB, Kashyap PC, Gopinath S, Naidu N, Choudhury B, Weimer BC, Monack DM, et al. Microbiota-liberated host sugars facilitate post-antibiotic expansion of enteric pathogens. Nature 2013; 502:96–9.
63. Centanni M, Ferguson SA, Sims IM, Biswas A, Tannock GW. Bifidobacterium bifidum ATCC 15696 and Bifidobacterium breve 24b Metabolic Interaction Based on 2'-O-Fucosyl-Lactose Studied in Steady-State Cultures in a Freter-Style Chemostat. Appl Environ Microbiol 2019; 85.

64. Sonnenburg ED, Smits SA, Tikhonov M, Higginbottom SK, Wingreen NS, Sonnenburg JL. Diet-induced extinctions in the gut microbiota compound over generations. Nature 2016; 529:212–5.
65. Lewis ZT, Totten SM, Smilowitz JT, Popovic M, Parker E, Lemay DG, Van Tassell ML, Miller MJ, Jin Y-S, German JB, et al. Maternal fucosyltransferase 2 status affects the gut bifidobacterial communities of breastfed infants. Microbiome 2015; 3:13.
66. Frese SA, Hutton AA, Contreras LN, Shaw CA, Palumbo MC, Casaburi G, Xu G, Davis JCC, Lebrilla CB, Henrick BM, et al. Persistence of Supplemented Bifidobacterium longum subsp. infantis EVC001 in Breastfed Infants. mSphere 2017; 2.
67. De Leoz MLA, Kalanetra KM, Bokulich NA, Strum JS, Underwood MA, German JB, Mills DA, Lebrilla CB. Human milk glycomics and gut microbial genomics in infant feces show a correlation between human milk oligosaccharides and gut microbiota: a proof-of-concept study. J Proteome Res 2015; 14:491–502.
68. Laursen MF, Pekmez CT, Larsson MW, Lind MV, Yonemitsu C, Larnkjær A, Mølgaard C, Bode L, Dragsted LO, Michaelsen KF, et al. Maternal milk microbiota and oligosaccharides contribute to the infant gut microbiota assembly. ISME COMMUN 2021; 1:21.
69. Tannock GW, Lee PS, Wong KH, Lawley B. Why don't all infants have bifidobacteria in their stool? Front Microbiol 2016; 7:834.
70. Vatanen T, Plichta DR, Somani J, Münch PC, Arthur TD, Hall AB, Rudolf S, Oakeley EJ, Ke X, Young RA, et al. Genomic variation and strain-specific functional adaptation in the human gut microbiome during early life. Nat Microbiol 2019; 4:470–9.
71. Lawley B, Otal A, Moloney-Geany K, Diana A, Houghton L, Heath A-LM, Taylor RW, Tannock GW. Fecal Microbiotas of Indonesian and New Zealand Children Differ in Complexity and Bifidobacterial Taxa during the First Year of Life. Appl Environ Microbiol 2019; 85.
72. Tso L, Bonham KS, Fishbein A, Rowland S, RESONANCE consortium, Klepac-Ceraj V. Targeted high-resolution taxonomic identification of *Bifidobacterium longum* subsp. *infantis* using human milk oligosaccharide metabolizing genes. BioRxiv 2021;
73. Seppo AE, Bu K, Jumabaeva M, Thakar J, Choudhury R, Yonemitsu C, Bode L, Martina CA, Allen M, Tamburini S, et al. Infant Gut Microbiome Is Enriched with Bifidobacteria longumssp. infantisin Old Order Mennoniteswith Traditional Farming Lifestyle. Allergy 2021;
74. Lewis ZT, Mills DA. Differential establishment of bifidobacteria in the breastfed infant gut. Nestle Nutr Inst Workshop Ser 2017; 88:149–59.
75. Casaburi G, Duar RM, Brown H, Mitchell RD, Kazi S, Chew S, Cagney O, Flannery RL, Sylvester KG, Frese SA, et al. Metagenomic insights of the infant microbiome community structure and function across multiple sites in the United States. Sci Rep 2021; 11:1472.
76. Huda MN, Ahmad SM, Alam MJ, Khanam A, Kalanetra KM, Taft DH, Raqib R, Underwood MA, Mills DA, Stephensen CB. Bifidobacterium abundance in early infancy and vaccine response at 2 years of age. Pediatrics 2019; 143.
77. Cukrowska B, Bierła JB, Zakrzewska M, Klukowski M, Maciorkowska E. The Relationship between the Infant Gut Microbiota and Allergy. The Role of Bifidobacterium breve and Prebiotic Oligosaccharides in the Activation of Anti-Allergic Mechanisms in Early Life. Nutrients 2020; 12.

78. Karav S, Casaburi G, Frese SA. Reduced colonic mucin degradation in breastfed infants colonized by Bifidobacterium longum subsp. infantis EVC001. FEBS Open Bio 2018; 8:1649–57.
79. Casaburi G, Frese SA. Colonization of breastfed infants by Bifidobacterium longum subsp. infantis EVC001 reduces virulence gene abundance. Human Microbiome Journal 2018; 9:7–10.
80. Taft DH, Liu J, Maldonado-Gomez MX, Akre S, Huda MN, Ahmad SM, Stephensen CB, Mills DA. Bifidobacterial dominance of the gut in early life and acquisition of antimicrobial resistance. mSphere 2018; 3.
81. Casaburi G, Duar RM, Vance DP, Mitchell R, Contreras L, Frese SA, Smilowitz JT, Underwood MA. Early-life gut microbiome modulation reduces the abundance of antibiotic-resistant bacteria. Antimicrob Resist Infect Control 2019; 8:131.
82. He F, Ouwehand AC, Isolauri E, Hashimoto H, Benno Y, Salminen S. Comparison of mucosal adhesion and species identification of bifidobacteria isolated from healthy and allergic infants. FEMS Immunol Med Microbiol 2001; 30:43–7.
83. Tobias J, Olyaei A, Laraway B, Jordan BK, Dickinson S, Arroyo LG, Fialkowski E, Owora A, Scottoline B. Feeding Activated *Bifidobacterium infantis* EVC001 to Very Low Birth Weight Infants is Associated with Significant Reduction in Rates of Necrotizing Enterocolitis. medRxiv 2021;
84. Henrick BM, Rodriguez L, Lakshmikanth T, Pou C, Henckel E, Arzoomand A, Olin A, Wang J, Mikes J, Tan Z, et al. Bifidobacteria-mediated immune system imprinting early in life. Cell 2021;
85. Duar RM, Henrick BM, Casaburi G, Frese SA. Integrating the Ecosystem Services Framework to Define Dysbiosis of the Breastfed Infant Gut: The Role of B. infantis and Human Milk Oligosaccharides. Front Nutr 2020; 7:33.
86. Kristensen NB, Bryrup T, Allin KH, Nielsen T, Hansen TH, Pedersen O. Alterations in fecal microbiota composition by probiotic supplementation in healthy adults: a systematic review of randomized controlled trials. Genome Med 2016; 8:52.
87. Shepherd ES, DeLoache WC, Pruss KM, Whitaker WR, Sonnenburg JL. An exclusive metabolic niche enables strain engraftment in the gut microbiota. Nature 2018; 557:434–8.
88. Krumbeck JA, Maldonado-Gomez MX, Martínez I, Frese SA, Burkey TE, Rasineni K, Ramer-Tait AE, Harris EN, Hutkins RW, Walter J. In vivo selection to identify bacterial strains with enhanced ecological performance in synbiotic applications. Appl Environ Microbiol 2015; 81:2455–65.
89. O'Brien CE, Meier AK, Cernioglo K, Mitchell RD, Casaburi G, Frese SA, Henrick BM, Underwood MA, Smilowitz JT. Early probiotic supplementation with B. infantis in breastfed infants leads to persistent colonization at 1 year. Pediatr Res 2021;
90. Duar RM, Casaburi G, Mitchell RD, Scofield LNC, Ortega Ramirez CA, Barile D, Henrick BM, Frese SA. Comparative Genome Analysis of Bifidobacterium longum subsp. infantis Strains Reveals Variation in Human Milk Oligosaccharide Utilization Genes among Commercial Probiotics. Nutrients 2020; 12.
91. Heiss B, Ehrlich A, Maldonado-Gomez M, Taft D, Larke J, Goodson M, Slupsky C, Tancredi D, Raybould H, Mills D. Bifidobacterium catabolism of human milk oligosaccharides overrides endogenous competitive exclusion driving colonization and protection. Gut Microbes 2021;

92. Davis JCC, Lewis ZT, Krishnan S, Bernstein RM, Moore SE, Prentice AM, Mills DA, Lebrilla CB, Zivkovic AM. Growth and morbidity of Gambian infants are influenced by maternal milk oligosaccharides and infant gut microbiota. Sci Rep 2017; 7:40466.
93. Alcon-Giner C, Dalby MJ, Caim S, Ketskemety J, Shaw A, Sim K, Lawson MAE, Kiu R, Leclaire C, Chalklen L, et al. Microbiota Supplementation with Bifidobacterium and Lactobacillus Modifies the Preterm Infant Gut Microbiota and Metabolome: An Observational Study. Cell Rep Med 2020; 1:100077.
94. Costeloe K, Bowler U, Brocklehurst P, Hardy P, Heal P, Juszczak E, King A, Panton N, Stacey F, Whiley A, et al. A randomised controlled trial of the probiotic Bifidobacterium breve BBG-001 in preterm babies to prevent sepsis, necrotising enterocolitis and death: the Probiotics in Preterm infantS (PiPS) trial. Health Technol Assess 2016; 20:1–194.
95. Suez J, Zmora N, Segal E, Elinav E. The pros, cons, and many unknowns of probiotics. Nat Med 2019; 25:716–29.
96. Yousuf EI, Carvalho M, Dizzell SE, Kim S, Gunn E, Twiss J, Giglia L, Stuart C, Hutton EK, Morrison KM, et al. Persistence of suspected probiotic organisms in preterm infant gut microbiota weeks after probiotic supplementation in the NICU. Front Microbiol 2020; 11:574137.
97. Underwood MA, Davis JCC, Kalanetra KM, Gehlot S, Patole S, Tancredi DJ, Mills DA, Lebrilla CB, Simmer K. Digestion of Human Milk Oligosaccharides by Bifidobacterium breve in the Premature Infant. J Pediatr Gastroenterol Nutr 2017; 65:449–55.
98. Henrick BM, Chew S, Casaburi G, Brown HK, Frese SA, Zhou Y, Underwood MA, Smilowitz JT. Colonization by B. infantis EVC001 modulates enteric inflammation in exclusively breastfed infants. Pediatr Res 2019; 86:749–57.
99. Breastfeeding Report Card United States, 2020. 2020;
100. Fleming P, Wilks M, Eaton S, Panton N, Hutchinson R, Akyempon A, Hardy P, Millar MR, Costeloe K. Bifidobacterium breve BBG-001 and intestinal barrier function in preterm babies: Exploratory Studies from the PiPS Trial. Pediatr Res 2020;

Chapter 2

Bifidobacterium catabolism of human milk oligosaccharides overrides endogenous competitive exclusion driving colonization and protection

Britta E. Heiss,[1,5] Amy M. Ehrlich,[2] Maria X. Maldonado-Gomez,[1,5] Diana H. Taft, [1,5] Jules A. Larke,[3] Michael L. Goodson,[2] Carolyn M. Slupsky,[1,3,5] Daniel J. Tancredi,[4] Helen E. Raybould[2,5] and David A. Mills,[1,5]

[1]Department of Food Science and Technology, University of California-Davis, Davis, CA.
[2]Department of Anatomy, Physiology, and Cell Biology, School of Veterinary Medicine, University of California-Davis, Davis, CA.
[3]Department of Nutrition, University of California-Davis, Davis, CA.
[4]Center for Healthcare Policy and Research, Department of Pediatrics, University of California-Davis, Davis, CA.
[5]Foods for Health Institute, University of California-Davis, Davis, CA.

Accepted by Gut Microbes August 2021.

2.1 Abstract

Understanding how exogenous microbes stably colonize the animal gut is essential to reveal mechanisms of action and tailor effective probiotic treatments. *Bifidobacterium* species are naturally enriched in the gastrointestinal tract of breast-fed infants. Human milk oligosaccharides (HMOs) are associated with this enrichment. However, direct mechanistic proof of the importance of HMOs in this colonization is lacking given milk contains additional factors that impact the gut microbiota. This study examined mice supplemented with the HMO 2'fucosyllactose (2'FL) together with a 2'FL-consuming strain, *Bifidobacterium pseudocatenulatum* MP80. 2'FL supplementation creates a niche for high levels of *B.p.* MP80 persistence, similar to *Bifidobacterium* levels seen in breast fed infants. This synergism impacted gut microbiota composition, activated anti-inflammatory pathways and protected against chemically-induced colitis. These results demonstrate that bacterial-milk glycan interactions alone drive enrichment of beneficial *Bifidobacterium* and provide a model for tunable colonization thus facilitating insight into their mechanisms of health promotion in neonates.

2.2 Introduction

Probiotics are commercially available supplements that are increasingly examined for their role in preventing a number of diseases including necrotizing enterocolitis and antibiotic-associated diarrhea among others.[1,2] Despite potential benefits, the specific role of probiotics in mitigating diseases remains controversial.[3] One aspect of this debate is the relative lack of persistence of supplemented probiotics in gut ecosystems due to the inherent heterogeneity and colonization resistance of the human gut microbiota.[4] Most probiotic species survive passage through the intestinal tract, but persistence of the microbe, that is, detection of elevated levels of the strain post-bacterial supplementation due to substantive growth and metabolism, is infrequent.[5] The persistence of a species is defined as the time between its emergence and extinction within a defined region.[6] Persistence time of a species is determined by the environmental conditions in the habitat, presence of additional species, and access to nutrient resources. In the case of bacterial persistence, specific conditions permit the microbe to replicate at an equal or greater rate than washout.[5] In short, the low abundance, lack of persistence, and likely low metabolite production from a probiotic population that diminishes after supplementation ceases are potential factors in the variable impact of probiotics on health outcomes. Thus, one means to address these concerns is to identify a mechanism that results in multiplication and persistence of specific microbes in the gastrointestinal tract, thereby allowing more robust examination of host-probiotic interactions and facilitating mechanistic exploration of the resulting health outcomes. A recent study demonstrated in mice that provision of a unique dietary carbohydrate, also known as a privileged nutrient niche, can facilitate engraftment of *Bacteroides* strains competent in catabolism of such carbohydrates.[7,8] However, no examination of colonization-associated health outcomes, a key factor in defining probiotics, was undertaken.

One model for the sustained diet-driven persistence of a specific beneficial bacterial taxa in the human gut is the common observation of *Bifidobacterium* enrichment during nursing. Numerous studies have identified associations between early, and predominant, colonization of infant borne *Bifidobacterium* and beneficial health outcomes in breast-fed infants.[9–14] A number of studies have illustrated possible mechanisms by which probiotic *Bifidobacterium* impact host health including production of acetate, indole-

3-lactic acid, exopolysaccharide, and pili.[15–19] While characteristic, high relative abundance *Bifidobacterium* colonization of infants has been associated with positive health outcomes, results on the clinical use of specific *Bifidobacterium* probiotics to address human disease remains varied.[20,21]

While the underlying mechanisms for seeding, expansion, and predominance of *Bifidobacterium* in the infant gut are not fully resolved, human milk oligosaccharides (HMOs) are considered a privileged nutrient enabling enrichment of a HMO-catabolizing *Bifidobacterium* population.[22–24] HMOs are structurally complex molecules composed of a range of monomers and linkages which require a complex assembly of bacterial glycosyl hydrolases and transport systems to catabolize them, making them a privileged nutrient that few microbes are capable of consuming. Several studies identified associations in breast-fed infants between HMO consumption, enrichment of certain *Bifidobacterium* strains, and higher fecal acetate and lactate (end products of *Bifidobacterium* fermentation).[23,25] However, considering the constellation of bioactive factors in human milk, notably antimicrobial factors such as lysozyme, lactoferrin and antimicrobial peptides, the magnitude of the effect that HMOs have in the assembly of the developing infant gut microbiome remains unclear.

The aim of the study was to address two associated questions: do HMOs alone act as a privileged nutrient enabling enrichment of a cognate HMO-consuming *Bifidobacterium* in a complex established gut ecosystem of the adult mouse and if *Bifidobacterium* enrichment occurs, does it provide a health benefit? This research is important in establishing the dominant role of HMOs in the colonization of the breast-fed infant gut by *Bifidobacterium*. Moreover, this work illustrates a path whereby provision of a specific nutrient for a supplemented probiotic could drive high level persistence in the gastrointestinal tract and impact host health.

2.3 Results

2.3.1 *B. pseudocatenulatum* persistence associated with genetic capability to catabolize 2'FL

To determine if the interaction between HMOs and *Bifidobacterium* would enable persistence of the strain, we administered 2'-fucosyllactose (2'FL), a predominant HMO in breast milk, and infant-isolate *B. pseudocatenulatum* MP80 to mice **(Figure 2.1a)**. *B.p.* MP80 grows robustly on 2'FL and possesses a unique genetic operon linked to catabolism of this HMO **(Figure 2.1b)**.[26] C57BL/6 mice received *B.p.* MP80 for 5 days by oral gavage and simultaneously 2'FL was provided in the drinking water (10% w/v; average consumption of 550 mg/day; **Figure 2.1a).** 2'FL supplementation continued for 5 additional days after *B.p.* MP80 gavage ended. On day 5 (the last day of bacterial oral gavage), *B.p.* MP80 was detected at a high level (>10e10 cells/gram of feces) in mice treated with 2'FL, compared to mice receiving *B.p.* MP80 and water (day 5, <10e7 cells/gram of feces, one-way ANOVA, p = 0.008; **Figure 2.1c**). After discontinuation of bacterial gavage, *B.p* MP80 persisted in mice that continued to receive 2'FL, but not in mice that received drinking water alone (day 10, one-way ANOVA, p = 0.0007; **Figure 2.1c**). Ten days after the end of 2'FL supplementation, *B.p.* MP80 levels were below the limit of detection (day 20, washout; **Figure 2.1c**).

We evaluated 2'FL catabolism by metabolite profiling of mouse colon contents using ^{1}H-NMR spectroscopy. Comparison across treatments resulted in no p values <0.05 after FDR correction (ANOVA with post hoc Games Howell test; **Supplemental table 2.2)**. Due to the small sample size and high number of metabolite features, effect size (Hedge's g) was calculated to compliment hypothesis testing by providing an estimate of treatment effects.[27] Hedge's g effect sizes revealed several medium (|g|> 0.5) and large (|g|> 0.8) treatment effects **(Supplemental figure 2.1)**. Notably, during 2'FL supplementation the fucose catabolism end product 1,2-propanediol was elevated in the colon luminal contents of *B.p.* MP80 + 2'FL treated mice relative to 2'FL alone (Hedge's g; |g| = 1.48; **Supplemental figure 2.1d**) or untreated control mice (Hedge's g; |g| = 1.47).

Despite repeated attempts we were unable to transform *B.p.* MP80 for creation of genetic knockouts. Thus, to evaluate whether a 2'FL gene cluster is necessary for *Bifidobacterium* persistence, we administered *B. pseudocatenulatum* JCM11661 which lacks α-fucosidases and fails to grow on 2'FL, to mice (**Figure 2.1d**).[26] Genome comparison[28] of *B.p.* JCM11661 to *B.p.* MP80 revealed that 72% of their genomes had a similarity of >75%. *B.p.* JCM11661 was detected during bacterial gavage (day 5, >10e8 cells/gram of feces; **Figure 2.1d**), but failed to persist during 2'FL supplementation alone (day 10; **Figure 2.1d**). In addition, there was no significant difference in *B.p.* JCM11611 levels between mice given 2'FL or drinking water.

Additional mouse experiments evaluated the frequency of bacterial gavage and the concentration of 2'FL required for *B.p.* MP80 persistence. Three days of *B.p.* MP80 gavage is sufficient for elevated persistence after bacterial gavage discontinuation (day 10, >10e9 cells/g feces) and 10% 2'FL yielded the highest persistence (day 10, >10e10 cells/g feces; **Supplemental figure 2.2a**). 2'FL at 5% and 2.5% resulted in lower persistence than 10% (day 10, <10e8 cells/g feces), indicating that adjusting 2'FL concentration controls strain abundance **(Supplemental figure 2.2b).**

2.3.2 2'FL driven *B.p.* MP80 persistence impacts microbial community membership

To understand the overall impact of persistence of *B.p.* MP80 on α-diversity, microbial community membership, and *Bifidobacterium* levels, 16S rRNA gene amplicon sequencing was performed. *Bifidobacteriaceae* was elevated from approximately <1% to 40% relative abundance in mice treated with *B.p.* MP80 + 2'FL from day 0 (baseline) through day 10 (end of 2'FL supplementation) **(Figure 2.2a).** In mice treated with *B.p.* MP80 or 2'FL alone, relative abundance of *Bifidobacteriaceae* only reached approximately 5% or 11%, respectively **(Figure 2.2a)**.

A linear regression with sandwich variance estimates to account for heteroskedasticity was used to estimate the effect of the interaction between *B.p.* MP80 in the presence of 2'FL on α-diversity in comparison to *B.p.* JCM11611. Administration of *B. p.* MP80 and 2'FL is associated with reduced α-diversity (Shannon Index; t-statistic = -3.17, p = 0.013; **Supplemental table 2.3**) compared to *B.p.* JCM11661 and 2'FL.

Microbial community structure differed for *B.p.* MP80 + 2'FL mice by day as measured by β-diversity (Bray Curtis, PERMANOVA, $p = 0.011$; **Figure 2.2b).** Community structure clearly shifts from baseline (day 0) during days of 2'FL supplementation and returns to baseline during washout **(Figure 2.2b).** Post-hoc testing for community structure differences between days of 2'FL-dependent *B.p.* MP80 persistence (day 10) was significant when compared to baseline (day 0, pairwise PERMANOVA, $p = 0.028$) and washout (day 20, pairwise PERMANOVA, $p = 0.005$; **Figure 2.2b).** As expected, provision of *B.p.* MP80 to mice generated changes in microbial community structure for treatments *B.p.* MP80 + 2'FL and *B.p.* MP80 (**Figure 2.2b and Supplemental figure 2.3a)**. However, a more dramatic disruption in community membership occurred when 2'FL was paired with *B.p.* MP80, based on dissimilarity community measures (Bray Curtis, baseline (day 0) vs final *B.p.* MP80 gavage (day 5), Mann-Whitney test, $p = 0.022$; **Supplemental figure 2.3b**). During *B.p.* MP80 persistence (day 10), comparison of overall microbial community structure by treatment was significant (PERMANOVA, $p = 0.001$; **Figure 2.2c**) although 2'FL alone and *B.p.* MP80 + 2'FL were not distinct from each other (pairwise PERMANOVA, $p = 0.358$; **Supplemental table 2.4**).

2.3.3 *B.p.* MP80 + 2'FL treatment enriches *Bifidobacteriaceae* relative to *Lachnospiraceae* and *Ruminococcaceae*

Microbial differential abundance testing evaluated whether specific ASVs were being increased relative to other taxa. The log ratio of *Bifidobacteriaceae* ASVs to the combination of *Lachnospiraceae* and *Ruminococcaceae* ASVs was identified by songbird and was significantly increased by treatment during 2'FL supplementation (one-way ANOVA, $p < 0.001$; **Figure 2.2d**).[29] During persistence of *B.p.* MP80, the *Bifidobacteriaceae:Lachnospiraceae* and *Ruminococcaceae* log ratio from *B.p.* MP80 + 2'FL treated mice were significantly higher than that found in untreated (Tukey's test, $p < 0.001$) and 2'FL treated mice (Tukey's test, $p = 0.017$; **Supplemental table 2.5**). Absolute abundance measured by qPCR confirms with a ~2 log increase of *Bifidobacterium* in *B.p.* MP80 mice during 2'FL supplementation (baseline vs day 10, Kruskal Wallis, $p = 0.011$; **Supplemental figure 2.3c**).

2.3.4 2'FL enriches *Bacteroidaceae* and *Bifidobacteriaceae* relative to *Lachnospiraceae* and *Ruminococcaceae*

Although the mouse-associated microbiota has not been naturally selected to catabolize HMOs, we examined the 2'FL control group to assess how 2'FL may effect change in an established microbiota. β-diversity (Bray Curtis) varied significantly by day (PERMANOVA, $p = 0.021$; **Figure 2.2e**) and 2'FL supplemented days were distinct from non-2'FL days (pairwise PERMANOVA, $p = 0.037$). Although no *Bifidobacterium* was provided, increased *Bifidobacteriaceae* relative abundance is noted **(Figure 2.2a)**. Absolute abundance of *Bifidobacterium* increased by 1-2 logs between baseline (day 0) and day 10 of 2'FL supplementation (Kruskal Wallis, $p = 0.024$; **Supplemental figure 2.3c**). In contrast to untreated control mice, 2'FL treatment results in high log ratios of *Bacteroidaceae* and *Bifidobacteriaceae* relative to *Lachnospiraceae* and *Ruminococcaceae* ASVs (student's t test, $p = 0.003$; **Figure 2.2f**).

2.3.5 Effects of *B.p.* MP80 + 2'FL treatment in healthy mice

Treatment with *B.p.* MP80, 2'FL, or *B.p.* MP80 + 2'FL compared to untreated control mice had no significant effect on food or fluid intake, body weight gain, or spleen or liver weights **(Supplemental table 2.9)**. Total cecum weight (cecal tissue plus content) was significantly increased in *B.p.* MP80 + 2'FL compared to other groups, suggesting fermentation was increased (untreated, *B.p.* MP80- and 2'FL-treated mice; $p < 0.0001$, $p < 0.0001$, $p = 0.0005$; **Supplemental table 2.9**). Treatment with *B.p.* MP80 + 2'FL induced changes in expression in a number of genes, which varied depending on the region of the gut **(Figure 2.3, Supplemental tables 2.10-2.16**). Changes in gene expression were more evident in the cecum with an increase in expression of both anti-inflammatory and pro-inflammatory markers including MyD88, Nrf2 targets (Gpx2, Hmox1, and Nqo1), and Pfkfb3 and Slc2a1 **(Supplemental figure 2.4)**. Treatments had little effect on colon and liver pro- or anti-inflammatory gene expression. *B.p.* MP80 + 2'FL reduced expression of Il1b in the colon ($p = 0.009$; **Supplemental figure 2.5, Supplemental tables 2.10-2.11**).

2.3.6 *B.p. MP80* + 2'FL treatment attenuates DSS-induced colitis

The DSS-induced colitis decrease in body weight was significantly attenuated by treatment with *B.p.* MP80 + 2'FL (one-way ANOVA with FDR correction, $p < 0.0001$, DSS vs untreated; $p = 0.0004$, DSS

vs DSS + *B.p* MP80 + 2'FL; **Figure 2.4a-c**) and significantly attenuated by pretreatment with 2'FL alone (p = 0.005, DSS vs DSS + 2'FL; **Figure 2.4c, Supplemental table 2.17**). There was no significant difference in water intake between any groups throughout the experimental period, indicating that all groups received the same amount of DSS (**Supplemental table 2.17**). DSS-induced immune cell infiltration, increase in colon length, disrupted mucosal architecture, and muscle thickening in the colon were significantly attenuated by *B.p*. MP80 + 2'FL treatment (one-way ANOVA with FDR correction, p = 0.0001, DSS vs untreated; p = 0.005, DSS vs DSS + *B.p* MP80 + 2'FL; **Figure 2.4d-e**;), but not by *B.p.* MP80 or 2'FL treatments alone (p = 0.90, DSS vs DSS + *B.p* MP80; p = 0.82, DSS vs DSS + 2'FL). Expression of occludin was significantly reduced by DSS compared to untreated (Wilcoxon Rank Sum with FDR correction, p = 0.024; **Figure 2.4f, Supplemental table 2.19**); treatment with *B.p.* MP80 + 2'FL significantly attenuated this reduction (p = 0.75, untreated vs DSS + *B.p* MP80 + 2'FL; p = 0.05, DSS vs DSS + *B.p* MP80 + 2'FL; **Supplemental tables 2.18-2.21**). Impairment of intestinal barrier function was assessed by measuring plasma levels of LPS binding protein (LBP); plasma LBP was significantly increased in mice with DSS ($p < 0.0001$, untreated vs DSS) which was significantly reduced by *B.p.* MP80 + 2'FL treatment (one-way ANOVA with FDR correction, p = 0.42, untreated vs DSS + *B.p* MP80 + 2'FL; $p < 0.0001$ DSS vs DSS + *B.p* MP80 + 2'FL; **Figure 2.4g**).

DSS significantly increased the expression of inflammatory markers IL-1β, IL-6, and Ccl2 and decreased expression of a number of anti-inflammatory pathways including Tgfβ and AhR in the colon compared to controls (Wilcoxon Rank Sum with FDR correction, p = 0.024 for each gene respectively; **Supplemental figure 2.7; Supplemental tables 2.18-2.19**). *B.p.* MP80 + 2'FL pre-treatment prevented the DSS-induced increases in IL-6 and Ccl2 (p = 0.024, respectively). Similar trends were observed in the liver where *B.p.* MP80 + 2'FL treatment attenuated DSS-induced increase in Lcn and decrease in Tgfβ (p = 0.013, p = 0.020, DSS vs DSS + *B.p* MP80 + 2'FL; **Supplemental figure 2.9, Supplemental tables 2.22-2.23**). Commensal microbes such as *Lactobacillus* and *Bifidobacterium spp.* produce agonists that activate the aryl hydrocarbon receptor (AhR) pathway shown to be involved in intestinal homeostasis.[30]

Specifically, *Bifidobacterium* produce indole metabolites such as indole-3-lactate which is an agonist for the AhR and interacts with the serotonin reuptake transporter, Slc6a4.[31,32] Decreases in Slc6a4 are associated with colitis whereby activation of AhR is associated with improved disease outcomes.[33] Here we show that *B.p.* MP80 + 2'FL prevented the colonic DSS-induced decrease in AhR ($p = 0.036$, DSS vs DSS + *B.p* MP80 + 2'FL; **Figure 2.4f, Supplemental tables 2.18-2.19**). The decrease in serum LBP and increase in AhR and colon length were significantly correlated to *B.p.* MP80 qPCR numbers (Spearman's correlation, $p = 0.008$, $p = 0.004$, $p = 0.001$, **Supplemental figure 2.11, Supplemental table 2.24;**). When administered simultaneously the data show that the effect of *B.p.* MP80 + 2'FL treatment on DSS-colitis was significantly greater than treatment with either *B.p.* MP80 or 2'FL alone.

Pre-treatment with *B.p.* MP80 + 2'FL shifted serum metabolite profiles to be more consistent with profiles of untreated mice in comparison to DSS mice (**Supplemental figure 2.12a).** Treatment effects (Hedge's g, $|g| > 0.5$) showed an increase in the serum metabolites glucose, 3-hydroxybutyrate, acetate and formate in DSS + *B.p.* MP80 + 2'FL mice versus mice receiving DSS alone (**Supplemental figure 2.12d**). Conversely, DSS mice had elevated branch chain amino acids (leucine, isoleucine and valine) in addition to lysine, phenylalanine and pyruvate (Hedge's g, $|g| > 0.5$) relative to DSS + *B.p.* MP80 + 2'FL mice (**Supplemental figure 2.12d**).

2.3.7 Attenuated neuroinflammation after treatment with *B.p.* MP80 and 2'FL

Systemic peripheral inflammation has been reported to induce neuroinflammation, therefore, we assessed brain samples from DSS-challenged animals to determine severity in this model and the effects of *B.p.* MP80 + 2'FL treatment.[34] DSS induced pro-inflammatory cytokine Cxcl1 expression in the hypothalamus (Wilcoxon Rank Sum with FDR correction, $p = 0.014$; **Supplemental figure 2.13).** Cxcl1 induction was prevented in the hypothalamus by *B.p.* MP80 + 2'FL treatment ($p = 0.014$). This effect on Cxcl1suggests further investigation is needed.

2.4 Discussion

Numerous clinical trials of probiotic administration have failed to show significant impact on the host microbiota partly because engraftment of a supplemented microbe into a stable microbial community has proven challenging.[20,35] One strategy for enriching probiotics *in situ* is to provide a unique substrate preferentially catabolized by the supplemented bacteria.[1] Such synbiotic pairings have been shown to elevate the microbe's abundance in the gut during simultaneous administration, however, detection of the microbe post-bacterial gavage (i.e. beyond supplementation) is not typically measured.[36,37] Bacterial persistence was demonstrated with *Bacteroides* strains engrafting in mice microbiota dependent upon the presence of porphyran as a substrate for the supplemented strains.[7,8] Similarly, in breast-fed infants high *Bifidobacterium* levels are associated with the ability to catabolize HMOs.[23] In preterm infants supplemented with *Lactobacillus* and *Bifidobacterium*, only *Bifidobacterium* robustly persisted and was correlated to milk metabolism.[38] Frese et al.[39] showed dramatic and persistent colonization of an HMO-catabolizing strain of *Bifidobacterium longum* subsp. *infantis* in supplemented breast-fed infants. This is in concordance with the findings presented here that, in the absence of other human milk factors, the milk glycan 2'FL is sufficient to enable persistence and enrich populations of cognate *Bifidobacterium* while competing with endogenous bacterial groups.

Our data show that 2'FL, an HMO nutrient resource exogenous to the mouse intestine, provides a fitness advantage to *B. pseudocatenulatum* that possess 2'FL catabolism genes. In the presence of 2'FL, *B.p.* MP80 persisted robustly while *B.p.* JCM11661 failed, suggesting the fucosylated HMO gene cluster is required for persistence and possession of HMO catabolism genes provide a growth advantage. Degradation of 2'FL was detected by the fucose catabolism byproduct 1,2-propanediol, of which *B.p.* MP80 is known to produce.[40] 1,2-propanediol is a differentiating serum marker between breast-fed and formula fed infants linked to *Bifidobacterium* metabolism.[41] Here, high fecal *B.p.* MP80 is associated with 1,2-propanediol in the colon contents suggesting that 2'FL is being catabolized by *B.p.* MP80 through fucose catabolism. This catabolism provides a growth advantage that enables persistence and consequently ensures active metabolism that may be connected to host benefits.

Synbiotic treatment with *B.p.* MP80 and 2'FL is associated with a reduction in α-diversity (Shannon Index) in contrast to *B.p.* JCM11661. Thus, *B.p.* MP80 in the presence of 2'FL successfully reduced the richness and evenness of the endogenous microbial community species (Shannon Index) which are associated with colonization resistance.[4] These results are emblematic of the diversity-invasion effect, where survival of a microbial invader is negatively associated with species richness and evenness.[4]

The microbial community, as measured by β-diversity and differential abundance, was restructured by 2'FL supplementation alone. 2'FL is likely more accessible to a murine endogenous microbiota than previously studied substrates.[7,8] Given HMOs resemble mucin glycans, mouse endogenous *Bacteroidaceae* and *Bifidobacteriaceae* likely possess α-fucosidases capable of cleaving 2'FL. 2'FL enrichment of *Bacteroidaceae* and *Bifidobacteriaceae* implies that an invading *Bifidobacterium* must outcompete these endogenous microbes for 2'FL; the persistence of *B.p* MP80 suggests that it is a strong competitor. Further research is warranted to investigate how glycan specificity, host microbial barriers, and microbial genetic capabilities influence *Bifidobacterium* fitness in a more competitive environment, such as the mature human gut, and whether a more selective nutrient resource would increase fitness of cognate *Bifidobacterium* strains.

Bifidobacterium supplementation has previously been associated with reduced DSS-induced colitis inflammation although effects seem to be strain-specific.[42] In prior synbiotic experiments continuous gavage of *Bifidobacterium* was required for colitis amelioration.[43] Here we show *B.p.* MP80 persistence maintained by the presence of 2'FL significantly reduces the severity of DSS-induced colitis, an example of bacterial-carbohydrate synergy impacting host physiology. The ability of *B.p.* MP80 in the presence of 2'FL to reduce colitis severity is in marked contrast to the lack of effect of *B.p.* MP80 alone. *B.p.* MP80 + 2'FL was associated with decreased expression of pro-inflammatory cytokines IL-6, IL1-β and CCl2, previously induced in colitis models and with increased expression of Tgfβ.[44] Tgfβ administration is associated with improved health outcomes while anti-Tgfβ worsened outcomes.[45,46] Consistent with reports of *Bifidobacterium* preserving intestinal barrier function, *B.p.* MP80 in the presence of 2'FL increased

occludin expression and decreased plasma LBP levels.[42,47] The increase in Tgfβ and occludin positively correlate with 2'FL-dependent *B.p.* MP80 abundance.

Prior *in vitro* experiments identified *Bifidobacterium*-produced metabolite indole-3-lactic acid (ILA) acts upon AhR and Nrf2 pathways.[16] The transcription factor hypoxia inducible factor (HIF) can be activated through cytoprotective AhR and Nrf2 pathways, creating a hypoxic environment which plays a role in mucosal protection *in vivo*.[48,49] There was increased expression of AhR in the colon of DSS + *B.p.* MP80 + 2'FL treated mice suggesting activation of this pathway. However, further research is required to identify specific metabolites that are activating the AhR, Nrf2, and serotonin pathways *in vivo*.

Glucose, 3-hydroxybutyrate, acetate and formate were higher in the serum of DSS + *B.p.* MP80 + 2'FL mice relative to DSS mice. Notably, breast-fed infant serum metabolites are elevated in acetate and formate.[41] *B.p.* MP80 *in vitro* growth on 2'FL produces acetate and formate as major fermentation products. Increased acetate concentrations are associated with higher *Bifidobacterium* abundance and is shown to provide a protective effect during inflammatory challenge of mice.[15,50] Acetate is absorbed in the cecum and colon and is subsequently detected in venous blood.[51–54] Conversely, DSS mice exhibited decreases in serum glucose and 3-hydroxybutyrate alongside increased branch chain amino acids relative to DSS + *B.p.* MP80 + 2'FL treated mice. Others have suggested this metabolic imbalance is likely indicative of tissue catabolism to rectify the loss of energy intake through diet in DSS challenged mice.[55]

2'FL treatment alone has some beneficial effects in DSS-induced colitis, including attenuation of body weight change and reduced serum LBP although there was no effect on colon histology scores or spleen weight. 2'FL has been shown to reduce systemic inflammation in mice.[56] 2'FL is likely acting via both direct impact on host cells and indirect catabolism of 2'FL by endogenous microbes, including *Bifidobacterium*, to produce bioactive metabolites. This is supported by 2'FL alone activating similar pathways, including AhR/Nrf2 target genes Gpx2, Nqo1, and Hmox1 in the cecum. 2'FL alone reduces inflammation, however the provision of an anti-inflammatory *Bifidobacterium* with a HMO has a synergistic protective effect, noticeably improving health outcomes when compared to *B.p.*MP80 or 2'FL alone.

It is challenging to predict how amenable a mature microbiota is to microbial engraftment, in this current study *B.p.* MP80 paired with 2'FL consistently persisted in multiple cohorts and bacterial abundance was correlated to the concentration of 2'FL provided to the mice. We conclude that by providing a bacterial-carbohydrate pairing that is biologically relevant and evolutionarily-selected, we improved the likelihood of engraftment and associated beneficial health outcomes in mice. This concept is directly applicable toward development of symbiotic pairings for other live bacterial therapeutics targeting mature microbiotas.

At present, the specific role of HMOs in the neonatal enrichment of a *Bifidobacterium* population is solely associative as there are multiple factors in milk known to shape the infant gut microbiome.[57,58] However, the data presented here show a single HMO (2'FL) is able to promote enrichment of a cognate 2'FL-consuming *Bifidobacterium* strain within a complex gut ecosystem. This argues that HMOs alone are sufficient to drive this outcome and provides a novel model to examine the specific influences of HMO-*Bifidobacterium* axis in isolation. While disparities between our mouse model and the human intestine may limit our conclusions, they also provide future research questions. The established mouse microbial community is not characteristic of the naïve infant's microbial community structure or colonization resistance. The infant gut initially possesses fewer bacterial species, however, those bacteria are being selected based on their capacity to catabolize nutrients found in breast milk. Therefore, the impact of founder effect, bacterial fitness differences, and inter-species competition of *Bifidobacterium* strains should be investigated in the future.

This research suggests that HMOs act as a privileged nutrient resource, enriching bacterium capable of catabolism even when high colonization resistance is present. This is an important concept for clinicians when addressing infant gastrointestinal microbiota development and adult GI inflammatory diseases. It provides critical information on bacterial characteristics that should be considered when recommending probiotics or live biotherapeutics and may increase the likelihood of conferring health benefits. Furthermore, these findings demonstrate the critical role of HMOs in colonization of *Bifidobacterium* which is associated with lifelong health impacts for infants and supports current efforts to encourage breast feeding.

2.5 Methods

2.5.1 Mouse studies

Animals were handled and maintained in accordance with protocols approved by the Institutional Animal Care and Use Committee of University of California, Davis (IACUC Protocol: 21900). Male C57BL/6J mice (5-6 weeks old, Jackson Labs) were group housed (3 per cage) and maintained at 22C with 12-hour light-dark cycle. Before commencing experiments, mice were co-housed and acclimated for a minimum of one week at the facility. Food (5058 Irradiated Pico Mouse Lab Diet) and water were provided *ad libitum.* 2'FL was provided in the drinking water as a 10% (w/v) solution. *Bifidobacterium* (10e9 cfu/ml in PBS) or phosphate buffered saline was administered via oral gavage (100µl). Mice were euthanized via CO_2 asphyxiation, excluding DSS experiments where mice were euthanized with FatalPlus. Supplemental methods contain further details on experimental design, preparation of bacterial inoculum and 2'FL, and ^{1}H-NMR metabolite sample preparation and analysis.

2.5.2 Quantification of bacterial strains by qPCR

B.p. JCM11661 was quantified with strain-specific primers designed for this study while *B.p.* MP80 and *Bifidobacterium* primers were previously generated (**Supplemental table 1**).[35,59,60] Primer validation and PCR program located in supplemental methods.

2.5.3 Fecal extraction, microbiota DNA sequencing, and differential abundance testing

Fecal samples were collected from individual mice within 1 hour of the light cycle's start. DNA was extracted from 30 to 100 mg of stool sample using the Quick-DNA Fecal/Soil Microbe Miniprep Kit, Catalog No. D6010 (ZYMO, Irvine, CA, USA). The extraction protocol was in accordance with the manufacturer's instructions including a bead-beating step using a FastPrep-24 Instrument (MP Biomedicals, Santa Ana, CA, USA) for a total of 2 min at 25°C at a speed of 6.5 m/s. In triplicate, the V4 region of the *16S rRNA* gene was amplified with barcoded PCR primers F515 (5′-CACGGTCGKCGGCGCCATT-3′) and R806 (5-′GGACTACHVGGGTWTCTAAT-3′) modified to contain an adapter region for sequencing on the Illumina MiSeq platform.[61] Amplicons were verified by gel electrophoresis, combined, purified, and sent to the UC Davis Genome Center for library preparation

and high throughput 250-bp paired-end sequencing using the Illumina MiSeq platform. Raw sequencing data was demultiplexed and quality filtered before import into QIIME2-2019.7.[62] Samples with poor quality data were excluded from analysis. After trimming, reads were processed with DADA2.[63] Filtered sequences were aligned and taxonomy was assigned using the 99% SILVA naïve Bayesian classifier in QIIME 2 v2019.7.[64] Samples were rarified to 2000 sequences. Differential abundance was evaluated with Songbird which ranks the log-fold changes between selected taxa or ASVs, identifying ASVs as high or low ranked.[29] The Songbird formula for differential abundance testing between all treatments tested the interaction between *B.p.* MP80 and 2'FL while accounting for the longitudinal nature of data. For 2'FL differential abundance, mice supplemented with a *Bifidobacterium* were excluded from analysis and only 2'FL and PBS treatments were evaluated. Taxa *Bifidobaceriaceae* and *Bacteroidaceae* were chosen as the numerator for respective analyses based on high and low Songbird rankings. For both respective analyses, the lowest 25% of ranked ASVs were selected and *Lachnospiraceae* and *Ruminococcaceae* ASVs identified within that selected range were chosen as the denominator when calculating log-fold changes. **Supplemental tables 6 and 7** list ASVs used for each log ratio. The NCBI BioProject ID for raw 16S sequencing data is PRJNA669815. Analysis of microbial ecosystem characteristics and statistics located in supplemental methods.

2.5.4 Plasma and tissue collection

Blood was collected via cardiac puncture into EDTA-coated vaccutainers. After centrifugation (40°C; 10,000 RCF, 15 min), plasma was obtained and stored at -80C. Luminal contents and tissue from small and large intestine, liver, and brain were collected onto dry ice before storage at -80°C.

2.5.5 Barrier function assessment

GI tract was cut along the mesenteric border and mounted in Ussing chambers inserts exposing 0.1 cm^2 tissue surface area (Physiologic Instruments, San Diego, CA, USA). The mucosal tissue side was exposed to a Ringers-mannitol (10mM) solution and the serosal was exposed to a Ringers-glucose (10mM) solution. Both compartments were oxygenated, and tissue maintained at 37°C. To measure paracellular and transcellular permeability, FITC- labelled dextran (400ug/ml, FD-4, Sigma Aldrich) and horse radish

peroxidase (200ug/ml, HRP Type VI, Sigma Aldrich), respectively, were added to the mucosal compartment. Every 30 minutes for the next 2 hours, serosal samples were collected. Concentration of FD-4 was measured with fluorescence (485nm excitation, 538nm emission) whereas HRP was detected by O-dianisidine (450nm absorbance). Data was calculated as flux (ng/cm2/hr).

3.5.6 Plasma lipopolysaccharide-binding protein (LBP)

LBP were measured in plasma samples via ELISA as per manufacturer instructions (Biometec GmbH, Greifswald, Germany).

2.5.7 Histology

Colon sections from DSS-treated mice were embedded in paraffin and cut into 10μM sections, mounted on slide and processed for hematoxylin and eosin staining. Images were taken at 200X using the MetaMorph Basic v. 7.7.0 image-analyzer software on an Olympus BX61 microscope. Tissues were scored blindly from 3 sections from every mouse on a scale of 1-4 based on inflammatory cell infiltration, goblet cell loss, mucosal architecture, muscle thickening, edema, and crypt abscess as previously described.[65,66]

2.5.8 RNA extraction and qRT-PCR

RNA was extracted from all intestine sections, liver, and brain using the TRIzol method (Life technologies, 15596018). Quality and quantity of RNA was assessed using a NanoDrop Spectrophotometer (Thermo Scientific). cDNA synthesis was performed (1ug RNA) with iScript cDNA synthesis kit (BioRad, 1708890) (primer sequences in **Supplemental table 6**). Real-time PCR was performed using Quantstudio 6 Flex real-time PCR machine with PowerUp SYBR Green Master Mix (Thermo Fisher, A25742) for detection. Ribosomal protein L13a was used as a housekeeping gene in accordance to the $2^{\Delta\Delta CT}$ method. Gene expression data are normalized to untreated control mice. In the heat maps, measured genes are expressed as the Log_2 transformed fold change in mRNA expression levels relative to the untreated group.

2.5.9 Colitis model statistics

Data are expressed as means +/- SEM and are analyzed by Kruskal-Wallis test with FDR correction and post hoc Wilcoxon Rank Sum test with FDR correction ($p < 0.05$ as significant). Outliers excluded

based on Grubbs' test $\alpha = 0.05$. Spearman's test calculated correlations between DSS inflammatory measures (qRT-PCR) and *B.p*. MP80 abundance (qPCR) (**Supplemental table 24**).

Data Availability: The NCBI BioProject ID for raw 16S sequencing data is PRJNA669815.

Acknowledgements: We thank Wendie Vang for assisting in mouse necropsy and Heather Romasko, Julia Wong, Dadne Lopez, and James Thach for performing mouse fecal DNA and mouse tissue RNA extractions. Thank you to Dr. Randall Robinson of the Barile Lab for testing the purity of multiple 2'-fucosyllactose lots.

Funding: This study was supported by National Institutes of Health awards 5T32AI060555 (BEH), F32HD093185 (DHT) and RO1AT008759 (DAM, HER). CMS acknowledges the Kinsella Endowed Chair in Food, Nutrition, and Health, and is supported by the USDA National Institute of Food and Agriculture Hatch project 1021411. DAM acknowledges the Peter J. Shields Endowed Chair in Dairy Food Science.

Author Contributions: Mouse studies including host analysis conducted by AME, BEH, MLG, MXMG, and DHT. Microbiota analysis and statistics performed by BEH, DHT, MXMG, and DJT. JAL completed metabolite profiling. AME, BEH, HER, and DAM wrote the manuscript with all collaborators providing input.

Competing Interests: DAM is a co-founder of Evolve Biosystems, a company focused on diet-based manipulation of the gut microbiota and BCD Biosciences, a company advancing novel bioactive glycans. Neither Evolve Biosystems nor BCD Biosciences had a role in the conceptualization, design, data collection, analysis, or preparation of this manuscript. MXMG is a current employee of BCD Biosciences.

2.6 References

1. Swanson KS, Gibson GR, Hutkins R, Reimer RA, Reid G, Verbeke K, Scott KP, Holscher HD, Azad MB, Delzenne NM, et al. The International Scientific Association for Probiotics and Prebiotics (ISAPP) consensus statement on the definition and scope of synbiotics. Nat Rev Gastroenterol Hepatol 2020; 17:687–701.
2. Wang Q, Dong J, Zhu Y. Probiotic supplement reduces risk of necrotizing enterocolitis and mortality in preterm very low-birth-weight infants: an updated meta-analysis of 20 randomized, controlled trials. J Pediatr Surg 2012; 47:241–8.
3. Suez J, Zmora N, Segal E, Elinav E. The pros, cons, and many unknowns of probiotics. Nat Med 2019; 25:716–29.
4. Mallon CA, Elsas JD van, Salles JF. Microbial invasions: the process, patterns, and mechanisms. Trends Microbiol 2015; 23:719–29.
5. Walter J, Maldonado-Gómez MX, Martínez I. To engraft or not to engraft: an ecological framework for gut microbiome modulation with live microbes. Curr Opin Biotechnol 2018; 49:129–39.
6. Bertuzzo E, Suweis S, Mari L, Maritan A, Rodríguez-Iturbe I, Rinaldo A. Spatial effects on species persistence and implications for biodiversity. Proc Natl Acad Sci USA 2011; 108:4346–51.
7. Shepherd ES, DeLoache WC, Pruss KM, Whitaker WR, Sonnenburg JL. An exclusive metabolic niche enables strain engraftment in the gut microbiota. Nature 2018; 557:434–8.
8. Kearney SM, Gibbons SM, Erdman SE, Alm EJ. Orthogonal dietary niche enables reversible engraftment of a gut bacterial commensal. Cell Rep 2018; 24:1842–51.
9. Taft DH, Liu J, Maldonado-Gomez MX, Akre S, Huda MN, Ahmad SM, Stephensen CB, Mills DA. Bifidobacterial dominance of the gut in early life and acquisition of antimicrobial resistance. mSphere 2018; 3.
10. Huda MN, Ahmad SM, Alam MJ, Khanam A, Kalanetra KM, Taft DH, Raqib R, Underwood MA, Mills DA, Stephensen CB. Bifidobacterium abundance in early infancy and vaccine response at 2 years of age. Pediatrics 2019; 143.
11. Vatanen T, Kostic AD, d'Hennezel E, Siljander H, Franzosa EA, Yassour M, Kolde R, Vlamakis H, Arthur TD, Hämäläinen A-M, et al. Variation in microbiome LPS immunogenicity contributes to autoimmunity in humans. Cell 2016; 165:842–53.
12. Henrick BM, Chew S, Casaburi G, Brown HK, Frese SA, Zhou Y, Underwood MA, Smilowitz JT. Colonization by B. infantis EVC001 modulates enteric inflammation in exclusively breastfed infants. Pediatr Res 2019; 86:749–57.
13. Karav S, Casaburi G, Frese SA. Reduced colonic mucin degradation in breastfed infants colonized by Bifidobacterium longum subsp. infantis EVC001. FEBS Open Bio 2018; 8:1649–57.
14. Casaburi G, Duar RM, Vance DP, Mitchell R, Contreras L, Frese SA, Smilowitz JT, Underwood MA. Early-life gut microbiome modulation reduces the abundance of antibiotic-resistant bacteria. Antimicrob Resist Infect Control 2019; 8:131.
15. Fukuda S, Toh H, Taylor TD, Ohno H, Hattori M. Acetate-producing bifidobacteria protect the host from enteropathogenic infection via carbohydrate transporters. Gut Microbes 2012; 3:449–54.
16. Ehrlich AM, Pacheco AR, Henrick BM, Taft DH, Xu G, Huda MN, Mishchuck D, Goodson ML, Slupsky C, Barile D, et al. Indole-3-lactic acid associated with Bifidobacterium-dominated microbiota significantly decreases inflammation in intestinal epithelial cells. BMC Microbiology 2020;
17. Meng D, Sommella E, Salviati E, Campiglia P, Ganguli K, Djebali K, Zhu W, Walker WA. Indole-3-lactic acid, a metabolite of tryptophan, secreted by Bifidobacterium longum subspecies infantis is anti-inflammatory in the immature intestine. Pediatr Res 2020; 88:209–17.
18. Fanning S, Hall LJ, Cronin M, Zomer A, MacSharry J, Goulding D, Motherway MO, Shanahan F, Nally K, Dougan G, et al. Bifidobacterial surface-exopolysaccharide facilitates commensal-host interaction through immune modulation and pathogen protection. Proc Natl Acad Sci USA 2012; 109:2108–13.

19. Turroni F, Serafini F, Foroni E, Duranti S, O'Connell Motherway M, Taverniti V, Mangifesta M, Milani C, Viappiani A, Roversi T, et al. Role of sortase-dependent pili of Bifidobacterium bifidum PRL2010 in modulating bacterium-host interactions. Proc Natl Acad Sci USA 2013; 110:11151–6.
20. Kristensen NB, Bryrup T, Allin KH, Nielsen T, Hansen TH, Pedersen O. Alterations in fecal microbiota composition by probiotic supplementation in healthy adults: a systematic review of randomized controlled trials. Genome Med 2016; 8:52.
21. Vujkovic-Cvijin I, Sklar J, Jiang L, Natarajan L, Knight R, Belkaid Y. Host variables confound gut microbiota studies of human disease. Nature 2020; 587:448–54.
22. Garrido D, Ruiz-Moyano S, Kirmiz N, Davis JC, Totten SM, Lemay DG, Ugalde JA, German JB, Lebrilla CB, Mills DA. A novel gene cluster allows preferential utilization of fucosylated milk oligosaccharides in Bifidobacterium longum subsp. longum SC596. Sci Rep 2016; 6:35045.
23. Sakanaka M, Hansen ME, Gotoh A, Katoh T, Yoshida K, Odamaki T, Yachi H, Sugiyama Y, Kurihara S, Hirose J, et al. Evolutionary adaptation in fucosyllactose uptake systems supports bifidobacteria-infant symbiosis. Sci Adv 2019; 5:eaaw7696.
24. Yu Z-T, Chen C, Kling DE, Liu B, McCoy JM, Merighi M, Heidtman M, Newburg DS. The principal fucosylated oligosaccharides of human milk exhibit prebiotic properties on cultured infant microbiota. Glycobiology 2013; 23:169–77.
25. Matsuki T, Yahagi K, Mori H, Matsumoto H, Hara T, Tajima S, Ogawa E, Kodama H, Yamamoto K, Yamada T, et al. A key genetic factor for fucosyllactose utilization affects infant gut microbiota development. Nat Commun 2016; 7:11939.
26. Shani G. Species, Subspecies, and Strain Specific Adaptations of Bifidobacteria to the Human Gut, and Their Implications . 2017;
27. Mutter S, Worden C, Paxton K, Mäkinen V-P. Statistical reporting of metabolomics data: experience from a high-throughput NMR platform and epidemiological applications. Metabolomics 2019; 16:5.
28. Cabanettes F, Klopp C. D-GENIES: dot plot large genomes in an interactive, efficient and simple way. PeerJ 2018; 6:e4958.
29. Morton JT, Marotz C, Washburne A, Silverman J, Zaramela LS, Edlund A, Zengler K, Knight R. Establishing microbial composition measurement standards with reference frames. Nat Commun 2019; 10:2719.
30. Agus A, Planchais J, Sokol H. Gut microbiota regulation of tryptophan metabolism in health and disease. Cell Host Microbe 2018; 23:716–24.
31. Aragozzini F, Ferrari A, Pacini N, Gualandris R. Indole-3-lactic acid as a tryptophan metabolite produced by Bifidobacterium spp. Appl Environ Microbiol 1979; 38:544–6.
32. Denhart DJ, Deskus JA, Ditta JL, Gao Q, Dalton King H, Kozlowski ES, Meng Z, LaPaglia MA, Mattson GK, Molski TF, et al. Conformationally restricted homotryptamines. Part 5: 3-(trans-2-aminomethylcyclopentyl)indoles as potent selective serotonin reuptake inhibitors. Bioorg Med Chem Lett 2009; 19:4031–3.
33. Coates MD, Mahoney CR, Linden DR, Sampson JE, Chen J, Blaszyk H, Crowell MD, Sharkey KA, Gershon MD, Mawe GM. Molecular defects in mucosal serotonin content and decreased serotonin reuptake transporter in ulcerative colitis and irritable bowel syndrome 1 ☆. Gastroenterology 2004; 126:1657–64.
34. Guo S, Nighot M, Al-Sadi R, Alhmoud T, Nighot P, Ma TY. Lipopolysaccharide regulation of intestinal tight junction permeability is mediated by TLR4 signal transduction pathway activation of FAK and myd88. J Immunol 2015; 195:4999–5010.
35. Maldonado-Gómez MX, Martínez I, Bottacini F, O'Callaghan A, Ventura M, van Sinderen D, Hillmann B, Vangay P, Knights D, Hutkins RW, et al. Stable Engraftment of Bifidobacterium longum AH1206 in the Human Gut Depends on Individualized Features of the Resident Microbiome. Cell Host Microbe 2016; 20:515–26.
36. Krumbeck JA, Walter J, Hutkins RW. Synbiotics for improved human health: recent developments, challenges, and opportunities. Annu Rev Food Sci Technol 2018; 9:451–79.

37. Mischke M, Arora T, Tims S, Engels E, Sommer N, van Limpt K, Baars A, Oozeer R, Oosting A, Bäckhed F, et al. Specific synbiotics in early life protect against diet-induced obesity in adult mice. Diabetes Obes Metab 2018; 20:1408–18.
38. Alcon-Giner C, Dalby MJ, Caim S, Ketskemety J, Shaw A, Sim K, Lawson MAE, Kiu R, Leclaire C, Chalklen L, et al. Microbiota Supplementation with Bifidobacterium and Lactobacillus Modifies the Preterm Infant Gut Microbiota and Metabolome: An Observational Study. Cell Rep Med 2020; 1:100077.
39. Frese SA, Hutton AA, Contreras LN, Shaw CA, Palumbo MC, Casaburi G, Xu G, Davis JCC, Lebrilla CB, Henrick BM, et al. Persistence of Supplemented Bifidobacterium longum subsp. infantis EVC001 in Breastfed Infants. mSphere 2017; 2.
40. Zabel B, Yde CC, Roos P, Marcussen J, Jensen HM, Salli K, Hirvonen J, Ouwehand AC, Morovic W. Novel Genes and Metabolite Trends in Bifidobacterium longum subsp. infantis Bi-26 Metabolism of Human Milk Oligosaccharide 2'-fucosyllactose. Sci Rep 2019; 9:7983.
41. He X, Parenti M, Grip T, Domellöf M, Lönnerdal B, Hernell O, Timby N, Slupsky CM. Metabolic phenotype of breast-fed infants, and infants fed standard formula or bovine MFGM supplemented formula: a randomized controlled trial. Sci Rep 2019; 9:339.
42. Srutkova D, Schwarzer M, Hudcovic T, Zakostelska Z, Drab V, Spanova A, Rittich B, Kozakova H, Schabussova I. Bifidobacterium longum CCM 7952 Promotes Epithelial Barrier Function and Prevents Acute DSS-Induced Colitis in Strictly Strain-Specific Manner. PLoS One 2015; 10:e0134050.
43. Sheng K, He S, Sun M, Zhang G, Kong X, Wang J, Wang Y. Synbiotic supplementation containing Bifidobacterium infantis and xylooligosaccharides alleviates dextran sulfate sodium-induced ulcerative colitis. Food Funct 2020; 11:3964–74.
44. Alex P, Zachos NC, Nguyen T, Gonzales L, Chen T-E, Conklin LS, Centola M, Li X. Distinct cytokine patterns identified from multiplex profiles of murine DSS and TNBS-induced colitis. Inflamm Bowel Dis 2009; 15:341–52.
45. Giladi G, Raz E, Karmeli F, Okon E, Rachmilewitz D. Transforming growth factor-beta gene therapy ameliorates experimental colitis in rats. European Journal of Gastroenterology & Hepatology, 1995; 7:341–7.
46. Fuss IJ, Boirivant M, Lacy B, Strober W. The interrelated roles of TGF-beta and IL-10 in the regulation of experimental colitis. J Immunol 2002; 168:900–8.
47. Krumbeck JA, Rasmussen HE, Hutkins RW, Clarke J, Shawron K, Keshavarzian A, Walter J. Probiotic Bifidobacterium strains and galactooligosaccharides improve intestinal barrier function in obese adults but show no synergism when used together as synbiotics. Microbiome 2018; 6:121.
48. Tumova S, Kerimi A, Williamson G. Long term treatment with quercetin in contrast to the sulfate and glucuronide conjugates affects HIF1α stability and Nrf2 signaling in endothelial cells and leads to changes in glucose metabolism. Free Radic Biol Med 2019; 137:158–68.
49. Karhausen J, Furuta GT, Tomaszewski JE, Johnson RS, Colgan SP, Haase VH. Epithelial hypoxia-inducible factor-1 is protective in murine experimental colitis. J Clin Invest 2004; 114:1098–106.
50. Aoki R, Kamikado K, Suda W, Takii H, Mikami Y, Suganuma N, Hattori M, Koga Y. A proliferative probiotic Bifidobacterium strain in the gut ameliorates progression of metabolic disorders via microbiota modulation and acetate elevation. Sci Rep 2017; 7:43522.
51. Pomare EW, Branch WJ, Cummings JH. Carbohydrate fermentation in the human colon and its relation to acetate concentrations in venous blood. J Clin Invest 1985; 75:1448–54.
52. Buckley BM, Williamson DH. Origins of blood acetate in the rat. Biochem J 1977; 166:539–45.
53. Fleming SE, Choi SY, Fitch MD. Absorption of short-chain fatty acids from the rat cecum in vivo. J Nutr 1991; 121:1787–97.
54. Umesaki Y, Yajima T, Yokokura T, Mutai M. Effect of organic acid absorption on bicarbonate transport in rat colon. Pflugers Arch 1979; 379:43–7.
55. Dong F, Zhang L, Hao F, Tang H, Wang Y. Systemic responses of mice to dextran sulfate sodium-induced acute ulcerative colitis using 1H NMR spectroscopy. J Proteome Res 2013; 12:2958–66.

56. Lee S, Goodson M, Vang W, Kalanetra K, Barile D, Raybould H. 2'-fucosyllactose Supplementation Improves Gut-Brain Signaling and Diet-Induced Obese Phenotype and Changes the Gut Microbiota in High Fat-Fed Mice. Nutrients 2020; 12.
57. Kirmiz N, Robinson RC, Shah IM, Barile D, Mills DA. Milk Glycans and Their Interaction with the Infant-Gut Microbiota. Annu Rev Food Sci Technol 2018; 9:429–50.
58. Lönnerdal B. Bioactive proteins in breast milk. J Paediatr Child Health 2013; 49 Suppl 1:1–7.
59. Rinttilä T, Kassinen A, Malinen E, Krogius L, Palva A. Development of an extensive set of 16S rDNA-targeted primers for quantification of pathogenic and indigenous bacteria in faecal samples by real-time PCR. J Appl Microbiol 2004; 97:1166–77.
60. Matsuki T, Watanabe K, Fujimoto J, Kado Y, Takada T, Matsumoto K, Tanaka R. Quantitative PCR with 16S rRNA-gene-targeted species-specific primers for analysis of human intestinal bifidobacteria. Appl Environ Microbiol 2004; 70:167–73.
61. Caporaso JG, Lauber CL, Walters WA, Berg-Lyons D, Lozupone CA, Turnbaugh PJ, Fierer N, Knight R. Global patterns of 16S rRNA diversity at a depth of millions of sequences per sample. Proc Natl Acad Sci USA 2011; 108 Suppl 1:4516–22.
62. Bolyen E, Rideout JR, Dillon MR, Bokulich NA, Abnet CC, Al-Ghalith GA, Alexander H, Alm EJ, Arumugam M, Asnicar F, et al. Reproducible, interactive, scalable and extensible microbiome data science using QIIME 2. Nat Biotechnol 2019; 37:852–7.
63. Callahan BJ, McMurdie PJ, Rosen MJ, Han AW, Johnson AJA, Holmes SP. DADA2: High-resolution sample inference from Illumina amplicon data. Nat Methods 2016; 13:581–3.
64. Quast C, Pruesse E, Yilmaz P, Gerken J, Schweer T, Yarza P, Peplies J, Glöckner FO. The SILVA ribosomal RNA gene database project: improved data processing and web-based tools. Nucleic Acids Res 2013; 41:D590-6.
65. Appleyard CB, Wallace JL. Reactivation of hapten-induced colitis and its prevention by anti-inflammatory drugs. Am J Physiol 1995; 269:G119-25.
66. Erben U, Loddenkemper C, Doerfel K, Spieckermann S, Haller D, Heimesaat MM, Zeitz M, Siegmund B, Kühl AA. A guide to histomorphological evaluation of intestinal inflammation in mouse models. Int J Clin Exp Pathol 2014; 7:4557–76.

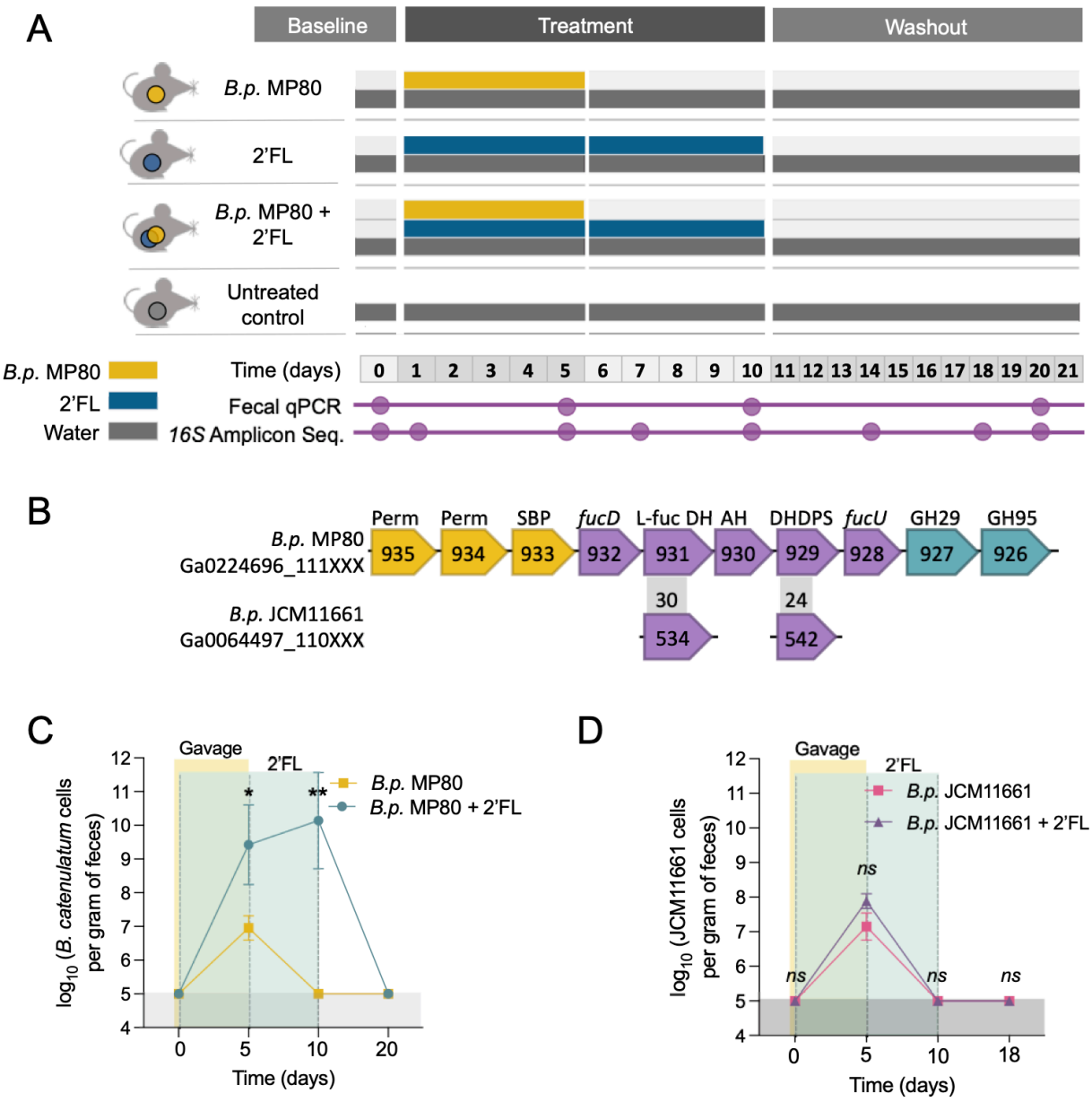

Figure 2.1. *Bifidobacterium* persistence during 2'FL supplementation in mice. (A) Mouse experimental design; (B) fucosylated HMO utilization gene cluster comparison; (C) quantification of *B.p.* MP80 by qPCR in fecal DNA of treatment groups *B.p.* MP80 + 2'FL (n = 6) and *B.p.* MP80 (n = 6); and (D) quantification of *B.p.* JCM11661 by qPCR in fecal DNA of treatment groups *B.p.* JCM11661 + 2'FL (n = 3) and *B.p.* JCM11661 (n = 3). In (A) treatments consisted of 4 groups of mice; untreated = oral gavage of PBS (day 1-5) and drinking water (day 1-20); *B.p.* MP80 = oral gavage of *B.p.* MP80 (day 1-5) and drinking water

(day 1-20); 2'FL = oral gavage of PBS (day 1-5) and 2'FL in drinking water (day 1-10); *B.p.* MP80 + 2'FL = oral gavage of *B.p.* MP80 (day 1-5) and 2'FL in drinking water (day 1-10); $n = 6$ per treatment group. In (B) arrows represent genes and inset numbers indicate the locus tag number for the respective genome from the Joint Genome Institute. Number in gray box indicates percent identity between corresponding gene and homologs relative to strain *B.p.* MP80. Colors are indicative of the primary function: oligosaccharide transport (yellow), carbohydrate feeder pathways (purple) and glycosyl hydrolases (blue). Perm: ABC Permease; SBP: Solute Binding Protein; L-Fuc DH: L-fuconate dehydrogenase; DHDPS: Dihydropicolinate synthase; FucU: L-fucose mutarotase. In (C) and (D) day 0: baseline, after acclimation to the animal facility; day 5: *Bifidobacterium* or PBS gavage days; day 10: 2'FL supplementation; day 20: washout of 2'FL, day before necropsy. One-way ANOVA with multiple comparison testing between treatments at individual time points; * $p<0.05$, ** $p<0.01$, *** $p<0.001$, *ns* = not significant.

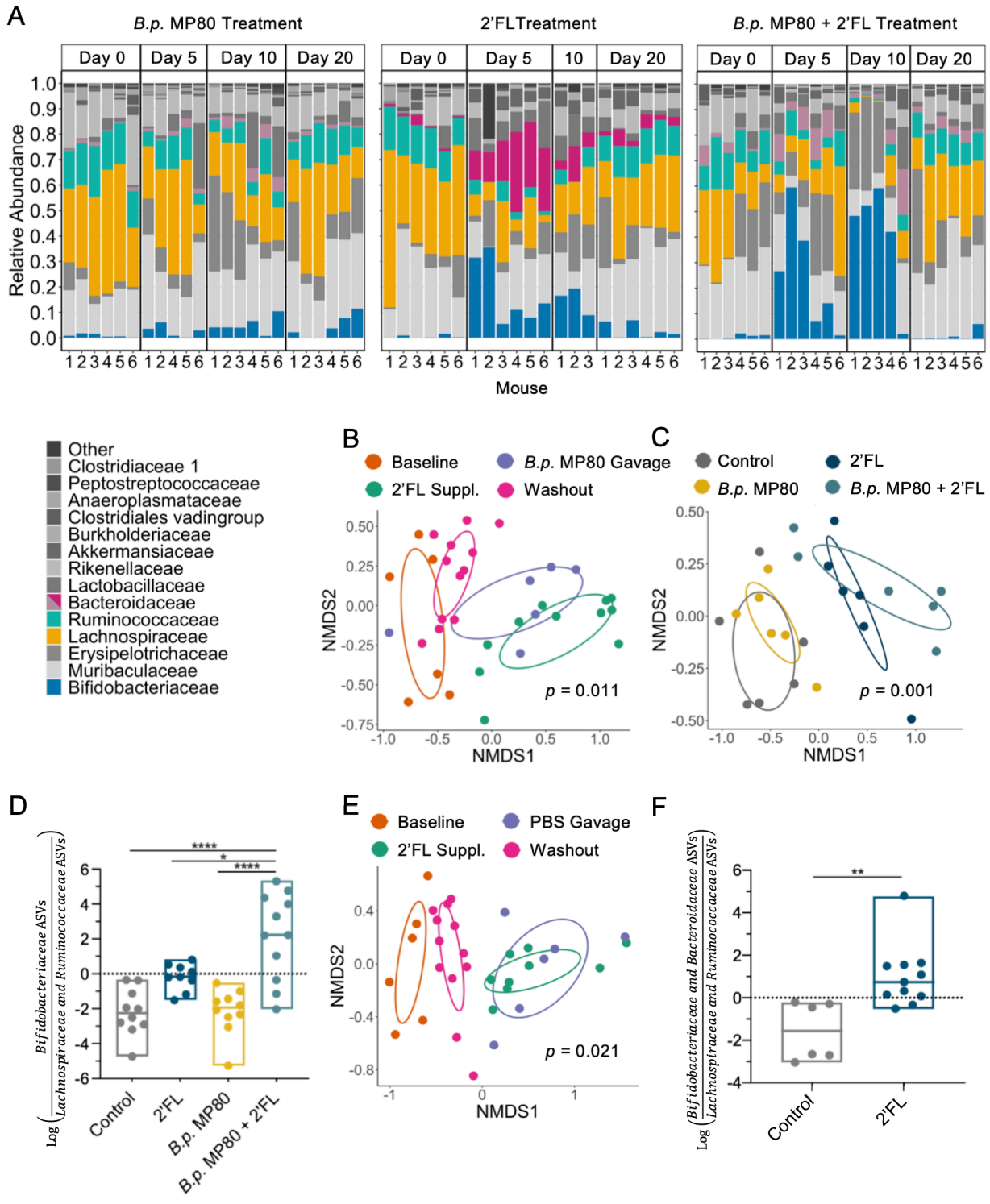

Figure 2.2. Microbial community structure changes during treatments. (A) Barplots of bacterial family relative abundance for individual mice from treatment groups *B.p.* MP80, 2'FL, and *B.p.* MP80 + 2'FL (*n* = 6 per treatment) at four time points (day 0: baseline; day 5: final day of *B.p.* MP80 or PBS gavage; day

10: final day of 2'FL supplementation; day 20: after 10 days washout of 2'FL, day before necropsy). Numbers along the x-axis indicate individual mice. To highlight key bacterial families identified in differential abundance testing, *Bacteroidaceae* is colored deep pink for 2'FL treatment, while *Bacteroidaceae* is grey-pink for *B.p.* MP80 and *B.p.* MP80 + 2'FL. (B) Non-metric Multi-dimensional Scaling (NMDS) plot of the β-diversity index Bray-Curtis for *B.p.* MP80 + 2'FL treatment group, time periods separated by color; (C) NMDS plot of β-diversity index Bray-Curtis on final day of 2'FL supplementation (day 10), colored by treatment; (D) log ratio of *Bifidobacteriaceae* relative to low ranked *Lachnospiraceae* and *Ruminococcaceae* ASVs on the final day of 2'FL supplementation (day 10); (E) NMDS plot of the β-diversity index Bray-Curtis for 2'FL treatment group, time periods separated by color; and (F) 2'FL treatment log ratio of *Bifidobacteriaceae* and *Bacteroidaceae* relative to low ranked *Lachnospiraceae* and *Ruminococcaceae* ASVs on the final day of 2'FL supplementation (day 10). In (D) and (F) one-way ANOVA with Tukey's multiple comparisons test; * $p<0.05$, ** $p<0.01$, *** $p<0.001$.

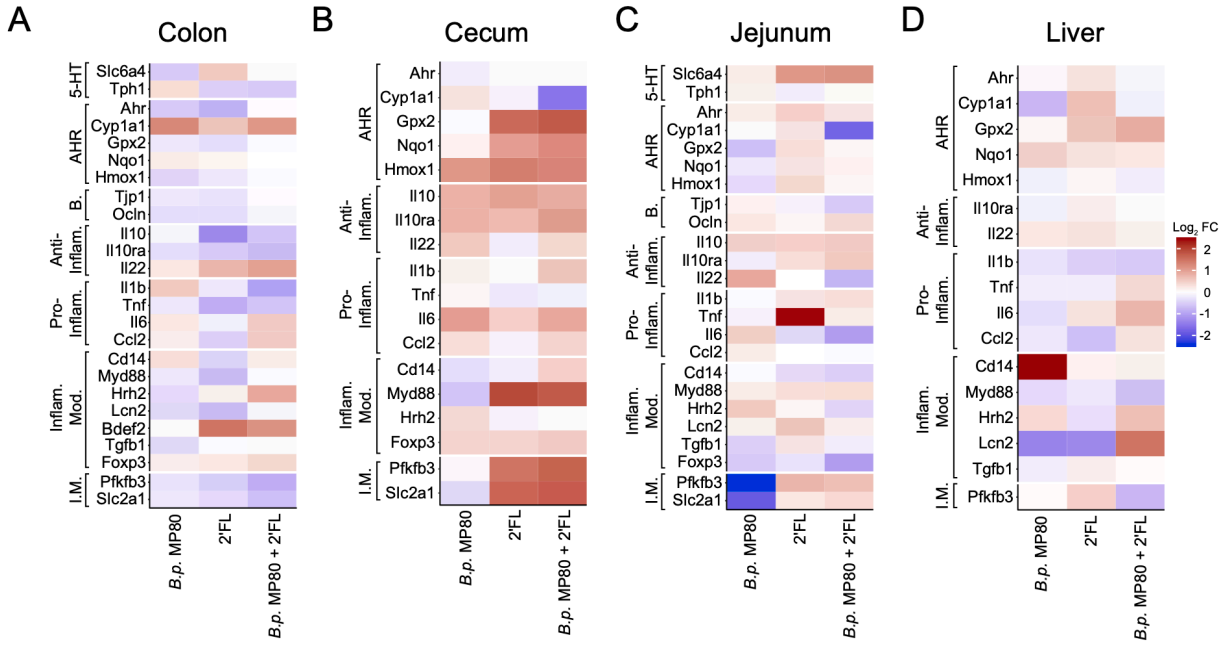

Figure 2.3. Heat maps of gene expression changes in mice in the (A) distal colon, (B) cecum, (C) jejunum, and (D) liver. Log_2 transformed fold changes are expressed relative to untreated control mice (n = 6 per treatment). Genes were grouped according to known function: serotonin (5-HT) regulatory targets, aryl hydrocarbon receptor (AhR) pathway targets, intestinal barrier markers, anti-inflammatory, pro-inflammatory, inflammatory modulating, and inflammatory metabolism. Statistical analysis for this data is in supplemental figures 4-6 and supplemental tables 10-16.

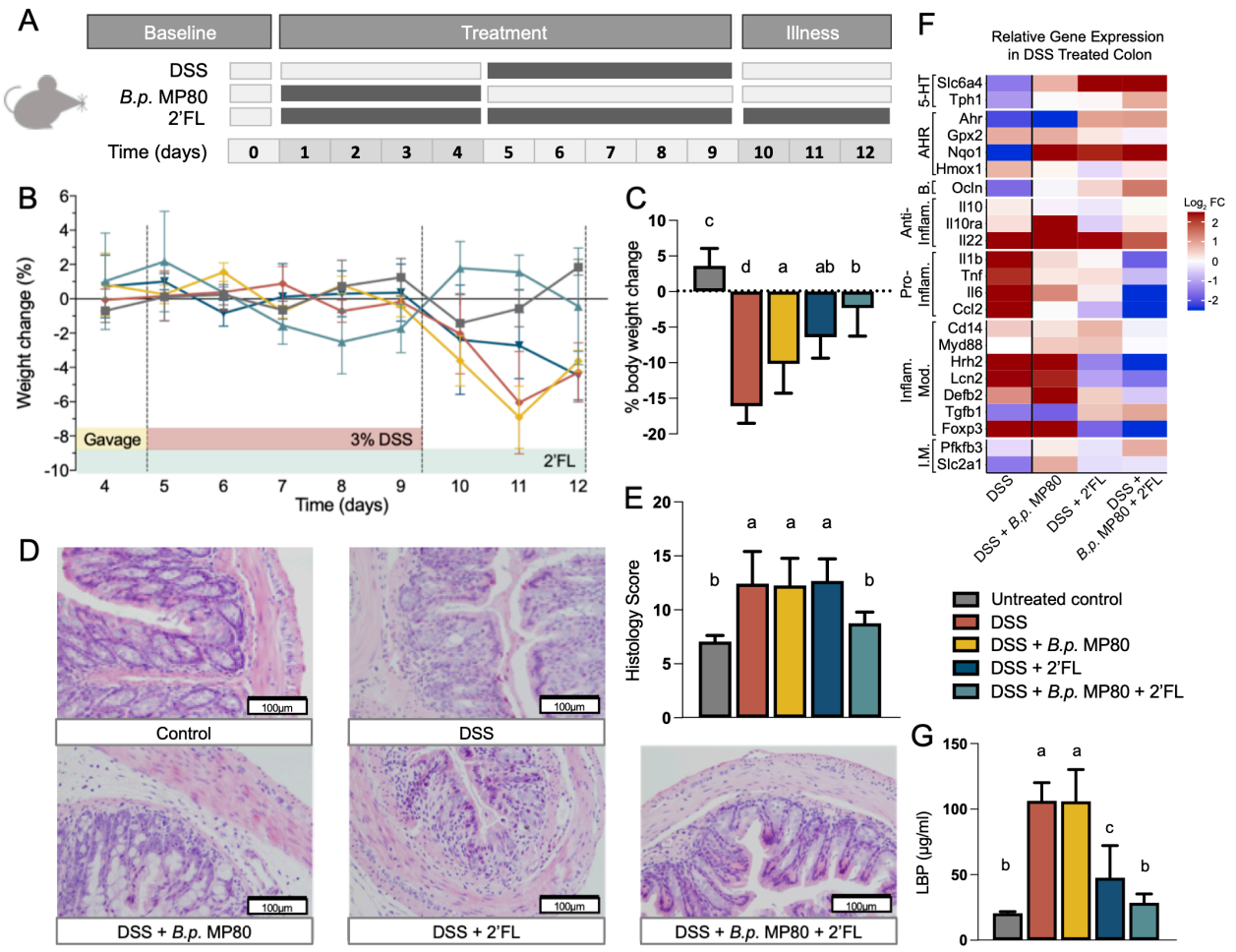

Figure 2.4. Effects of *B.p.* MP80 and 2'FL supplementation in mice challenged with DSS-induced colitis. (A) Experimental timeline (n = 6 per treatment); (B) percent change in weight, as compared to the previous day, during and following DSS challenge; (C) percentage weight change measured from before DSS exposure (day 4) to necropsy (day 12); (D) representative images (200x magnification) of colon H and E sections; (E) histology scores based on inflammatory cell infiltration, goblet cell loss, mucosal architecture, muscle thickening, edema, and crypt abscess; (F) heatmap of relative gene expression changes in the colon of DSS challenged mice during 2'FL supplementation; and (G) serum levels of LPS binding protein (LBP). In (A) treatments consisted of 5 groups of mice: untreated = oral gavage of PBS (day 1-4) and drinking water (day 1-12); DSS = oral gavage of PBS (day 1-4) and DSS in drinking water (day 5-9); DSS + *B.p.* MP80 = oral gavage of *B.p.* MP80 (day 1-4) and DSS in drinking water (day 5-9); DSS + 2'FL = oral gavage of PBS (day 1-4), DSS in drinking water (day 5-9), and 2'FL in drinking water (day 1-12); DSS +

B.p. MP80 + 2'FL = oral gavage of *B.p.* MP80 (day 1-4), DSS in drinking water (day 5-9), and 2'FL in drinking water (day 1-12); $n = 6$ per treatment group. In (C), (E), and (G) the different letters signify statistical difference between treatments (one-way ANOVA with FDR correction; $p < 0.05$). In (B) outliers were excluded using Grubb's test ($\alpha = 0.05$). In (F) Log_2 transformed fold changes are expressed with DSS alone challenged mice values expressed relative to untreated control mice and all other DSS-challenged mice expressed relative to DSS alone challenged mice (statistical analysis contained in supplemental figure 7 and supplemental tables 18-19). Genes were grouped according to known function: serotonin (5-HT) regulatory targets, aryl hydrocarbon receptor (AhR) pathway targets, intestinal barrier markers, anti-inflammatory, pro-inflammatory, inflammatory modulating, and inflammatory metabolism.

2.7 Supplemental Information

Study Design

Sample size was determined based on a preliminary *Bifidobacterium* + 2'FL experiment that resulted in consistent persistence. Therefore, we conducted two *B.p.* MP80 persistence experiments at two distinct time points to account for cage effects and different indigenous mouse microbiotas; $n = 3$ mice per treatment per experiment. Two separate DSS experiments were conducted for replication with an $n = 3$ for each. The preliminary experiment also revealed that after a washout period of 10 days the supplemented *Bifidobacterium* was below the limit of detection which is how we chose our end point. Mice were randomly assigned into treatment groups 4-6 days prior to initiating experiments. Researchers served as animal caretakers and were aware of treatments provided to each cage, therefore, the mouse experiments were not conducted blind. Histological assessment was conducted blind.

Mouse experimental design

Persistence experiments: B.p. MP80 or *B.p.* JCM11661 were provided for 5 days by oral gavage starting from experimental day 1. 2'FL was provided in the drinking water from experimental days 1 to 10. During days 11 through 21, all treatment groups underwent a washout period with drinking water alone. Fecal samples were collected every 2-4 days throughout the experiment. For health phenotyping experiments, *B.p.* MP80 was the only *Bifidobacterium* administered.

DSS phenotype experiments: B.p. MP80 was provided for 4 days by oral gavage starting from experimental day 1. 2'FL was provided in the drinking water from experimental days 1 to 12. DSS was provided in the drinking water at 3% w/v during days 6-10. Fecal samples were collected every 2-4 days throughout the experiment. Food and water intakes and mouse body weights were measured daily. Mice were sacrificed on day 12.

Preparation of bacterial inoculum and 2'-fucosyllactose for mice

B.p. MP80 was previously isolated in the Mills lab from an infant fecal sample. *Bifidobacterium* strains were grown under anaerobic conditions at 37°C and propagated in de Man, Rogosa, and Sharpe media (BD Difco Microbiology, Houston, TX) supplemented with 0.05% w/v L-cysteine (Sigma-Aldrich,

St. Louis, MO). For mouse bacterial inoculation stocks, strains were separately grown, harvested at late exponential phase, washed with reduced PBS under anaerobic conditions, pelleted by centrifugation (8000 x g for 10 min), and then re-suspended in pre-reduced PBS with a final concentration of 10% v/v glycerol (pH 7). Quantitative culture revealed approximately 10^9 CFU/ml after freeze thaw. 2'-fucosyllactose (Advanced Protein Technologies, South Korea) was diluted into sterile drinking water at a concentration of 0.10 grams per milliliter and filter sterilized.

Quantification of bacterial strains by qPCR

B.p. JCM11661 was quantified by designing strain-specific primers to target genes identified to be unique by comparing the genome against a selection of closely related strains and bacteria common to mouse gastrointestinal tracts using JGI/IMG tools (**Supplemental table 2.1**).[1] Primers' strain specificity was tested in silico by conducting a BLAST search against the NCBI database. Primers were tested using qPCR against fecal DNA from acclimation periods, and confirmed to produce no to very low background amplification. *B.p.* MP80 and *Bifidobacterium* were quantified by previously evaluated primers (**Supplemental table 2.1**).[2,3] Cell numbers of strains were quantified by absolute quantification using a standard curve prepared with DNA isolated from bacterial cultures with a CFU/ml determined by quantitative culture. Standard curves were prepared by using pure cultures of each microorganism harvested at late exponential phase, determined by growth curves generated for each strain under anaerobic conditions. qPCR was performed using a 7500 Fast Real-Time PCR System (Applied Biosystems, Waltham, MA, USA), with PCR reaction volumes of 20 µl using PowerUp SYBR Green qPCR master mix (Applied Biosystems, Waltham, MA, USA), 0.8 µM primer concentrations, and 1 µl DNA template.

^{1}H-NMR metabolite sample preparation and analysis

Colon contents were weighed, resuspended in ice cold PBS, vortexed for 2 minutes, incubated on ice for 5 min and vortexed again before centrifugation (6000 x RCF, 15 minutes, 4C). Supernatant was removed, the pellets were dried in miVac sample concentrator, and weighed to determine dry fecal weight. After an additional centrifugation step (14000xRCF, 10 minutes, 40C), the supernatants were transferred to 3 kDa filters and centrifuged again (14000xRCF, 60 minutes, 40C). 207 µL of the filtrates were

transferred to a new tube, and 23 μL of an internal standard consisting of 5 mM DSS-d6 containing 0.2% NaN3 (to inhibit bacterial growth) in 99.8% D2O (for locking) was added. pH was adjusted to 6.7-6.9 with NaOH or HCl as described in He et al[4]. Sera were thawed on ice and transferred to 3 kDa filters. After 60 minutes of centrifugation (4 C, 14000x RCF) 207 μL of filtrate was combined with 23 μL of 5 mM DSS-d6. pH was adjusted to to 6.7-6.9 with NaOH or HCl before transfer to 3mm NMR tubes.

^{1}H NMR spectra were acquired at 298K using the NOESY 1H presaturation experiment ('noesypr1d') on a Bruker Avance 600 MHz NMR spectrometer (Bruker BioSpin, Germany). Data acquisition was achieved with the following parameters; 8 dummy scans and 32 transients over a spectral width of 12 ppm and a total acquisition time of 2.5 s. Water saturation was applied during relaxation delay (2.5 s) and mixing time (100 ms). The resulting spectra were Fourier transformed with zero filling to 128 k data points and the Free Induction Decays (FIDs) were transformed with an exponential apodization function corresponding to a line broadening of 0.5 Hz. Chenomx NMR Suite v8.4 (Chenomx Inc, Edmonton, Alberta, Canada) was used to manually phase and correct baseline spectra. Each metabolite was assigned manually and quantified using Chenomx Profiler.

All statistical analyses for metabolites were completed in R (v4.0.2). Normality was assessed by generating Q-Q plots and observing deviations in the residuals in addition to Shapiro-Wilk testing. Metabolites in groups with non-normal distributions were log transformed ($\log(y + \sqrt{y^2 + 1})$) to approximate normality. Heteroskedastic data was evaluated with Welch's t-test, followed by Games Howell post hoc testing, whereas normally distributed data with homogeneous variances was tested with ANOVA followed by Tukey's HSD. Effect sizes were calculated using Hedge's g formula to account for small sample sizes with medium and large effects considered as $|g| > 0.5$ and > 0.8 respectively. All p-values were corrected for multiple testing by FDR correction with significance assessed as $p < 0.05$ and statistical trends considered as $p < 0.1$ (**Supplemental table 2.2**).

Microbial ecosystem statistics

Statistical analysis was performed in R (version 3.6.3).[5] α-diversity was measured with Shannon Index values for each mouse fecal sample (vegan::diversity). Shannon values were log transformed and each mouse subject's α-diversity geometric mean was calculated from day 8 and day 10 log values. These days were selected as they are post-*Bifidobacterium* gavage and yet during 2'FL supplementation. We used a linear regression to test the effect of *B.p.* MP80 and 2'FL on α-diversity with *B.p.* JCM11661 as the control comparison. Included in the GLM analysis (lme4::glm) were robust sandwich variance estimates (clubSandwich::vcovCR) and a degrees of freedom Satterthwaite correction (clubSandwich::coef_test).[6,7] β-diversity was measured by Bray-Curtis distances (vegan::metaMDS, dist = "bray") which were visualized using non-metric multidimensional scaling (NMDS) (vegan::metaMDS, k=2) with ellipses (vegan::veganCovEllipse).[8] Differences in β-diversity were detected by checking dispersion (vegan::betadisper), a permutational multivariate ANOVA (vegan::adonis2, 999 permutations), and post hoc testing (RVAideMemoire::pairwise.perm.manova, nperm = "500").[9] The strata argument was used to constrain by mouse when longitudinal data was examined. Log ratio ASV differences between all treatment groups was tested with an ANOVA with Tukey's Test (stats::aov and stats::TukeyHSD).[5] Log ratio ASV differences between 2'FL and untreated mice was tested with a student's t test (stats::t.test).

References

1. Maldonado-Gómez MX, Martínez I, Bottacini F, O'Callaghan A, Ventura M, van Sinderen D, Hillmann B, Vangay P, Knights D, Hutkins RW, et al. Stable Engraftment of Bifidobacterium longum AH1206 in the Human Gut Depends on Individualized Features of the Resident Microbiome. Cell Host Microbe 2016; 20:515–26.
2. Rinttilä T, Kassinen A, Malinen E, Krogius L, Palva A. Development of an extensive set of 16S rDNA-targeted primers for quantification of pathogenic and indigenous bacteria in faecal samples by real-time PCR. J Appl Microbiol 2004; 97:1166–77.
3. Matsuki T, Watanabe K, Fujimoto J, Kado Y, Takada T, Matsumoto K, Tanaka R. Quantitative PCR with 16S rRNA-gene-targeted species-specific primers for analysis of human intestinal bifidobacteria. Appl Environ Microbiol 2004; 70:167–73.
4. He X, Parenti M, Grip T, Domellöf M, Lönnerdal B, Hernell O, Timby N, Slupsky CM. Metabolic phenotype of breast-fed infants, and infants fed standard formula or bovine MFGM supplemented formula: a randomized controlled trial. Sci Rep 2019; 9:339.
5. R Core Team. R: A Language and Environment for Statistical Computing. R Foundation for Statistical Computing; 2020.
6. Bates D, Mächler M, Bolker B, Walker S. Fitting linear mixed-effects models using lme4. J Stat Softw 2015; 67:1–48.
7. Pustejovsky J. clubSandwich: Cluster-Robust (Sandwich) Variance Estimators with Small-Sample

Corrections. R; 2020.
8. Oksanen J, Blanchet FG, Friendly M, Kindt R, Legendre P, McGlinn D, Minchin PR, O'Hara RB, Simpson GL, Solymos P, et al. vegan: Community Ecology Package [Internet]. R; 2019 [cited 2020 Jul 20]. Available from: https://CRAN.R-project.org/package=vegan
9. Hervé M. RVAideMemoire: Testing and Plotting Procedures for Biostatistics. R; 2020.

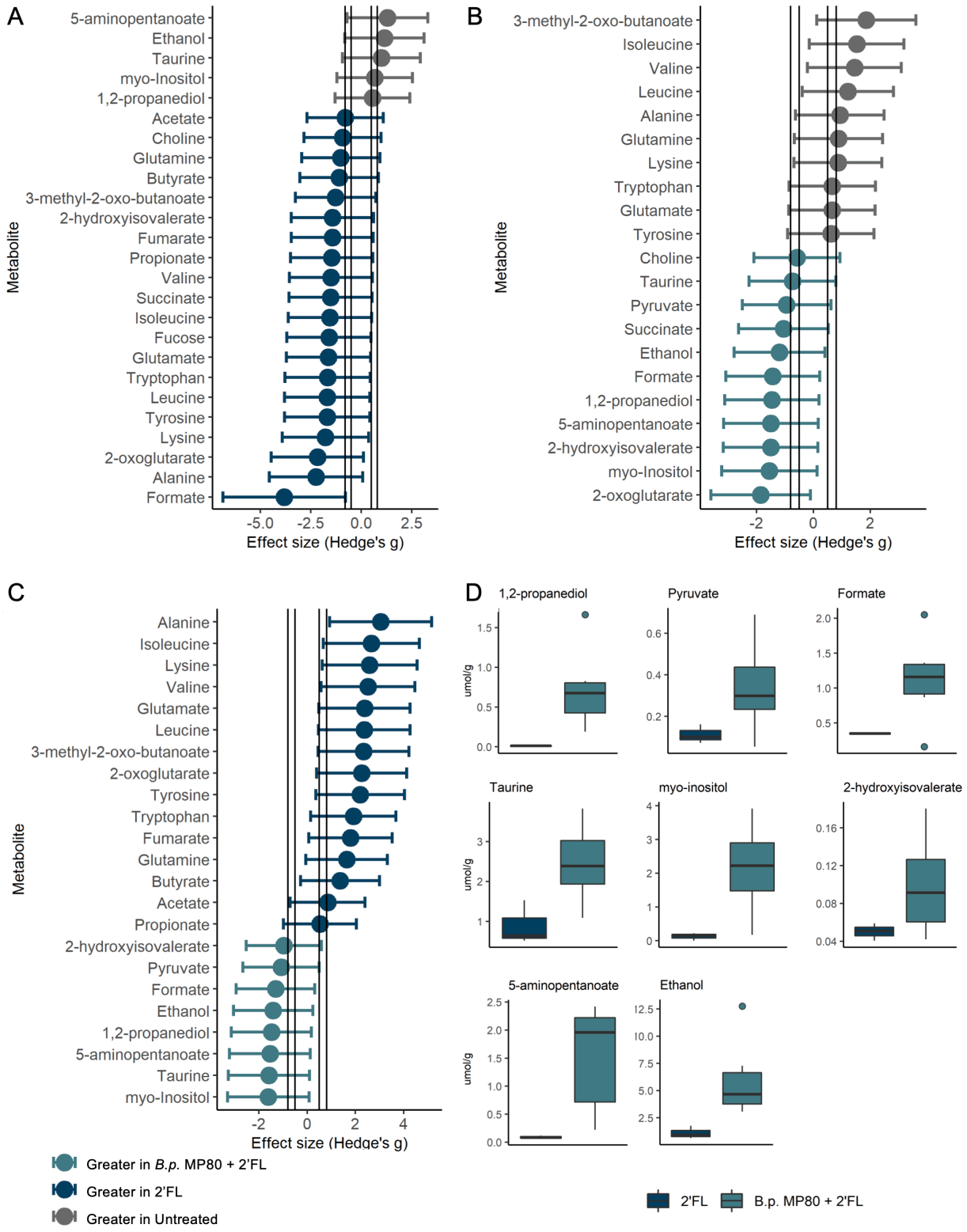

Supplemental figure 2.1. Colon content metabolites profiled by ^{1}H NMR reveals differences between untreated, 2'FL, and *B.p.* MP80 + 2'FL. Effect sizes between (A) 2'FL and untreated, (B) *B.p.* MP80 +

2'FL and untreated, and (C) *B.p.* MP80 + 2'FL and 2'FL; (D) individual metabolite concentrations for metabolites greater in *B.p.* MP80 + 2'FL treatment versus 2'FL treatment. Medium and large effect sizes (|0.5| and |0.8| respectively) are displayed as vertical lines on each plot *(n* = 6 per group). The 95% confidence interval was estimated using the normal distribution. The boxplots represent medians and interquartile range (IQR) with whisker end points equal to the maximum and minimum values below or above the median at 1.5 times the IQR.

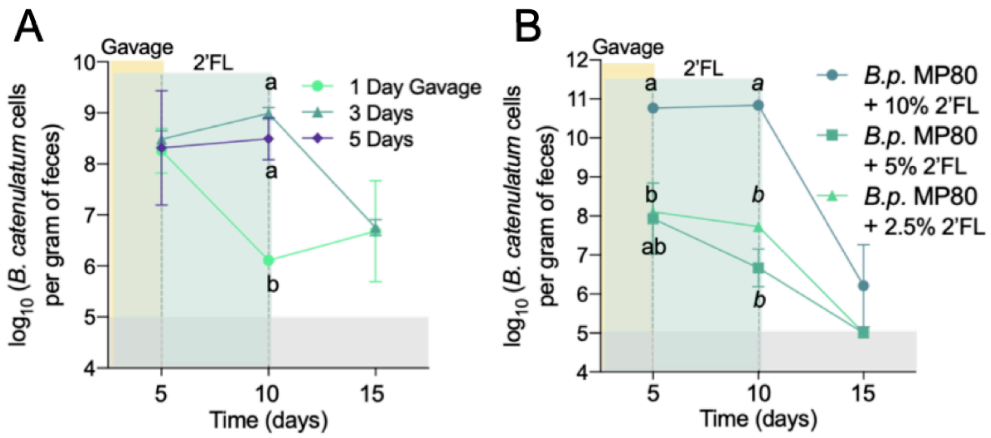

Supplemental figure 2.2. Supplemental mouse experiments to characterize *B.p.* MP80 persistence during 2'FL administration. (A) *B.p.* MP80 quantification by qPCR in an experiment varying the number of *B.p.* MP80 gavage days (n = 2 per treatment group); and (B) *B.p.* MP80 quantification by qPCR from a mouse experiment with varying concentrations of 2'FL provided to mice for 5 days post *B.p.* MP80 gavage (n = 3 per treatment group). In (A) and (B), 5: final day of *B.p.* MP80 gavage; 10: final day of 2'FL supplementation; 15: washout of 2'FL, day before necropsy. The experimental groups labeled with different letters are significantly different at each time point (one-way ANOVA with Tukey's multiple comparisons; $p < 0.05$).

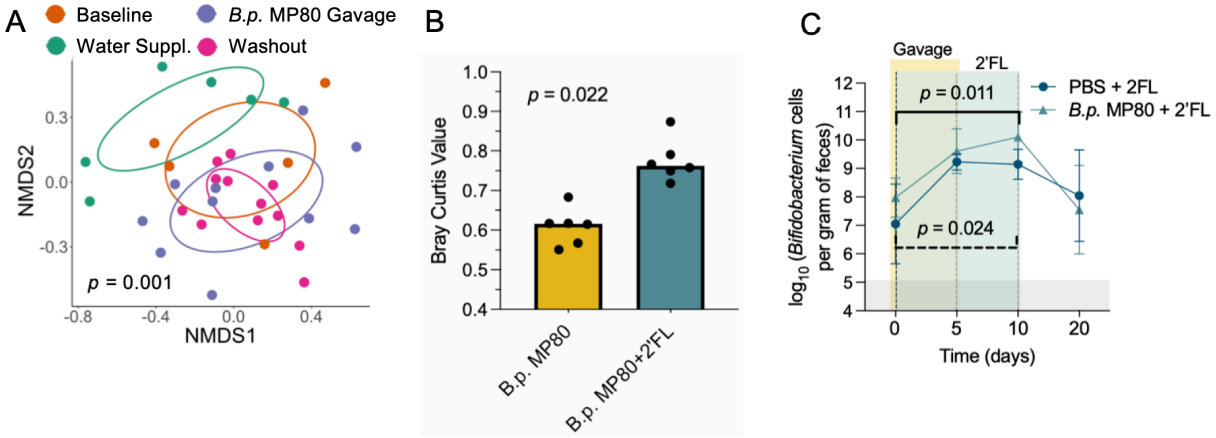

Supplemental figure 2.3. *B.p.* MP80 microbial community effects and supplemental *Bifidobacterium* qPCR. (A) NMDS plot of the β-diversity index Bray-Curtis for *B.p.* MP80 treatment, colored by time (n = 6); (B) Bray Curtis matrix values from baseline (day 0) vs. final *B.p.* MP80 gavage (day 6) with a Mann Whitney test (n = 6 per treatment); and (C) *Bifidobacterium* quantification by qPCR in fecal DNA for 2'FL (dashed line) and *B.p.* MP80 + 2'FL (solid line) treatments with a Kruskal Wallis test (n = 6).

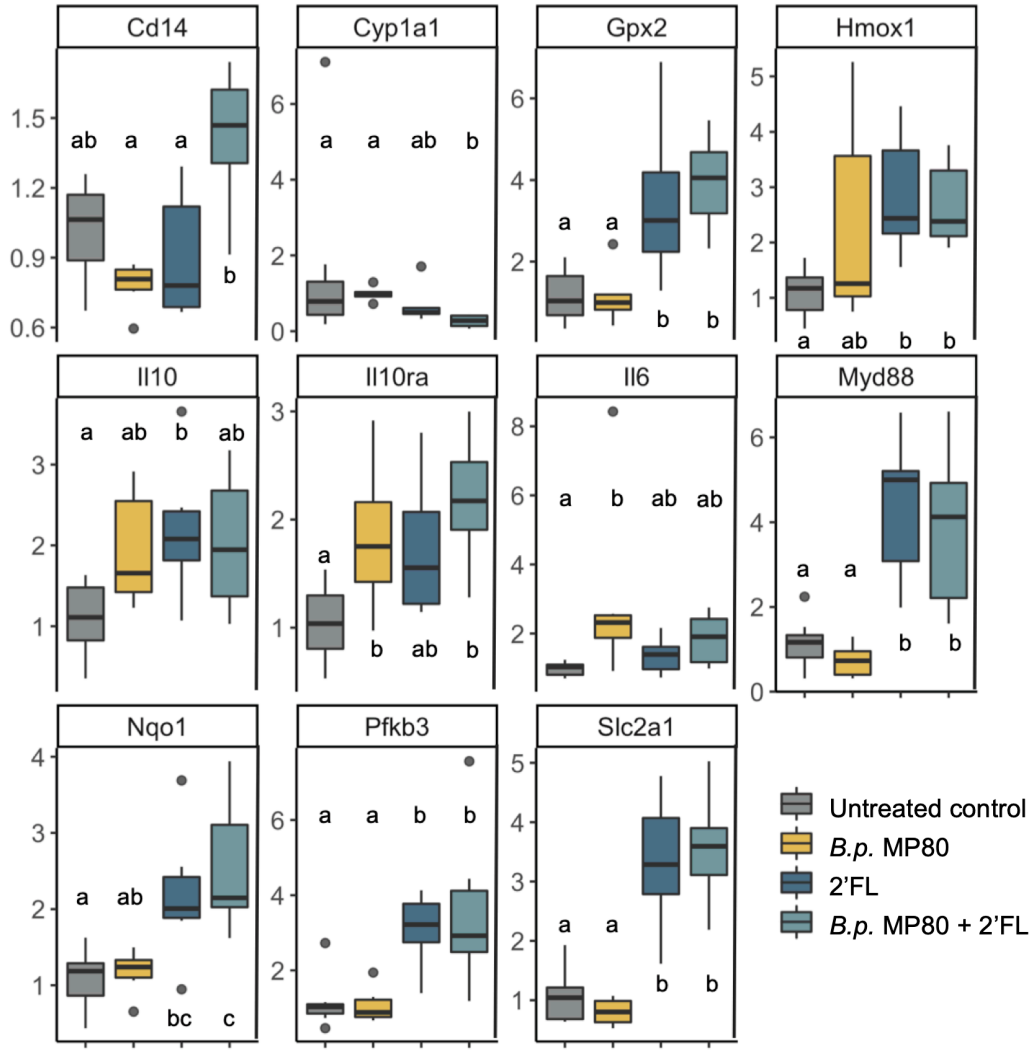

Supplemental figure 2.4. Cecum gene expression for *B.p.* MP80 persistence experiments. Untreated mice (n = 6-9), *B.p.* MP80 mice (n = 6), 2'FL mice (n = 6), and *B.p.* MP80 + 2'FL mice (n = 6). Select genes significant by Kruskal-Wallis test with FDR correction. Different letters signify statistical difference between treatments (post hoc Wilcoxon Rank Sum with FDR correction; $p < 0.05$).

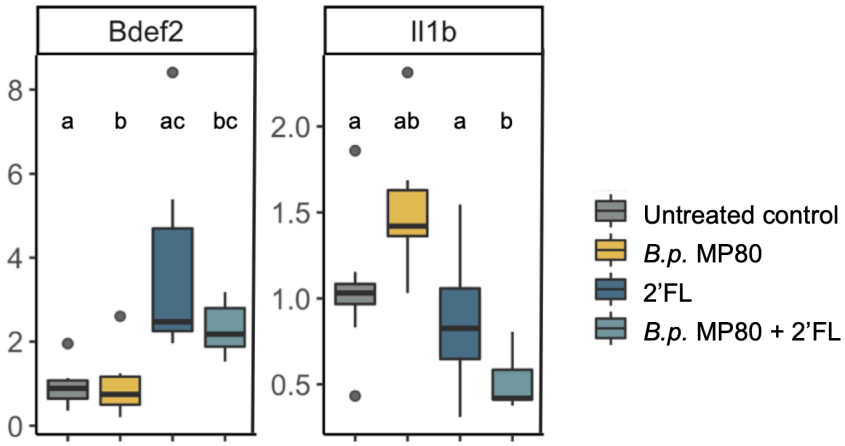

Supplemental figure 2.5. Colon gene expression for *B.p.* MP80 persistence experiments. Untreated mice (n = 6-9), *B.p.* MP80 mice (n = 6), 2'FL mice (n = 6), and *B.p.* MP80 + 2'FL mice (n = 6). Select genes significant by Kruskal-Wallis test with FDR correction. Different letters signify statistical difference between treatments (post hoc Wilcoxon Rank Sum with FDR correction; $p < 0.05$).

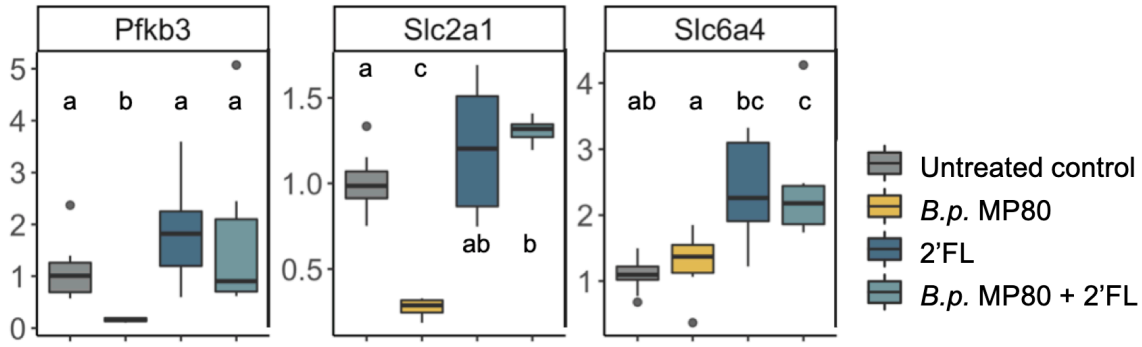

Supplemental figure 2.6. Jejunum gene expression for *B.p.* MP80 persistence experiments. Untreated mice (n = 6-9), *B.p.* MP80 mice (n = 6), 2'FL mice (n = 6), and *B.p.* MP80 + 2'FL mice (n = 6). Select genes significant by Kruskal-Wallis test with FDR correction. Different letters signify statistical difference between treatments (post hoc Wilcoxon Rank Sum with FDR correction; $p < 0.05$).

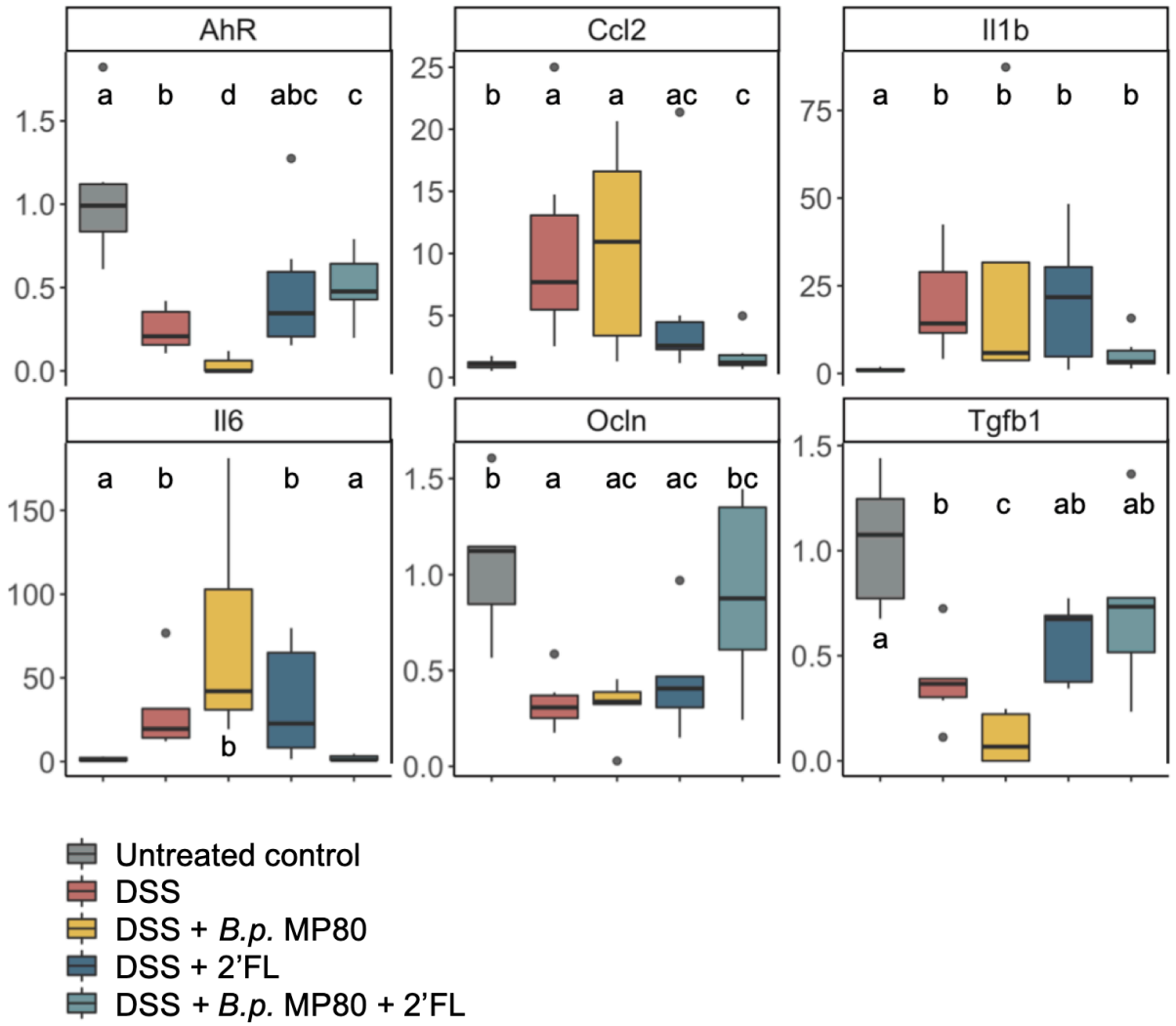

Supplemental figure 2.7. Colon gene expression for DSS-induced colitis experiments. Untreated mice (*n* = 6), DSS mice (*n* = 6), DSS + *B.p.* MP80 mice (*n* = 6), DSS + 2'FL mice (*n* = 6), and DSS + *B.p.* MP80 + 2'FL mice (*n* = 6). Select genes significant by Kruskal-Wallis test with FDR correction. Different letters signify statistical difference between treatments (post hoc Wilcoxon Rank Sum with FDR correction; $p < 0.05$).

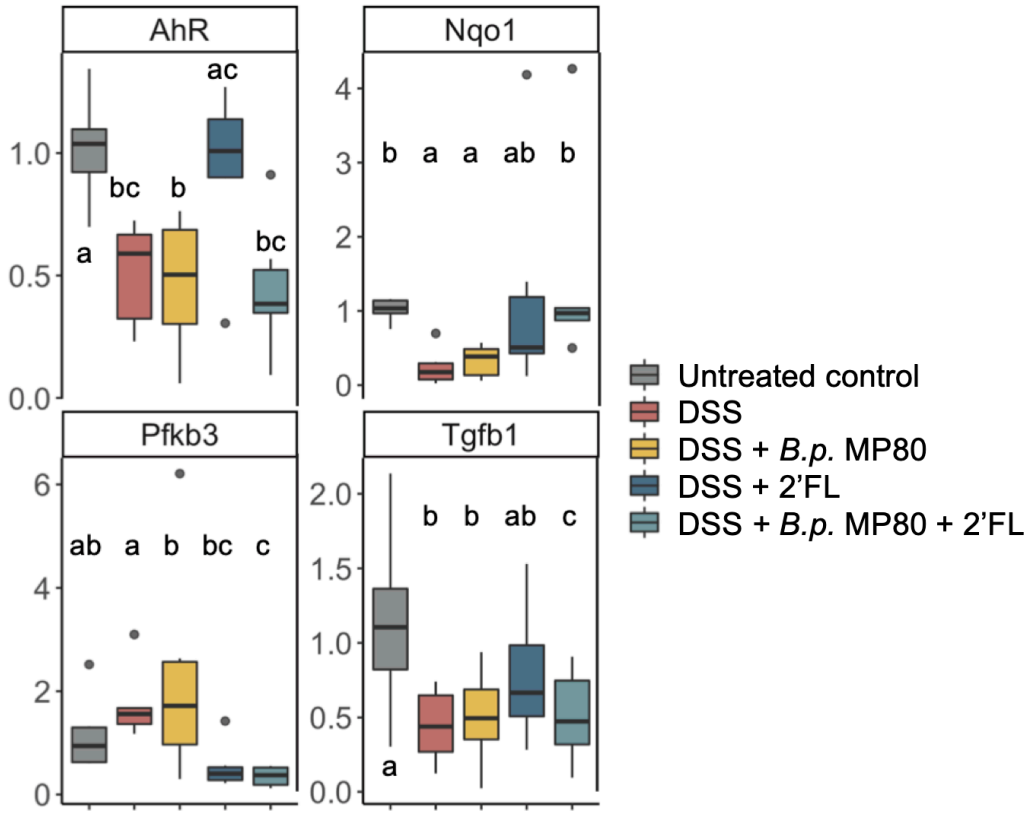

Supplemental figure 2.8. Jejunum gene expression from DSS-induced colitis experiments. Untreated mice ($n = 6$), DSS mice ($n = 6$), DSS + *B.p.* MP80 mice ($n = 6$), DSS + 2'FL mice ($n = 6$), and DSS + *B.p.* MP80 + 2'FL mice ($n = 6$). Select genes significant by Kruskal-Wallis test with FDR correction. Different letters signify statistical difference between treatments (post hoc Wilcoxon Rank Sum with FDR correction; $p < 0.05$).

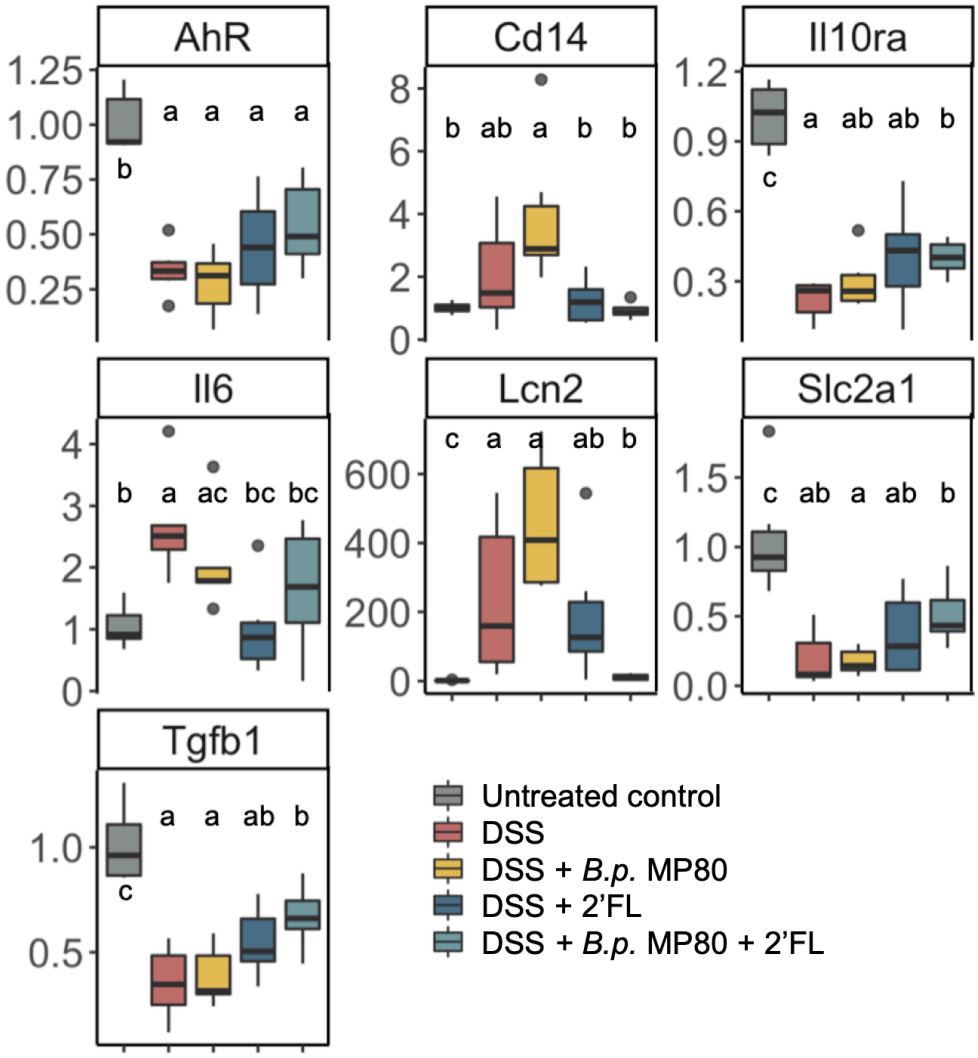

Supplemental figure 2.9. Liver gene expression from DSS-induced colitis experiments. Untreated mice (*n* = 6), DSS mice (*n* = 6), DSS + *B.p.* MP80 mice (*n* = 6), DSS + 2'FL mice (*n* = 6), and DSS + *B.p.* MP80 + 2'FL mice (*n* = 6). Select genes significant by Kruskal-Wallis test with FDR correction. Different letters signify statistical difference between treatments (post hoc Wilcoxon Rank Sum with FDR correction; $p < 0.05$).

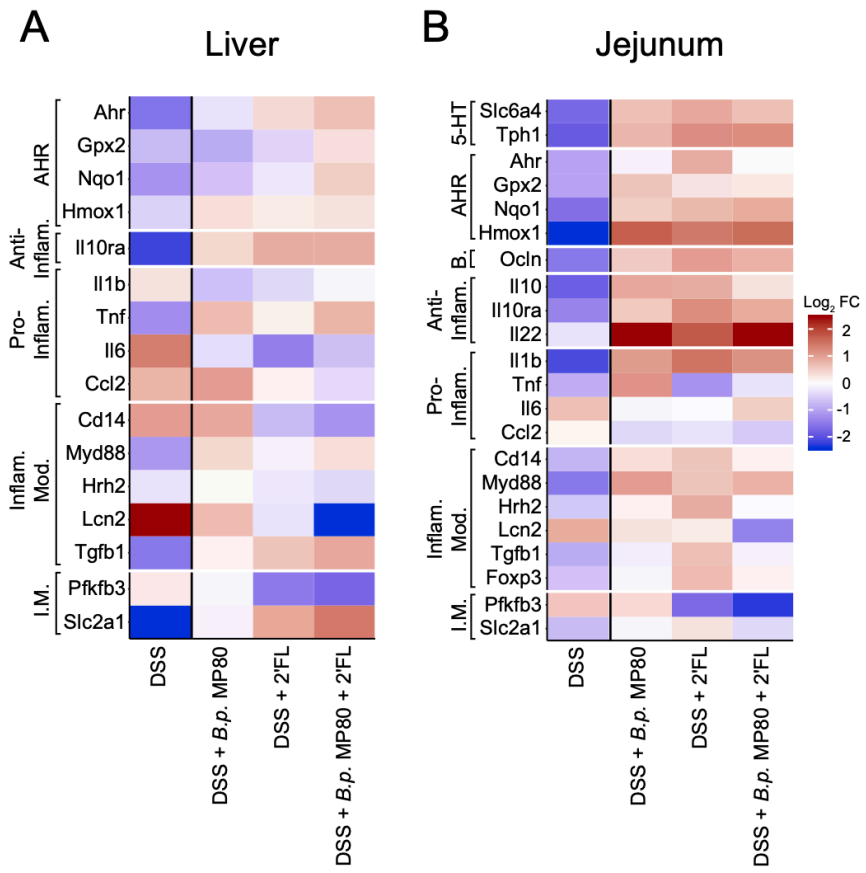

Supplemental figure 2.10. Heat maps of gene expression changes in DSS challenged mice in (A) liver; and (B) jejunum (n = 6 per treatment). Log_2 transformed fold changes are expressed with DSS alone challenged mice values expressed relative to untreated control mice and all other DSS-challenged mice expressed relative to DSS alone challenged mice (statistical analysis contained in supplemental figures 8-9 and supplemental tables 20-23). Genes were grouped according to known function: serotonin (5-HT) regulatory targets, aryl hydrocarbon receptor (AhR) pathway targets, intestinal barrier markers, anti-inflammatory, pro-inflammatory, inflammatory modulating, and inflammatory metabolism.

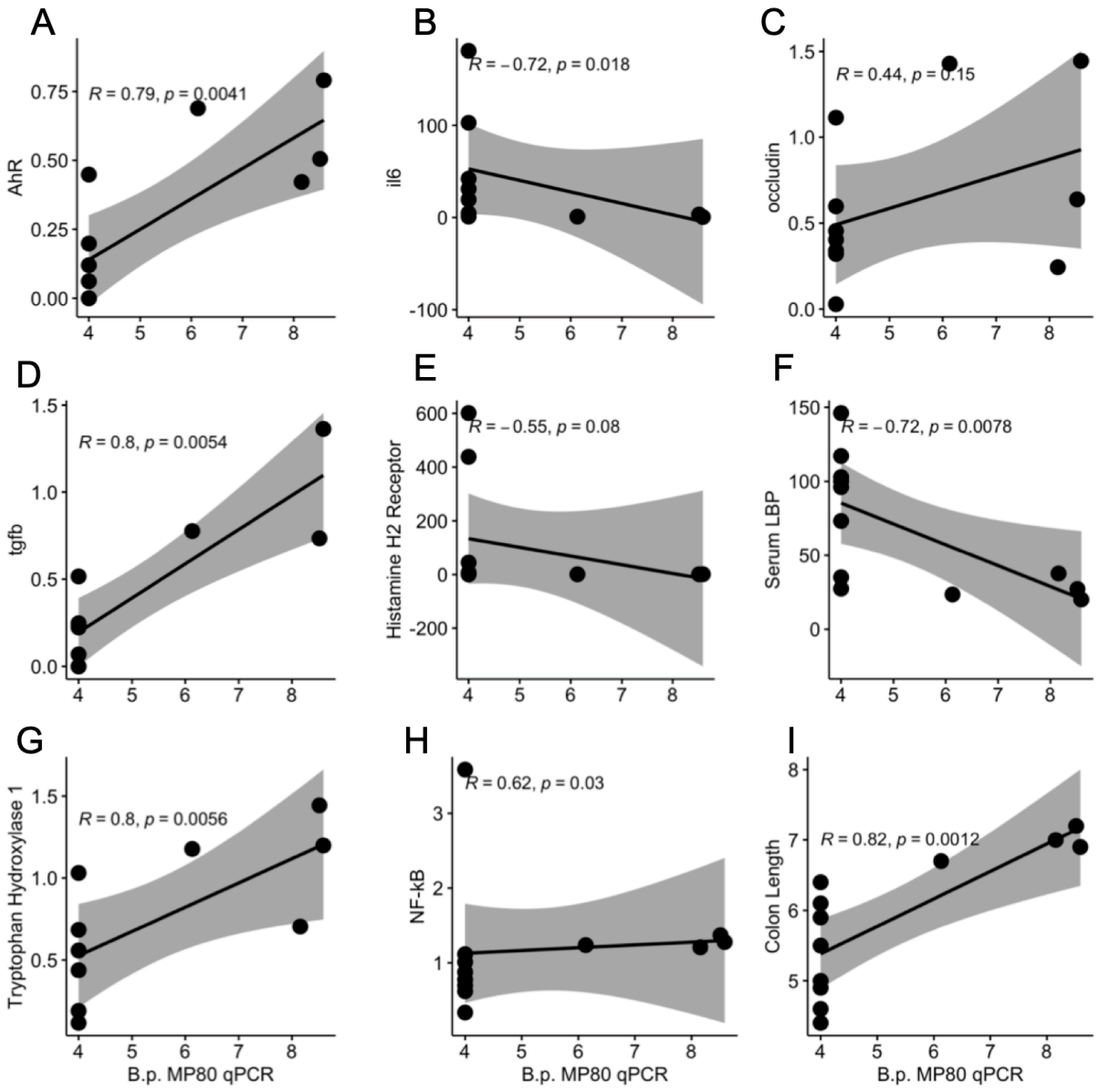

Supplemental figure 2.11. Select Spearman's correlations between colon gene expression and fecal *B.p.* MP80 abundance for treatment groups DSS + *B.p.* MP80 and DSS + *B.p.* MP80 + 2'FL at day of necropsy. Correlations and associated *p* value for inflammatory markers (A) AhR, (B) Il6, (C) Ocln, (D) Tgfb1, (E) Hrh2, (F) serum LPS binding protein, (G) Tph1, (H) NFkB, (I) colon length (n = 6 per treatment).

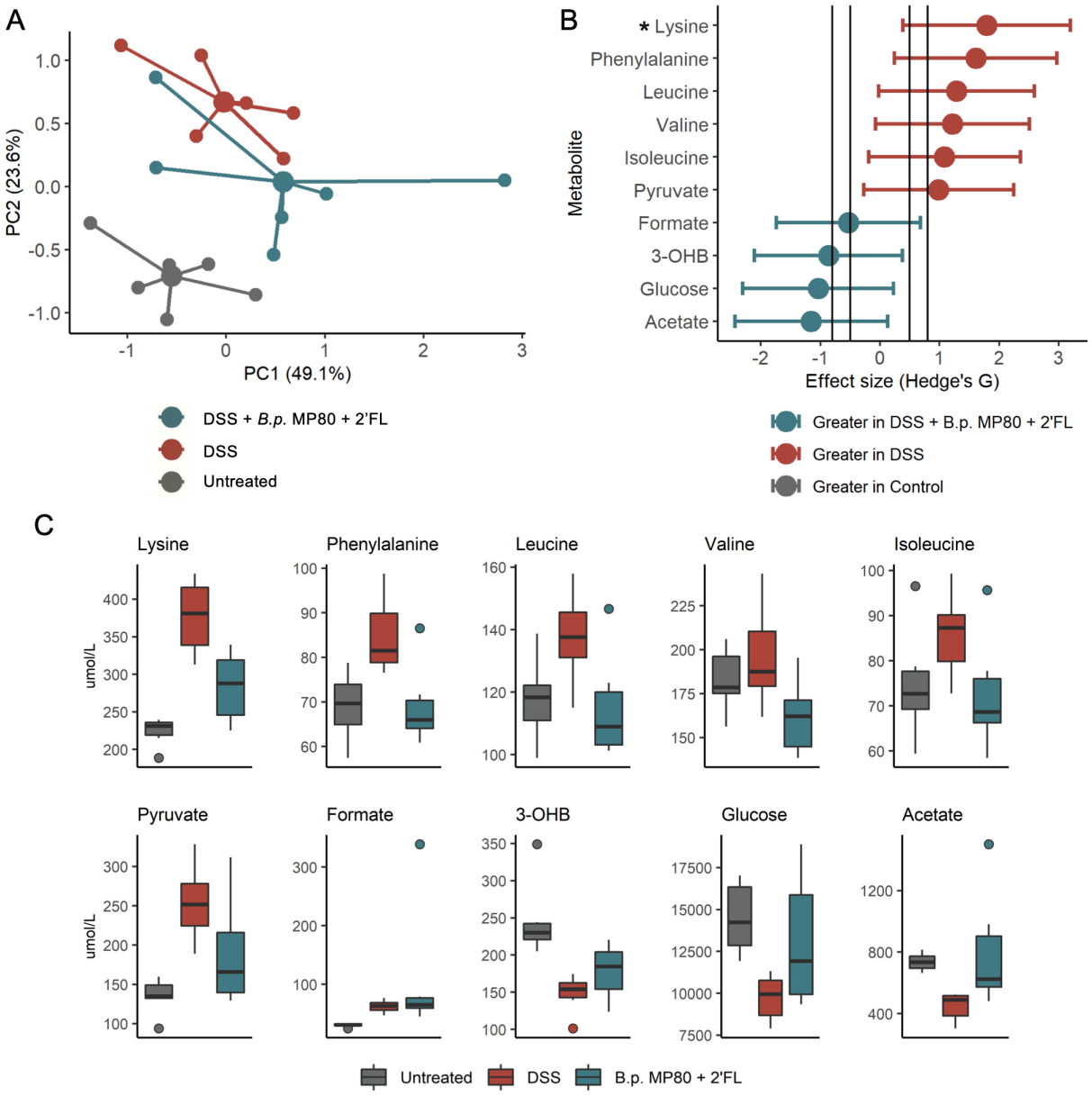

Supplemental figure 2.12. Serum metabolites assessed by ^{1}H NMR reveals differences between untreated (gray), DSS (red), and DSS + *B.p.* MP80 + 2'FL (blue) (n = 6 per treatment). (A) Principal component analysis (PCA) of generalized log transformed data; (B) serum metabolite effect sizes between DSS + *B.p.* MP80 + 2'FL and DSS; and (C) individual metabolite concentrations by treatment group. Medium and large effect sizes (|0.5| and |0.8| respectively) are displayed as vertical lines on each plot. The 95% confidence interval was estimated using the normal distribution. The boxplots represent medians and

interquartile range (IQR) with whisker end points equal to the maximum and minimum values below or above the median at 1.5 times the IQR. * signifies $p < 0.05$ after FDR correction.

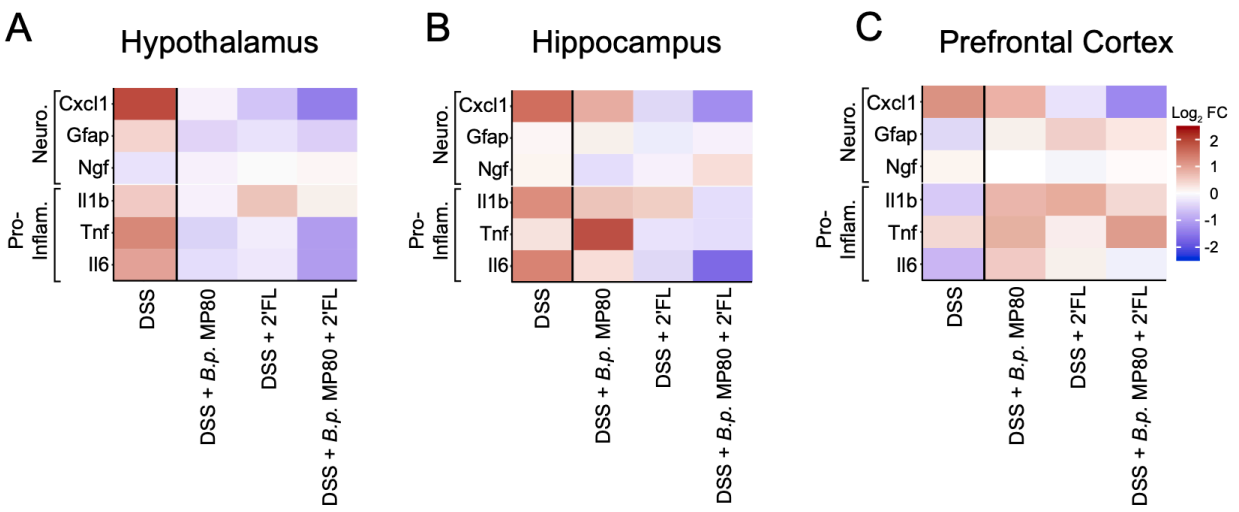

Supplemental figure 2.13. Heat maps of regional brain gene expression changes in DSS challenged mice in (A) hypothalamus, (B) hippocampus, and (C) prefrontal cortex. Log_2 transformed fold changes are expressed with DSS alone challenged mice values expressed relative to untreated control mice and all other DSS-challenged mice expressed relative to DSS alone challenged mice (n = 6 per treatment). Genes were grouped according to known function: neurological and pro-inflammatory.

Primer Target Forward and Reverse Sequences (5' – 3')	Product Size (bp)	Annealing Temp (C)	Source
Bifidobacterium			
TCGCGTC(C/T)GGTGTGAAAG	243	58	Rinttila et al.
CCACATCCAGC(A/G)TCCAC			*(53)*
B. catenulatum			
CGGATGCTCCGACTCCT	285	58	Matsuki et al.
CGAAGGCTTGCTCCCGAT			*(54)*
B .pseudocatenulatum JCM11661			
AAAACGGCGTGACCTACAAC	158	60	This Study
GGAGGTCTGGTTGGTCTTGA			
B. pseudocatenulatum MP80			
Fucosidases	212	60	This Study
AGTGGAATACACGTTGCGCT			
CCGCATGCTGGTAGCAAAAA			

Supplemental table 2.1: List of primers used for bacterial absolute quantification (qPCR) all of which used SYBR Green ® as the detection chemistry.

	p value			FDR-adjusted *q* value		
	Untreated – 2'FL	Untreated – *B.p.* MP80 + 2FL	2'FL – *B.p.* MP80 + 2'FL	Untreated – 2'FL	Untreated – *B.p.* MP80 + 2FL	2'FL – *B.p.* MP80 + 2'FL
2-hydroxyisovalerate	0.232	**0.038**	0.154	0.352	0.154	0.328
2-oxoglutarate	0.140	**0.017**	0.215	0.328	0.145	0.352
3-methyl-2-oxo-butanoate	0.315	0.146	0.224	0.426	0.328	0.352
5-aminopentanoate	0.229	**0.030**	**0.026**	0.352	0.151	0.150
Acetate	0.519	0.664	0.154	0.622	0.757	0.328
Alanine	0.079	0.120	**0.006**	0.246	0.314	0.145
Butyrate	0.197	0.353	0.058	0.352	0.454	0.198
Choline	0.474	0.351	0.522	0.581	0.454	0.622
Ethanol	0.307	**0.011**	**0.009**	0.421	0.145	0.145
Formate	**0.023**	**0.035**	0.052	0.145	0.151	0.198
Fucose	0.144	0.767	1.000	0.328	0.839	1.000
Fumarate	0.265	0.964	0.271	0.376	0.988	0.378
Glutamate	0.174	0.250	0.059	0.352	0.362	0.198
Glutamine	0.396	0.198	0.096	0.494	0.352	0.277
Isoleucine	0.217	**0.029**	**0.010**	0.352	0.151	0.145
Lactate	0.692	0.846	0.937	0.770	0.902	0.973
Leucine	0.192	0.054	**0.010**	0.352	0.198	0.145
Lysine	0.130	0.190	**0.021**	0.328	0.352	0.145
Myo-inositol	0.207	0.904	0.237	0.352	0.951	0.352
Propionate	0.694	**0.022**	**0.021**	0.770	0.145	0.145
1,2-propanediol	0.847	0.171	0.106	0.902	0.352	0.297
Pyruvate	0.190	0.120	0.997	0.352	0.314	1.000
Succinate	0.377	0.554	0.086	0.477	0.650	0.258
Taurine	0.213	0.334	0.078	0.352	0.444	0.246
Tryptophan	0.149	0.237	**0.035**	0.328	0.352	0.151
Tyrosine	0.239	**0.035**	**0.011**	0.352	0.151	0.145
Valine	0.607	**0.018**	**0.013**	0.703	0.145	0.145

Supplemental table 2.2: Colon content metabolite comparisons with Games Howell post hoc test before and after FDR adjustment for *B.p.* MP80 + 2'FL persistence experiments. Metabolites with a $p < 0.05$ are shown in bold. q values are FDR corrected by the number of metabolites tested (48).

	Beta Coefficients	t-statistic	Lower 95% CI	Upper 95% CI	*p*-value
B. p. MP80:2'FL	-0.42	-3.17	-0.73	-0.12	**0.013**
B.p. MP80	0.14	6.02	0.08	0.21	**0.004**
B.p. JCM11661:2'FL	-0.08	-1.66	-0.22	0.05	0.172

Supplemental table 2.3: Linear regression model of Shannon Index (α-diversity) values evaluating the interaction (denoted by :) between 2'FL supplementation and *B.p.* MP80 ($n = 6$) versus *B.p.* JCM11661 ($n = 3$). Robust sandwich variance estimates and degrees of Satterthwaite correction incorporated. Values in bold are $p < 0.05$.

	B.p. MP80 + 2'FL	*B.p.* MP80	2'FL
B.p. MP80	**0.008**		
2'FL	0.358	**0.008**	
Untreated	**0.008**	0.488	**0.008**

Supplemental table 2.4: Pairwise comparisons of PERMANOVA for Bray Curtis values (β-diversity) evaluating differences between microbial communities of all treatments (n = 6 mice per treatment) on day 10, the final day of 2'FL supplementation (nperm = 200). Values in bold are $p < 0.05$.

	Differential	Lower 95% CI	Upper 95% CI	*p value*
B. p. MP80 + 2FL – Untreated	4.35	2.39	6.29	**< 0.001**
B.p. MP80 + 2'FL – *B.p.* MP80	4.31	2.36	6.26	**< 0.001**
B.p. MP80 + 2'FL – 2'FL	2.34	0.33	4.34	**0.017**
Untreated – *B. p.* MP80	0.04	-2.04	1.96	> 0.999
Untreated – 2'FL	2.01	-4.06	0.04	0.056
B.p. MP80 – 2'FL	-1.97	-4.03	0.08	0.063

Supplemental table 2.5: Tukey's multiple comparison testing of the log ratio of *Bifidobacteriaceae* ASVs relative to low ranked *Lachnospiraceae* and *Ruminococcaceae* ASVs by treatment. Values in bold are $p < 0.05$.

ASV Feature ID	Bacterial Family	Log Ratio Classification
46ef1a1d163d392f75bd877a6b6eb7cc	*Bifidobacteriaceae*	Numerator
931fff02d94342afd4b68703cebc9d13	*Bifidobacteriaceae*	Numerator
ce6eabf2d84da6efcea6fbc168c92d03	*Bifidobacteriaceae*	Numerator
f4f5cf8d8d238c12682888d27859fa3f	*Bifidobacteriaceae*	Numerator
12fab84068d560d5ddaf5e4c1d1182fd	*Ruminococcaceae*	Denominator
ac6858e21fdfd6b1a2863e73180d8caf	*Lachnospiraceae*	Denominator
1e22f1407ca878c2d0448f300ab7d817	*Ruminococcaceae*	Denominator
32fa1e9dfd85f3c7fe5765158d07a1fd	*Lachnospiraceae*	Denominator
74804ec12dd657a69648c9da08abd597	*Ruminococcaceae*	Denominator
4e6dacec034d4b1431ef7f9e57d9490a	*Ruminococcaceae*	Denominator
61dda49be7ef2e6ba371ae50a17afc10	*Ruminococcaceae*	Denominator
30584d9aed923c0c1d895d6201f19924	*Lachnospiraceae*	Denominator
f6fee0996809fffc3b3b8d32845466e7	*Lachnospiraceae*	Denominator
5bcabac8d78720c0db64155569782725	*Lachnospiraceae*	Denominator
f3cb623fafc2eae95b22949eebc0ac80	*Lachnospiraceae*	Denominator
e72e247bda1d9d5a1e30dc21fa920ec4	*Ruminococcaceae*	Denominator
74778997f2b404d99413cdbb92be937e	*Ruminococcaceae*	Denominator
df2d1dcce96a59a12330e5f955a2847f	*Lachnospiraceae*	Denominator
2097c2310c94b63b7aa3f1d282720fe1	*Ruminococcaceae*	Denominator
1c728cf6c1d5828eeaf57e83c39f0600	*Ruminococcaceae*	Denominator
7f9ac6505ff478702b26a9e0ca12f2e4	*Lachnospiraceae*	Denominator
9e4b28d37cdaf716c79a07f62d856852	*Ruminococcaceae*	Denominator
9873f6eaf55845b58e027d51407ee056	*Lachnospiraceae*	Denominator
39a2666452fe7cb00aa9d17a2ba9b7d8	*Lachnospiraceae*	Denominator
584f07ed2c373c887dc223e744047d5c	*Ruminococcaceae*	Denominator
ae439e26c93eacd8002fd7bc06eafe22	*Lachnospiraceae*	Denominator
501737a85ba32f8232caf28f6ff3b84e	*Ruminococcaceae*	Denominator
e29666e119130822c19d1415430c039b	*Lachnospiraceae*	Denominator
4d0d4fcf2265051d832c34fea4396739	*Lachnospiraceae*	Denominator
6d15b963bd8adbf52bb4d46bd85e6f59	*Lachnospiraceae*	Denominator
c2a737924e989ece22452a86bbeaf775	*Lachnospiraceae*	Denominator
6c9202c2a41df232d8a39d13017c4982	*Lachnospiraceae*	Denominator
acb734be7481d4f49f61bb4f3d46b92c	*Lachnospiraceae*	Denominator
6df4225cb7b6423e58e4a82daff43001	*Ruminococcaceae*	Denominator
438545090161435c29c5c96c5181a746	*Ruminococcaceae*	Denominator
ec0ede08845dad4df7113237e1838fe5	*Ruminococcaceae*	Denominator
5872de8f236ebe7df78bdcb54cb6837e	*Lachnospiraceae*	Denominator
cf15f944ae602f0e3111e32570d0b545	*Lachnospiraceae*	Denominator
bef4daf8c571b34fee9f7e9219d4e584	*Lachnospiraceae*	Denominator
dd6593e0cd2e878bf2220f5d8670f8ca	*Lachnospiraceae*	Denominator
556fefa5d5dc7afdeb72b5bebade25a0	*Lachnospiraceae*	Denominator

a6788561949b316d9018742a8d14b638	*Lachnospiraceae*	Denominator
0bb16df5759b121505f224e3efd23072	*Lachnospiraceae*	Denominator
28018a6f7c334b8fb92d616bac5cbdcb	*Lachnospiraceae*	Denominator
0e098e232ddc310d4b654d82d1b0c82e	*Lachnospiraceae*	Denominator
127a8e50dfc16470d189ed4173e4badb	*Lachnospiraceae*	Denominator
32495f2b8edbb6a142b3f8a6a081857a	*Lachnospiraceae*	Denominator
640f30c84bf18f225e048bed207e63c7	*Lachnospiraceae*	Denominator
6022dc18fc918874fe68e467d878af20	*Lachnospiraceae*	Denominator
db74e3bce11f81adf607afa3ade2cc70	*Ruminococcaceae*	Denominator
68b76711c0d2a0cd069e729df926548f	*Lachnospiraceae*	Denominator
ed92e36ec94dc479c844e4df424908ce	*Ruminococcaceae*	Denominator

Supplemental table 2.6: Feature IDs selected using Songbird to generate a log ratio to calculate differential abundance between *B.p.* MP80 + 2'FL treatment and treatments *B.p.* MP80, 2'FL, and untreated control. *Lachnospiraceae* and *Ruminococcaceae* ASVs were selected from the lowest 25% ranked ASVs.

ASV Feature ID	Bacterial Family	Log Ratio Classification
46ef1a1d163d392f75bd877a6b6eb7cc	*Bifidobacteriaceae*	Numerator
59044bba9492389101d12888fb981b19	*Bacteroidaceae*	Numerator
61143439625764e98d254209f9d10304	*Bacteroidaceae*	Numerator
ce6eabf2d84da6efcea6fbc168c92d03	*Bifidobacteriaceae*	Numerator
ae439e26c93eacd8002fd7bc06eafe22	*Lachnospiraceae*	Denominator
b73a98840df0e8eabd9e04684a9fd40e	*Lachnospiraceae*	Denominator
ac6858e21fdfd6b1a2863e73180d8caf	*Lachnospiraceae*	Denominator
1c728cf6c1d5828eeaf57e83c39f0600	*Ruminococcaceae*	Denominator
34d57454243e07e31b65c276f869b6a6	*Lachnospiraceae*	Denominator
12fab84068d560d5ddaf5e4c1d1182fd	*Ruminococcaceae*	Denominator
2a2b8eb747cafad379a264737faeca63	*Lachnospiraceae*	Denominator
f6fee0996809fffc3b3b8d32845466e7	*Lachnospiraceae*	Denominator
1e22f1407ca878c2d0448f300ab7d817	*Ruminococcaceae*	Denominator
1dd2c20574f2b4bf58db53648b30cd0c	*Lachnospiraceae*	Denominator
9e4b28d37cdaf716c79a07f62d856852	*Ruminococcaceae*	Denominator
356afb7a82f0050f844d2e6d907c3fa2	*Lachnospiraceae*	Denominator
6d15b963bd8adbf52bb4d46bd85e6f59	*Lachnospiraceae*	Denominator
35cb1ff0165c6176cf381d53d0652d72	*Lachnospiraceae*	Denominator
e72e247bda1d9d5a1e30dc21fa920ec4	*Ruminococcaceae*	Denominator
9873f6eaf55845b58e027d51407ee056	*Lachnospiraceae*	Denominator
28018a6f7c334b8fb92d616bac5cbdcb	*Lachnospiraceae*	Denominator
f3cb623fafc2eae95b22949eebc0ac80	*Lachnospiraceae*	Denominator
dd6593e0cd2e878bf2220f5d8670f8ca	*Lachnospiraceae*	Denominator
88cd10c71ba0e12387ef9c6e5a3c602b	*Ruminococcaceae*	Denominator
d7ec692f6ed54afb0111f6ad30945350	*Lachnospiraceae*	Denominator
d8537b5c60fa537157d25264c3734bdf	*Ruminococcaceae*	Denominator
a6788561949b316d9018742a8d14b638	*Lachnospiraceae*	Denominator
5872de8f236ebe7df78bdcb54cb6837e	*Lachnospiraceae*	Denominator
718230c252b3e24f132152ee42b6b3f0	*Lachnospiraceae*	Denominator
74804ec12dd657a69648c9da08abd597	*Ruminococcaceae*	Denominator
ed92e36ec94dc479c844e4df424908ce	*Ruminococcaceae*	Denominator
95bef9cd263b65a4710cf63b52347d9d	*Ruminococcaceae*	Denominator
be5338ba42939fb0be20c865f881ae42	*Lachnospiraceae*	Denominator
b4043718f2da6bf61bbeaabdef4c9ff9	*Lachnospiraceae*	Denominator
5bcabac8d78720c0db64155569782725	*Lachnospiraceae*	Denominator
aa935103e3f612d4a45a649b5acab4e0	*Ruminococcaceae*	Denominator
cf15f944ae602f0e3111e32570d0b545	*Lachnospiraceae*	Denominator
e760e34a170a081eeeb51eda08ba47c3	*Ruminococcaceae*	Denominator
2ab756065c27e6163ad4259a5609c5b1	*Lachnospiraceae*	Denominator
c2a737924e989ece22452a86bbeaf775	*Lachnospiraceae*	Denominator

ec0ede08845dad4df7113237e1838fe5	*Ruminococcaceae*	Denominator
48b1bd255e8dec337da1d05e1bc27780	*Lachnospiraceae*	Denominator
5f5944bbc4632122fcd45e2a8ab335b9	*Lachnospiraceae*	Denominator

Supplemental table 2.7: Feature IDs selected using Songbird to generate a log ratio to calculate differential abundance between 2'FL and untreated control mice. *Lachnospiraceae* and *Ruminococcaceae* ASVs were selected from the lowest 25% ranked ASVs.

Code	*Genes*	*Forward (5' – 3')*	*Reverse (5' – 3')*
Ahr	aryl hydrocarbon receptor	CTGACAGAAATGGAGGCCAGGA	AGAAGACCAAGGCATCTGCTGT
Bdef2	beta-defensin 2	CACTCCAGCTGTTGGAAGTTTA	GCTCTGACACAGTACCCTCC
Ccl2	hemokine (C-C motif) ligand 2	CCACTCACCTGCTGCTACTCAT	GAAGTGCTTGAGGTGGTTGTGG
Cd14	cluster of differentiation 14	ACAACAGGCTGGATAGGAACCC	TTGACGAGGACCCTCAGAAACC
Cyp1a1	Cytochrome P450, family 1, subfamily A	ATTCCTGTCCTCCGTTACCTGC	ATGAGGCTGTCTGTGATGTCCC
Foxp3	forkhead box P3	AGGCTGATCCCCCTCTAGCA	AGCAGAGCTGTGTCTGGTGG
Gdnf	Glial cell-derived neurotrophic factor	AGAGGGGCAAAAATCGGGG	CCGCTGCAATATCGAAAGATCA
Gfap	Glial fibrillary acidic protein	GCGGCTGCTCTTGTAGTGAA	AGGGCCACATACCAGTAAAAC
Gpx2	Glutathione peroxidase 2	TCGGACATCAGGAGAACTGTC	TGCCCATTGACGTCACACTT
Hmox1	heme oxygenase 1	GCCCCACCAAGTTCAAACAG	GCTCCTCAAACAGCTCAATGT
H2R	Histamine Receptor H2	TGCCCTTCTCTGCCATTTACCA	TTGAGGATGGAAGCTGTGCAGA
Iba1	Ionized calcium binding adaptor molecule 1	CGCTCCTAGTGGGTCACATC	ATCAGCCATAGCAACCCCAT
Il-10	Interleukin 10	TTCCCTGGGTGAGAAGCTGAAG	TCACTCTTCACCTGCTCCACTG
Il-10r	Interleukin 10 receptor	CATTGCATACGGGACAGAACTGC	TTTCCGTACTGTTTGAGGGCCA
Il-22	Interleukin 22	ACTTGTGCGATCTCTGATGGCT	TATGGCTGCTGGAAGTTGGACA
Il1b	Interleukin 1 beta	TGCCACCTTTTGACAGTGATGA	CCCAGGTCAAAGGTTTGGAAGC
Il6	Interleukin 6	ACCCCAATTTCCAATGCTCTCC	AACGCACTAGGTTTGCCGAGTA
Myd88	Myeloid differentiation primary response 88	CCTGAGCAACTAGGACTGCCTT	GGAGGCATGTGTGTACTGAGGT
Ngf1	nerve growth factor 1	GGAGCGCATCGAGTTTTGG	CCTCACTGCGGCCAGTATAG
Nqo1	NAD(P)H dehydrogenase [quinone] 1	GGTAGCGGCTCCATGTACTC	CGCAGGATGCCACTCTGAAT
Ocln	Occludin	ATGGCAAGCGATCATACCCAGA	GGTTACCAATTGCTGCTGTACCG
Pfkfb3	6-Phosphofructo-2-Kinase/Fructose-2,6-Biphosphatase 3	CCCAGAGCCGGGTACAGAA	GGGGAGTTGGTCAGCTTCG
Rpl13a	60S ribosomal protein L13a	CTGCTGCTCTCAAGGTTGTTCG	TGTCACTGCCTGGTACTTCCAC
Rplp0	Ribosomal Protein Lateral Stalk Subunit P0	CCATGATGCGCAAGGCTATCAG	TGCCTCTGGAGATTTTCGTGGT

Slc2a1	facilitated glucose transporter member 1	CAGTTCGGCTATAACACTGGTG	GCCCCCGACAGAGAAGATG
Slc64a	sodium-dependent serotonin transporter	TTGATGAGTCCACCCCAACTCC	AATGCGCTCCTTAAGTGTCCCT
Tgfb	Transforming growth factor beta	AGGAGACGGAATACAGGGCT	GGGGCTGATCCCGTTGATTT
Tjp	tight junction protein	AGCCTTGAACTTTGACCTCTGC	ACAGAAATCGTGCTGATGTGCC
Tnf-a	tumor necrosis factor alpha	TTCGAGTGACAAGCCTGTAGCC	GATAGCAAATCGGCTGACGGTG
Tph1	tryptophan hydroxylase 1	CTACACTCCAGAGCCAGACACC	GTCTCCTCTGAAGCTCCAAGGG

Supplemental table 2.8: Primers and full gene name for qRT-PCR of mouse tissue samples.

	Untreated	*B.p.* MP80	2'FL	*B.p.* MP80 + 2'FL
Starting Weight (g)	24.7 ± 1.05 [a]	21.2 ± 0.54 [b]	22.4 ± 0.68 [ab]	24.5 ± 0.67 [a]
Ending Weight (g)	27.4 ± 1.20 [a]	22.9 ± 0.63 [b]	23.9 ± 0.67 [bc]	27.2 ± 0.90 [ac]
Body Weight Change (%)	9.9 ± 1.83 [a]	7.3 ± 0.74 [a]	6.4 ± 0.53 [a]	9.7 ± 1.79 [a]
Spleen Weight (mg/g)	3.3 ± 0.26 [a]	3.5 ± 0.22 [a]	3.1 ± 0.07 [a]	3.0 ± 0.15 [a]
Liver Weight (mg/g)	54.4 ± 3.55 [a]	51.3 ± 3.00 [a]	52.4 ± 1.51 [a]	51.4 ± 0.75 [a]
Cecum Weight (w/ content) (mg/g)	17.0 ± 0.86 [a]	16.9 ± 2.12 [a]	26.8 ± 2.26 [a]	47.6 ± 5.16 [b]
Cecum Weight (w/o content) (mg/g)	5.0 ± 0.32 [a]	4.7 ± 0.28 [a]	8.1 ± 0.74 [b]	9.8 ± 0.75 [b]
LPS Binding Protein (unit)	9.3 ± 1.35 [a]	4.1 ± 0.37 [b]	6.5 ± 0.43 [ab]	8.6 ± 0.89 [a]
*Paracellular Perm. Ileum (ng/cm^2/hr)	2664 ± 503 [a]	3503 ± 1844 [a]	3573 ± 744 [a]	3147 ± 1121 [a]
Transcellular Perm. Ileum (ng/cm^2/hr)	1357 ± 337 [a]	1120 ± 346 [a]	1641 ± 671 [a]	1225 ± 528 [a]
Paracellular Perm. Colon (ng/cm^2/hr)	2143 ± 638 [a]	1988 ± 125 [a]	1204 ± 194 [a]	1527 ± 169 [a]
Transcellular Perm. Colon (ng/cm^2/hr)	1288 ± 311 [a]	1281 ± 208 [a]	376 ± 77.4 [b]	668 ± 144 [ab]
Food Intake (g/day/cage)	9.83 ± 0.34 [a]	9.47 ± 0.57 [a]	11.3 ± 2.79 [a]	9.3 ± 1.04 [a]
Water Intake (ml/day/mouse)	6.36 ± 0.25 [a]	5.02 ± 0.66 [a]	5.08 ± 0.32 [a]	5.75 ± 0.29 [a]

*Permeability measures conducted using ussing chambers.

Supplemental table 2.9: Healthy mouse physiological data expressed as means +/- SEM and analyzed by one-way ANOVA with Tukey's multiple comparisons.

	Untreated			*B.p* MP80			2'FL			*B.p* MP80 + 2'FL		
Ahr	1.11	±	0.13	0.81	±	0.03	0.87	±	0.27	1.20	±	0.28
Bdef2	0.97	±	0.23	1.00	±	0.35	3.82	±	1.05	2.31	±	0.27
Ccl2	0.93	±	0.11	1.13	±	0.17	0.70	±	0.16	1.46	±	0.22
Cd14	1.13	±	0.11	1.26	±	0.05	0.96	±	0.18	1.13	±	0.11
Cyp1a1	1.51	±	0.51	2.57	±	0.51	1.65	±	0.43	2.27	±	0.59
Fox3p	1.01	±	0.06	1.14	±	0.14	1.19	±	0.21	1.23	±	0.14
Gpx2	1.03	±	0.11	0.87	±	0.04	1.32	±	0.54	1.00	±	0.10
Hmox1	1.23	±	0.22	0.97	±	0.22	0.87	±	0.09	1.03	±	0.17
Hrh2	1.02	±	0.21	0.65	±	0.07	1.09	±	0.15	1.57	±	0.20
Il10	0.99	±	0.11	0.92	±	0.17	0.40	±	0.12	0.66	±	0.08
Il10ra	1.05	±	0.15	0.40	±	0.12	0.92	±	0.17	0.66	±	0.08
Il1b	1.04	±	0.12	1.54	±	0.18	0.87	±	0.18	0.51	±	0.07
Il22	1.15	±	0.32	1.05	±	0.21	1.48	±	0.23	2.00	±	0.26
Il6	1.07	±	0.19	1.06	±	0.16	1.34	±	0.54	1.32	±	0.12
Lcn2	1.08	±	0.17	0.81	±	0.09	0.91	±	0.27	1.27	±	0.25
Myd88	1.10	±	0.16	0.92	±	0.07	0.84	±	0.19	1.07	±	0.16
Nqo1	1.07	±	0.17	1.22	±	0.09	1.13	±	0.18	1.05	±	0.11
Ocln	1.01	±	0.12	0.86	±	0.05	1.08	±	0.34	1.01	±	0.14
Pfkb3	1.12	±	0.11	0.92	±	0.06	0.78	±	0.12	0.61	±	0.08
Sl6a4	1.13	±	0.33	0.76	±	0.18	1.44	±	0.32	1.16	±	0.36
Slc2a1	1.07	±	0.18	0.81	±	0.11	0.82	±	0.21	0.66	±	0.15
Tgfb	1.04	±	0.10	0.78	±	0.10	1.02	±	0.21	1.01	±	0.20
Tjp1	0.95	±	0.07	0.81	±	0.07	1.02	±	0.26	1.02	±	0.08
Tnfa	1.30	±	0.31	1.11	±	0.13	1.06	±	0.38	0.86	±	0.18
Tph1	1.04	±	0.11	1.39	±	0.15	1.07	±	0.40	0.83	±	0.13

Supplemental table 2.10: Colon tissue gene expression data expressed as means +/- SEM and analyzed by Kruskal-Wallis test with FDR corrected *p* values (genes with *p* values < 0.05 in bold).

	Untreated – *B.p.* MP80	Untreated – 2'FL	Untreated – *B.p.* MP80 + 2'FL	*B.p.* MP80 – 2'FL	*B.p.* MP80 – *B.p.* MP80 + 2'FL	2'FL – *B.p.* MP80 + 2'FL
Bdef2	**0.009**	0.940	**0.026**	**0.036**	0.370	0.052
Il1b	0.420	0.062	**0.009**	0.062	0.180	**0.009**

Supplemental table 2.11: Colon tissue gene expression *p* values calculated by post hoc Wilcoxon Rank Sum test with FDR corrected *p* values. Genes selected based on Kruskal Wallis test with FDR correction and bold values are $p < 0.05$.

	Untreated			*B.p.* MP80			2'FL			*B.p* MP80 + 2'FL		
AhR	1.05	±	0.13	1.02	±	0.18	1.95	±	0.33	1.69	±	0.13
Ccl2	0.83	±	0.14	1.04	±	0.14	0.89	±	0.18	1.19	±	0.35
Cd14	0.98	±	0.11	0.95	±	0.12	0.75	±	0.15	0.69	±	0.08
Cyp1a1	1.09	±	0.35	1.05	±	0.24	1.32	±	0.68	0.32	±	0.05
Foxp3	1.04	±	0.11	0.82	±	0.11	0.84	±	0.13	0.58	±	0.08
Gpx2	1.03	±	0.10	0.66	±	0.11	1.30	±	0.18	1.09	±	0.12
Hmox1	1.03	±	0.09	0.79	±	0.17	1.36	±	0.16	1.09	±	0.12
Hrh2	1.14	±	0.16	1.70	±	0.18	1.19	±	0.23	0.83	±	0.08
Il10	0.88	±	0.08	1.31	±	0.15	1.29	±	0.38	1.34	±	0.26
Il10ra	1.11	±	0.17	0.99	±	0.10	1.40	±	0.31	1.65	±	0.17
Il1b	1.04	±	0.10	0.85	±	0.14	1.55	±	0.31	1.63	±	0.36
Il22	0.93	±	0.10	1.78	±	0.82	0.93	±	0.15	0.54	±	0.21
Il6	1.00	±	0.14	1.44	±	0.32	0.75	±	0.17	0.49	±	0.09
Lcn2	0.93	±	0.12	1.04	±	0.26	1.41	±	0.26	1.84	±	0.80
Myd88	1.09	±	0.17	1.25	±	0.16	1.36	±	0.19	1.40	±	0.09
Nqo1	1.01	±	0.06	0.86	±	0.07	1.22	±	0.10	1.10	±	0.11
Ocln	1.00	±	0.13	1.20	±	0.16	1.05	±	0.13	1.32	±	0.08
Pfkb3	1.11	±	0.21	0.16	±	0.02	1.87	±	0.43	1.77	±	0.72
Slc2a1	1.01	±	0.06	0.28	±	0.02	1.20	±	0.16	1.31	±	0.03
Slc6a4	1.10	±	0.09	1.27	±	0.21	2.37	±	0.34	2.44	±	0.38
Tgfb	1.07	±	0.14	0.76	±	0.12	1.29	±	0.19	0.94	±	0.04
Tjp1	1.09	±	0.11	1.18	±	0.09	1.00	±	0.24	0.74	±	0.04
Tnf	0.98	±	0.31	0.90	±	0.25	5.33	±	2.30	1.14	±	0.37
Tph1	1.33	±	0.13	1.49	±	0.22	1.18	±	0.43	1.38	±	0.32

Supplemental table 2.12: Jejunum tissue gene expression data expressed as means +/- SEM and analyzed by Kruskal-Wallis test with FDR corrected *p* values (genes with *p* values < 0.05 in bold).

	Untreated – *B.p.* MP80	Untreated – 2'FL	Untreated – *B.p.* MP80 + 2'FL	*B.p.* MP80 – 2'FL	*B.p.* MP80 – *B.p.* MP80 + 2'FL	2'FL – *B.p.* MP80 + 2'FL
Pfkb3	**0.004**	0.340	0.850	**0.005**	**0.005**	0.870
Slc2a1	**0.004**	0.590	**0.006**	**0.005**	**0.005**	0.710
Slc6a4	0.450	0.005	**0.004**	**0.043**	**0.016**	0.940

Supplemental table 2.13: Jejunum tissue gene expression *p* values calculated by post hoc Wilcoxon Rank Sum test with FDR corrected *p* values. Genes selected based on Kruskal Wallis test with FDR correction and bold values are $p < 0.05$.

	Untreated			*B.p* MP80			2'FL			*B.p* MP80 + 2'FL		
AhR	0.94	±	0.06	0.83	±	0.07	0.96	±	0.14	0.960	±	0.150
Ccl2	1.10	±	0.15	1.40	±	0.34	1.01	±	0.18	1.490	±	0.270
Cd14	1.01	±	0.07	0.78	±	0.04	0.90	±	0.11	1.420	±	0.120
Cyp1a1	1.42	±	0.65	0.98	±	0.08	0.72	±	0.25	0.270	±	0.070
Fox3p	1.05	±	0.12	1.33	±	0.23	1.33	±	0.13	1.300	±	0.170
Gpx2	1.16	±	0.21	1.15	±	0.28	3.46	±	0.82	3.950	±	0.480
Hmox1	1.08	±	0.14	2.30	±	0.80	2.84	±	0.47	2.680	±	0.320
Hrh2	0.93	±	0.13	1.21	±	0.24	0.85	±	0.19	0.900	±	0.200
Il10	1.10	±	0.15	1.94	±	0.30	2.19	±	0.35	2.030	±	0.350
Il10ra	1.06	±	0.12	1.83	±	0.28	1.73	±	0.27	2.180	±	0.250
Il1b	1.00	±	0.11	1.77	±	0.60	0.95	±	0.32	2.370	±	0.860
Il22	0.95	±	0.10	1.41	±	0.54	0.83	±	0.18	1.270	±	0.410
Il6	0.98	±	0.07	3.05	±	1.10	1.36	±	0.22	1.840	±	0.310
Myd88	1.14	±	0.19	0.73	±	0.16	4.38	±	0.73	3.870	±	0.800
Nqo1	1.08	±	0.13	1.17	±	0.12	2.18	±	0.37	2.540	±	0.370
Pfkb3	1.11	±	0.21	1.07	±	0.20	3.08	±	0.40	3.580	±	0.910
Slc2a1	1.07	±	0.15	0.80	±	0.09	3.32	±	0.47	3.560	±	0.390
Tnfa	1.03	±	0.13	1.07	±	0.17	0.88	±	0.16	0.920	±	0.130

Supplemental table 2.14: Cecum tissue gene expression data expressed as means +/- SEM and analyzed by Kruskal-Wallis test with FDR corrected *p* values (genes with *p* values < 0.05 in bold).

	Untreated – *B.p.* MP80	Untreated – 2'FL	Untreated – *B.p.* MP80 + 2'FL	*B.p.* MP80 – 2'FL	*B.p.* MP80 – *B.p.* MP80 + 2'FL	2'FL – *B.p.* MP80 + 2'FL
Cd14	0.054	0.670	0.028	0.870	**0.009**	**0.034**
Cyp1a1	0.700	0.870	**0.028**	0.210	**0.009**	0.062
Gpx2	0.950	**0.015**	**0.008**	**0.023**	**0.014**	0.530
Hmox1	0.600	**0.008**	**0.008**	0.450	0.530	0.870
Il10	0.068	**0.022**	0.068	0.710	0.950	0.810
Il10ra	**0.039**	0.068	**0.010**	0.870	0.630	0.360
Il6	**0.022**	0.290	0.086	0.073	0.710	0.360
Myd88	0.290	**0.008**	**0.009**	**0.009**	**0.009**	0.530
Nqo1	0.720	**0.028**	**0.008**	0.073	**0.009**	0.530
Pfkb3	0.910	**0.009**	**0.010**	**0.014**	**0.023**	0.950
Slc2a1	0.350	**0.008**	**0.008**	**0.009**	**0.009**	0.870

Supplemental table 2.15: Cecum tissue gene expression *p* values calculated by post hoc Wilcoxon Rank Sum test with FDR corrected *p* values. Genes selected based on Kruskal Wallis test with FDR correction and bold values are $p < 0.05$.

	Untreated			*B.p* MP80			2'FL			*B.p* MP80 + 2'FL		
AhR	1.00	±	0.15	0.96	±	0.14	1.24	±	0.40	0.94	±	0.15
Ccl2	1.23	±	0.34	1.03	±	0.25	0.93	±	0.18	1.53	±	0.27
Cd14	1.08	±	0.23	9.26	±	1.46	1.19	±	0.19	1.60	±	0.43
Cyp1a1	1.40	±	0.44	0.77	±	0.11	1.76	±	0.39	1.54	±	0.44
Gpx2	1.02	±	0.10	1.08	±	0.11	1.56	±	0.15	1.85	±	0.25
Hmox1	0.86	±	0.12	0.77	±	0.12	0.90	±	0.08	0.77	±	0.09
Hrh2	0.84	±	0.33	1.09	±	0.23	1.06	±	0.40	2.75	±	1.44
Il10ra	0.95	±	0.14	0.85	±	0.16	1.08	±	0.24	0.98	±	0.23
Il1b	1.17	±	0.33	0.96	±	0.20	0.83	±	0.21	0.78	±	0.24
Il22	1.08	±	0.17	1.27	±	0.48	1.33	±	0.56	1.20	±	0.07
Il6	1.06	±	0.16	0.83	±	0.09	1.28	±	0.14	1.82	±	0.36
Lcn2	3.67	±	1.95	1.44	±	0.47	1.46	±	0.98	10.39	±	6.12
Myd88	0.99	±	0.16	0.76	±	0.08	0.82	±	0.27	0.61	±	0.15
Nqo1	1.02	±	0.11	1.44	±	0.10	1.25	±	0.18	1.21	±	0.08
Pfkb3	0.94	±	0.24	0.94	±	0.17	1.71	±	0.51	0.71	±	0.18
Tgfb	1.01	±	0.08	0.90	±	0.11	1.15	±	0.11	1.02	±	0.04
Tnfa	0.99	±	0.31	0.89	±	0.22	2.12	±	1.26	2.26	±	1.01

Supplemental table 2.16: Liver tissue gene expression data expressed as means +/- SEM and analyzed by Kruskal-Wallis test with FDR corrected *p* values (genes with *p* values < 0.05 in bold).

	Untreated	DSS	DSS +*B.p.* MP80	DSS +2'FL	DSS +*B.p.* MP80 + 2'FL
Starting Weight (g)	24.0 ± 0.5	25.4 ± 1.3	25.0 ± 0.9	25.9 ± 0.1	25.1 ± 0.9
Ending Weight (g)	24.9 ± 0.2	21.9 ± 1.4	22.7 ± 0.9	24.3 ± 0.5	24.5 ± 0.3
Body Weight Change (%)	3.6 ± 1.4 [c]	-16.1 ± 1.4 [d]	-10.2 ± 2.4 [a]	-6.4 ± 1.7 [ab]	-2.3 ± 2.3 [b]
Spleen Weight (mg/g)	3.0 ± 0.2 [b]	5.7 ± 0.3 [a]	6.3 ± 0.8 [a]	5.6 ± 0.9 [a]	3.6 ± 0.6 [b]
Liver Weight (mg/g)	24.9 ± 0.2 [b]	49.7 ± 0.8 [a]	48.8 ± 1.4 [a]	49.1 ± 4.4 [a]	51.9 ± 2.9 [a]
Colon Length (cm)	7.3 ± 0.3 [b]	5.5 ± 0.3 [a]	5.3 ± 0.3 [a]	6.2 ± 0.4 [ac]	6.5 ± 0.3 [c]
Cecum Weight (w/ content) (mg/g)	18.5 ± 0.4 [a]	11.2 ± 2.1 [a]	13.1 ± 2.8 [a]	47.8 ± 10.1 [b]	50.0 ± 8.6 [b]
Cecum Weight (w/o content) (mg/g)	4.7 ± 0.2 [a]	7.5 ± 1.2 [ab]	6.0 ± 1.4 [ab]	8.7 ± 0.4 [b]	9.6 ± 0.6 [b]
Fluid intake before DSS (ml/day/cage)	9.3 ± 1.3	12.8 ± 2.4	12.2 ± 1.7	10.2 ± 0.8	8.2 ± 0.5
Fluid intake during DSS (ml/day/cage)	10.9 ± 2.5	13.9 ± 2.6	13.8 ± 2.8	9.1 ± 1.4	12.4 ± 1.8
Food intake before DSS (g/day/cage)	9.2 ± 0.4	8.9 ± 1.0	10.3 ± 1.1	7.9 ± 0.7	7.8 ± 1.0
Food intake during DSS (g/day/cage)	9.6 ± 2.0 [a]	8.6 ± 1.5 [b]	10.4 ± 2.1 [a]	7.8 ± 0.6 [bc]	7.6 ± 0.6 [c]

Supplemental table 2.17: DSS-colitis experiment mouse physiological data expressed as means +/- SEM and analyzed by one-way ANOVA with FDR corrected *p* values (different letters signify statistical difference between treatments)

	Untreated			DSS			DSS + *B.p* MP80			DSS + 2'FL			*DSS* + *B.p* MP80 + 2'FL		
AhR	1.06	±	0.17	0.25	±	0.05	0.04	±	0.02	0.49	±	0.17	0.51	±	0.09
Bdef2	1.12	±	0.21	2.55	±	0.68	59.42	±	36.54	3.61	±	2.87	1.72	±	0.87
Ccl2	1.07	±	0.17	10.41	±	3.37	10.53	±	3.34	5.82	±	3.15	1.82	±	0.65
Cd14	1.06	±	0.18	1.53	±	0.21	1.89	±	0.68	2.64	±	0.51	1.37	±	0.32
Foxp3	1.03	±	0.12	7.36	±	2.86	10.53	±	7.57	2.19	±	1.64	0.97	±	0.22
Gpx2	1.16	±	0.30	1.63	±	0.54	2.49	±	0.85	1.92	±	0.38	1.48	±	0.36
Hmox1	1.07	±	0.17	1.86	±	0.31	2.01	±	0.78	1.43	±	0.14	1.88	±	0.57
Hrh2	1.05	±	0.16	9.43	±	3.40	5.43	±	0.96	3.68	±	2.95	0.94	±	0.14
Il10	1.15	±	0.27	1.31	±	0.21	1.21	±	0.39	1.11	±	0.37	1.35	±	0.30
Il10ra	1.05	±	0.14	1.32	±	0.53	9.97	±	5.00	2.67	±	1.76	1.56	±	0.50
Il1b	1.07	±	0.19	19.94	±	6.03	26.41	±	16.13	20.87	±	7.59	5.65	±	2.19
Il22	1.13	±	0.26	27.37	±	7.39	209.94	±	155.77	147.61	±	93.73	94.66	±	65.21
Il6	1.41	±	0.50	30.95	±	11.93	75.32	±	30.11	34.93	±	14.28	2.11	±	0.82
Lcn2	1.02	±	0.08	5.58	±	1.89	26.50	±	14.10	2.74	±	0.48	1.86	±	0.39
Myd88	1.06	±	0.16	1.07	±	0.24	1.59	±	0.29	1.64	±	0.84	1.05	±	0.20
Nqo1	1.08	±	0.18	0.40	±	0.29	0.68	±	0.23	0.51	±	0.08	0.75	±	0.22
Ocln	1.05	±	0.15	0.33	±	0.06	0.31	±	0.06	0.45	±	0.11	0.91	±	0.20
Pfkb3	1.01	±	0.07	0.78	±	0.22	0.89	±	0.76	0.63	±	0.14	1.41	±	0.88
Slc2a1	1.25	±	0.18	0.38	±	0.12	0.68	±	0.58	0.30	±	0.08	0.31	±	0.06
Slc6a4	1.08	±	0.19	0.39	±	0.18	0.68	±	0.23	2.15	±	0.99	3.10	±	1.33
Tgfb	1.04	±	0.13	0.38	±	0.08	0.11	±	0.05	0.57	±	0.09	0.73	±	0.19
Tnfa	1.21	±	0.35	2.40	±	0.70	6.53	±	2.21	6.87	±	2.11	3.31	±	1.07
Tph1	1.08	±	0.18	0.49	±	0.07	0.51	±	0.22	0.52	±	0.09	0.92	±	0.17

Supplemental table 2.18: Colon tissue gene expression data from chemically-induced colitis experiments expressed as means +/- SEM and are analyzed by Kruskal-Wallis test with FDR corrected *p* values (genes with *p* values < 0.05 in bold).

	Untreated – DSS	Untreated – DSS MP80	Untreated – DSS 2'FL	Untreated – DSS MP80 2FL	DSS – DSS MP80	DSS – DSS 2FL	DSS – DSS MP80 2FL	DSS MP80 – DSS 2FL	DSS MP80 – DSS MP80 2FL	DSS 2FL – DSS MP80 2FL
AhR	**0.024**	**0.024**	0.110	**0.024**	**0.032**	0.490	**0.036**	**0.024**	**0.024**	0.490
Ccl2	**0.024**	**0.024**	**0.024**	0.650	0.950	0.200	**0.024**	0.650	**0.050**	0.110
Il1b	**0.024**	**0.024**	**0.050**	**0.024**	0.630	0.950	0.073	0.830	0.190	0.490
Il6	**0.024**	**0.024**	**0.024**	0.520	0.320	1.000	**0.024**	0.260	**0.024**	**0.040**
Ocln	**0.024**	**0.024**	**0.024**	0.750	0.750	0.580	**0.050**	0.490	0.073	0.150
Tgfb	**0.024**	**0.024**	0.057	0.450	**0.048**	0.450	0.190	**0.031**	**0.047**	0.630

Supplemental table 2.19: Colon tissue gene expression data from chemically-induced colitis experiments *p* values calculated by post hoc Wilcoxon Rank Sum test with FDR corrected *p* values. Genes selected based on Kruskal Wallis test with FDR correction and bold values are $p < 0.05$.

	Untreated	DSS	DSS + *B.p* MP80	DSS + 2'FL	*DSS* + *B.p* MP80 + 2'FL
AhR	1.02 ± 0.09	0.51 ± 0.09	0.47 ± 0.11	0.94 ± 0.14	0.45 ± 0.11
Ccl2	1.07 ± 0.18	1.14 ± 0.24	0.86 ± 0.17	0.94 ± 0.18	0.78 ± 0.17
Cd14	1.05 ± 0.15	0.60 ± 0.13	0.76 ± 0.10	0.93 ± 0.10	0.65 ± 0.11
Foxp3	1.04 ± 0.13	0.66 ± 0.10	0.62 ± 0.09	1.08 ± 0.19	0.72 ± 0.16
Gpx2	1.45 ± 0.59	0.52 ± 0.21	0.79 ± 0.20	0.63 ± 0.24	0.62 ± 0.27
Hmox1	0.89 ± 0.19	0.23 ± 0.08	0.49 ± 0.09	0.41 ± 0.07	0.45 ± 0.09
Hrh2	1.05 ± 0.13	0.70 ± 0.08	0.76 ± 0.17	1.28 ± 0.28	0.69 ± 0.18
Il10	1.05 ± 0.14	0.30 ± 0.11	0.56 ± 0.15	0.53 ± 0.11	0.36 ± 0.09
Il10ra	1.01 ± 0.07	0.39 ± 0.07	0.82 ± 0.26	0.91 ± 0.20	0.72 ± 0.19
IL1b	1.12 ± 0.21	0.26 ± 0.11	0.53 ± 0.11	0.71 ± 0.14	0.57 ± 0.13
Il22	1.02 ± 0.12	0.82 ± 0.35	33.64 ± 30.74	2.81 ± 1.01	5.60 ± 4.52
Il6	1.03 ± 0.11	1.61 ± 0.46	1.69 ± 0.28	1.40 ± 0.25	2.03 ± 0.46
Lcn2	1.20 ± 0.37	1.36 ± 0.39	1.65 ± 0.44	1.82 ± 0.50	0.84 ± 0.25
Myd88	1.29 ± 0.37	0.33 ± 0.15	0.68 ± 0.11	0.52 ± 0.18	0.59 ± 0.17
Nqo1	1.01 ± 0.07	0.24 ± 0.10	0.33 ± 0.09	1.19 ± 0.62	1.53 ± 0.69
Ocln	1.01 ± 0.16	0.35 ± 0.13	0.52 ± 0.08	0.72 ± 0.18	0.63 ± 0.16
Pfkb3	1.16 ± 0.30	1.73 ± 0.28	2.25 ± 0.87	0.54 ± 0.18	0.35 ± 0.08
Slc2a1	1.01 ± 0.08	0.60 ± 0.13	0.57 ± 0.09	0.74 ± 0.14	0.45 ± 0.08
Slc6a4	0.90 ± 0.16	0.32 ± 0.08	0.51 ± 0.08	0.59 ± 0.08	0.51 ± 0.12
Tgfb	1.13 ± 0.15	0.44 ± 0.07	0.51 ± 0.08	0.77 ± 0.11	0.51 ± 0.08
Tnfa	1.14 ± 0.35	0.54 ± 0.24	3.02 ± 1.88	0.24 ± 0.06	0.37 ± 0.10
Tph1	0.89 ± 0.14	0.24 ± 0.07	0.42 ± 0.07	0.55 ± 0.09	0.48 ± 0.10

Supplemental table 2.20: Jejunum tissue gene expression data from chemically-induced colitis experiments expressed as means +/- SEM and are analyzed by Kruskal-Wallis test with FDR corrected *p* values (genes with *p* values < 0.05 in bold).

	Untreated – DSS	Untreated – DSS MP80	Untreated – DSS 2'FL	Untreated – DSS MP80 2FL	DSS – DSS MP80	DSS – DSS 2FL	DSS – DSS MP80 2FL	DSS MP80 – DSS 2FL	DSS MP80 – DSS MP80 2FL	DSS 2FL – DSS MP80 2FL
AhR	**0.019**	**0.019**	1.000	**0.027**	0.910	0.065	0.820	**0.065**	0.990	0.160
Nqo1	**0.019**	**0.019**	0.610	0.910	0.640	0.130	**0.027**	0.480	**0.027**	0.490
Pfkb3	0.160	0.640	0.097	**0.017**	0.910	**0.027**	**0.017**	0.130	**0.043**	0.710
Tgfb	**0.015**	**0.017**	0.150	**0.017**	0.640	0.100	0.640	0.290	1.000	0.190

Supplemental table 2.21: Jejunum tissue gene expression data from chemically-induced colitis experiments *p* values calculated by post hoc Wilcoxon Rank Sum test with FDR corrected *p* values. Genes selected based on Kruskal Wallis test with FDR correction and bold values are $p < 0.05$.

	Untreated	DSS	DSS + *B.p* MP80	DSS + 2'FL	*DSS* + *B.p* MP80 + 2'FL
AhR	1.01 ± 0.06	0.3383 ± 0.046	0.2792 ± 0.0597	0.443 ± 0.097	0.541 ± 0.08
Ccl2	1.09 ± 0.2	1.8844 ± 0.353	3.8259 ± 1.3452	2.0459 ± 0.506	1.448 ± 0.46
Cd14	1.01 ± 0.07	2.0541 ± 0.673	3.8954 ± 0.952	1.2344 ± 0.29	0.921 ± 0.1
Gpx2	1.11 ± 0.18	0.9351 ± 0.341	0.3561 ± 0.0748	0.5002 ± 0.077	0.843 ± 0.24
Hmox1	1.27 ± 0.39	1.0577 ± 0.437	0.835 ± 0.1909	0.7494 ± 0.089	0.811 ± 0.17
Hrh2	1.02 ± 0.09	0.8353 ± 0.392	0.8646 ± 0.1706	0.7094 ± 0.164	0.629 ± 0.17
Il10ra	1.01 ± 0.06	0.2225 ± 0.034	0.2984 ± 0.0488	0.4066 ± 0.091	0.401 ± 0.03
Il1b	1.29 ± 0.41	1.5637 ± 0.818	0.9813 ± 0.3397	1.1802 ± 0.082	1.471 ± 0.28
Il6	1.04 ± 0.14	2.6899 ± 0.411	2.0999 ± 0.3979	1.0022 ± 0.299	1.659 ± 0.41
Lcn2	1.47 ± 0.5	234.73 ± 93.32	462.1 ± 89.649	189.49 ± 78.75	11.4 ± 3.45
Myd88	1.31 ± 0.38	0.5961 ± 0.204	0.7929 ± 0.3084	0.5518 ± 0.059	0.755 ± 0.22
Nqo1	0.86 ± 0.14	0.2545 ± 0.12	0.2283 ± 0.0613	0.3356 ± 0.04	0.493 ± 0.11
Pfkb3	1.02 ± 0.09	1.1991 ± 0.751	1.1343 ± 0.4344	0.4304 ± 0.091	0.361 ± 0.13
Slc2a1	1.06 ± 0.17	0.1919 ± 0.083	0.1746 ± 0.0427	0.3673 ± 0.121	0.509 ± 0.09
Tgfb	1.01 ± 0.07	0.353 ± 0.071	0.3818 ± 0.0593	0.5457 ± 0.067	0.669 ± 0.06
Tnfa	1.08 ± 0.35	0.4499 ± 0.2	0.7323 ± 0.3258	0.4991 ± 0.211	0.777 ± 0.22

Supplemental table 2.22: Liver tissue gene expression data from chemically-induced colitis experiments expressed as means +/- SEM and are analyzed by Kruskal-Wallis test with FDR corrected *p* values (genes with *p* values < 0.05 in bold).

	Untreated – DSS	Untreated – DSS MP80	Untreated – DSS 2'FL	Untreated – DSS MP80 2FL	DSS – DSS MP80	DSS – DSS 2FL	DSS – DSS MP80 2FL	DSS MP80 – DSS 2FL	DSS MP80 – DSS MP80 2FL	DSS 2FL – DSS MP80 2FL
AhR	**0.009**	**0.009**	**0.009**	**0.009**	0.660	0.660	0.160	0.410	0.053	0.480
Cd14	0.340	**0.009**	0.940	0.480	0.210	0.660	0.210	**0.013**	**0.009**	0.870
Il10ra	**0.009**	**0.009**	**0.009**	**0.009**	0.480	0.340	**0.009**	0.410	0.160	0.940
Il6	**0.013**	**0.020**	0.750	0.340	0.410	**0.038**	0.350	0.100	0.720	0.340
Lcn2	**0.009**	**0.013**	**0.009**	**0.020**	0.210	0.940	**0.013**	0.061	**0.013**	0.053
Slc2a1	**0.009**	**0.013**	**0.013**	**0.020**	0.720	0.160	0.120	0.640	**0.020**	0.480
Tgfb	**0.009**	**0.009**	**0.009**	**0.020**	0.940	0.280	**0.020**	0.160	**0.020**	0.480

Supplemental table 2.23: Liver tissue gene expression data from chemically-induced colitis experiments *p* values calculated by post hoc Wilcoxon Rank Sum test with FDR corrected *p* values. Genes selected based on Kruskal Wallis test with FDR correction and bold values are $p < 0.05$.

	Spearman's Correlation	*p* value
Slc6a4	0.104	0.748
Tph1	0.799	**0.006**
AhR	0.786	**0.004**
Nqo1	0.158	0.643
Hmox1	0.104	0.761
Ocln	0.441	0.151
Il10ra	-0.104	0.748
Il1b	-0.095	0.782
Tnf	-0.295	0.351
Il6	-0.723	**0.018**
Ccl2	-0.478	0.116
Cd14	-0.250	0.434
Hrh2	-0.549	0.080
Lcn2	-0.300	0.344
Tgfb	0.800	**0.005**
Nfkb	0.624	**0.030**
Colon Length	0.815	**0.001**
LBP in Serum	-0.724	**0.008**
Spleen Weight	-0.528	0.077

Supplemental table 2.24: Spearman's correlation between colon inflammatory markers and *B.p.* MP80 abundance as measured by qPCR with a fucosidase primer for treatment groups DSS + *B.p.* MP80 + 2'FL and DSS + *B.p.* MP80 (n = 6 per treatment group).

Chapter 3

Persistence of *Bifidobacterium pseudocatenulatum* MP80 shifts local and systemic microbial metabolome when paired with 2'-fucosyllactose in conventionally colonized mice

Britta E. Heiss[1], Jules A. Larke[2], Amy M. Ehrlich[3], Diana H. Taft[1], Helen E. Raybould[3], and David A. Mills[1], Carolyn M. Slupsky[1,2]

[1]Department of Food Science and Technology, [2]Department of Nutrition, [3]Department of Anatomy, Physiology, and Cell Biology, School of Veterinary Medicine, University of California, Davis, Davis, CA, USA

3.1 Abstract

Bifidobacteria represent an important gut commensal in humans particularly during initial microbiome assembly in the first year of life. In this context, enrichment of *Bifidobacterium* is mediated though the utilization of human milk oligosaccharides (HMOs) whereby several human-adapted species have dedicated genomic loci for transport and metabolism of these glycans. This creates a competitive advantage that enables Bifidobacteria expansion, persistence and the subsequent release of fermentation products into the gut lumen which may offer physiological benefits to the host. Following infancy, the stable gut microbial community is more resistant to colonization by external microbes as the indigenous members compete for available resources. Synbiotic pairing of probiotic species with a cognate prebiotic delivers a competitive advantage when establishing residence in the gut by utilizing the provided nutrient niche. To determine the fitness advantage and metabolic characteristics of an HMO-catabolizing *Bifidobacterium* strain in the presence or absence of 2'-fucosyllactose (2'-FL), conventionally colonized mice received probiotic treatment of *Bifidobacterium pseudocatenulatum* MP80 (*B. p.* MP80) during the first three days of the experiment with or without 2'-FL supplementation throughout the study. 16S rRNA amplicon sequencing revealed that mice provided only the probiotic, *B. p.* MP80, were observed to have a similar microbiome composition with a consistently low proportion of *Bifidobacteriaceae*. Furthermore, using ^{1}H NMR spectroscopy we observed similar metabolic profiles of gut luminal contents and serum for probiotic-treated mice relative to untreated mice. In contrast, synbiotic supplemented mice exhibited shifts in their community structure across time with an overall increased, yet variable, proportion of *Bifidobacteriaceae* following oral inoculation. Parsing the synbiotic group into high and low bifidobacteria persistence based on the median proportion of *Bifidobacteriaceae*, we observed significant differences in gut microbial diversity and metabolite profiles. Notably, metabolites associated with the fermentation of 2'-FL by bifidobacteria were significantly greater in mice with a high proportion of *Bifidobacteriaceae* in the gut suggesting metabolite production scales with population density. This study demonstrates the

importance of modeling persistent, rather than transient, microbial populations for characterizing the functional output of probiotic supplementation.

3.2 Introduction

Early, dominant, infant borne *Bifidobacterium* colonization in breastfed infants is favored by the consumption of human milk oligosaccharides (HMOs) due to their prebiotic nature.[1] These structurally-complex oligosaccharides comprised of a range of monomers and linkages[2,3] establish a nutrient niche in the gut that selectively enrich several *Bifidobacterium* species.[4,5] In infant cohort studies, associations between human milk oligosaccharide (HMO) degradation, enrichment of select *Bifidobacterium* species, higher fecal acetate and lactate, and advantageous health outcomes have been observed.[6–13] As such, robust colonization of *Bifidobacterium* during infancy has been linked with improved markers for T1D[12], reduced likelihood of obesity[13,14], robust vaccine responses[15] and lower antimicrobial resistance gene carriage.[8,16,17]

Given the associations of *Bifidobacterium* and health outcomes in infants, there is an increased interest to promote *Bifidobacterium* populations in later human life stages and model colonization of this organism to scrutinize mechanisms of action. Probiotic supplementation is a commonly used strategy to manipulate the gut microbiota, however, efficacy is influenced by inter-individual variation of host related factors including genetics, diet, and microbiome composition.[18–22] As such, deriving health benefits from the probiotic may be case specific in which only certain diet and/or microbiome configurations promote metabolic or other microbial activities responsible for the benefit.[23] While probiotic bacteria are often capable of surviving passage through the gastrointestinal tract, most probiotics do not colonize, and little is known about their interaction with indigenous microbiota and gut accessible nutrient resources. However, synbiotics, comprised of both probiotic and prebiotic substrate selectively utilized by the microbe act synergistically to enhance colonization and functionality in the gut.[24] With this targeted enrichment strategy, there is a greater likelihood of colonization through which health outcomes can be achieved.

The persistence of a species is defined as the time between its emergence and extinction within a region.[25] Nutrient availability, environmental conditions, and competition between species influences whether a microbe persists. Bacterial persistence consists of a microbe replicating at an equal or greater rate than washout.[26] A prior synbiotic rodent model pairing a fermented milk product and five food-borne

bacterial strains found that the supplemented bacteria were quantifiable in the feces during the feeding periods with only a subset of rats continuing to shed one of the five strains 2 days post-supplementation.[27] Researchers concluded that a subset of rats were permissive to probiotic persistence while others were resistant. Alternatively, by exploiting the established, evolutionary-selected, complementary milk glycan-bacterial synbiotic pairing, we established a persistent population of *Bifidobacterium pseudocatenulatum* MP80 (*B. p*. MP80), a breastfed infant bacterial isolate, with continuous supplementation of the HMO 2'-fucosyllactose (2'-FL).[28] When mice were subjected to a chemically-induced colitis model, synbiotic treatment improved health outcomes and reduced inflammation suggesting a synergistic protective effect. Given the evidence of *Bifidobacterium* engraftment among probiotic supplemented breastfed infants[29,30], this mouse persistence model was designed to recapitulate the critical role HMOs play in the colonization of HMO-consuming *Bifidobacterium*.

Here, we sought to investigate how provision of 2'-FL may augment the colonization and metabolic output of *B. p.* MP80 in the murine gut. We approached this question by evaluating the gut microbiota and metabolic profiles of mice provided synbiotic treatment containing 2'-FL and *B. p.* MP80 compared with supplementation of either 2'-FL or *B. p.* MP80 alone. This allowed us to gauge the effect of 2'-FL on sustaining *Bifidobacterium* populations in the gut and the corresponding metabolite profiles. Determining how the indigenous microbiota can be modulated by probiotic or synbiotic colonization and the resultant metabolic outputs are critical to understanding how synbiotics may facilitate health outcomes.

3.3 Results

To measure changes in metabolism upon supplementation of the bifidobacterial strain, mice (n=39) were divided into four groups and provided either the *B.p.* MP80 probiotic (n=9; PRO), 2'-FL as a prebiotic (n=9: PRE), both *B.p.* MP80 and 2'-FL (n=12, SYN), or a saline control (n=9; CON). The probiotic was provided as an oral gavage each day for three days for the PRO and SYN groups and the prebiotic was provided as a 10% solution of 2'-FL for the PRE and SYN groups every day throughout the experiment (**Figure 3.1**).

3.3.1 *B.p.* MP80 persists only when supplemented as a synbiotic

Persistence of *B.p.* MP80 was determined using 16S rRNA amplicon sequencing of the fecal microbial community structure. Mice in the SYN group had statistically significant microbial community structure shifts by day of treatment, from baseline (day 0) to the final time point (day 9) (**Figure 3.2a**, PERMANOVA, $p < 0.001$). Post hoc testing revealed statistical significance between baseline and the subsequent time points ($p < 0.005$). Community structure in the PRO treated mice corresponded to smaller, non-significant shifts during the experiment (**Figure 3.2b**, PERMANOVA, $p < 0.181$). Persistence of *Bifidobacteriaceae* was observed in the SYN group with significantly higher proportions of *Bifidobacteriaceae* relative to the PRO group at completion of the experiment (**Figure 3.2c**, Wilcoxon rank-sum test, $p < 0.01$), although there was a high variance. Pairwise comparison of the weighted Unifrac distance revealed that the microbial community structure was statistically different on the final day between each group with the exception of CON and PRO groups (**Table 3.1**, PERMANOVA, $p < 0.05$), suggesting that provision of *B.p.* MP80 alone failed to impact the membership of the microbial community. However, β-diversity at baseline also differed significantly from PRE to CON and SYN treatment groups (**Table 3.1**, PERMANOVA, $p < 0.001$) and the three experimental trials (**Supplementary Table 3.1**, PERMANOVA, $p < 0.001$).

3.3.2 Gut microbial communities shift dynamically in response to synbiotic treatment

Following oral gavage on day 4, we observed a high coefficient of variation in proportions of *Bifidobacteriaceae* in the synbiotic treatment arm (**Figure 3.2c**). We therefore decided to evaluate the

microbial diversity within these mice by dividing the group into high and low bifidobacterial persistence based on the median relative abundance of *Bifidobacteriaceae* (50.5%). Microbiota composition was not significantly different at baseline for either α-diversity (t-test, $p = 0.221$) or β-diversity (weighted unifrac, $p = 0.256$) suggesting similar initial microbial distribution within and between synbiotic treated mice (**Supplementary figure 3.1**). Using a linear mixed effects model with sandwich variance to account for baseline, Shannon index, and day of gavage, we examined α-diversity over the course of 2'-FL supplementation. Interestingly, mice with high bifidobacterial persistence had significantly reduced α-diversity compared to mice with low bifidobacterial persistence (**Table 3.2**). A classification tree explored baseline differences between mice categorized as high and low bifidobacteria persistence. The tree identified that 4 of 5 mice with high bifidobacterial persistence possessed <0.9% relative abundance *Erysipelotrichaceae* (**Figure 3.3a)**. Using a chi-squared test to further explore these results, mice with <0.9% relative abundance *Erysipelotrichaeae* were significantly more likely to have high bifidobacterial persistence (X-squared = 6.185, $p = 0.0227$). To capture the stability of the gut microbial communities in mice with high versus low persistence we used linear regression with sandwich variance to estimate changes in Morisita-Horn distance from baseline to the day following oral gavage. Mice with high *Bifidobacteriaceae* persistence had a significantly increased Morisita-Horn distance compared to mice with low persistence (t-test, $p = 0.049$) indicating a reduced community stability over the course of *B.p*. MP80 gavage (**Figure 3.3b**). At the final time point (day 9), β-diversity was significantly different in mice with high compared to low persistence of *Bifidobacteriaceae* (**Figure 3.3c**, PERMANOVA, $p = 0.002$). Furthermore, differential abundance testing indicated a significantly higher log ratio of *Bifidobacteriaceae* to *Lachnospiraceae* and *Ruminococcaceae* in mice classified with high bifidobacterial persistence compared to low persistence (**Figure 3.3d**, t-test, $p = 0.001$). Moreover, the overall median proportions of *Lachnospiraceae* in the high and low persistence groups were 0.1% and 12.4% respectively while *Ruminococcaceae* was less than 0.05% and 4.1% respectively (**Supplementary figure 3.2**), further reflecting the differences in gut microbial representation across synbiotic-treated mice.

3.3.3 Microbial metabolic changes in the gut occur with pre- and syn- but not pro-biotic treatment

The metabolic output of the gut microbiota depends on the composition of microbes, substrate availability, and their related metabolic activities. We examined the metabolome of the colonic contents obtained at necropsy (day 10) using proton NMR spectroscopy. Non-metric multidimensional scaling (NMDS) revealed considerable overlap of PRO compared with CON group mice suggesting the probiotic alone does not have an effect on microbial metabolites within the gut lumen, one week after the end of supplementation (**Figure 3.4a**). The metabolite profile of prebiotic-treated mice were distinct from treatments due to changes driven primarily by monomeric fucose, propionate and succinate. Synbiotic treatment resulted in high dispersion in which five mice had distinct gut metabolite profiles that correlated with high lactate, pyruvate, formate and 1,2-propanediol (1,2-PD). Notably, these mice were those with high bifidobacteria persistence (> 50.5% *Bifidobacteriaceae*), indicating a relationship between these metabolites and the degree of colonization by bifidobacteria. Using the cutoff of 50.5% *Bifidobacteriaceae*, we compared several discriminating metabolites indicated by NMDS. Lactate, formate and 1,2-PD were all significantly higher in mice with high persistence, whereas acetate, propionate and butyrate were significantly lower in mice with low (< 50.5%) *Bifidobacteriaceae* (**Figure 3.4b**, Wilcoxon rank-sum test, $p < 0.05$). The organic acid composition in the gut was determined by summing the seven acids at highest concentration and dividing by their total to provide an overview of the relative metabolite profile by treatment (**Figure 3.4c**). Acetate was the dominate metabolite comprising over 60 percent of the total organic acid content for all except the SYN group, which was approximately 40 percent of the total. Consistent with the NMDS loadings plot, we observed elevated propionate and succinate in the PRE group relative to the other groups. Moreover, CON and PRO treated mice had similar organic acid profiles to each other which featured higher butyrate concentrations compared to PRE and SYN treated mice.

3.3.4 Changes in gut metabolite concentrations are associated with alterations in the gut microbiota

To evaluate associations between gut luminal metabolites and corresponding microbiota composition we used median metabolite concentrations as a cutoff to assess differences in overall microbial community structure and differential abundance of selected bacterial families at the final time point (day 10). Here meaning, microbial communities were evaluated by differential abundance testing and β diversity

using above and below the median metabolite concentrations as the variable being compared between groups. Mice with higher butyrate concentrations had a significantly higher log ratio of *Lachnospiraceae* and *Ruminococcaceae* relative to *Bifidobacteriaceae* (**Figure 3.5a**, Wilcoxon rank-sum test, $p = 0.003$). In mice provided 2'-FL (PRE and SYN), colonic propionate at the median cutoff was discriminatory for microbial community structure (**Figure 3.5b**, PERMANOVA, $p = 0.004$). Additionally, a significant log ratio increase of *Bacteroidaceae* to *Bifidobacteriaceae* was observed in the high propionate group (**Figure 3.5c**, Wilcoxon rank-sum test, $p = 0.015$). For mice receiving 2'-FL (PRE and SYN), the metabolite 1,2-PD produced during microbial fermentation of fucose was associated with differences in microbial communities (**Figure 3.5d**, PERMANOVA, $p = 0.028$) and a significant increase in the ratio of *Bifidobacteriaceae* to *Lachnospiraceae* and *Ruminococcaceae* (**Figure 3.5e**, t-test, $p = 0.01$).

In addition to differential abundance testing, groups were compared across treatment arms for the purpose of assessing changes in the microbiota associated with probiotic, prebiotic or synbiotic administration. Proportions of *Lachnospiraceae* and *Ruminococcaceae* were observed to be significantly higher in CON and PRO groups at the final day of sample collection (**Figure 3.6a, b**, Dunn's test, $p < 0.05$). The proportion of *Bacteroidaceae* in PRE treated mice was significantly enriched at the final day of sample collection relative to the CON group with concomitantly higher concentrations of free fucose (**Figure 3.6c, d**, Dunn's test, $p < 0.01$). Furthermore, a high correlation between *Bacteroidaceae* and propionate was detected in mice provided 2'-FL (PRE and SYN groups) (Figure 6e, Pearson's r, $r^2 = 0.741$, $p = 0.00019$), strengthening the link between the co-occurrence of *Bacteroidaceae* with high propionate levels (**Figure 3.5e**).

3.3.5 Synbiotic treatment affects systemic metabolism

Serum obtained on the final day was analyzed for metabolomics to discern changes in systemic metabolites related to treatment. Ordination by NMDS showed similar results as observed with colon content metabolites; overlap of CON and PRO groups followed by some separation with PRE treatment and diffuse SYN group dispersion (**Figure 3.7a**). Notably, the five mice exhibiting the greatest separation away from the control groups on the basis of plasma metabolome were identified as those with high

persistence (> 50.5% *Bifidobacteriaceae*) and distinct gut metabolite profiles (see **Figure 3.4a**). Metabolic features related to separation in serum were predominately fucose, formate and 1,2-PD. The higher concentrations of the fucose metabolite 1,2-PD found in the colon contents of mice with high bifidobacterial persistence were also significantly higher in the serum of these same animals (**Figure 3.7b**, t-test, $p < 0.05$) suggesting increased absorption across the gut epithelium**.** Lastly, we examined the liver and brain to determine if the perfusion of blood with enriched microbial metabolites equilibrated with these organs. Notably, only synbiotic treated mice showed detectable concentrations of 1,2-PD in liver and brain samples with none detected in the control animals (**Figure 3.7c**). Together, only persistent colonization corresponded to an increase in the microbial fermentation products 1,2-PD observed in circulation. The presence of 1,2-PD in liver and brain further indicates a systemic distribution of metabolites that occurs during synbiotic treatment.

3.4 Discussion

Previous work established that the HMO 2'-FL is sufficient to facilitate persistence of *B.p.* MP80 in a competitive environment.[28] Concordant with that study, we observed synbiotic treatment, in contrast to probiotic treatment alone, resulted in persistent colonization of *Bifidobacterium*. However, in this study amongst the synbiotic treated mice, *Bifidobacterium* populations were more heterogeneous than in the previous study, resulting in mice having either a high or low bifidobacteria count. The inability of a novel intestinal microbe to compete with the indigenous microbial community is well established, with studies indicating the degree of individual permissiveness to an invading microbe is contingent on the baseline microbial composition.[18,19,31] However, in this study no differences in baseline microbial community (α-diversity or β-diversity) were found between groups with high and low persistence of *Bifidobacteriaceae*. It should be noted that absolute bacterial values and functional capacity via metagenomics remains to be investigated. Stratification into high and low proportions of bifidobacteria were distinct throughout the experiment by α-diversity, exemplifying the diversity-invasion effect where a survival of an invader, *B.p.* MP80, is inversely correlated to species richness and evenness.[32,33] A classification tree and subsequent statistical testing identified very low baseline *Erysipelotrichaceae* relative abundance being associated with high bifidobacterial persistence. Currently, an unknown aspect of *Erysipelotrichaceae* appears to be preventing *B.p.* MP80 from effectively exploiting the 2-FL nutrient niche and outcompeting baseline microbes. Further investigation of *Eryispelotrichaceae* and colonization resistance to synbiotic treatment is required. At the final time point, the microbial community structure (β-diversity) was distinct within the symbiotic-treated group, resulting from the division of high and low *Bifidobacteriaceae* persistence.

In infants, the functional capacity to catabolize HMOs is associated with high levels of *Bifidobacterium* and their metabolites.[4,17,29,34,35] In our mouse model, a persistent, predominant *B.p.* MP80 population generated discrete metabolic profiles defined by elevated lactate, formate and 1,2-PD in the colon. Additionally, this metabolic capacity aligns with prior *in vitro* analysis of *B.p.* MP80 2'-FL catabolism.[36] Thus, the degree of *B.p.* MP80 colonization *in vivo* is commensurate with the enrichment of 2'-FL metabolites produced by *Bifidobacterium* including lactate and 1,2-PD. 2'-FL metabolites were not

enriched in mice with low *B. p.* MP80 abundance, only mice with high degrees of colonization. Lactate and 1,2-PD are found in considerably lower quantities in the adult gut due to a reduced capacity for metabolite production and/or their utilization by other microbial inhabitants.[37] As such, a lower diversity ecosystem dominated with bifidobacterial, as observed in the mice with high persistence of bifidobacterial, has greater potential to accumulate these products.

Diet-driven microbial metabolic effects have been widely studied in humans and animal models due to associated health benefits.[38–40] Here, we identified gut microbiota compositions are distinguished by their metabolic output (butyrate, propionate, and 1,2-PD). Butyrate-producing bacteria create a functional cohort where the two most abundant groups include *Eubacterium rectale/Roseburia spp.* (*Lachnospiraceae*) and *Faecalibacterium prausnitzii* (*Ruminococcaceae*). [41] As butyrate production is due to the breakdown of complex polysaccharides that reach the colon, it is expected to find butyrate concentrations associated with enrichment of *Lachnospiraceae* and *Ruminococcaceae* families in mice where chow was the predominant fiber source. However, in mice with 2'-FL supplementation, butyrate concentrations were proportionally lower, coinciding with a previous report in which 2'-FL supplementation in mice was associated with reduced butyrate.[42] We observed provision of 2'-FL in the prebiotic and symbiotic treated mice corresponded with enrichment of *Bacteroidaceae* in the murine gut at each sampling period. *Bacteroides* species typically possess several polysaccharide utilization loci in their genomes that enable cleavage of a variety of glycosidic linkages including HMO.[43] Metabolically, *Bacteroides* is a primary producer of propionate in the gut microbiome via the succinate pathway.[44,45] Therefore, in cases where 2'-FL provision resulted in high propionate, indigenous *Bacteroidaceae* likely outcompeted the autochthonous microbial community in prebiotic fed mice and *B.p.* MP80 in those receiving the symbiotic treatment. These data are similar to previous reports that describe the high prevalence of *Bacteroides* in the gut microbiota of breastfed infants[46] which likely arises from the opportunistic utilization of HMOs. Competition between *Bacteroides* and *Bifidobacterium* for the HMO nutrient niche[47] is recapitulated in this mouse model, as evidenced by the greater enrichment of *Bacteroidaceae* in the mice receiving only 2'-FL relative to those provided the synbiotic which had higher

proportions of *Bifidobacteriaceae*. Additionally, mice with high concentrations of 1,2-PD in the gut were enriched in *Bifidobacteriaceae*. The propanediol pathway, common to *Bifidobacterium*, characteristically produces 1,2-PD from the metabolism of fucose, and is found to be elevated in infants enriched with *Bifidobacteriaceae.*[46,47] [36,48,49] In our model, high concentrations of 1,2-PD were observed only in mice with high *Bifidobacteriaceae* suggesting a related source of this metabolite.

Some microbial metabolites produced in the intestine can be absorbed across the gut epithelium into systemic circulation. We found that each treatment group exhibited a similar pattern of serum and colonic content metabolite profiles. Notably, significantly higher concentrations of 1,2-PD in serum was observed in mice with high persistence of *Bifidobacteriaceae*, suggesting that in this model probiotic persistence (enabled by co-administration of prebiotic 2'FL) is necessary to produce metabolites at a sufficient concentration to be detected systemically. Evidence of this relationship has been shown in human adults in which the provision of *Bifidobacterium animalis* subsp. *lactis* (*B. lactis*) and fructooligosaccharides had resulted in higher concentrations of serum metabolites compared to *B. lactis* alone.[50] The absorption of microbial metabolites into the circulation has the potential to interact with receptors expressed peripheral tissues and to influence their function. Metabolite profiles in liver and brain were similar between control and synbiotic treated mice, with the exception of 1,2-PD which was only detected in the liver and brain of synbiotic treated mice with high persistence of *Bifidobacteriaceae*. Based on these data, we conclude that the high concentration of 1,2-PD in the gut generated by microbial fermentation of fucose is absorbed and reaches peripheral tissues such as the brain. Prior work using ^{13}C-labeled 2'-FL orally administered to mice showed that ^{13}C enrichment occurred in tissues including liver and brain.[51] Moreover, ^{13}C label was not detected in tissues following 2'-FL administered to germ-free mice indicating that the gut microbiota is fundamental to enrichment of 2'-FL. Additionally, intravenous administration resulted in excretion of ^{13}C in urine, further supporting that microbial metabolism is a precursor to tissue incorporation. Here we provide evidence that fermentation of 2'-FL by gut microbes produce metabolites that enter the circulation. This is potentially important considering the assembly of the gut microbiota in early life could tune host metabolic processes that impact cognitive and metabolic

development. Understanding the contribution of microbial metabolites at this stage of life will be instrumental in the development and use of biologics to confer well-being throughout the lifespan.

In summary, we found that introducing *B.p.* MP80 into the colonized murine gut environment requires concomitant provision of a nutrient niche (2'-FL) to modulate metabolism at the local and systemic level. Without this advantage, colonization resistance cannot be overcome as the community structure reconfigures to the pre-treatment condition following probiotic inoculation. Additionally, this reinforces the finding that HMO act as a privileged nutrient resource for a competitive population of *Bifidobacterium*, although the permissiveness to colonization does have variability. Moreover, enrichment of microbial metabolites is dependent on persistent colonization of *B.p.* MP80 and are reflected by bifidobacterial products of 2'-FL catabolism throughout the host organism.

Our study does have limitations; although mice were ordered from the same vendor and facility, the baseline microbial community structure was distinct between cohorts. This limitation directly affected differential abundance testing where ASVs were grouped by bacterial family for data processing. While this reduced analysis granularity, the fact that differential abundance at the bacterial family level was statistically significant demonstrates how strongly associated diet and microbial communities were within this study. Additionally, the number of mice in each group were not evenly distributed amongst experimental groups and cohorts which may also contribute to microbial community differences between treatments at baseline. The established microbial community of the mouse gut does not perfectly exemplify the human gut microbiota nor identically capture the competition for resources and available physical niches. This model assessed how infant-borne *Bifidobacterium* strains are competitive, persistent and metabolically active when a privileged nutrient source is provided, even in a non-indigenous environment. Developing an ecological framework through the use of synbiotics or their components is crucial for discovering the underlying mechanisms of synbiotic-associated health outcomes. Overall, such findings will aid in pinpointing synbiotic pairings that possess a higher likelihood of conferring health benefits to the host.

3.5 Methods

3.5.1 Mouse study design

Animals were maintained in accordance with IACUC Protocol 21900 approved by the Institutional Animal Care and Use Committee of University of California, Davis. Male C57BL/6J mice (5-6 weeks old, Jackson Labs) were group housed (3 per cage) and maintained at 22C with 12-hour light-dark cycle. Before commencing experiments, mice were acclimated for a minimum of one week at the facility. Food (5058 Irradiated Pico Mouse Lab Diet) and water were provided *ad libitum*. 2'-FL was provided in the drinking water as a 10% (w/v) solution. Under anaerobic conditions at 37°C, *B.p.* MP80 was grown in de Man, Rogosa, and Sharpe media (BD Difco Microbiology, Houston, TX) supplemented with 0.05% w/v L-cysteine (Sigma-Aldrich, St. Louis, MO). *B.p.* MP80 (10^9 cfu/ml in PBS) or phosphate buffered saline was administered via oral gavage (100µl) for three days. Within 1 hour of the light cycle's start fecal samples were collected from individual mice. For validation, experiments were conducted in three separate cohorts. The experimental protocols were identical between cohorts although the number of sampling days and final time point varied. For cohorts 1 and 2, samples were collected at baseline (day 0) and days 2, 4, 6 and a final time point at either day 9 or 10, respectively. For cohort 3, samples were collected at baseline and days 4 and 10. Mice were euthanized via CO_2 asphyxiation.

3.5.2 Fecal extraction and microbial DNA sequencing

DNA was extracted from stool samples (30-100 mg) using the Quick-DNA Fecal/Soil Microbe Miniprep Kit, Catalog No. D6010 (ZYMO, Irvine, CA, USA). Following the manufacturer's instructions, the extraction protocol included a bead-beating step using a FastPrep-24 Instrument (MP Biomedicals, Santa Ana, CA, USA) for a total of 2 min at 25°C at a speed of 6.5 m/s. The V4 region of the 16S rRNA gene was amplified in triplicate with barcoded PCR primers F515 (5′-CACGGTCGKCGGCGCCATT-3′) and R806 (5-′GGACTACHVGGGTWTCTAAT-3′) modified to contain an adapter region for sequencing on the Illumina MiSeq platform.[52] Amplicons were verified by gel electrophoresis, combined, purified, and sent to the UC Davis Genome Center for library preparation and high throughput 250-bp paired-end sequencing. Raw sequencing data was demultiplexed and quality filtered before import into QIIME2-

2019.7.[53] Samples with poor quality data were excluded from analysis. After trimming, reads were processed with DADA2.[54] Filtered sequences were aligned and taxonomy was assigned using the 99% SILVA naïve Bayesian classifier.[55] Samples were rarified to 3000 sequences. The NCBI BioProject ID for raw 16s sequencing data is PRJNA725904.

3.5.3 Statistics (Microbial ecosystem)

Microbial community statistical analysis was performed in R (version 4.0.2). For each fecal sample, α-diversity was measured with Shannon Index values (vegan::diversity). A linear regression was used to test α-diversity differences between high and low bifidobacteria groups amongst *B.p.* MP80+2'-FL treated mice. Included in the LME analysis (lme4::lmer)[56] were robust sandwich variance estimates (clubSandwich::vcovCR)[57] and a degrees of freedom Satterthwaite correction (clubSandwich::coef_test). The GLM analysis (lme4::glm) for Morisita-Horn stability (vegan::vegdist, method = "horn") also included robust sandwich variance estimates and a degrees of freedom Satterthwaite correction. β-diversity was measured by Unifrac distances (GUnifrac) and visualized using non-metric multidimensional scaling (NMDS) (vegan::metaMDS, k=2).[58] β-diversity statistical analysis consisted of checking dispersion (vegan::betadisper), a permutational multivariate ANOVA (vegan::adonis2, 999 permutations), and post hoc testing (RVAideMemoire::pairwise.perm.manova, nperm = "500").[59] The strata argument was used to constrain by mouse subject when longitudinal data was examined. Songbird was employed for differential abundance testing which ranks the log-fold changes between selected features.[60] Due to a lack of ASV overlap between cohorts, ASVs were aggregated by bacterial family for Songbird analysis. Songbird analysis to differentiate between high and low bifidobacteria categories included samples from SYN treated mice at the final time point and accounted for experimental trial differences. Songbird formulas tested the association between final time point microbial communities and metabolites (butyrate, propionate, and 1,2-PD) while accounting for experimental trials. For statistical testing, the metabolite median was used as a cut off for high or low metabolite production. Based on being the highest or lowest ranked features, bacterial families *Bifidobaceriaceae*, *Bacteroidaceae*, *Lachnospiraceae* and *Ruminococcaceae* were chosen as the

numerator or denominator for respective analyses. Differential abundance associations with propionate resulted in a lower number of log ratios because two samples failed to have any *Bacteroidaceae* reads, resulting in no log ratio for two fecal samples. Differential abundance log ratios were assessed for normality using a Shapiro-Wilk test which determined whether a Student's t-Test or Wilcoxon Rank Sum test was employed. A classification tree was generated to differentiate between high and low bifidobacteria categorized mice with the minimum split reduced due to a small number of subjects (rpart::rpart, minsplit = 2).[61] Post hoc testing of associations were conducted with Pearson's Chi-squared test (stats::chisq.test). Corrections were applied for multiple comparisons by Benjamini-Hochberg.

3.5.4 Metabolomics sample preparation

Colon contents were weighed and combined with 500 µL aliquots of ice-cold PBS. Samples were then vortexed for 2 minutes, incubated on ice for 5 minutes and vortexed for 2 additional minutes before centrifugation (6000 x RCF, 15 minutes, 4° C). Supernatant was transferred to a new tube and the pellets were dried in a miVac sample concentrator to determine dry weight. After an additional centrifugation step (14k RCF, 10 minutes, 4° C), the supernatant was transferred to 3 kDa filters and centrifuged again (14k RCF, 60 minutes, 4° C). 207 µL of filtrate was transferred to a new tube, and combined with 23 µL of internal standard consisting of 4.8 mM DSS-d_6 containing 0.2% NaN3 (to inhibit bacterial growth) in 99.8% D2O. pH was adjusted to 6.7-6.9 with NaOH or HCl prior to transfer to 3mm NMR tubes. Sera were thawed on ice and transferred to 3 kDa filters. After 60 minutes of centrifugation (4° C, 14000 x RCF) 207 µL of filtrate was combined with 23 µL of 4.8 mM DSS-d_6. pH was adjusted to to 6.7-6.9 with NaOH or HCl. Thawed liver samples were weighed and combined with 900 µL of ice-cold PBS in an MB Bio Lysing matrix D bead beating tube (MP Biomedicals, USA). Samples were homogenized using a FastPrep-24 bead beater (MP Biomedicals, USA) for 60 seconds at six meters per second and repeated for a total of two minutes. Liver homogenate was centrifuged for 10 seconds and cooled on ice for one minute followed by additional centrifugation for 15 minutes (14k RCF, 4° C). Supernatant was then transferred to a new tube and spun down for 10 minutes at 14k RCF and 4° C. Supernatant was transferred to a 3 kD molecular

weight filter and centrifuged for 45 minutes at 14k RCF and 4° C. 207 µL of filtrate was transferred to a new tube and combined with 23 µL of 4.8 mM DSS-d_6 and pH was adjusted to between 6.7 and 6.9. Brain samples were thawed, weighed and combined with 550 µL of ice-cold PBS followed by homogenization by bead beating using MB Bio Lysing matrix D bead beating tube (MP Biomedicals, USA) for one minute at six meters per second and repeated for a total of two minutes. Samples were spun down for 10 seconds and incubated on ice for 1 minute followed by centrifugation for 15 minutes at 14k RCF and 4° C. Supernatant was transferred to a new tube and centrifuged for 10 min at 14k RCF and 4° C and then transferred to a 3 kD molecular weight filter followed by an additional centrifugation for 45 minutes at 14k RCF and 4° C. 207 µL of filtrate was combined with 23 µL of 4.8 mM DSS-d_6 in a new tube and pH was adjusted to between 6.7 and 6.9.

3.5.5 Acquisition parameters for ^{1}H-NMR

^{1}H NMR spectra were acquired at 298K using the NOESY 1H pre-saturation experiment ('noesypr1d') on a Bruker Avance 600 MHz NMR spectrometer (Bruker BioSpin, Germany). Data acquisition was achieved with the following parameters; 8 dummy scans and 32 transients over a spectral width of 12 ppm and a total acquisition time of 2.5 s. Water saturation was applied during relaxation delay (2.5 s) and mixing time (100 ms). The resulting spectra were Fourier transformed with zero filling to 128k data points and the Free Induction Decays (FIDs) were transformed with an exponential apodization function corresponding to a line broadening of 0.5 Hz. Chenomx NMR Suite v8.4 (Chenomx Inc, Edmonton, Alberta, Canada) was used to manually phase and correct baseline spectra. Each metabolite was assigned manually and quantified using Chenomx Profiler.

3.5.6 Statistics (Metabolites)

All metabolite statistical analyses and graphics were generated using R (v4.0.2). Non-metric multidimensional scaling (NMDS) plots were generated (vegan::metaMDS, k = 2, distance = "euclidian"). Normality was assessed using the Shapiro-Wilk test in addition to observing deviations in the residuals of Quantile-Quantile plots. Group comparisons were evaluated using Student's t-test. Corrections were

applied for multiple comparisons by either false discovery rate correction or Benjamini-Hochberg when appropriate. Statistical significance was considered as $\alpha < 0.05$ and statistical trends for $\alpha < 0.1$.

3.6 References

1. Gyorgy P, Norris RF, Rose CS. Bifidus factor. I. A variant of Lactobacillus bifidus requiring a special growth factor. Arch Biochem Biophys 1954; 48:193–201.

2. Davis JCC, Totten SM, Huang JO, Nagshbandi S, Kirmiz N, Garrido DA, Lewis ZT, Wu LD, Smilowitz JT, German JB, et al. Identification of Oligosaccharides in Feces of Breast-fed Infants and Their Correlation with the Gut Microbial Community. Mol Cell Proteomics 2016; 15:2987–3002.

3. Totten SM, Zivkovic AM, Wu S, Ngyuen U, Freeman SL, Ruhaak LR, Darboe MK, German JB, Prentice AM, Lebrilla CB. Comprehensive profiles of human milk oligosaccharides yield highly sensitive and specific markers for determining secretor status in lactating mothers. J Proteome Res 2012; 11:6124–33.

4. Sakanaka M, Hansen ME, Gotoh A, Katoh T, Yoshida K, Odamaki T, Yachi H, Sugiyama Y, Kurihara S, Hirose J, et al. Evolutionary adaptation in fucosyllactose uptake systems supports bifidobacteria-infant symbiosis. Sci Adv 2019; 5:eaaw7696.

5. Lawson MAE, O'Neill IJ, Kujawska M, Gowrinadh Javvadi S, Wijeyesekera A, Flegg Z, Chalklen L, Hall LJ. Breast milk-derived human milk oligosaccharides promote Bifidobacterium interactions within a single ecosystem. ISME J 2020; 14:635–48.

6. Vatanen T, Plichta DR, Somani J, Münch PC, Arthur TD, Hall AB, Rudolf S, Oakeley EJ, Ke X, Young RA, et al. Genomic variation and strain-specific functional adaptation in the human gut microbiome during early life. Nat Microbiol 2019; 4:470–9.

7. Karav S, Casaburi G, Frese SA. Reduced colonic mucin degradation in breastfed infants colonized by Bifidobacterium longum subsp. infantis EVC001. FEBS Open Bio 2018; 8:1649–57.

8. Casaburi G, Duar RM, Vance DP, Mitchell R, Contreras L, Frese SA, Smilowitz JT, Underwood MA. Early-life gut microbiome modulation reduces the abundance of antibiotic-resistant bacteria. Antimicrob Resist Infect Control 2019; 8:131.

9. Matsuki T, Yahagi K, Mori H, Matsumoto H, Hara T, Tajima S, Ogawa E, Kodama H, Yamamoto K, Yamada T, et al. A key genetic factor for fucosyllactose utilization affects infant gut microbiota development. Nat Commun 2016; 7:11939.

10. Henrick BM, Chew S, Casaburi G, Brown HK, Frese SA, Zhou Y, Underwood MA, Smilowitz JT. Colonization by B. infantis EVC001 modulates enteric inflammation in exclusively breastfed infants. Pediatr Res 2019; 86:749–57.

11. Lewis ZT, Totten SM, Smilowitz JT, Popovic M, Parker E, Lemay DG, Van Tassell ML, Miller MJ, Jin Y-S, German JB, et al. Maternal fucosyltransferase 2 status affects the gut bifidobacterial communities of breastfed infants. Microbiome 2015; 3:13.

12. Vatanen T, Kostic AD, d'Hennezel E, Siljander H, Franzosa EA, Yassour M, Kolde R, Vlamakis H, Arthur TD, Hämäläinen A-M, et al. Variation in microbiome LPS immunogenicity contributes to autoimmunity in humans. Cell 2016; 165:842–53.

13. Kalliomäki M, Collado MC, Salminen S, Isolauri E. Early differences in fecal microbiota composition in children may predict overweight. Am J Clin Nutr 2008; 87:534–8.

14. Stanislawski MA, Dabelea D, Wagner BD, Iszatt N, Dahl C, Sontag MK, Knight R, Lozupone CA, Eggesbø M. Gut Microbiota in the First 2 Years of Life and the Association with Body Mass Index at Age 12 in a Norwegian Birth Cohort. MBio 2018; 9.

15. Huda MN, Ahmad SM, Alam MJ, Khanam A, Kalanetra KM, Taft DH, Raqib R, Underwood MA, Mills DA, Stephensen CB. Bifidobacterium abundance in early infancy and vaccine response at 2 years of age. Pediatrics 2019; 143.

16. Taft DH, Liu J, Maldonado-Gomez MX, Akre S, Huda MN, Ahmad SM, Stephensen CB, Mills DA. Bifidobacterial dominance of the gut in early life and acquisition of antimicrobial resistance. mSphere 2018; 3.

17. Nguyen M, Holdbrooks H, Mishra P, Abrantes MA, Eskew S, Garma M, Oca C-G, McGuckin C, Hein CB, Mitchell RD, et al. Impact of Probiotic B. infantis EVC001 Feeding in Premature Infants on the Gut Microbiome, Nosocomially Acquired Antibiotic Resistance, and Enteric Inflammation. Front Pediatr 2021; 9:618009.

18. Zmora N, Zilberman-Schapira G, Suez J, Mor U, Dori-Bachash M, Bashiardes S, Kotler E, Zur M, Regev-Lehavi D, Brik RB-Z, et al. Personalized Gut Mucosal Colonization Resistance to Empiric Probiotics Is Associated with Unique Host and Microbiome Features. Cell 2018; 174:1388–1405.e21.

19. Maldonado-Gómez MX, Martínez I, Bottacini F, O'Callaghan A, Ventura M, van Sinderen D, Hillmann B, Vangay P, Knights D, Hutkins RW, et al. Stable Engraftment of Bifidobacterium longum AH1206 in the Human Gut Depends on Individualized Features of the Resident Microbiome. Cell Host Microbe 2016; 20:515–26.

20. Martínez I, Maldonado-Gomez MX, Gomes-Neto JC, Kittana H, Ding H, Schmaltz R, Joglekar P, Cardona RJ, Marsteller NL, Kembel SW, et al. Experimental evaluation of the importance of colonization history in early-life gut microbiota assembly. Elife 2018; 7.

21. Benson AK, Kelly SA, Legge R, Ma F, Low SJ, Kim J, Zhang M, Oh PL, Nehrenberg D, Hua K, et al. Individuality in gut microbiota composition is a complex polygenic trait shaped by multiple environmental and host genetic factors. Proc Natl Acad Sci USA 2010; 107:18933–8.

22. Carmody RN, Gerber GK, Luevano JM, Gatti DM, Somes L, Svenson KL, Turnbaugh PJ. Diet dominates host genotype in shaping the murine gut microbiota. Cell Host Microbe 2015; 17:72–84.

23. Suez J, Zmora N, Segal E, Elinav E. The pros, cons, and many unknowns of probiotics. Nat Med 2019; 25:716–29.

24. Swanson KS, Gibson GR, Hutkins R, Reimer RA, Reid G, Verbeke K, Scott KP, Holscher HD, Azad MB, Delzenne NM, et al. The International Scientific Association for Probiotics and Prebiotics (ISAPP) consensus statement on the definition and scope of synbiotics. Nat Rev Gastroenterol Hepatol 2020; 17:687–701.

25. Bertuzzo E, Suweis S, Mari L, Maritan A, Rodríguez-Iturbe I, Rinaldo A. Spatial effects on species persistence and implications for biodiversity. Proc Natl Acad Sci USA 2011; 108:4346–51.

26. Walter J, Maldonado-Gómez MX, Martínez I. To engraft or not to engraft: an ecological framework for gut microbiome modulation with live microbes. Curr Opin Biotechnol 2018; 49:129–39.

27. Zhang C, Derrien M, Levenez F, Brazeilles R, Ballal SA, Kim J, Degivry M-C, Quéré G, Garault P, van Hylckama Vlieg JET, et al. Ecological robustness of the gut microbiota in response to ingestion of transient food-borne microbes. ISME J 2016; 10:2235–45.

28. Heiss B, Ehrlich A, Maldonado-Gomez M, Taft D, Larke J, Goodson M, Slupsky C, Tancredi D, Raybould H, Mills D. Bifidobacterium catabolism of human milk oligosaccharides overrides endogenous competitive exclusion driving colonization and protection. Gut Microbes 2021;

29. Frese SA, Hutton AA, Contreras LN, Shaw CA, Palumbo MC, Casaburi G, Xu G, Davis JCC, Lebrilla CB, Henrick BM, et al. Persistence of Supplemented Bifidobacterium longum subsp. infantis EVC001 in Breastfed Infants. mSphere 2017; 2.

30. O'Brien CE, Meier AK, Cernioglo K, Mitchell RD, Casaburi G, Frese SA, Henrick BM, Underwood MA, Smilowitz JT. Early probiotic supplementation with B. infantis in breastfed infants leads to persistent colonization at 1 year. Pediatr Res 2021;

31. Davis L, Martínez I, Walter J, Goin C, Hutkins R. Barcoded Pyrosequencing Reveals That Consumption of Galactooligosaccharides Results in a Highly Specific Bifidogenic Response in Humans. PLoS One 2011; 6.

32. Mallon CA, Elsas JD van, Salles JF. Microbial invasions: the process, patterns, and mechanisms. Trends Microbiol 2015; 23:719–29.

33. van Elsas JD, Chiurazzi M, Mallon CA, Elhottova D, Kristufek V, Salles JF. Microbial diversity determines the invasion of soil by a bacterial pathogen. Proc Natl Acad Sci USA 2012; 109:1159–64.

34. Chow J, Panasevich MR, Alexander D, Vester Boler BM, Rossoni Serao MC, Faber TA, Bauer LL, Fahey GC. Fecal metabolomics of healthy breast-fed versus formula-fed infants before and during in vitro batch culture fermentation. J Proteome Res 2014; 13:2534–42.

35. He X, Parenti M, Grip T, Lönnerdal B, Timby N, Domellöf M, Hernell O, Slupsky CM. Fecal microbiome and metabolome of infants fed bovine MFGM supplemented formula or standard formula with breast-fed infants as reference: a randomized controlled trial. Sci Rep 2019; 9:11589.

36. Shani G, Hoeflinger J, Heiss B, Masarweh C, Larke J, Jensen N, Wickramasinghe S, Davis J, Goonatilleke E, El-Hawiet A, et al. Fucosylated human milkoligosaccharide foraging within the species Bifidobacterium pseudocatenulatum is driven by glycosyl hydrolase content and specificity. 2021;

37. Flint HJ, Duncan SH, Scott KP, Louis P. Links between Diet, Gut Microbiota Composition and Gut Metabolism. Proc Nutr Soc 2015; 74:13–22.

38. So D, Whelan K, Rossi M, Morrison M, Holtmann G, Kelly J, Shanahan E, Staudacher H, Campbell K. Dietary fiber intervention on gut microbiota composition in healthy adults: a systematic review and meta-analysis. Am J Clin Nutr 2018; 107:965–83.

39. Krumbeck JA, Walter J, Hutkins RW. Synbiotics for improved human health: recent developments, challenges, and opportunities. Annu Rev Food Sci Technol 2018; 9:451–79.

40. Krumbeck JA, Maldonado-Gomez MX, Ramer-Tait AE, Hutkins RW. Prebiotics and synbiotics: dietary strategies for improving gut health. Curr Opin Gastroenterol 2016; 32:110–9.

41. Louis P, Flint HJ. Diversity, metabolism and microbial ecology of butyrate-producing bacteria from the human large intestine. FEMS Microbiol Lett 2009; 294:1–8.

42. Lee S, Goodson M, Vang W, Kalanetra K, Barile D, Raybould H. 2'-fucosyllactose Supplementation Improves Gut-Brain Signaling and Diet-Induced Obese Phenotype and Changes the Gut Microbiota in High Fat-Fed Mice. Nutrients 2020; 12.

43. Marcobal A, Sonnenburg JL. Human milk oligosaccharide consumption by intestinal microbiota. Clin Microbiol Infect 2012; 18 Suppl 4:12–5.

44. Salonen A, Lahti L, Salojärvi J, Holtrop G, Korpela K, Duncan SH, Date P, Farquharson F, Johnstone AM, Lobley GE, et al. Impact of diet and individual variation on intestinal microbiota composition and fermentation products in obese men. ISME J 2014; 8:2218–30.

45. Louis P, Flint HJ. Formation of propionate and butyrate by the human colonic microbiota. Environ Microbiol 2017; 19:29–41.

46. Rotimi V, Duerden B. THE DEVELOPMENT OF THE BACTERIAL FLORA IN NORMAL NEONATES. J Med Microbiol 1981;

47. Marcobal A, Barboza M, Sonnenburg ED, Pudlo N, Martens EC, Desai P, Lebrilla CB, Weimer BC, Mills DA, German JB, et al. Bacteroides in the infant gut consume milk oligosaccharides via mucus-utilization pathways. Cell Host Microbe 2011; 10:507–14.

48. He X, Parenti M, Grip T, Domellöf M, Lönnerdal B, Hernell O, Timby N, Slupsky CM. Metabolic phenotype of breast-fed infants, and infants fed standard formula or bovine MFGM supplemented formula: a randomized controlled trial. Sci Rep 2019; 9:339.

49. Lee H, Slupsky CM, Heckmann AB, Christensen B, Peng Y, Li X, Hernell O, Lönnerdal B, Li Z. Milk Fat Globule Membrane as a Modulator of Infant Metabolism and Gut Microbiota: A Formula Supplement Narrowing the Metabolic Differences between Breastfed and Formula-Fed Infants. Mol Nutr Food Res 2021; 65:e2000603.

50. Crovesy L, El-Bacha T, Rosado EL. Modulation of the gut microbiota by probiotics and symbiotics is associated with changes in serum metabolite profile related to a decrease in inflammation and overall benefits to metabolic health: a double-blind randomized controlled clinical trial in women with obesity. Food Funct 2021; 12:2161–70.

51. Kuntz S, Kunz C, Borsch C, Vazquez E, Buck R, Reutzel M, Eckert GP, Rudloff S. Metabolic Fate and Distribution of 2´-Fucosyllactose: Direct Influence on Gut Microbial Activity but not on Brain. Mol Nutr Food Res 2019; :e1900035.

52. Caporaso JG, Lauber CL, Walters WA, Berg-Lyons D, Lozupone CA, Turnbaugh PJ, Fierer N, Knight R. Global patterns of 16S rRNA diversity at a depth of millions of sequences per sample. Proc Natl Acad Sci USA 2011; 108 Suppl 1:4516–22.

53. Bolyen E, Rideout JR, Dillon MR, Bokulich NA, Abnet CC, Al-Ghalith GA, Alexander H, Alm EJ, Arumugam M, Asnicar F, et al. Reproducible, interactive, scalable and extensible microbiome data science using QIIME 2. Nat Biotechnol 2019; 37:852–7.

54. Callahan BJ, McMurdie PJ, Rosen MJ, Han AW, Johnson AJA, Holmes SP. DADA2: High-resolution sample inference from Illumina amplicon data. Nat Methods 2016; 13:581–3.

55. Quast C, Pruesse E, Yilmaz P, Gerken J, Schweer T, Yarza P, Peplies J, Glöckner FO. The SILVA ribosomal RNA gene database project: improved data processing and web-based tools. Nucleic Acids Res 2013; 41:D590-6.

56. Bates D, Mächler M, Bolker B, Walker S. Fitting linear mixed-effects models using lme4. J Stat Softw 2015; 67:1–48.

57. Pustejovsky J. clubSandwich: Cluster-Robust (Sandwich) Variance Estimators with Small-Sample Corrections. R; 2020.

58. Oksanen J, Blanchet FG, Friendly M, Kindt R, Legendre P, McGlinn D, Minchin PR, O'Hara RB, Simpson GL, Solymos P, et al. vegan: Community Ecology Package [Internet]. R; 2019 [cited 2020 Jul 20]. Available from: https://CRAN.R-project.org/package=vegan

59. Hervé M. RVAideMemoire: Testing and Plotting Procedures for Biostatistics. R; 2020.

60. Morton JT, Marotz C, Washburne A, Silverman J, Zaramela LS, Edlund A, Zengler K, Knight R. Establishing microbial composition measurement standards with reference frames. Nat Commun 2019; 10:2719.

61. Therneau T, Atkinson E. An Introduction to Recursive Partitioning Using the RPART Routines. 2019;

Table 3.1. Pairwise comparisons of weighted UniFrac measures between treatment groups at the baseline and final time points.

	Baseline		
	Synbiotic	Probiotic	Prebiotic
Untreated Control	0.567	0.311	**0.040**
Prebiotic	**0.024**	0.40	
Probiotic	0.311		
	Final		
	Synbiotic	Probiotic	Prebiotic
Untreated Control	**0.024**	0.076	**0.006**
Prebiotic	**0.008**	**0.006**	
Probiotic	**0.009**		

Table 3.2. Linear regression model of Shannon Index (α-diversity) values for Synbiotic (*B.p.* MP80 + 2'FL) treated mice.

	Beta Coefficients	t-statistic	Lower 95% CI	Upper 95% CI	*p*-value*
High Bif. persistence	-0.578	-2.74	-1.07	-0.09	**0.0271**
Baseline Shannon Index	1.393	3.06	0.27	2.52	**0.0232**
Day of Gavage	0.651	4.33	0.32	0.98	**<0.001**

Supplementary Table 3.1. Pairwise comparisons* of weighted UniFrac measures between experimental cohorts at baseline.

	First Exp. Cohort	Second Exp. Cohort
Second Experimental Cohort	**0.021**	
Third Experimental Cohort	**0.021**	0.148

*Comparisons were evaluated using PERMANOVA and FDR adjustment.
p-values with statistical significance are denoted in bold.

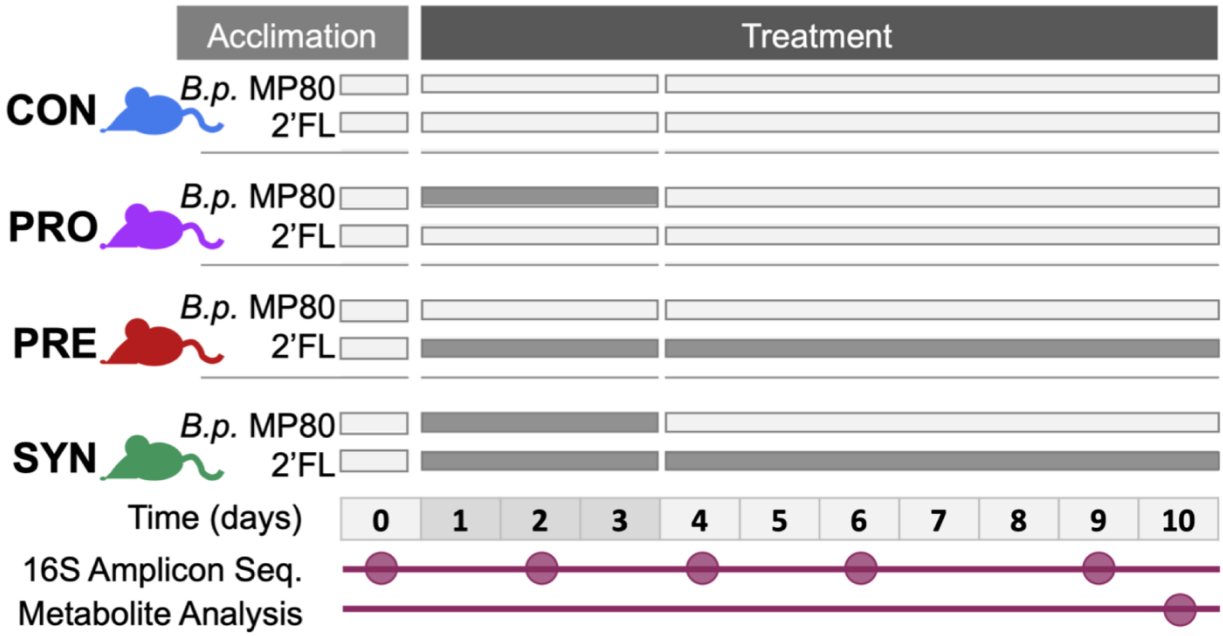

Figure 3.1. Mouse experimental design as a timeline. Treatment groups consisted of untreated control (CON): oral gavage of PBS (day 1-3) and drinking water (day 1-10), probiotic (PRO): oral gavage of *B.p.* MP80 (day 1-3) and drinking water (day 1-10), prebiotic (PRE): oral gavage of PBS (day 1-3) and 2-FL in drinking water (day 1-10), and synbiotic (SYN): oral gavage of *B.p.* MP80 (day 1-3) and 2-FL in drinking water (day 1-10). Fecal samples collected for 16S amplicon sequencing throughout the experiment, samples for metabolite analysis were collected at necropsy.

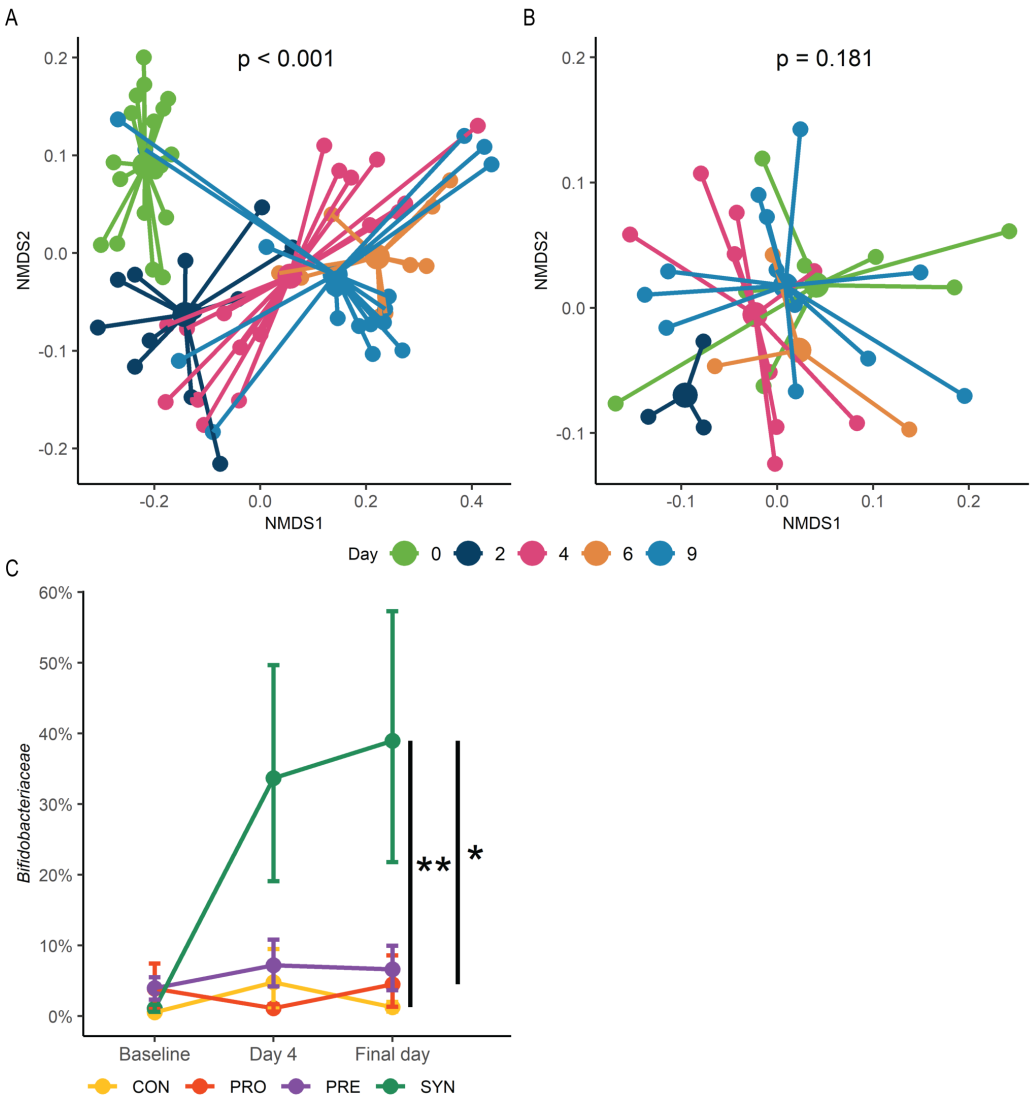

Figure 3.2. Microbial community structure changes during synbiotic treatment. (A) Microbial community NMDS plot of synbiotic-treated mice (day 0 to final time point) colored by day (n = 12); (B) microbial community NMDS plot of probiotic-treated mice (day 0 to final time point) colored by day (n = 9); and (C) relative abundance of *Bifidobacteriaceae* in synbiotic (n = 12) and probiotic (n = 9) groups from baseline, after oral gavage (day 4) and one week following (final day). Final day, while grouped as day 9 for A, consists of day 9 or 10 depending on the experiment. NMDS was generated using β-diversity index weighted unifrac distance in two dimensions. Error bars for relative abundance data is represented as mean and standard error from bootstrapped confidence intervals with 1000 iterations.

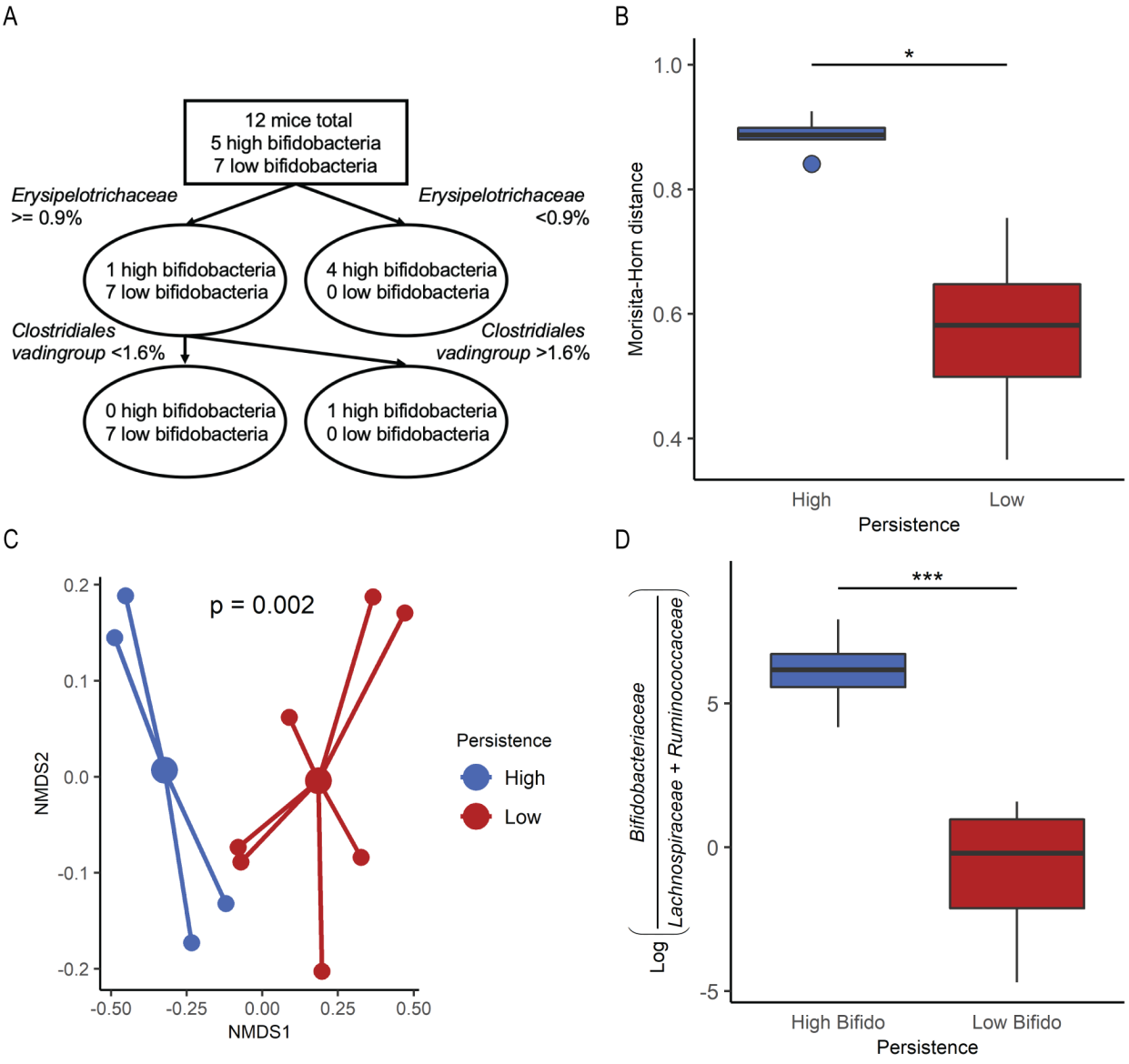

10

11 **Figure 3.3.** Microbial community differences between high and low bifidobacteria categorizations within
12 symbiotic-treated mice. (A) Classification tree distinguishes mice with high and low bifidobacteria based
13 on other microbial taxa; (B) Morisita-Horn distances for synbiotic-treated mice grouped as high ($n = 4$) and
14 low ($n = 7$) bifidobacteria; (C) microbial community NMDS plot of high and low bifidobacteria groups at
15 the final time point, colored by high and low; (D) log ratio of *Bifidobacteriaceae* relative to
16 *Lachnospiraceae* and *Ruminococcaceae* on the final day of the experiment. Boxplots represent medians
17 and interquartile range (IQR) with whisker end points equal to the maximum and minimum values below

or above the median at 1.5 times the IQR. NMDS was generated using β-diversity index weighted unifrac distance in two dimensions.

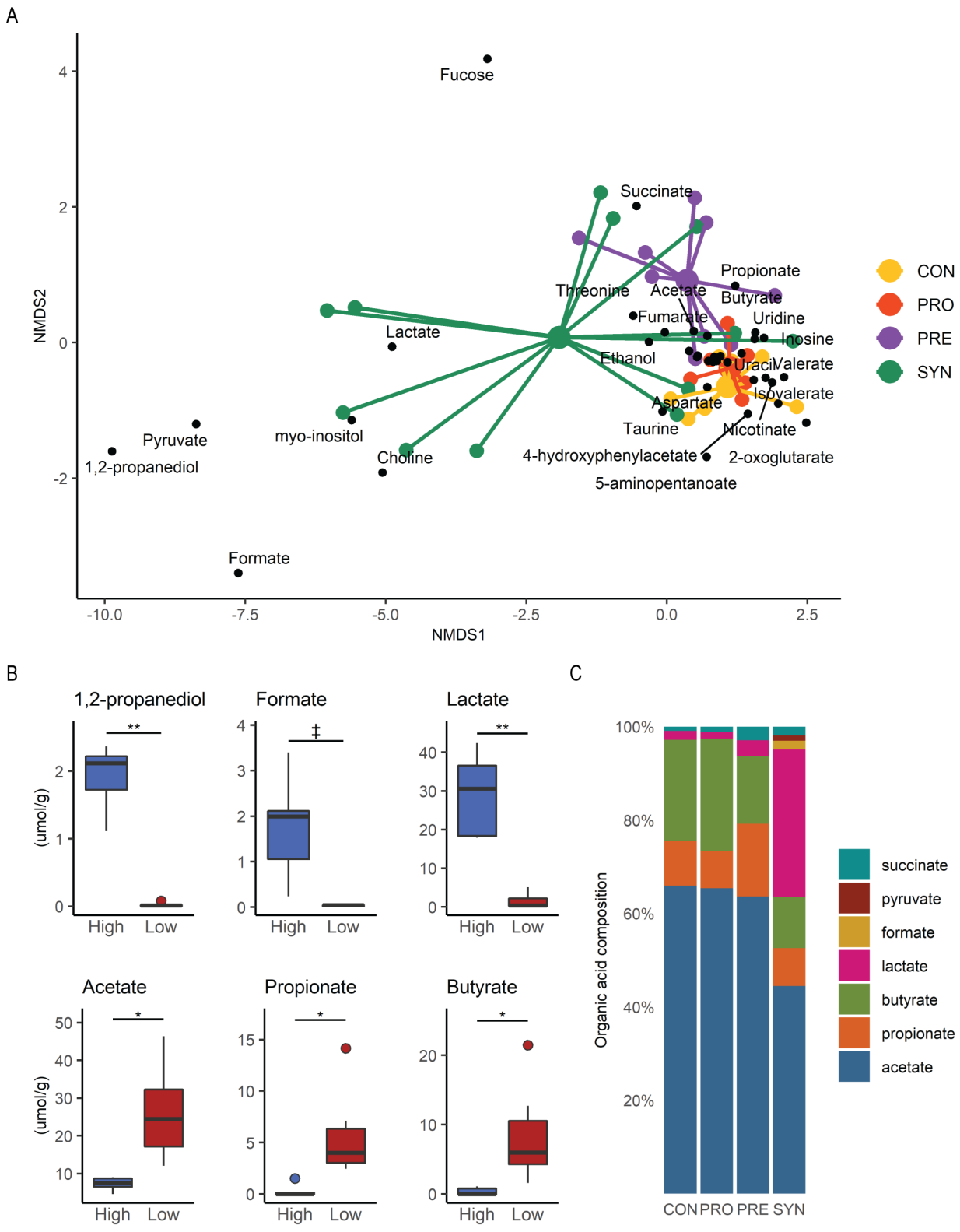

Figure 3.4. Metabolic profiling of colon contents reveal distinct compositions in synbiotic-treated mice

with high persistence of bifidobacteria. (A) NMDS plot of mouse colonic metabolome at the final experimental time point; (B) colonic metabolites differ across high and low persistence of *Bifidobacteriaceae* by high (n = 4) and low (n = 7); and (C) organic acid composition across treatment groups. ** $p < 0.01$, * $p = < 0.05$, ‡ $p < 0.1$. NMDS was generated using Euclidian distance in two dimensions. Boxplots represent medians and interquartile range (IQR) with whisker end points equal to the maximum and minimum values below or above the median at 1.5 times the IQR. Organic acid composition was derived by the sum of each acid divided by the total.

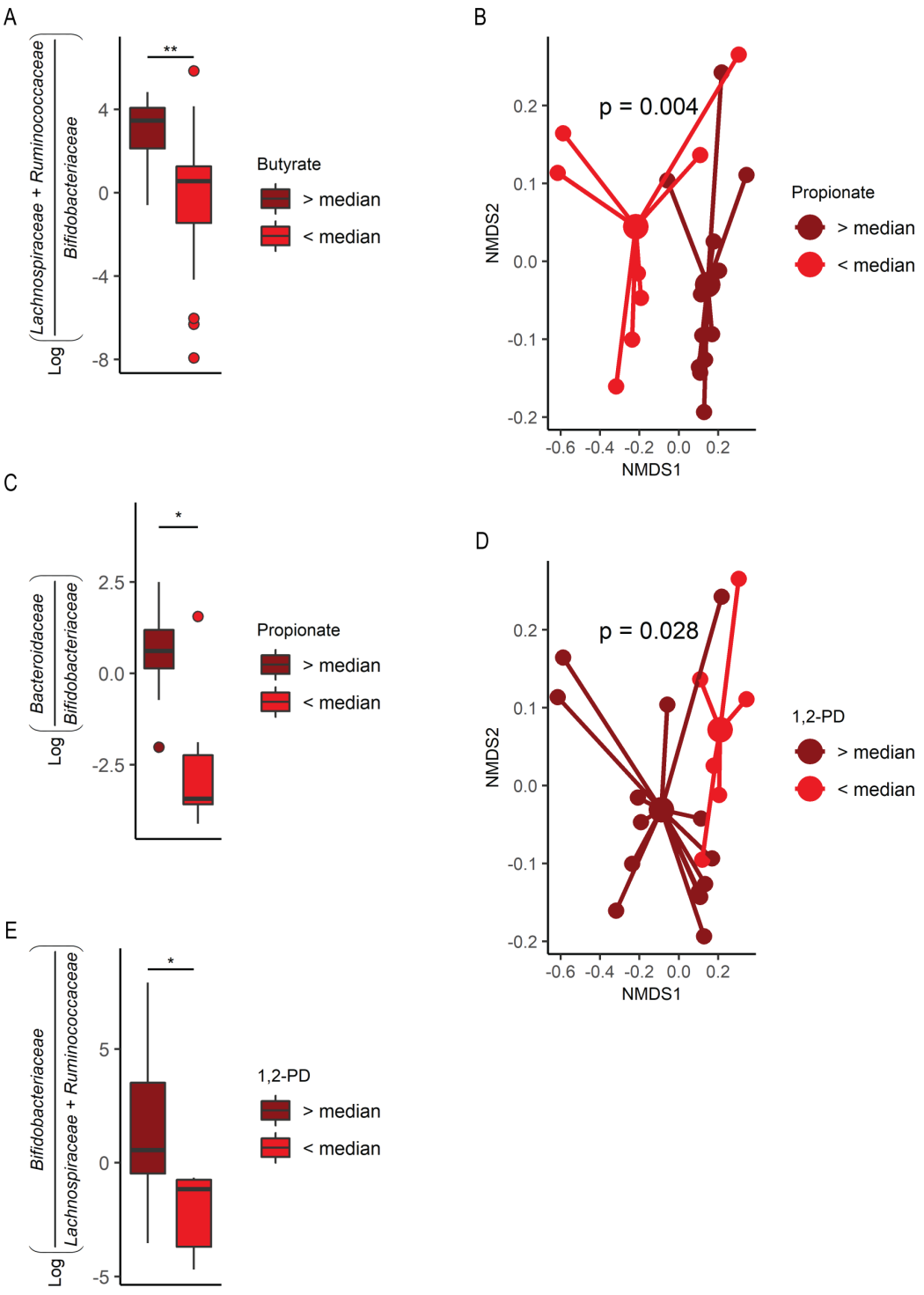

29

30 **Figure 3.5.** Microbial community differences are associated with distinct metabolite profiles at the final
31 time point. (A) Log ratio of *Lachnospiraceae* and *Ruminococcaceae* relative to *Bifidobacteriaceae* for all
32 treatments, grouped as either above (n = 19) or below (n = 19) the median butyrate concentration; (B) log

ratio of *Bacteroidaceae* relative to *Bifidobacteriaceae* for all 2-FL mice, grouped as either above (n = 12) or below (n = 8) the median propionate concentration; (C) microbial community NMDS plot grouped as above and below the median propionate concentration; (D) log ratio of *Bifidobacteriaceae* relative to *Lachnospiraceae* and *Ruminococcaceae* for all 2-FL mice, grouped as either above (n = 14) or below (n = 6) the median 1,2-propanediol (1,2-PD) concentration; and (E) microbial community NMDS plot grouped as above and below the median 1,2-PD concentration. Boxplots represent medians and interquartile range (IQR) with whisker end points equal to the maximum and minimum values below or above the median at 1.5 times the IQR. NMDS was generated using β-diversity index weighted unifrac distance in two dimensions.

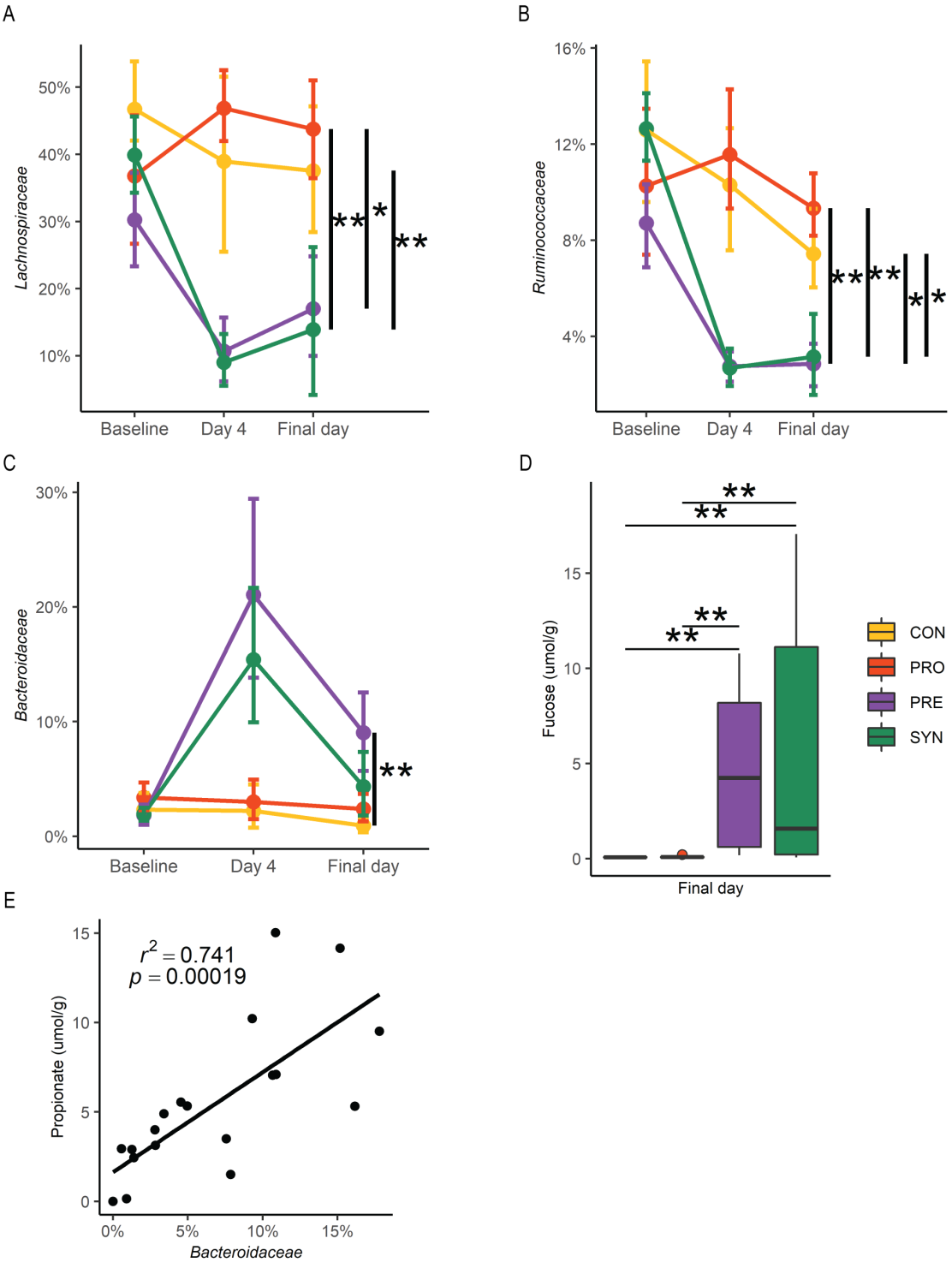

42

43 **Figure 3.6.** Bacterial relative abundance by treatment group. Relative abundance of (A) *Lachnospiraceae*,

44 (B) *Ruminococcaceae,* and (C) *Bacteroidaceae* in control (n = 9), probiotic (n = 9), prebiotic (n = 9), and

45 synbiotic (n = 12) groups from baseline, after oral gavage (day 4) and one week following (final day); and

(D) free fucose (μmol/g) at the final day for all treatments. Boxplots represent medians and interquartile range (IQR) with whisker end points equal to the maximum and minimum values below or above the median at 1.5 times the IQR. Error bars for relative abundance data is represented as mean and standard error from bootstrapped confidence intervals with 1000 iterations

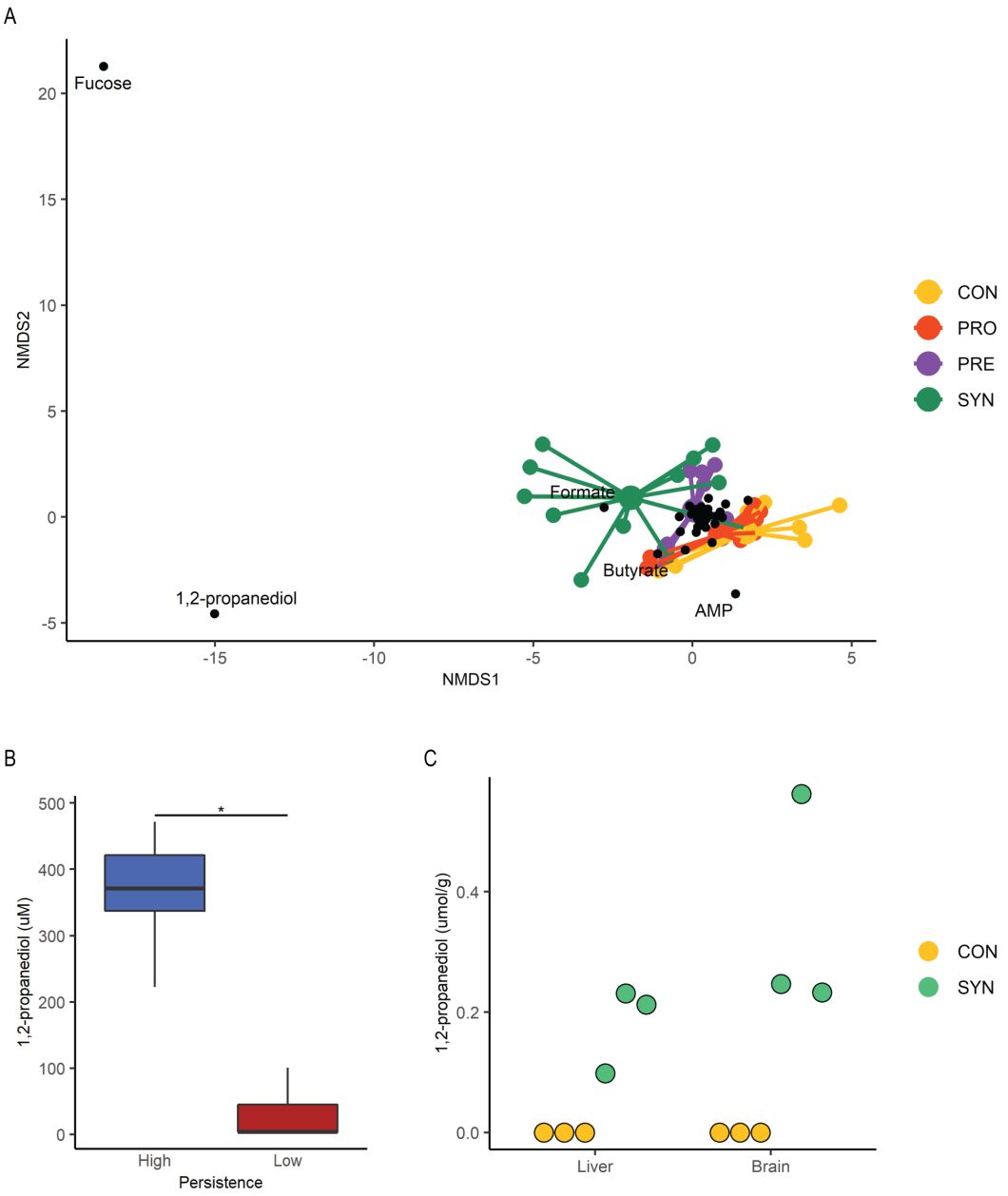

Figure 3.7. Systemic metabolome changes associated with synbiotic treatment. (A) NMDS plot of mouse serum metabolome at the final experimental time point, with metabolites highlighted that drive differentiation of samples, colored by treatment group; (B) serum 1,2-propanediol (µmol/g) by high and low bifidobacteria categorization of synbiotic treated mice; and (C) liver and brain 1,2-propanediol for control ($n = 3$) and synbiotic ($n = 3$) mice from experimental trial one. NMDS was generated using Euclidian

distance in two dimensions. Boxplots represent medians and interquartile range (IQR) with whisker end points equal to the maximum and minimum values below or above the median at 1.5 times the IQR.

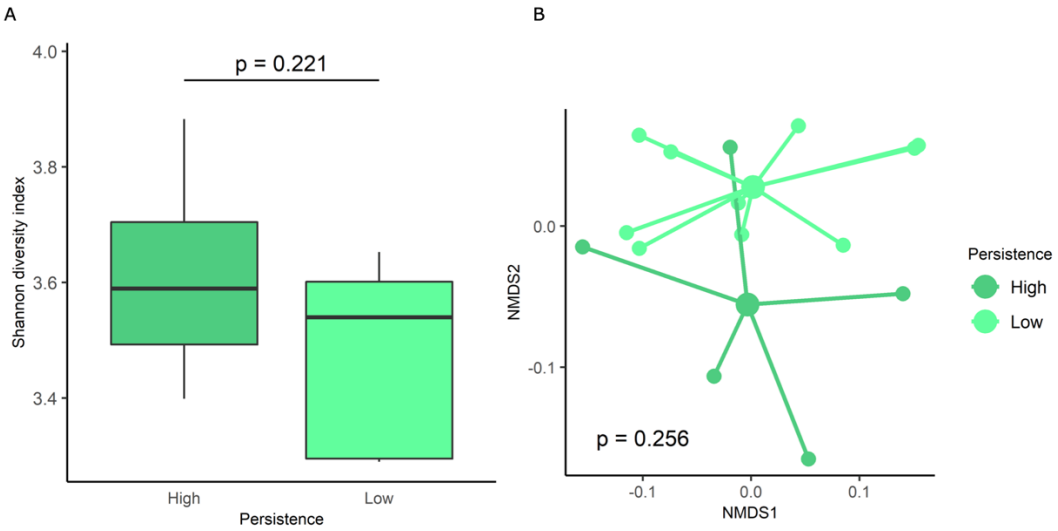

Supplementary Figure 3.1. Baseline differences not significant between high and low bifidobacteria categorizations of synbiotic treated mice. (A) Shannon α-diversity index values at baseline for synbiotic treated mice grouped as high (n = 4) and low (n = 7) bifidobacteria; and (B) NMDS plot of β-diversity index weighted unifrac for high and low bifidobacteria groups at baseline. Boxplots represent medians and interquartile range (IQR) with whisker end points equal to the maximum and minimum values below or above the median at 1.5 times the IQR.

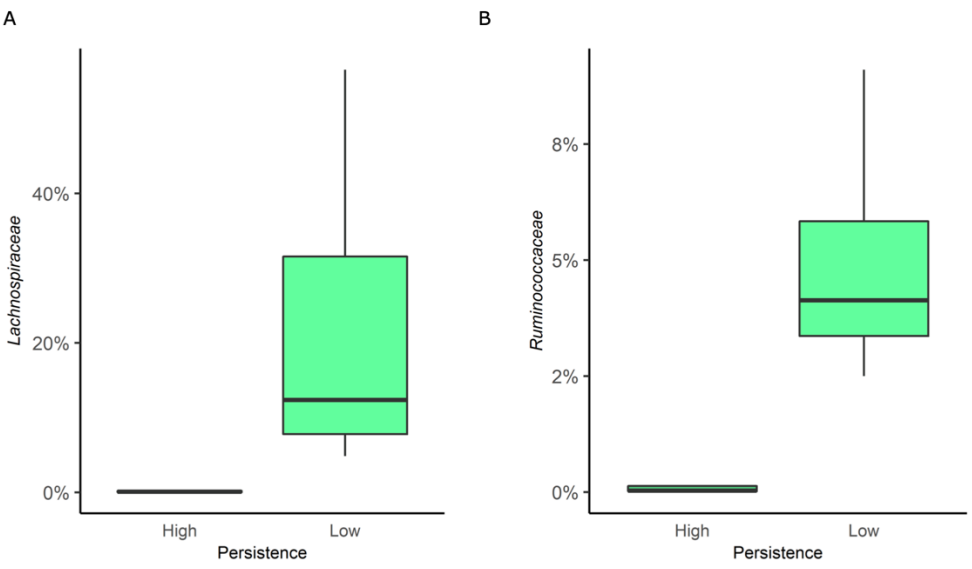

Supplemental Figure 3.2. Correlation between propionate concentrations and the relative abundance of *Bacteroidaceae* at the final time point for 2-FL treated mice. Pearson correlation between the relative abundance of *Bacteroidaceae* and propionate (μmol/g) for synbiotic (n = 12) and prebiotic (n = 9) treated mice at the final time point. Boxplots represent medians and interquartile range (IQR) with whisker end points equal to the maximum and minimum values below or above the median at 1.5 times the IQR.

Chapter 4

Persistence variability between *Bifidobacterium* species influenced by human milk oligosaccharide catabolism strategy and resource partitioning

Britta E. Heiss,[1] Amy M. Ehrlich,[2] Maria X. Maldonado-Gomez,[1] Diana H. Taft, [1] Helen E. Raybould[2] and David A. Mills[1]

[1]Department of Food Science and Technology, University of California-Davis, Davis, CA.

[2]Department of Anatomy, Physiology, and Cell Biology, School of Veterinary Medicine, University of California-Davis, Davis, CA.

4.1 Abstract

The human milk oligosaccharide 2'-fucosyllactose (2'FL) creates a resource niche for high levels of *Bifidobacterium pseudocatenulatum* MP80 persistence in mice. The bacterial-milk glycan pairing of *B. pseudocatenulatum* MP80 with 2'FL successfully enriched *B. pseudocatenulatum* after bacterial administration ended. Further questions arise regarding additional infant-isolated *Bifidobacterium* species' capability to use this resource niche. Specifically, fitness differences associated with bifidobacterial catabolism strategies and the possession of fucosylated HMO utilization genes should be examined. The ability to persist when mice are supplemented with 2'FL was tested with an intracellular (*Bifidobacterium longum* SC596) and extracellular (*Bifidobacterium bifidum* SC555) 2'FL utilizing strains to evaluate bifidobacterial molecular mechanisms for glycan catabolism. Additionally, non-2'FL catabolizing strains, *Bifidobacterium pseudocatenulatum* JCM11661 and *Bifidobacterium longum* DJO10A tested the necessity of fucosylated HMO genes. Persistence of *Bifidobacterium* species was inconsistent between experimental cohorts and the bacterial species supplemented. Individual mice were categorized as responders or non-responders based on qPCR persistence data. A baseline microbiota difference between responders and non-responders was not identified as statistically significant. These results suggest that not every bifidobacterial-milk glycan interaction is capable of overcoming colonization resistance. Further, the persistence of a strain that cannot catabolize 2'FL indicates the enrichment of *Bifidobacterium* is not always due to a direct access to 2'FL. This provides insight into how molecular mechanisms and functional capacities influence *in vivo* fitness differences between *Bifidobacterium* in complex microbial communities.

4.2 Introduction

Bifidobacterium pseudocatenulatum MP80 contains a fucosylated HMO gene cluster (**Figure 4.1a**); growth of *B. pseudocatenulatum* MP80 on 2'-FL increased expression of these genes 21-42 fold.[1] We have previously shown that persistence of *Bifidobacterium pseudocatenulatum* MP80 was achieved in mice when the human milk oligosaccharide (HMO) 2'-fucosyllactose (2'FL) was supplemented (Chapter 2).[2] To assess persistence, the 2'FL-catabolizing *B. pseudocatenulatum* MP80 strain was orally gavaged for the first 5 experimental days and 2'FL was supplemented to mice for 10 days (i.e. 5 days beyond cessation of the bacterial gavage).[2] When bacterial gavage was discontinued, during 2'FL administration, *B. pseudocatenulatum* MP80 was detected at high levels in the feces of mice (**Figure 4.1b)**. However, *B. pseudocatenulatum* MP80 decreased to below the limit of detection when mice received water alone (**Figure 4.1b**). Microbial community membership analysis found that *B. pseudocatenulatum* MP80 + 2'FL treatment increased *Bifidobacteriaceae* relative abundance, reaching ~40% during persistence (day 10). Furthermore, the ratio of *Bifidobacteriaceae* ASVs relative to the combination of *Lachnospiraceae* and *Ruminococcaceae* ASVs was significant by treatment and the log ratio was significantly higher in *B.p.* MP80 + 2'FL treated mice versus untreated control and 2'FL treated mice (**Chapter 2, Figure 2.2d**). Thus, *B. pseudocatenulatum* MP80 + 2'FL treatment enriched *Bifidobacteriaceae* ASVs, supporting the qPCR findings. In contrast, *Bifidobacterium pseudocatenulatum* JCM11661 which lacks the fucosylated HMO gene cluster and fails to grow *in vitro* on 2'FL, did not persist in the mouse gut in the presence of 2'-FL (Chapter 2).[2] This research led us to conclude that within a complex microbial community, a single HMO, 2'FL, was capable of enriching of the 2'FL utilizing *B. pseudocatenulatum* MP80 strain.

These findings spurred further questions regarding bacterial-carbohydrate synergy. First, would additional *Bifidobacterium* strains capable of 2'FL catabolism persist comparably? The fucosylated HMO cluster present in *B. pseudocatenulatum* MP80 has also been identified in *Bifidobacterium longum* subsp. *longum* SC596.[3] When grown on pooled HMO, *B. longum* SC596 preferentially utilized fucosylated HMOs first with the α(1-2) fucosyl linkage containing 2'FL and lacto-difucosyllactose (LDFT) reaching 100% consumption rates by mid exponential phase.[3] Therefore, *B. longum* SC596 can be tested as another *Bifidobacterium* species that prefers fucosylated HMOs and may be able to exploit the supplemented 2'FL resource niche.

Second, does variation in *Bifidobacterium* catabolism strategy (intracellular vs. extracellular) result in an altered growth advantage during 2'FL supplementation? Many *Bifidobacterium* utilize an import-and-degrade strategy for HMO catabolism, and others deploy extracellular glycosyl hydrolases which degrade HMOs into mono- and disaccharides which are then imported and catabolized internally.[4,5] This degrade-and-import strategy is characteristic of *Bifidobacterium bifidum.*[4,5] One possible outcome of extracellular catabolism could be reduced reproductive success (fitness) as this strategy may not provide the microbe with a competitive advantage when it comes to HMOs. It is interesting to note that a fucosylated HMO ABC transporter has been identified as a key colonization factor amongst infant gut microbes.[6] Alternatively, external sialidases have been shown to improve host mucosal adhesion which could subsequently increase colonization success.[7]

Third, are non-2'FL catabolizing strains capable of persistence, or elongated washout periods, during 2'FL supplementation? *Bifidobacterium* strains associated with poor or inefficient HMO catabolism are present in infant gut microbial communities and sometimes are even the predominant *Bifidobacterium* taxa.[8] A fecal metagenomic cross-section of US infants found that,

despite high levels of *B. longum* subsp. *longum, B. bifidum, or B. breve,* infant microbial communities contained a limited functional capacity for catabolizing HMOs.[9] An uneven distribution of carbohydrate-active enzymes is believed to suggest diverging colonization strategies between *B. longum* spp., as some appear better adapted for plant versus HMO glycans.[10] Testing non-2'FL catabolizing strains will further our understanding of *Bifidobacterium* strains which commonly colonize infants, even when HMO catabolism genes are absent.

To address each of these three questions, three individual *Bifidobacterium* species were tested in a mouse model supplemented with 2'FL (in addition to *B. pseudocatenulatum* MP80 and JCM11661, Chapter 2). *B. longum* SC596 tested whether a similar level of persistence could be achieved by another *Bifidobacterium* species with a catabolism strategy and preference for fucosylated HMOs similar to *B. pseudocatenulatum* MP80. Comparison of *Bifidobacterium* intracellular and extracellular catabolism strategies was evaluated with the extracellularly catabolizing *B. bifidum* SC555. As a contrast to *B. pseudocatenulatum* MP80, *B. pseudocatenulatum* JCM11661 was previously evaluated to test a non-2'FL catabolizing strain from the same bacterial species (Chapter 2). Therefore, to complement provision of *B. longum* SC596, a non-2'FL catabolizing *B. longum* strain was tested, *B. longum* DJO10A.

4.3 Methods

4.3.1 Mouse experimental trial design

Animals were maintained in accordance with IACUC Protocol 21900, University of California, Davis. Male C57BL/6J mice (5-6 weeks old, Jackson Labs) were randomly assigned to treatment groups (n = 6 mice per treatment). Two cohorts of n = 3 mice each were tested. Mice were sourced from different Jackson Labs locations for each experimental cohort. For one week prior to the experiment, mice were acclimatized to the facility. *Bifidobacterium* (10^9 CFU in PBS) or phosphate buffered saline was administered via oral gavage (100µl) for 5 days. A 10% (w/v) 2'FL solution was provided in drinking water *ad libitum* for 10 days. Body weights and food intake were measured 2-3 times per week and water intake was measured daily. Mice were euthanized via CO_2 asphyxiation. Fecal samples were collected at baseline and days 2, 6, 8, 10, 14, 18, 19 and a final time point at either day 18 or 20, depending on the experiment. Mice were euthanized via CO_2 asphyxiation.

Persistence experiment timeline: Either PBS or *Bifidobacterium* (*B.p.* MP80, *B.l.* SC596, *B.b.* SC555, *B.p.* JCM11661, or *B.l.* DJO10A) were provided for 5 days by oral gavage beginning on day 1. Either 2'FL or water alone was provided from days 1 to 10. During days 10 through 20, all treatment groups underwent a washout period with drinking water alone. Fecal samples were collected every 2-4 days throughout the experiment.

4.3.2 Quantification of bacterial strains by qPCR

B. pseudocatenulatum MP80 primers were previously generated while strain-specific primers were designed for *B. longum* SC596, *B. bifidum* SC555, *B. pseudocatenulatum* JCM11661, and *B. longum* DJO10A in this study (**Table 4.1**).[11–13] Primers were designed by identifying target genes determined unique by comparing the bacterial genome against a selection

of closely related strains and bacteria common to mouse gastrointestinal tracts using JGI/IMG tools. In silico primer specificity was tested by conducting a BLAST search against the NCBI database. Cell numbers consist of absolute quantification using a standard curve. qPCR was performed using a 7500 Fast Real-Time PCR System (Applied Biosystems, Waltham, MA, USA), with PCR reaction volumes of 20 µl using PowerUp SYBR Green qPCR master mix (Applied Biosystems, Waltham, MA, USA), 0.8 µM primer concentrations, and 1 µl DNA template.

4.3.3 Fecal DNA extraction and microbial DNA sequencing

DNA was extracted from stool samples (30-100 mg) using the Quick-DNA Fecal/Soil Microbe Miniprep Kit, Catalog No. D6010 (ZYMO, Irvine, CA, USA). The extraction protocol included a bead-beating step using a FastPrep-24 Instrument (MP Biomedicals, Santa Ana, CA, USA) for a total of 2 min at 25°C at a speed of 6.5 m/s. The V4 region of the 16S rRNA gene was amplified in triplicate with barcoded PCR primers F515 (5′-CACGGTCGKCGGCGCCATT-3′) and R806 (5-′GGACTACHVGGGTWTCTAAT-3′) modified to contain an adapter region for sequencing on the Illumina MiSeq platform.[14] Amplicons were verified by gel electrophoresis, combined, purified, and sent to the UC Davis Genome Center for library preparation and high throughput 250-bp paired-end sequencing. Raw sequencing data was demultiplexed and quality filtered before import into QIIME2-2019.7.[15] Samples with poor quality data were excluded from analysis. After trimming, reads were processed with DADA2.[16] Filtered sequences were aligned and taxonomy was assigned using the 99% SILVA naïve Bayesian classifier.[17] Samples were rarified to 2860 sequences.

4.3.4 Microbial ecosystem statistics and differential abundance testing

Microbial community statistical analysis was performed in R (version 4.0.2).[18] β-diversity was measured by Unifrac distances (GUnifrac) and visualized using non-metric multidimensional

scaling (NMDS) (vegan::metaMDS, k=2).[19] β-diversity statistical analysis consisted of checking dispersion (vegan::betadisper), a permutational multivariate ANOVA (vegan::adonis2, 999 permutations), and post hoc testing (RVAideMemoire:: pairwise.perm.manova, nperm = "500").[20] Differential abundance testing was conducted with songbird which ranks the log-fold changes between selected features.[21] Songbird analysis used samples from mice treated with *B. longum* DJO10A + 2'FL and *B. longum* DJO10A + water during 2'FL supplementation, post bacterial gavage (days 6, 8, 10) and accounted for differences by day. The high ranked *Bacteroidaceae* ASVs were chosen as the numerator while the low ranked *Lachnospiraceae* and *Ruminococcaceae* ASVs served as the denominator in the log ratio. Differential abundance log ratios were assessed for normality using a Shapiro-Wilk test which determined whether a Student's t-Test or Wilcoxon Rank Sum test was employed. A classification tree was generated to differentiate responder:non-responder categorized mice at baseline with the minimum split reduced due to a small number of subjects (rpart::rpart, minsplit = 2).[22] A linear regression was used to test the effect of discriminatory baseline microbial taxa, the 2'FL-metabolizing *Bifidobacterium* administered, and experimental trial to predict log transformed *Bifidobacterium* strain-specific qPCR values from day 10. Analysis conducted in R for GLM (stats::glm) and confidence intervals (stats::confint).[23]

4.3.5 Bifidobacterium in vitro growth assays

Bacteroides and *Bifidobacterium* strains were grown on modified MRS medium (mMRS), devoid of glucose and supplemented with 0.05% (w/v) L-cysteine, 0.5% (w/v) beef extract, and 2% (w/v) of substrate. Strains were grown on three sole carbon sources: lactose, fucose, and 2'FL. A 1% inoculation (v/v) of *B. theta* overnight culture was added to mMRS+substrate and grown for 24 hours before being spun down. *B. theta* supernatant was filter sterilized and adjusted to ~6.5 pH for *Bifidobacterium* growth. An inoculation of 2.5% (v/v) of *B.l* DJO10A or *B.p.* JCM11661

was added to a 96 well microtiter plate filled with media. Three biological replicates were performed for each bacterial strain for each carbohydrate source. Incubation was at 37 °C in an anaerobic chamber (Coy Laboratory Products, Grass Lake, MI) where cell growth was monitored every 30 min by optical density (OD) at 600nm using a BioTek PowerWave 340 plate reader (BioTek, Winoosky, VT). Analysis of growth curves was conducted in R v.4.1.0 (growthcurver::SummarizeGrowthByPlate).

4.4 Results

4.4.1 *Bifidobacterium* persistence diverges by strain and experiment

To determine whether possessing fucosylated HMO catabolism genes is sufficient for *Bifidobacterium* persistence, we tested strains capable of *in vitro* growth on 2'FL (in addition to *B. pseudocatenulatum* MP80 already studied; Chapter 2). Further bifidobacterial species were tested to evaluate species-specific colonization resistance. *B. longum* subsp. *longum* is associated with metabolism of plant glycans, lacto-N-tetraose (LNT), and lacto-N-biose (LNB) although strains that grow on fucosylated HMOs[3,10] have been identified. *B. pseudocatenulatum* MP80 and *B. longum* subsp. *longum* SC596 possess fucosylated HMO gene clusters with a high percent sequence similarity to each other (**Figure 4.1a**). The fucose metabolism genes and two α-fucosidases are nearly identical between the two strains and have high sequence similarity to HMO cluster I from *B. longum* subp. *infantis*[1,3] Importation of 2'FL is thought to be via the ABC cassette (solute binding proteins and permeases).[1,24] In contrast, *B. bifidum* SC555 genes do not display high sequence similarity to *B. pseudocatenulatum* MP80, but it does possess at least one active α-fucosidase (**Figure 4.1a**) and grows on 2'FL *in vitro*.[5] Similar to *B. pseudocatenulatum* MP80, *B. longum* SC596 possesses putative intracellular α-fucosidases.[3] In contrast, *B. bifidum* SC555 is hypothesized to possess an extracellular degradation strategy, by which 2'FL is cleaved externally and individual subunits are imported.[25]

Two experimental cohorts of each *Bifidobacterium* were run to test reproducibility ($n = 3$ mice per cohort). Even though *B. longum* SC596 possesses a fucosylated HMO gene cluster with high sequence similarity to *B. pseudocatenulatum* MP80 (**Figure 4.1a**), persistence was comparable to *B. pseudocatenulatum* MP80 for only one cohort (day 10; **Figure 4.1d)**. On day 10, the final day of 2'FL supplementation, *B. longum* SC596 was detected at a high level (>10e9

cells/gram of feces) in the first cohort but failed to persist in the second (day 10, ANOVA Tukey's test, $p = 0.006$; **Figure 4.1d**). *B. bifidum* SC555 was below the limit of detection in all mice, failing to persist in both cohorts (day 10; **Figure 4.1d**).

4.4.2 Persistence diverges between non-2'FL catabolizing strains

These data suggest that the ability to utilize 2'FL did not predict colonization. Therefore, we tested the hypothesis that the absence of 2'FL catabolism genes prevents competitiveness, resulting in no persistence. Two *Bifidobacterium* strains that do not grow on 2'FL *in vitro* were tested to evaluate whether the strains would persist when 2'FL was supplemented to mice. Strains *B. longum* DJO10A and *B. pseudocatenulatum* JCM11661 were chosen because they are related to *B. longum* SC596 and *B. pseudocatenulatum* MP80, respectively, but fail to grow *in vitro* on 2'FL. *B. longum* DJO10A persisted (>10e9 cells/gram of feces) after bacterial gavage had ended while mice were receiving 2'FL (day 10; **Figure 4.2a**). *B. longum* DJO10A + 2'FL persistence was not statistically significant from that seen in mice not treated with 2'FL, possibly due to the high standard deviation and low number of mice (t test, $p = 0.073$). *B. longum* DJO10A was below the level of detection at day 18, 8 days after the end of 2'-FL supplementation. *B. pseudocatenulatum* JCM11661 was detected during bacterial gavage (day 5, >10e7 cells/gram of feces; **Figure 4.2b**), but failed to persist during 2'FL supplementation alone. Relative abundance of *Bifidobacteriaceae* was observed to be elevated in *B. longum* DJO10A + 2'FL mice, reaching ~50% relative abundance on day 10 in contrast to ~10% in *B. pseudocatenulatum* JCM11661 + 2'FL mice (**Figure 4.3).** Hence, persistence of a bifidobacterial species was facilitated by 2'FL even when direct consumption of the supplemented glycan was not occurring.

4.4.3 B. longum DJO10A + 2'FL treatment enriches *Bacteroidaceae* ASVs

Microbial differential abundance testing was conducted on mice treated with *B. longum* DJO10A and either 2'FL or water in an attempt to understand how *B. longum* DJO10A was persisting during 2'FL supplementation.[21] *Bacteroidaceae* ASV counts in comparison to *Lachnospiraceae* and *Ruminoccaceae* ASV counts were elevated in mice treated with *B. longum* DJO10A and 2'FL (t test, p = 7.31e-05; **Figure 4.2c)**. *Bifidobacterium* strains that cannot catabolize 2'FL may have a growth advantage by cross-feeding from the endogenous *Bacteroidaceae* population that are capable of HMO degradation. Cross-feeding between non-2'FL catabolizing strains and *Bacteroidaceae* was explored using spent media from *Bacteroides thetaiotomicron* grown on 2'FL as the growth media for *B. longum* DJO10A and *B. pseudocatenulatum* JCM11661 growth curves. Non-2'FL catabolizing strains *B. longum* DJO10A and *B. pseudocatenulatum* JCM11661 failed to grow on 2'FL-supplemented minimal media (**Figure 4.4a)**. However, when grown on spent media of *B. thetaiotaomicron* grown on 2'FL*, B. longum* DJO10A reached a higher max optical density (OD > 1.0) than growth *B. pseudocatenulatum* JCM11661 (OD ~ 0.8) (**Figure 4.4a**). However, growth rate (Wilcoxon, p = 0.7) and maximum OD (Wilcoxon, p = 0.7) were not statistically significant between the two bacteria (**Figure 4.4b-c**). These data suggest that 2'FL enrichment of *Bacteroidaceae* could result in cross-feeding of *B. longum* DJO10A, leading to detection of *B. longum* DJO10A during 2'FL supplementation *in vivo*. However, in an oversimplified *in vitro* system, there was no distinction in growth fitness measures between *B. longum* DJO10A and *B. pseudocatenulatum* JCM11661 when grown on 2'FL *B. thetaiotamicron* spent media. This supports the observation that persistence success is defined by multiple factors related to the endogenous microbial community and the supplemented strains.

4.4.4 β-diversity distinct between responders and non-responders during persistence

Mice treated with *Bifidobacterium* + 2'FL were classified as responders or non-responders based on strain-specific qPCR data. Responders possessed a detectable (qPCR) persistent population of the supplemented strain at day 10, demonstrating that the mice "responded" to the treatment provided. All mice from *Bifidobacterium* + 2'FL treatments were used in this analysis, regardless of strain. Based on this cutoff, responders consisted of all *B. pseudocatenulatum* MP80 + 2'FL mice, the first experiment of *B. longum* SC596 + 2'FL mice, and all *B. longum* DJO10A mice. Non-responders consisted of the second experiment of *B. longum* SC596 + 2'FL mice and all *B. bifidum* SC555 +2'FL and *B. pseudocatenulatum* JCM11661 + 2'FL mice. A bimodal distribution of *Bifidobacteriaceae* relative abundance during 2'FL supplementation was noted between responders and non-responders (median 47% and 2%, respectively) (Mann Whitney, $p < 0.001$; **Figure 4.5a)**. Thus, the *Bifidobacteriaceae* population is elevated when population growth of the supplemented *Bifidobacterium* exceeds washout. Increased absolute abundance of a *Bifidobacterium* correlated to a relative abundance shift. Microbial community structure as measured by β-diversity was distinct between responders:non-responders during 2'FL supplementation (weighted unifrac, PERMANOVA, $p = 0.001$, post-hoc pairwise, $p = 0.002$; **Figure 4.5b**). Therefore, amongst responders, the absolute abundance of the provided *Bifidobacterium* increased, and in contrast to non- responders there was a significant shift in the microbial community membership (relative abundance).

4.4.5 Influence of *Erysipelotrichaceae* colonization resistance potentially strain-dependent

The lack of *Bifidobacterium* persistence amongst non-responders may be due to an increased colonization resistance at baseline. We have previously shown using classification tree analysis of mouse microbial communities that when baseline *Erysipelotrichaceae* relative abundance was >0.9%, the relative abundance of *Bifidobacterium* was reduced and

Bifidobacterium-associated metabolites were not detected (Chapter 3). The microbes associated with colonization resistance are likely to be study-dependent, however, we tested the *Erysipelotrichaceae* association in this current study. The same *Erysipelotrichaceae* relative abundance cutoff was applied to the analysis of responder:non-responders. A large number of non-responders possessed *Erysipelotrichaceae* relative abundances >0.9% (10/12 non-responders), but a portion of the responders (6/12 responders) also possessed elevated *Eryspelotrichaceae* at baseline and *Erysipelotrichaceae* relative abundance was not significant between responder:non-responders (Wilcoxon Rank Sum, $p = 0.141$, **Figure 4.5c**). Within the responder group of mice, the highest baseline *Erysipelotrichaceae* relative abundances were in mice treated with *B.p.* MP80 ($n = 3$). This suggests that *B.p.* MP80 was capable of overcoming the higher *Erysipelotrichaceae* abundance to achieve persistence. In contrast, *B. longum* SC596 did not persist when *Erysipelotrichaceae* abundance was elevated at baseline ($n = 3$). Certain *Bifidobacterium* strains may be more competitive against endogenous *Erysipelotrichaceae*. These data suggest that the influence of *Erysipelotrichaceae* on persistence may be overcome by strain fitness.

4.5.6 Baseline microbial taxa was not significantly associated with responder:non-responder outcome

The relative abundance of *Erysipelotrichaceae* was not a clear discriminator between responders and non-responders, and a classification tree was used to investigate differences between baseline bacterial families in responders and non-responders. For this analysis we narrowed our question, focusing on mice treated with *Bifidobacterium* + 2'FL where the *Bifidobacterium* provided was capable of *in vitro* 2'FL metabolism (MP80, SC596, and SC555). Although *B. longum* DJO10A demonstrated persistence, this was likely dependent on a commensal relationship with *Bacteroidaceae* and inclusion of this group could potentially complicate baseline

bacterial taxa analysis by adding an additional factor to the model. Therefore, in an attempt to identify baseline colonization resistance to Bifidobacterium, data from mice treated with 2'FL-metabolizing *Bifidobacterium* only was used. The tree identified five distinguishing bacterial taxa between responder:non-responder (**Figure 4.6**). A linear regression model was used to explore if any variables were predictive of persistence. The bacterial strain administered and the experimental trial were significantly associated with whether a mouse was a responder or non-responder (**Table 4.2**). None of the bacterial families identified by the classification tree were associated with whether *Bifidobacterium* persisted or not (**Table 4.2**). Three experimental cohorts were conducted during this study in an effort to increase rigor and reproducibility. The baseline microbial community structure (β-diversity) was statistically different in each cohort (weighted unifrac, PERMANOVA, $p = 0.001$) but not by responder:non-responder ($p = 0.704$).

4.5. Discussion

Engraftment of a microbe into a stable microbial community has proven difficult. After probiotic administration, fecal microbiota community alterations (β diversity) are habitually found to be nonsignificant.[13,26,27] Here meaning, microbial communities are not restructuring based on probiotic administration, even when engraftment of the microbe occurs. We hypothesized that providing 2'FL, a privileged nutrient resource, would result in a growth advantage only to *Bifidobacterium* possessing 2'FL catabolism genes. Three 2'FL catabolizing strains were tested for persistence, but only *B. pseudocatenulatum* MP80 consistently persisted at high levels across two experimental trials.

Prior carbohydrate-bacterial pairing studies have demonstrated a ~10% increase in the relative abundance of taxa of interest.[28–30] Focusing on mice treated with *B. pseudocatenulatum* MP80 and 2'FL, *Bifidobacteriaceae* relative abundance reached ~40% during persistence. A strong competitor, *B. pseudocatenulatum* MP80 consistently persisted, even when mice were sourced from two Jackson Laboratories locations with varied baseline microbial communities. Prior work established that *Bifidobacterium* possesses a growth advantage over *Bacteroides* when co-colonizing a germ-free mouse supplemented with the HMO LNnT.[31] In this case, *B. pseudocatenulatum* MP80 is able to utilize HMO structures but is unable to degrade the mucin structures utilized by *Bacteroides*. As previously reported, in these experiments *B. pseudocatenulatum* MP80 is well adapted to catabolize 2'FL and outcompetes *Bacteroidaceae*, resulting in no *Bacteroidaceae* relative enrichment.

2'FL was provided with the intent of being a privileged resource, providing a selective growth advantage to only 2'FL-catabolizing *Bifidobacterium* over endogenous microbes. *B. longum* DJO10A and *B. pseudocatenulatum* JCM11661 fail to grow *in vitro* on 2'FL and their

respective genomes lack α-fucosidases. Thus, 2'FL should not serve as a privileged resource to these two *Bifidobacterium* strains. However, the data do not support this hypothesis. In a 2'FL safety and tolerance study in adult humans, *Bifidobacterium adolescentis*, a strain that generally fails to grow on 2'FL, was the main OTU responding to treatment.[32] Our previous study (Chapter 2) showed that treatment with 2'FL alone enriched endogenous *Bacteroidaceae* and *Bifidobacteriaceae* ASVs in mice.[2] *Bacteroides* species can upregulate distinct mucin-use genes to take advantage of HMOs as a nutrient resource.[31] In the present study, degradation of 2'FL by *Bacteroides* may cross-feed other microbes, such as *B. longum* DJO10A. Such cross-feeding relationships have been identified previously.[33–36] In this study, the enrichment of *Bacteroidaceae* ASVs in *B. longum* DJO10A + 2'FL treated mice supports this hypothesis.

Both of the non-2'FL catabolizing *Bifidobacterium* strains grew on the spent media from the growth of *B. thetaiotaomicron* on 2'FL. no fitness difference between strains was determined based on growth kinetics. Therefore, this data does not help parse why *B. longum* DJO10A had a fitness advantage when 2'FL was supplemented and *B. pseudocatenulatum* alternatively was not detectable. *Bifidobacterium* species lacking HMO catabolism genes are often present in infant gut microbial communities, which may be analogous to non-2'FL catabolizing *B. longum* DJO10A persistence seen in the present study. Evidence from a study in a preterm infants supplemented with a HMO-catabolizing *B. bifidum* probiotic suggested close species interaction, which could potentially be cross-feeding, between the supplemented *B. bifidum* and a native *B. breve* which lacked HMO catabolism genes.[37] The relative abundance of *B. bifidum* steadily declined after bacterial supplementation ended, failing to persist, while the relative abundance of the non-2'FL catabolizing *B. breve* increased.[37] Within individual infant microbial communities, Lawson et al. revealed cooperative and complementary relationships existing between *Bifidobacterium* HMO

catabolizing strains and non-HMO catabolizing strains.[36] Many *Bifidobacterium* possess the capacity to use the products of degraded HMOs *in vitro*, however, other factors likely play a role in persistence when taxa are competing against indigenous gut microbes. *Bifidobacterium* species may be resource partitioning in an attempt to reduce inter-species competition. In order to co-exist in a community, commensal organisms are metabolically flexible depending on resources available and whether they can harvest certain substrates more efficiently than competitors, termed resource partitioning. The concept that some non-HMO catabolizing *Bifidobacterium* strains may be more proficient at scavenging 2'FL metabolites and engaging in resource partitioning is a hypothesis that requires further exploration. Such research may advance our understanding of *Bifidobacterium* networks within infant microbial communities.

Not every *Bifidobacterium* strain capable of 2'FL catabolism achieved consistent, high levels of persistence. Based on strain-specific qPCR, *Bifidobacterium* + 2'FL treated mice were categorized as responders or non-responders. The differential response of adult conventionally raised mice to bacterial supplementation is a phenomenon noted throughout literature and has previously been explained either by colonization resistance[39], endogenous microbes filling the specific functional niche[13,40], the bacterial strain being adapted for a different host[41], or a nutrient that is not as selective as assumed.[27,42] In our experiment, infant isolated *Bifidobacterium* strains were provided to healthy, adult mice with established gut microbial communities. Therefore, it was not entirely unexpected to see a responder:non-responder categorization of individual mice. When testing *Bifidobacterium* catabolism strategies, we expected to see a difference in strain persistence as ABC transporters have been identified as factors in bacterial colonization success.[6,13,43] Glycosyl hydrolases expressed by *B. pseudocatenulatum* MP80 and *B. longum* SC596 are intracellular while *B. bifidum* SC555 are extracellular.[5] After cleaving fucose from the

lactose core, *B. bifidum* SC555 prioritizes lactose as a nutrient resource, discarding the fucose.[5] *B. bifidum* SC555 did not persist in all mice, thus, in this limited experiment, an external catabolism strategy failed to impart a fitness advantage capable of overcoming colonization resistance. *Bifidobacterium* with internalized catabolism strategies revealed species-level differences. *B. pseudocatenulatum* MP80 successfully persisted in both trials, all mice were categorized as responders. *B. longum* SC596 only persisted in the first trial, while the second trial mice were categorized as non-responders. An internal catabolism strategy alone does not provide an overwhelming growth advantage to *Bifidobacterium*, although internal catabolism strains were more successful in persistence. In a gnotobiotic mouse experiment, the colonization of *Bacteroides* strains was prevented only by members of the same species.[40] Future work could explore the presence of indigenous *B. longum* species across experimental trials to evaluate potential species-specific colonization resistance.

Notably, the microbial community structure was distinct between responders and non-responders during 2'FL supplementation, a result not always seen when comparing responder:nonresponder individuals.[13] Our previous analysis of *Bifidobacterium* supplemented mice found that *Erysipelotrichaceae* relative abundance at baseline was a factor in whether *Bifidobacterium* relative abundance reached high levels (>50.5%) (Chapter 3). However, in this study, baseline relative abundance of *Erysipelotrichaceae* greater than 0.9% was not significantly associated with the non-responder phenotype. Notably, *B. pseudocatenulatum* MP80, but not *B. longum* SC596, overcame the higher baseline *Erysipelotrichaceae*. Thus, the capacity to overcome the colonization resistance associated with *Erysipelotrichaceae* appears to be more species-specific. Additional investigation of the baseline *Bifidobacterium* population may also reveal species-specific interactions. For example, *B. longum* SC596 may be facing higher colonization

resistance than *B. pseudocatenulatum* MP80 from native, mouse *B. longum* species. *B. longum* may be enriched in these mice given the association of this subspecies with plant glycan metabolism; this would be consistent with other studies showing that colonization resistance was previously demonstrated to be species-specific.[40]

Further exploration of the baseline microbiota between responders and non-responders using a classification tree revealed bacterial families that when enriched were associated with reduced bifidobacterial persistence. A number of the identified taxa are associated with fiber degradation or have previously been enriched *in vitro* during 2'FL provision, for example *Erysipelotrichaceae* and *Lachnospiraceae*.[44] However, the relative abundance of discriminatory baseline bacterial taxa was not significantly associated with persistence. Instead, *Bifidobacterium* persistence was significantly associated with the *Bifidobacterium* strain administered and the experimental cohort. This reveals a study limitation as baseline bacterial taxa appear to be influencing persistence, but the heterogeneity of baseline microbiota and intrinsic competitive nature of *Bifidobacterium* strains are making it challenging to parse apart colonization resistance. For example, high *Erysipelotriochaceae* abundance appears to be associated with high colonization resistance, however, *B. pseudocatenulatum* MP80 is competitive enough to overcome such resistance. Therefore, the combination of different baseline microbial communities and distinct competitive differences by *Bifidobacterium* strains leads to inconclusive results.

In the present study, there was one mouse that was discrepant when considering persistence of *B. pseudocatenulatum* MP80. The microbial community structure (β-diversity) of subject 6, a responder, clustered more closely with the non-responder versus responder mice. Subject 6 also had the lowest *Bifidobacteriaceae* relative abundance of all responders (2%) during 2'FL supplementation and the lowest level of detected *B. pseudocatenulatum* MP80 by qPCR (>10e7

cells/gram of feces). Subject 6 also possessed elevated *Erysipelotrichaceae* at baseline (25%). Additional mice in that cage, (4 and 5), had similarly high *Erysipelotrichaceae* at baseline but had much higher detected *B. pseudocatenulatum* MP80 (>10e10 cells/gram of feces). Thus, subject 6 seems to be an outlier, it does however demonstrate the limitations of these studies and methods that focus on taxonomy alone. Therefore, it is necessary to understand the functional capacity of the microbial community to gain insight on the relationship between absolute abundance of *Bifidobacterium* persistence, relative abundance measurements, and quantifiable metabolites.

Conclusion

The present study shows that *Bifidobacterium* persistence was strongly influenced by resource availability, catabolism strategy, cross-feeding capabilities, and colonization resistance. Similar principles apply to the infant microbiota where microbial colonization and subsequent metabolic activity are driven by nutrient resources, bacterial metabolic capacity to exploit that resource, and interspecific competition resulting in resource partitioning. This mouse model, while not emblematic of an infant intestine, supports the hypothesis that HMOs can directly and indirectly drive persistence of *Bifidobacterium* strains. The functional capacity to utilize a privileged resource, 2'FL, was an advantage for *Bifidobacterium* strains. However, the capacity to exploit 2'FL did not overwhelmingly result in *Bifidobacterium* persistence. This study provides evidence to support that an intracellular catabolism strategy may improve fitness, but our results are not conclusive. In this study, persistence appears to be determined by 1) the intrinsic competitiveness of the *Bifidobacterium* strain for 2'FL, and 2) the baseline microbial environment. Understanding the functional capacity of the microbial community of responders and non-responders may provide further information as to why some *Bifidobacterium* strains were

incapable of persisting. Further research employing this mouse model could explore interspecies competition and cooperativity between *Bifidobacterium* strains.

4.6 References

1. Shani G, Hoeflinger J, Heiss B, Masarweh C, Larke J, Jensen N, Wickramasinghe S, Davis J, Goonatilleke E, El-Hawiet A, et al. Fucosylated human milkoligosaccharide foraging within the species Bifidobacteriumpseudocatenulatum is driven byglycosyl hydrolase content and specificity. 2021;
2. Heiss B, Ehrlich A, Maldonado-Gomez M, Taft D, Larke J, Goodson M, Slupsky C, Tancredi D, Raybould H, Mills D. Bifidobacterium catabolism of human milk oligosaccharides overrides endogenous competitive exclusion driving colonization and protection. Gut Microbes 2021;
3. Garrido D, Ruiz-Moyano S, Kirmiz N, Davis JC, Totten SM, Lemay DG, Ugalde JA, German JB, Lebrilla CB, Mills DA. A novel gene cluster allows preferential utilization of fucosylated milk oligosaccharides in Bifidobacterium longum subsp. longum SC596. Sci Rep 2016; 6:35045.
4. Kitaoka M. Bifidobacterial enzymes involved in the metabolism of human milk oligosaccharides. Adv Nutr 2012; 3:422S–9S.
5. Garrido D, Ruiz-Moyano S, Lemay DG, Sela DA, German JB, Mills DA. Comparative transcriptomics reveals key differences in the response to milk oligosaccharides of infant gut-associated bifidobacteria. Sci Rep 2015; 5:13517.
6. Matsuki T, Yahagi K, Mori H, Matsumoto H, Hara T, Tajima S, Ogawa E, Kodama H, Yamamoto K, Yamada T, et al. A key genetic factor for fucosyllactose utilization affects infant gut microbiota development. Nat Commun 2016; 7:11939.
7. Nishiyama K, Yamamoto Y, Sugiyama M, Takaki T, Urashima T, Fukiya S, Yokota A, Okada N, Mukai T. Bifidobacterium bifidum Extracellular Sialidase Enhances Adhesion to the Mucosal Surface and Supports Carbohydrate Assimilation. MBio 2017; 8.
8. Yang B, Ding M, Chen Y, Han F, Yang C, Zhao J, Malard P, Stanton C, Ross RP, Zhang H, et al. Development of gut microbiota and bifidobacterial communities of neonates in the first 6 weeks and their inheritance from mother. Gut Microbes 2021; 13:1–13.
9. Casaburi G, Duar RM, Brown H, Mitchell RD, Kazi S, Chew S, Cagney O, Flannery RL, Sylvester KG, Frese SA, et al. Metagenomic insights of the infant microbiome community structure and function across multiple sites in the United States. Sci Rep 2021; 11:1472.
10. Tarracchini C, Milani C, Lugli GA, Mancabelli L, Fontana F, Alessandri G, Longhi G, Anzalone R, Viappiani A, Turroni F, et al. Phylogenomic disentangling of the Bifidobacterium longum subsp. infantis taxon. Microb Genom 2021; 7.
11. Rinttilä T, Kassinen A, Malinen E, Krogius L, Palva A. Development of an extensive set of 16S rDNA-targeted primers for quantification of pathogenic and indigenous bacteria in faecal samples by real-time PCR. J Appl Microbiol 2004; 97:1166–77.
12. Matsuki T, Watanabe K, Fujimoto J, Kado Y, Takada T, Matsumoto K, Tanaka R. Quantitative PCR with 16S rRNA-gene-targeted species-specific primers for analysis of human intestinal bifidobacteria. Appl Environ Microbiol 2004; 70:167–73.
13. Maldonado-Gómez MX, Martínez I, Bottacini F, O'Callaghan A, Ventura M, van Sinderen D, Hillmann B, Vangay P, Knights D, Hutkins RW, et al. Stable Engraftment of Bifidobacterium longum AH1206 in the Human Gut Depends on Individualized Features of the Resident Microbiome. Cell Host Microbe 2016; 20:515–26.
14. Caporaso JG, Lauber CL, Walters WA, Berg-Lyons D, Lozupone CA, Turnbaugh PJ, Fierer N, Knight R. Global patterns of 16S rRNA diversity at a depth of millions of sequences per sample. Proc Natl Acad Sci USA 2011; 108 Suppl 1:4516–22.

15. Bolyen E, Rideout JR, Dillon MR, Bokulich NA, Abnet CC, Al-Ghalith GA, Alexander H, Alm EJ, Arumugam M, Asnicar F, et al. Reproducible, interactive, scalable and extensible microbiome data science using QIIME 2. Nat Biotechnol 2019; 37:852–7.
16. Callahan BJ, McMurdie PJ, Rosen MJ, Han AW, Johnson AJA, Holmes SP. DADA2: High-resolution sample inference from Illumina amplicon data. Nat Methods 2016; 13:581–3.
17. Quast C, Pruesse E, Yilmaz P, Gerken J, Schweer T, Yarza P, Peplies J, Glöckner FO. The SILVA ribosomal RNA gene database project: improved data processing and web-based tools. Nucleic Acids Res 2013; 41:D590-6.
18. R Core Team. R: A Language and Environment for Statistical Computing. R Foundation for Statistical Computing; 2020.
19. Oksanen J, Blanchet FG, Friendly M, Kindt R, Legendre P, McGlinn D, Minchin PR, O'Hara RB, Simpson GL, Solymos P, et al. vegan: Community Ecology Package [Internet]. R; 2019 [cited 2020 Jul 20]. Available from: https://CRAN.R-project.org/package=vegan
20. Hervé M. RVAideMemoire: Testing and Plotting Procedures for Biostatistics. R; 2020.
21. Morton JT, Marotz C, Washburne A, Silverman J, Zaramela LS, Edlund A, Zengler K, Knight R. Establishing microbial composition measurement standards with reference frames. Nat Commun 2019; 10:2719.
22. Therneau T, Atkinson E. An Introduction to Recursive Partitioning Using the RPART Routines. 2019;
23. Bates D, Mächler M, Bolker B, Walker S. Fitting linear mixed-effects models using lme4. J Stat Softw 2015; 67:1–48.
24. Garrido D, Kim JH, German JB, Raybould HE, Mills DA. Oligosaccharide binding proteins from Bifidobacterium longum subsp. infantis reveal a preference for host glycans. PLoS One 2011; 6:e17315.
25. Ruiz-Moyano S, Totten SM, Garrido DA, Smilowitz JT, German JB, Lebrilla CB, Mills DA. Variation in consumption of human milk oligosaccharides by infant gut-associated strains of Bifidobacterium breve. Appl Environ Microbiol 2013; 79:6040–9.
26. Kristensen NB, Bryrup T, Allin KH, Nielsen T, Hansen TH, Pedersen O. Alterations in fecal microbiota composition by probiotic supplementation in healthy adults: a systematic review of randomized controlled trials. Genome Med 2016; 8:52.
27. Krumbeck JA, Rasmussen HE, Hutkins RW, Clarke J, Shawron K, Keshavarzian A, Walter J. Probiotic Bifidobacterium strains and galactooligosaccharides improve intestinal barrier function in obese adults but show no synergism when used together as synbiotics. Microbiome 2018; 6:121.
28. Sheng K, He S, Sun M, Zhang G, Kong X, Wang J, Wang Y. Synbiotic supplementation containing Bifidobacterium infantis and xylooligosaccharides alleviates dextran sulfate sodium-induced ulcerative colitis. Food Funct 2020; 11:3964–74.
29. Kearney SM, Gibbons SM, Erdman SE, Alm EJ. Orthogonal dietary niche enables reversible engraftment of a gut bacterial commensal. Cell Rep 2018; 24:1842–51.
30. Mischke M, Arora T, Tims S, Engels E, Sommer N, van Limpt K, Baars A, Oozeer R, Oosting A, Bäckhed F, et al. Specific synbiotics in early life protect against diet-induced obesity in adult mice. Diabetes Obes Metab 2018; 20:1408–18.
31. Marcobal A, Barboza M, Sonnenburg ED, Pudlo N, Martens EC, Desai P, Lebrilla CB, Weimer BC, Mills DA, German JB, et al. Bacteroides in the infant gut consume milk

oligosaccharides via mucus-utilization pathways. Cell Host Microbe 2011; 10:507–14.
32. Elison E, Vigsnaes LK, Rindom Krogsgaard L, Rasmussen J, Sørensen N, McConnell B, Hennet T, Sommer MOA, Bytzer P. Oral supplementation of healthy adults with 2'-O-fucosyllactose and lacto-N-neotetraose is well tolerated and shifts the intestinal microbiota. Br J Nutr 2016; 116:1356–68.
33. Turroni F, Özcan E, Milani C, Mancabelli L, Viappiani A, van Sinderen D, Sela DA, Ventura M. Glycan cross-feeding activities between bifidobacteria under in vitro conditions. Front Microbiol 2015; 6:1030.
34. Turroni F, Milani C, Duranti S, Mahony J, van Sinderen D, Ventura M. Glycan Utilization and Cross-Feeding Activities by Bifidobacteria. Trends Microbiol 2018; 26:339–50.
35. De Vuyst L, Leroy F. Cross-feeding between bifidobacteria and butyrate-producing colon bacteria explains bifdobacterial competitiveness, butyrate production, and gas production. Int J Food Microbiol 2011; 149:73–80.
36. Lawson MAE, O'Neill IJ, Kujawska M, Gowrinadh Javvadi S, Wijeyesekera A, Flegg Z, Chalklen L, Hall LJ. Breast milk-derived human milk oligosaccharides promote Bifidobacterium interactions within a single ecosystem. ISME J 2020; 14:635–48.
37. Alcon-Giner C, Dalby MJ, Caim S, Ketskemety J, Shaw A, Sim K, Lawson MAE, Kiu R, Leclaire C, Chalklen L, et al. Microbiota Supplementation with Bifidobacterium and Lactobacillus Modifies the Preterm Infant Gut Microbiota and Metabolome: An Observational Study. Cell Rep Med 2020; 1:100077.
38. Centanni M, Ferguson SA, Sims IM, Biswas A, Tannock GW. Bifidobacterium bifidum ATCC 15696 and Bifidobacterium breve 24b Metabolic Interaction Based on 2'-O-Fucosyl-Lactose Studied in Steady-State Cultures in a Freter-Style Chemostat. Appl Environ Microbiol 2019; 85.
39. Zhang C, Derrien M, Levenez F, Brazeilles R, Ballal SA, Kim J, Degivry M-C, Quéré G, Garault P, van Hylckama Vlieg JET, et al. Ecological robustness of the gut microbiota in response to ingestion of transient food-borne microbes. ISME J 2016; 10:2235–45.
40. Lee SM, Donaldson GP, Mikulski Z, Boyajian S, Ley K, Mazmanian SK. Bacterial colonization factors control specificity and stability of the gut microbiota. Nature 2013; 501:426–9.
41. Duar RM, Frese SA, Lin XB, Fernando SC, Burkey TE, Tasseva G, Peterson DA, Blom J, Wenzel CQ, Szymanski CM, et al. Experimental Evaluation of Host Adaptation of Lactobacillus reuteri to Different Vertebrate Species. Appl Environ Microbiol 2017; 83.
42. Davis L, Martínez I, Walter J, Goin C, Hutkins R. Barcoded Pyrosequencing Reveals That Consumption of Galactooligosaccharides Results in a Highly Specific Bifidogenic Response in Humans. PLoS One 2011; 6.
43. Sakanaka M, Hansen ME, Gotoh A, Katoh T, Yoshida K, Odamaki T, Yachi H, Sugiyama Y, Kurihara S, Hirose J, et al. Evolutionary adaptation in fucosyllactose uptake systems supports bifidobacteria-infant symbiosis. Sci Adv 2019; 5:eaaw7696.
44. Nogacka AM, Arboleya S, Nikpoor N, Auger J, Salazar N, Cuesta I, Mantecón L, Solís G, Gueimonde M, Tompkins TA, et al. Influence of 2′-Fucosyllactose on the Microbiota Composition and Metabolic Activity of Fecal Cultures from Breastfed and Formula-Fed Infants at Two Months of Age. Microorganisms 2021; 9:1478.

Primer Target Forward and Reverse Sequences (5' – 3')	Product Size (bp)	Annealing Temp (C)	Source
Bifidobacterium TCGCGTC(C/T)GGTGTGAAAG CCACATCCAGC(A/G)TCCAC	243	58	Rinttila et al. *(53)*
B. catenulatum CGGATGCTCCGACTCCT CGAAGGCTTGCTCCCGAT	285	58	Matsuki et al. *(54)*
B. longum subsp. *longum* SC596 ACGAACTGGCAAAAATGCTT ATCCCGTGGAGACATTGAAA	217	60	This Study
B. bifidum SC555 AGAACCGCAACGGAATGA TTGTAAGTCTGGCAGTTCGTC	170	60	This Study
B .pseudocatenulatum JCM11661 AAAACGGCGTGACCTACAAC GGAGGTCTGGTTGGTCTTGA	158	60	This Study
B. longum DJO10A ATTCGTCCGAGTGGAACAAG GAACAGTGTGCCTTGGGTCT	155	60	This Study

Table 4.1: Primers for quantification of bacterial species, all used a Sybr Green as the polymerase.

	Beta coeff.	t-statistic	Lower 95% CI	Upper 95% CI	*p*-value*
Experimental cohort	-3.12	-2.32	-5.88	-0.49	**0.045**
B. pseudocatenulatum MP80	6.26	5.20	3.90	8.62	**< 0.001**
B. longum SC596	3.62	3.20	1.41	5.83	**0.012**
Anaeroplasmataceae	94.52	1.82	-7.52	196.55	0.103
Burkholderiaceae	-6.53	-0.02	-875	862	0.988
Clostridiales vadingroup	1.94	0.08	-48.03	51.90	0.676
Erysipelotrichaceae	3.69	0.43	-13.11	20.49	0.941
Lachnospiraceae	0.31	0.04	-16.36	16.98	0.972

Table 4.2: Generalized linear regression model for predicting persistence on experimental day 10 for *Bifidobacterium* + 2'FL treated mice (2'FL-metabolizing strains). To assess persistence, Log10 transformed *Bifidobacterium* strain-specific qPCR values on day 10 were the outcome. Experimental cohort, *Bifidobacterium* supplemented, and baseline distinguishing bacterial taxa were variables included in linear regression. Variable is considered significant if $p < 0.05$ and are shown in bold.

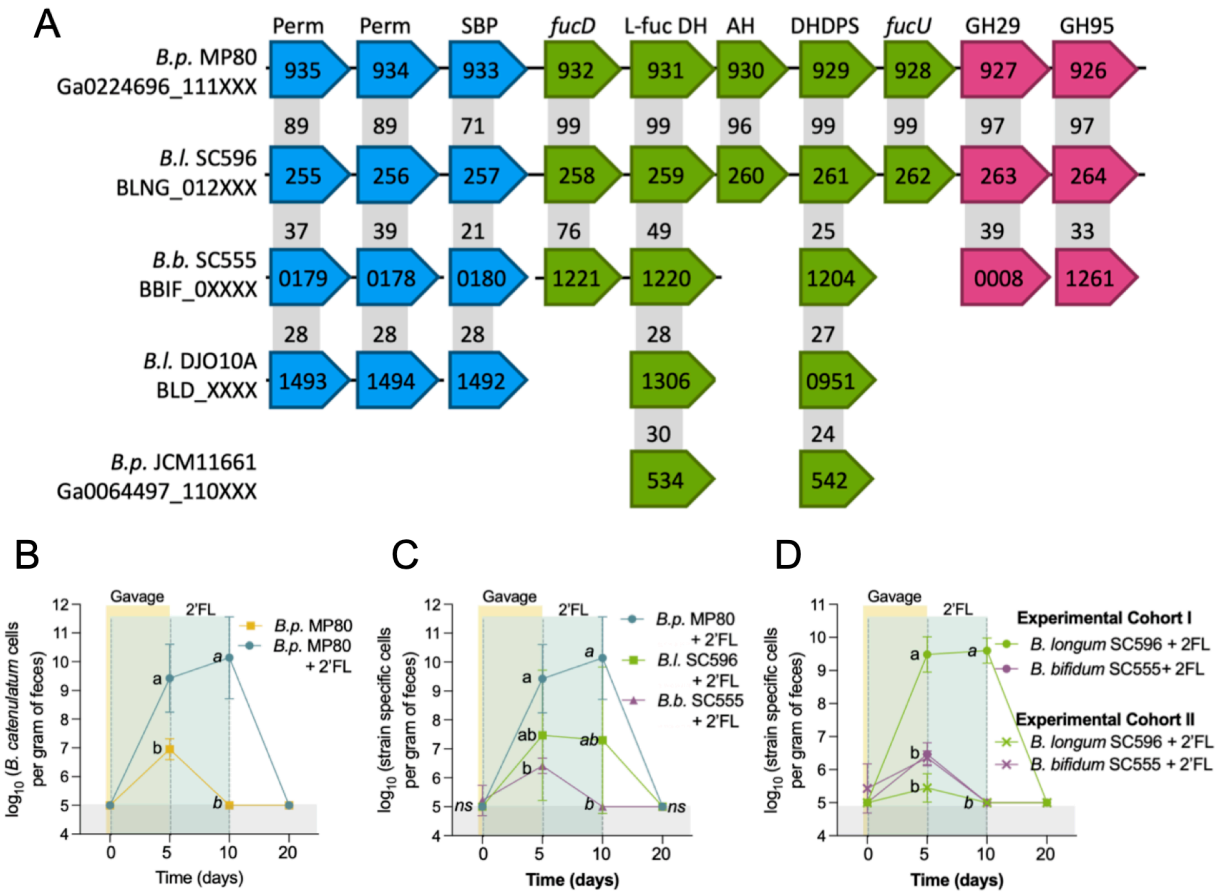

Figure 4.1. Genetic capacity and persistence of *Bifidobacterium* strains in mice. (A) Comparison of fucosylated HMO utilization gene cluster amongst *Bifidobacterium* strains; (B) quantification of *B. pseudocatenulatum* MP80 by qPCR in fecal DNA of treatment groups *B.p.* MP80 + 2'FL (n = 6) and *B.p.* MP80 (n = 6); (C) quantification with strain-specific primers by qPCR in fecal DNA of treatments *B. pseuodocatenulatum* MP80 + 2'FL, *B. longum* SC596 + 2'FL, and *B. bifidum* SC555 (n = 6 per treatment), and (D) quantification with strain-specific primers by qPCR in fecal DNA of *B. longum* SC596 + 2'FL and *B. bifidum* SC555 separated by experimental cohort (n = 3 per trial); (E) log ratio of *Bifidobacteriaceae* ASVs relative to low ranked *Lachnospiraceae* and *Ruminococcaceae* ASVs on the final day of 2'FL supplementation (day 10) between control, *B. pseudocatenulatum* MP80, 2'FL, and *B. pseudocatenulatum* MP80 + 2'FL (n = 6 per treatment).

In (A) arrows represent genes and the number is the locus tag number for the respective genome (Joint Genome Institute). Number in gray box indicates percent identity between corresponding gene and homologs relative to strain *B. pseudocatenulatum* MP80. Colors are indicative of the primary function: oligosaccharide transport (blue), carbohydrate feeder pathways (green) and glycosyl hydrolases (pink). Perm: ABC Permease; SBP: Solute Binding Protein; L-Fuc DH: L-fuconate dehydrogenase; DHDPS: Dihydropicolinate synthase; FucU: L-fucose mutarotase. In (B), (C), and (D) day 0: baseline; day 5: *Bifidobacterium* or PBS gavage days (yellow); day 10: 2'FL supplementation (mint); day 20: washout of 2'FL, day before necropsy (no color). In (B), (C), and (D) different letters signify statistical difference between treatments by day (ANOVA with Tukey's multiple comparison testing; $p < 0.05$). Data from (B) reproduced from Heiss & Ehrlich et al., 2021.

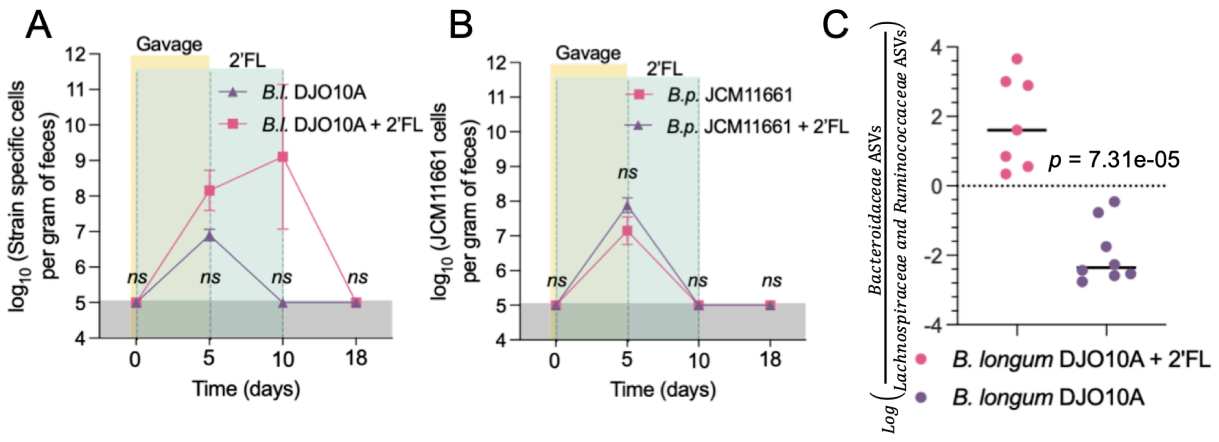

Figure 4.2. Persistence of non-2'FL catabolizing *Bifidobacterium* strains. (A) Quantification of *B. longum* DJO10A by qPCR in fecal DNA of treatment groups *B. longum* DJO10A + 2'FL and *B. longum* DJO10A (n = 3 per treatment); (B) quantification of *B. pseudocatenulatum* JCM11661 by qPCR in fecal DNA of treatment groups *B. pseudocatenulatum* JCM11661 + 2'FL and *B. pseudocatenulatum* JCM11661 (n = 3 per treatment), and (C) log ratio of *Bacteroidaceae* ASVs relative to low ranked *Lachnospiraceae* and *Ruminococcaceae* ASVs during 2'FL supplementation (days 6, 8 and 10) analyzed by t test. Multiple unpaired t tests for comparison of bacterial abundance between treatments by day.

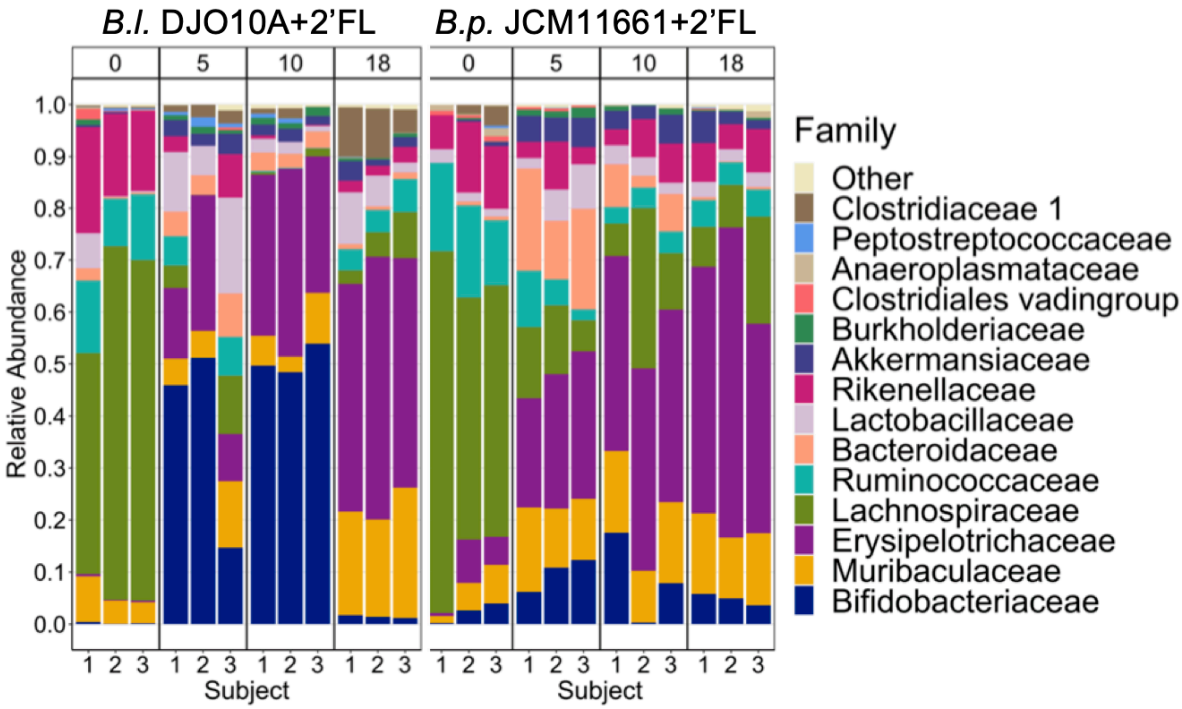

Figure 4.3. Barplots of bacterial family relative abundance for individual mice from treatment groups *B. longum* DJO10A + 2'FL and *B. pseudocatenulatum* JCM11661 +2'FL (n = 3 per treatment) at four time points (day 0: baseline, after one week of acclimation in the facility; day 5: last day of *Bifidobacterium* or PBS gavage; day 10: last day of 2'FL supplementation; day 18: after 8 days washout of 2'FL, day before necropsy). Numbers along the x-axis indicate individual mice.

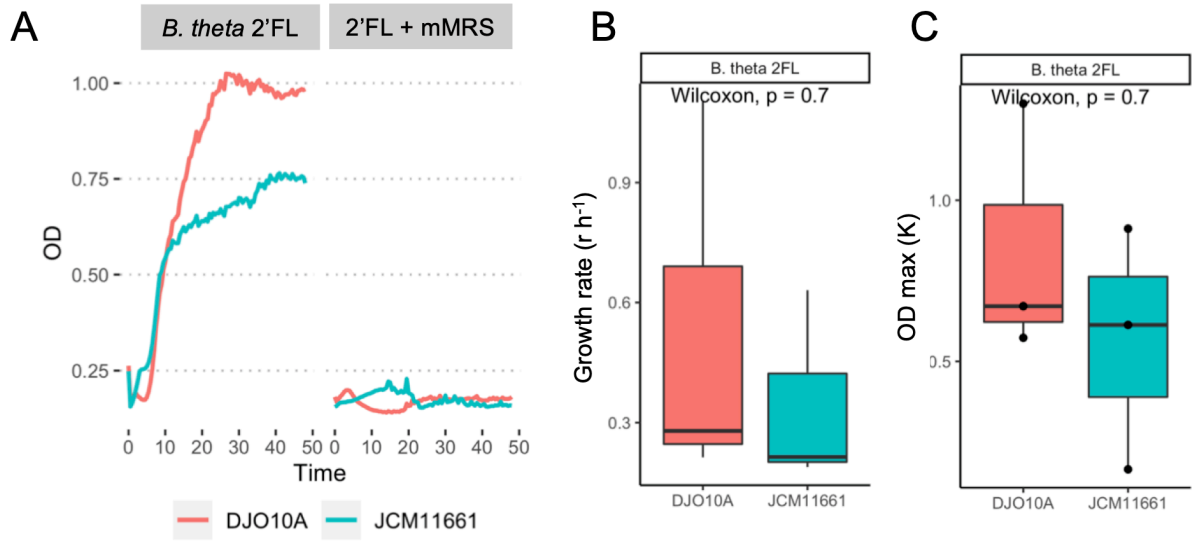

Figure 4.4. Cross-feeding growth curves and kinetics of non-2'FL catabolizing *Bifidobacterium* strains. (A) Growth curve of *B. longum* DJO10A and *B. pseudocatenulatum* JCM11661 on modified MRS (mMRS) + 2% 2'FL or filtered spent media from *B. thetaiotoamicron* grown on mMRS + 2% 2'FL (*n* = 3 biological replicates); (B) and (C) growth kinetics of *Bifidobacterium* strains grown on spent *B. thetaiotaomicron* media (Wilcoxon test).

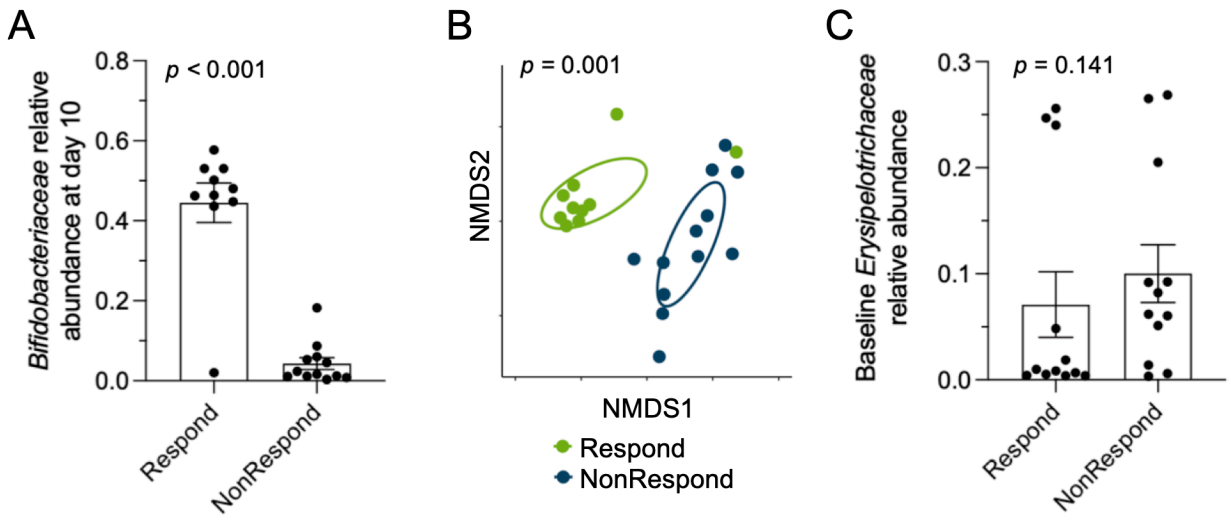

Figure 4.5. Microbial community structure changes between responders and non-responders. (A) *Bifidobacteriaceae* relative abundance at the final day of 2'FL supplementation (day 10) for responders (n = 12) and non-responders (n = 12); (B) microbial community NMDS plot of responder and non responders on day 10 (n = 12 per group); and (C) relative abundance of *Erysipelotrichaceae* in responder and non-responder groups at baseline (day 0) (n = 12 per group). NMDS was generated using β-diversity index weighted unifrac distance in two dimensions.

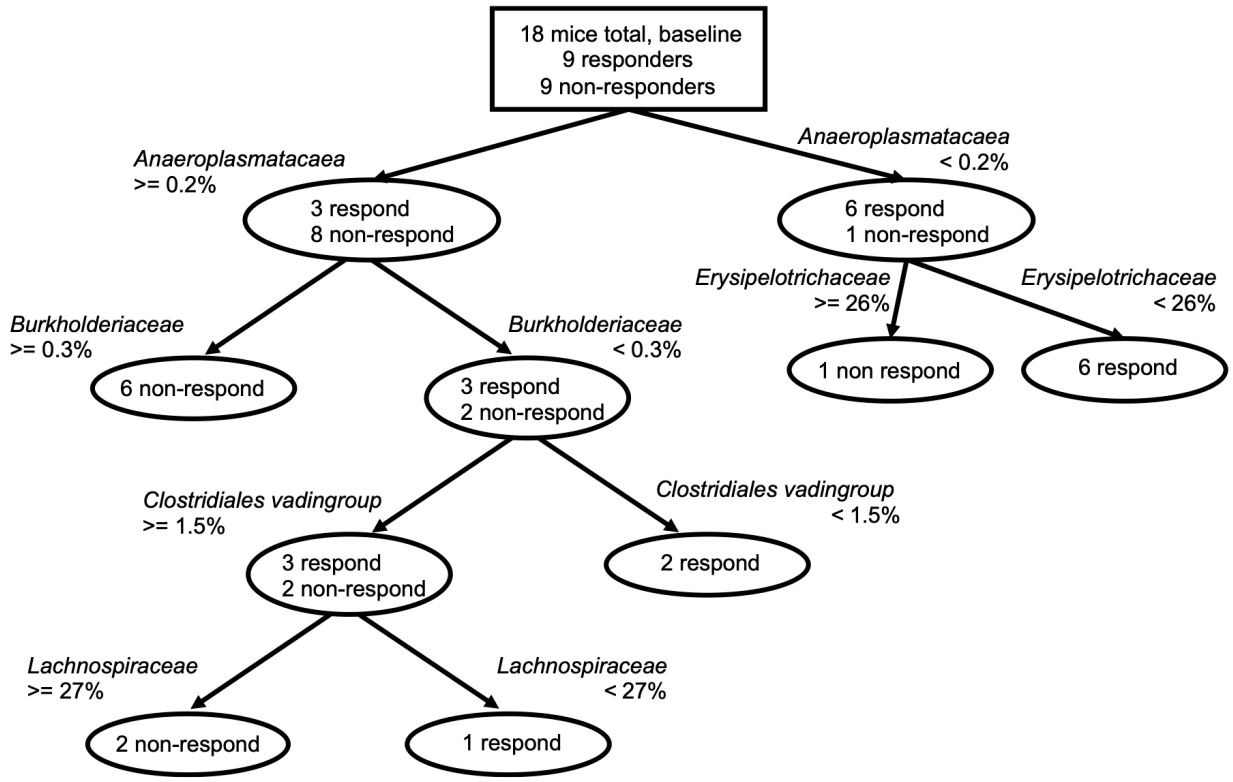

Figure 4.6. Classification tree baseline microbial taxa of *B. pseudocatenulatum* MP80 + 2'FL, *B. longum* SC596 + 2'FL, and *B. bifidum* SC555 + 2'FL treated mice at baseline to predict responder or non-responder.

Chapter 5: Addendum

Fucosylated human milk oligosaccharide foraging within the species *Bifidobacterium pseudocatenulatum* is driven by glycosyl hydrolase content and specificity

Guy Shani[1§], Jennifer L Hoeflinger[1‡], Britta E Heiss[1†], Chad F Masarweh[1], Jules A Larke[2], Nick M Jensen[1], Saumya Wickramasinghe[1], Jasmine C Davis[3], Elisha Goonatilleke[3], Amr El-Hawiet[4,5], Linh Nguyen[5], John S Klassen[5], Carolyn M Slupsky[2,6], Carlito B Lebrilla[3,6], David A Mills[1,6*]

Author Affiliations: [1]Department of Food Science and Technology, University of California Davis, Davis, CA, USA; [2]Department of Nutrition, University of California Davis, Davis, CA, USA, [3]Department of Chemistry, University of California Davis, Davis, CA, USA, [4]Department of Pharmacognosy, Faculty of Pharmacy, Alexandria University, Alexandria, [5]Alberta Glycomics Centre and Department of Chemistry, University of Alberta, Edmonton, AB, Canada, [6]Foods for Health Institute, University of California Davis, Davis, CA, USA

5.1 Preface

This project was initiated by Dr. Guy Shani and portions of this data set appear in their dissertation. This manuscript is included as an addendum to recognize the contributions I made. Specifically, I wrote portions of the manuscript, conducted qRT-PCR of bacteria grown on 2'FL, performed RNA-Seq and analyzed bacteria grown on 2'FL, lactose, and LNFPI, and collaborated on the metabolite profiling of *B. pseudocatenulatum* MP80. This was submitted to Applied and Environmental Microbiology.

5.2 Abstract

Human milk enriches members of the genus *Bifidobacterium* in the infant gut. One species, *Bifidobacterium pseudocatenulatum*, is found in the gastrointestinal tracts of adults and breastfed infants. In this study, *B. pseudocatenulatum* strains were isolated and characterized to identify genetic adaptations to the breastfed infant gut. During growth on pooled human milk oligosaccharides (HMO) we observed two distinct groups of *B. pseudocatenulatum*, isolates that readily consumed HMO and those that did not, a difference driven by variable catabolism of fucosylated HMO. A conserved gene cluster for fucosylated HMO utilization was identified in several sequenced *B. pseudocatenulatum* strains. One isolate, *B. pseudocatenulatum* MP80, which uniquely possessed GH95 and GH29 α-fucosidases consumed the majority of fucosylated HMO tested. Furthermore, *B. pseudocatenulatum* SC585, which possesses only a single GH95 α-fucosidase, lacked the ability to consume the complete repertoire of linkages within the fucosylated HMO pool. Analysis of the purified GH29 and GH95 fucosidase activities directly on HMO revealed complementing enzyme specificities with the GH95 enzyme preferring 1-2 fucosyl linkages and the GH29 enzyme favoring 1-3 and 1-4 linkages. The HMO binding specificity of the Family 1 solute binding protein component linked to the fucosylated HMO gene cluster in both SC585 and MP80 are similar, suggesting differential transport of fucosylated HMO is not a driving factor in each strain's distinct HMO consumption pattern. Taken together, this data indicates the presence or absence of specific α-fucosidases directs the strain-specific fucosylated HMO utilization pattern among bifidobacteria and likely influences competitive behavior for HMO foraging *in situ*.

5.3 Importance

Often isolated from the human gut, microbes from the bacterial family *Bifidobacteriaceae* commonly possess genes enabling carbohydrate utilization. Isolates from breast fed infants often grow *in vitro* on and possess genes capable of catabolizing human milk oligosaccharides (HMO) which are found in human breast milk. However, catabolism of structurally diverse HMO differs between bifidobacteria strains. This study identifies gene differences between *Bifidobacterium pseudocatenulatum* isolates that may impact whether a microbe successfully colonizes an infant gut. In this case, the presence of complementary α-fucosidases may provide an advantage to microbes seeking residence in the infant gut.

5.4 Introduction

In humans, colonization of the gut microbiome in early life is strongly influenced by various elements in human milk. Human milk is composed of lactose, fats, proteins, and numerous bioactive molecules. One key constituent known to influence the gut microbiota are human milk oligosaccharides (HMO). These highly abundant (10 - 15 g L^{-1})[1] and structurally diverse bioactive molecules consisting of neutral (non-fucosylated and fucosylated) and acidic sialylated oligosaccharides.[2] While energetically dense, HMO are not digested by the infant but rather fermented by intestinal microbes, often infant-borne bifidobacterial.[3] Only one species of *Bifidobacterium*, *Bifidobacterium longum* subsp. *infantis*, has been shown to consume the full constellation of HMO structures[4–6] while isolates of other infant-borne species, including *Bifidobacterium longum* subsp. *longum*[7], *Bifidobacterium breve*[8], *Bifidobacterium kashiwanohense*[9], and *Bifidobacterium bifidum*[10] have been shown to consume portions of the HMO pool. These differential consumption phenotypes suggest that HMO delivered to infants enrich a network of primary bifidobacterial consumers who target different components of the HMO pool. In addition, some primary consumers partially degrade HMO externally, releasing component sugars which are consumed by recipient strains.[11,12] Similar HMO consumption networks could be predicted from other HMO consuming taxa like *Bacteriodes* species[13], *Akkermensia* species[14], *Roseburia* species[15] among other taxa that degrade HMO externally. These HMO consumption networks, along with the conditioning of the environment from production of organic acids[16] and lowering of pH[17], generated by fermentation of HMO likely limits entry into the infant colonic ecosystem.

The genome of *B. longum* subsp. *infantis* ATCC15697 contains transporters, substrate-binding proteins (SBP), and glycosyl hydrolases (GH) organized in a 43 kb cluster specialized for HMO utilization.[18] While other *Bifidobacterium* species exhibit growth on HMO, none grow as robustly as *B. longum* subsp. *infantis*. Although the closely related *B. longum* subsp. *longum* can broadly consume type I core HMO, relatively few strains are capable of metabolizing fucosylated HMO and none are known to consume sialylated HMO.[7] These growth differences have a clear genetic basis in *B. longum* subsp. *longum* SC596, which encodes two β-galactosidases and two α-fucosidases but lacks a sialidase [7]. *B. breve* strains

generally consume type I and II core HMO[6,8,19], whereas fucosylated and sialylated HMO consumption is restricted to a few specific strains.[8] The secretory enzymes, lacto-*N*-biosidase[20], α-fucosidase GH29[21], and α-fucosidase GH95[22], are necessary for extracellular cleavage of HMO prior to importation and catabolism in *B. bifidum*. While *B. longum*, *B. breve* and *B. bifidum* are well-studied, they are not the only *Bifidobacterium* species detected in breastfed infant feces.

Bifidobacterium pseudocatenulatum is prevalent in the feces of breastfed infants[8,16,23–27] as well as adults.[28–30] The bacterial composition of the infant and adult gut microbiome is distinct [31,32] and attributable in part to differences in dietary intake. These dietary differences may select for distinct metabolic abilities in infant- and adult-derived *B. pseudocatenulatum* strains. Of six *B. pseudocatenulatum* isolates from a cohort of Japanese breastfed infants, only three showed growth on pooled HMO, preferentially consuming fucosylated HMO, which corresponded to the presence of an α-fucosidase GH95 [16]. On the other hand, an adult-derived *B. pseudocatenulatum* strain 1E was unable to consume type II core HMO even though *in silico* analysis revealed that its genome encoded β-galactosidases and a β-hexosaminidase.[30] Further research is needed to understand strain-specific HMO utilization in *B. pseudocatenulatum*. In this study, we explored the genetic basis of fucosylated HMO consumption in infant-derived, adult-derived and commercially available *B. pseudocatenulatum* strains.

5.5 Results

5.5.1 Isolation and phylogenetic analysis of *Bifidobacterium pseudocatenulatum*

To evaluate a diverse pool of *B. pseudocatenulatum* strains for HMO growth phenotypes isolates were obtained from many sources (**Table 5.1**). Most *B. pseudocatenulatum* strains were obtained from earlier studies (infant-derived)[8,33], culture collections (various sources) and colleagues (lamb-derived).[34] An adult-derived *B. pseudocatenulatum* GST210 was isolated from a fecal sample donated by an individual participant in a bovine milk oligosaccharide supplementation tolerance trial.[35] All *B. pseudocatenulatum* isolates (n = 62) were characterized with multilocus sequence typing. In total, 11 unique allelic profiles were observed (data not shown) and concatenated to construct a phylogenetic tree (**Figure S5.1**). While *B. pseudocatenulatum* DSM20438 had an identical allelic profile to *B. pseudocatenulatum* MP86, both isolates were included in this study since they came from two very different sources. All twelve *B. pseudocatenulatum* strains are listed in **Table 5.1**.

5.5.2 Growth of *B. pseudocatenulatum* isolates on pooled HMO and select purified fucosylated HMO

Isolates of *B. pseudocatenulatum* (n = 12) were examined for their ability to consume pooled HMO. All *B. pseudocatenulatum* isolates grew well on lactose (positive control, data not shown), whereas growth on pooled HMO varied (**Figure 5.1a-b**). The *B. pseudocatenulatum* isolates SC585, MP80, MP86, DSM20438 (infant-derived), and JCM7040 (human-derived) grew to a maximum OD ($0.94 \leq OD \leq 1.17$) similar to the positive control *B. longum* subsp. *infantis* ATCC15697 (OD = 1.13, **Figure 5.1a**). In contrast, the *B. pseudocatenulatum* isolates SC237, SC564, SC665, SC666 (infant-derived), JCM11661 (origin unknown), GST210 (adult-derived), and L15 (lamb-derived) grew to a maximum OD ($0.39 \leq OD \leq 0.59$), similar to the negative control *Bifidobacterium animalis* subsp. *lactis* ATCC27536 (OD = 0.51, **Figure 5.1b**). Since the purification of pooled HMO does not remove 100% of the lactose, it is common to observe minimal growth.

The specific HMO structures consumed by each *B. pseudocatenulatum* were characterized by mass spectrometry-based glycoprofiling of the spent media (**Figure 5.1c and Table S5.2**). Isomers lacto-*N*-tetraose (LNT) and lacto-*N*-neotetraose (LNnT) were depleted (>94%) by most *B. pseudocatenulatum*

isolates, but consumption was undetectable in *B. pseudocatenulatum* SC585 (infant-derived), SC237, and L15 (lamb-associated).

Consumption of fucosylated HMO by *B. pseudocatenulatum* isolates varied by structure. 2'-fucosyllactose (2'-FL) and lactodifucotetraose (LDFT) were depleted almost entirely by *B. pseudocatenulatum* SC585, MP80, MP86, JCM7040, and DSM20438 (all >97%). All *B. pseudocatenulatum* isolates exhibited some consumption of LDFT (26 – 47%). Lacto-*N*-fucopentaose type I and III (LNFP I and LNFP III, respectively) were consumed by *B. pseudocatenulatum* that consumed 2'-FL, albeit to a lesser extent (66-85%). Uniquely, *B. pseudocatenulatum* MP80 consumed Lacto-*N*-difucohexaose type I and II isomers (LNDFH I and LNDFH II, 55%). *B. longum* subsp. *infantis* ATCC15697 demonstrated an ability to consume higher-molecular weight HMO, whereas *B. pseudocatenulatum* isolates preferred lower-molecular weight fucosylated HMO (**Table S5.2**).

To explore subtle differences observed in growth on HMO pools (**Figure 5.1c**) select *B. pseudocatenulatum* strains were examined for growth on purified HMO species. Strains SC585, MP80, MP86, JCM7040, and DSM20438 grew on purified 2'-FL, 3'-fucosyllactose (3'-FL) (**Figure 5.2a-b).** While *B. pseudocatenulatum* JCM11661 consumed 2'-FL from pooled HMO (22%, **Figure 5.1c**), it failed to grow robustly on purified 2'-FL as the sole carbon source (**Figure 5.2a**). Notably SC585 was able to grow on LNT but failed to grow on LNnT while MP80 readily grew on both isomers **(Figure 5.2c)**. However, both MP80 and SC585 readily grew on LNFP1 which contains the LNnT type 2 core (**Figure 5.2d**).

Growth of *B. pseudocatenulatum* MP80 on 2'-FL and lactose produced the end products, acetate (44.71 mM ± 1.21 vs. 44.51 mM ± 0.20; p=0.185), lactate (19.06 mM ± 0.53 vs. 22.79 ± 0.12; p=0.027), and ethanol (0.92 mM ± 0.02, 0.35 mM ± 0.003; p<0.01). *B. pseudocatenulatum* MP80 produced significantly higher amounts of formate (6.20 mM ± 0.23 vs. 0.74 mM ± 0.002; p<0.01), pyruvate (2.82 mM ± 0.11 vs. 0.12 mM ± 0.002; p<0.01), and 1,2-propanediol (2.82 mM ± 0.18 vs. 0.00 mM ± 0.00; p<0.01) following growth on 2'-FL as compared to growth on lactose (**Table 5.2)**. The metabolites

observed provide functional validation of the MP80 fucose catabolism via the propanediol pathway observed in other fucosylated HMO (F-HMO) consuming bifidobacterial strains.[9]

5.5.3 Characterization of a fucosylated HMO utilization gene cluster

To identify genes required for fucosylated HMO consumption, we sequenced the genomes of *B. pseudocatenulatum* SC585, MP80, JCM7040, JCM11661, L15, and GST210 (refer to **Table S5.3** for a summary of the sequencing metrics). *B. pseudocatenulatum* L15 and GST210 were included as representative HMO "non-consumers." These newly sequenced *B. pseudocatenulatum* strains have comparable genome sizes and characteristics to *B. pseudocatenulatum* DSM20438.

A cluster of genes, predicted to be associated with the consumption of F-HMO, was readily observed in *B. pseudocatenulatum* SC585, MP80, JCM7040 and DSM20438 (**Figure 5.3**). Annotated genes in this cluster include two ATP-Binding Cassette (ABC) transporter permease components, a family-1 (oligosaccharide-binding) ABC transporter substrate-binding protein, a L-fuconate dehydratase, a L-fucose dehydrogenase, a metal-dependent hydrolase, a 4-hydroxy-tetrahydrodipicolinate synthase, and an α-fucosidase GH95. *B. pseudocatenulatum* L15 or GST210 did not contain the putative F-HMO gene cluster consistent with their inability to robustly consume F-HMO (**Figure 5.1c**). Interestingly, two additional genes, a fucose mutarotase and an α-fucosidase GH29, were observed in *B. pseudocatenulatum* MP80. These additional genes are homologous to the fucose mutarotase and α-fucosidase GH29 from *B. longum* subsp. *infantis* ATCC15697.

A survey of publicly available *B. pseudocatenulatum* genomes revealed a subset of strains possessing homologs of the fucosidase operon found in *B. pseudocatenulatum* SC585, MP80, and JCM7040 (**Figure 5.4**). Of this subset, strains CA-C29, CA-K29a, and CA-K29b are infant-derived, while, the *B. pseudocatenulatum* isolates TM10-1, AF17-20AC, and AF45-10BH were isolated from human feces of an unreported age. Unique among *B. pseudocatenulatum* isolates, *B. pseudocatenulatum* MP80 possessed two α-fucosidases (GH29 and GH95), resembling the genomes of *B. longum* subsp. *infantis* ATCC15697 and *B. longum* subsp. *longum* SC596.[7,36] This additional fucosidase presence in MP80 and absence in the other

F-HMO consuming *B. pseudocatenulatum* strains (SC585, JCM7040 and DSM20438) likely contributes to the differential F-HMO catabolism capacity describe above. Aside from some shared ABC transporter permeases, most *B. pseudocatenulatum* strains lack homologs of the fucosidase operon entirely **(Figure 5.4**).

While the presence or absence of this main F-HMO gene cluster clearly differentiated the more robust F-HMO consumer strains (MP80, SC585, JCM7040) from the "non-consumers" (L15, JCM11661, GST210) it did not explain other subtle differences in HMO consumption patterns between some strains. Notably, glycoprofiling revealed that strain SC585 did not consume LNT/LNnT (**Figure 5.1c**). While SC585 lacked ability to grow on LNnT and LNT it was able to grow well on LNFP1 which contains LNnT as a core (**Figure 5.2d**). Moreover, the shared presence of HMO-related GHs in sequenced strains MP80, JCM7040 and SC585 (**Figure 5.4b**) does not predict the differential consumption of LNnT/LNT in these strains, demonstrating the requirement for individual strain glycoprofiling of HMO consumption preferences (from HMO pools) as well as growth on individual HMO to truly decipher strain level HMO foraging behavior. At present the mechanism underlying the lack of growth of SC585 on LNnT remains unresolved.

Transcriptomics of MP80 grown on lactose, 2'-FL and LNFP1 revealed clear induction of the main F-HMO cluster (the cluster shown in Figure 3) with each gene of the cluster induced from 16- to 48-fold upon growth on the two F-HMO (**Table 5.3**). In addition, an LNB/GNB gene cluster common to many bifidobacteria including those that do not consume F-HMO[37] as strongly was upregulated during growth on LNFP1 but not on 2'FL, likely due to the fact that LNFP1 contains N-acetylglucosamine. This complements a previous observation of the lack of induction of the LNB/GNB cluster during growth on 2'FL in a *B. longum* strain that harbors a similar F-HMO cluster.[7] In a separate experiment using qRT-PCR, strain SC585, which possessed the similar gene cluster for fucose consumption to MP80 but lacks the GH29 fucosidase, showed a similar induced the GH95 fucosidase (Ga0064049_111413) and SBP (Ga0064049_111418) during growth on 2'-FL (**Figure S5.2**) suggesting a common regulation across strains harboring this F-HMO gene cluster.

5.5.4 B. pseudocatenulatum MP80's α-fucosidase substrate digestion specificity

In this work, most *B. pseudocatenulatum* strains that grow on F-HMO only contained a single GH95 class α-fucosidases. However, as shown in **Figure 5.3 and 5.4**, MP80 contained both GH95 and GH29 type α-fucosidases similar to those previously characterized in *B. longum* subsp. *infantis*[36] and *B. longum* subsp. *longum* SC596.[7] To understand the specificity of the MP80 α-fucosidases (GH29:Ga0224696_111927 and GH95:Ga0224696_111926) both were cloned, the enzymes purified and their activity assessed against an HMO pool as described previously.[7] While both α-fucosidases (GH29 and GH95) digested 2'-FL, the GH95 α-fucosidase showed higher activity (100%) as compared to the GH29 α-fucosidase (42.8%, **Table 5.4**). Overall, the GH95 α-fucosidase was more active than the GH29 α-fucosidase on 2-linked terminal fucose moieties (**Table 5.4**). Conversely, the GH29 α-fucosidase was more active than the GH95 α-fucosidase on 3- and 4-linked terminal fucose moieties (**Table 5.4**). In general, the addition of the GH29 enzyme (Ga0224696_111927) promoted cleavage of a range of HMO moieties poorly cleaved by the GH95 enzyme (Ga0224696_111926) (bolded structures in **Table 5.4**) suggesting the addition of the second α-fucosidase expanded the pool of fucosylated HMO catabolized by MP80 by comparison to strains like SC585 which only contain a single GH95 type α-fucosidase.

5.5.5 B. pseudocatenulatum MP80 and SC585 fucosidase operon SBP's substrate binding specificity

As shown above, strains MP80 and SC585 were able to consume fucosylated HMO however differences were noted, particularly consumption of higher MW HMO by MP80. Given we did not witness differences in SBP and GH95 expression between MP80 and SC585 we postulated ATP transporter specificity differences between the strains might also drive the HMO consumption differences in addition to the added GH29 fucosidase in MP80. Notably the SBPs from each strain (Ga00224696_111993 vs. Ga0064049_111418) were only 71% identical by comparison to the higher identity among the remaining genes in this operon between the two strains (**Figure 5.3**) which is clearly different than the near identical homology among the remaining genes in the cluster. The SBPs from *B. pseudocatenulatum* MP80 and SC585 were cloned, purified and substrate binding affinity to a variety of HMO structures was determined using the catch-and-release electrospray ionization mass spectrometry.[38,39] 2'-FL and 3'-FL had the

strongest binding affinity to SBPs from both *B. pseudocatenulatum* MP80 and SC585 (**Figure 5.5**). Several fucosylated HMO, including 2-, 3-, and 4-linked terminal fucose moieties, showed a moderate binding affinity to SBPs from *B. pseudocatenulatum* MP80 and SC585. Specifically, *B. pseudocatenulatum* SC585's SBP moderately bound fucosylated HMO with smaller (≤4 monomers) and unbranched backbone structures (3'-sialyl Lewis A and Blood group A antigen tetraose type 5). Of note, *B. pseudocatenulatum* MP80's SBP uniquely bound to longer (>4 monomers) and branched backbone structures (Difucosyllacto-*N*-hexaose A and Difucosyl-para-lacto-*N*-hexaose II). Sialylation did not prevent binding of either strain's SBP and binding affinity did not require fucosylation. A complete list of HMO structures evaluated is presented in **Table S5.5 and S5.6**.

5.6 Discussion

HMO serve as a nutritional source for the proliferation of *Bifidobacterium* species in breastfed infants.[40,41] The relative abundance and composition of *Bifidobacterium* species are correlated with maternal secretor status[33] and fucosylated HMO-consuming *Bifidobacterium* species promote beneficial intestinal metabolite profiles and microbiome compositions.[16] *B. pseudocatenulatum* is frequently detected member in the mammalian gut microbiota[30], including in breastfed infants[8,16,23–27] and adults.[28–30] Therefore, it is important to examine the genomic diversity of *B. pseudocatenulatum* strains to understand its presence in several distinct ecological contexts. Unlike other species common to breastfed neonates—such as *B. longum* subsp. *infantis*, *B. longum* subsp. *longum*, *B. breve*, or *B. bifidum—B. pseudocatenulatum* has been poorly studied despite its frequent presence in breastfed infant feces. In this study, a fucosylated HMO utilization gene cluster was identified and characterized in a subset of infant-derived *B. pseudocatenulatum* strains.

5.6.1 Presence of a fucosylated HMO gene cluster drives strain-dependent utilization

Growth studies revealed a subset of HMO-consuming *B. pseudocatenulatum* isolates originating from breastfed infants. Unlike these strains, other tested *B. pseudocatenulatum* isolates, including infant-, adult-, and lamb-derived specimens, did not consume HMO as a sole carbon source. It was not surprising to observe poor consumption of HMO in the adult- and lamb-derived *B. pseudocatenulatum* since HMO are not a part of an adult or lamb's diet. However, the differential HMO consumption in infant-derived *B. pseudocatenulatum* isolates may be due to the presence or absence of HMO catabolism genes.

Bifidobacterium species possess highly specialized HMO utilization gene clusters which promote assimilation and catabolism of neutral non-fucosylated/non-sialylated, neutral fucosylated and acidic sialylated HMO.[42] Not all isolated *Bifidobacterium* strains from breastfed infants are capable of consuming all HMO isomers, due to missing, incomplete or dysfunctional HMO utilization gene clusters.[8,16,27,43–45] Whole-genome sequencing of *B. pseudocatenulatum* SC585, MP80, and JCM7040 (all infant-derived) revealed an intact fucosylated HMO utilization gene cluster containing oligosaccharide transporters, a carbohydrate feeder pathway and glycosyl hydrolase genes (**Figure 5.3**). This gene cluster's structure and

composition is homologous to the fucosylated HMO utilization gene clusters in *B. longum* subsp. *infantis* ATCC15697[18], *B. longum* subsp. *longum* SC596[7], *Bifidobacterium kashiwanohense* PV20-2[9], and other *B. pseudocatenulatum* isolates (**Figure 5.4**).[16]

A broad analysis of publicly available *B. pseudocatenulatum* genomes illustrates a subset of *B. pseudocatenulatum* strains uniquely capable of consuming fucosylated HMO (**Figure 5.4)**. Additionally, *B. pseudocatenulatum* MP80 is unique among *B. pseudocatenulatum* isolates given that it possesses two α-fucosidases (GH29 and GH95). This gene cluster was missing in the fucosylated HMO non-consuming *B. pseudocatenulatum* strains JCM11661, L15, and GST210 included in this study. Previous studies and our analysis (**Figure 5.4**) demonstrate that the presence or absence of genes within this gene cluster separates *B. pseudocatenulatum* strains into either consumers or non-consumers of fucosylated HMO.[16,27] Matsuki and colleagues[16] concluded that the fucosylated HMO utilization pathway, present in other isolated *Bifidobacterium* species as well as a subset of *B. pseudocatenulatum*, was fundamental in their cohort of Japanese infants (n = 12). Infants consuming breastmilk from secretor mothers and harboring fucosylated HMO-consuming *Bifidobacterium* species (B1 cluster) were characterized by lower fecal pH and higher concentrations of fecal acetate. They concluded that fucosylated HMO-consuming *Bifidobacterium* species, including *B. pseudocatenulatum*, contributed to a beneficial infant gut microbiota.

5.6.2 *B. pseudocatenulatum* MP80, a robust fucosylated HMO consumer, possesses complementary α-fucosidases (GH29 and GH95)

Previous characterization of the fucosylated HMO utilization gene cluster in *B. pseudocatenulatum* strains found that a single α-fucosidase belonging to the GH95 family was associated with consumption of 2'-FL (16,27) and other fucosylated HMO.[16] However, the genome of *B. pseudocatenulatum* MP80 contains an additional α-fucosidase (GH29), consistent with the gene clusters in *B. longum* subsp. *infantis* ATCC15697[18] and several other *Bifidobacterium* species[7–9,16,27] but not seen previously in *B. pseudocatenulatum*.[16,27] Additionally, both α-fucosidases (GH29 and GH95) were required for robust growth on 2-, 3-, and 4-linked fucosylated HMO in *B. breve* SC95, SC154, and SC568.[8] The α-fucosidase GH29 has been shown to preferentially cleave 3- and 4-linked terminal fucose moieties[7,21,36],

complementing the α-fucosidase GH95's preference for 2-linked fucosylated HMO.[22,46] Enzymatic substrate digestion specificity confirmed that *B. pseudocatenulatum* MP80's α-fucosidase GH29 preferentially cleaved 3- and 4-linked terminal fucose moieties (**Table 5.4**). However, growth on 3- and 4-linked fucosylated HMO did not require an α-fucosidase GH29 because *B. pseudocatenulatum* strains SC585, JCM7040, and DSM20438 (lacking the α-fucosidase GH29) grew equally well on 2'-FL and 3'-FL. These data suggest that the α-fucosidase GH95 has some cross-reactivity on 3- and 4-linked fucosylated HMO in *B. pseudocatenulatum* strains (**Table 5.4)**. The catalytic specificity of α-fucosidase GH95s differs among *Bifidobacterium* species. Katayama and colleagues (2004) did not observe cleavage of 3- or 4-linked fucosylated HMO with *B. bifidum* JCM1254's extracellular GH95 α-fucosidase. However, *B. longum* subsp. *infantis* ATCC15697 moderately cleaved 3-linked fucosylated HMO[46] and several *B. breve* strains consumed 3'-FL with a single α-fucosidase GH95 and no α-fucosidase GH29.[8] The amino acid sequence of the GH95 α-fucosidase in *B. pseudocatenulatum* MP80, *B. longum* subsp. *infantis* ATCC15697 (78%) and *B. breve* JCM7019 (97%) are homologous while not being homologous to *B. bifidum* JCM 1254 (32%). While the presence of the α-fucosidase GH95 is sufficient for growth and cleavage of 3- and 4-linked fucosylated HMO *in vitro*, substrate competition *in vivo* may still show a growth advantage to *Bifidobacterium* possessing the complementary α-fucosidase GH29.

5.6.3 Expanded fucosylated HMO consumption in *B. pseudocatenulatum* MP80 cannot be attributed to a more divergent substrate-binding protein

The *B. longum* subsp. *infantis* ATCC15697 genome encodes a plethora of family 1 SBPs to facilitate transport of HMO via ABC permeases.[18,47] The *B. longum* subsp. *infantis* ATCC15697 SBP (Blon_2202) and ABC permeases (Blon_2203-2204) are homologous (71-90% identical amino acid sequences) to the *B. pseudocatenulatum* MP80 SBP (Ga0224696_111933) and ABC permeases (Ga0224696_111934-111935). The *B. longum* subsp. *infantis* ATCC15697 SBP (Blon_2202) has been shown to bind fucosylated HMO.[47,48] Given its proximity to fucosylated HMO catabolism genes and homology to *B. longum* subsp. *infantis* ATCC15697's SBP (Blon_2202), it is hypothesized that the SBP from *B. pseudocatenulatum* MP80 (Ga0224696_111933) also binds fucosylated HMO. Catch and release

electrospray ionization mass spectrometry assay showed moderate to strong binding of *B. pseudocatenulatum* MP80's SBP (Ga0224696_111933) to 2-, 3-, and 4-linked fucosylated HMO (**Figure 5.5**). Recently, the crystal structure and ligand binding site of *B. longum* subsp. *infantis* ATCC15697's SBP (Blon_2202) was resolved for binding both 2'-FL and 3'-FL with a rotation of 50° to accommodate the different fucose moiety linkages.[48] Therefore, the strong binding affinity for both 2'-FL and 3'-FL observed with *B. pseudocatenulatum* MP80's SBP (Ga0224696_111933) was not unexpected. Additionally, *B. pseudocatenulatum* MP80's SBP (Ga0224696_111933) moderately bound to several larger (DP >3) 2-, 3-, and 4-linked fucosylated HMO. Sakanaka and colleagues [48] suggest that the binding pocket features of *B. longum* subsp. *infantis* ATCC15697's SBP (Blon_2202) would likely accommodate larger fucosylated HMO (DP >3) at lower affinities.[48] Along with the presence of the α-fucosidase GH29, the divergent SBP (Ga0224696_111933) in *B. pseudocatenulatum* MP80 may allow access to a broader range of fucosylated HMO catabolism.

The infant-derived *B. pseudocatenulatum* SC585 strain, possessing one α-fucosidase (GH95), consumed less diverse fucosylated HMO structures (**Figure 5.1c**) as compared to *B. pseudocatenulatum* MP80. The homologous SBP (Ga0064049_111418) from *B. pseudocatenulatum* SC585 differed in amino acid sequence (71% similar) perhaps suggesting a slightly lower binding specificity for fucosylated HMO. However, catch and release electrospray ionization mass spectrometry assay did not show a significant difference in the binding specificity between the SBP's from *B. pseudocatenulatum* MP80 and SC585. This result was not surprising given the greater homology (91% amino acid sequence) between the SBPs from *B. pseudocatenulatum* SC585 (Ga0064049_111418) and *B. longum* subsp. *infantis* ATCC15697 (Blon_2202) and suggests that *B. pseudocatenulatum* MP80's complementary α-fucosidases (GH29 and GH95) promotes expanded fucosylated HMO consumption capability as compared to other infant-derived *B. pseudocatenulatum* strains.

5.6.4 Conclusion

B. pseudocatenulatum is a widely dispersed species isolated from a number of diverse environments. This study, among others, demonstrates a genetic basis for specialized fucosylated HMO

consumption in a subset of *B. pseudocatenulatum* strains isolated from breastfed infants.[16,27] In particular, the fucosylated HMO utilization gene cluster from *B. pseudocatenulatum* MP80 indicates that the presence of complementary α-fucosidases (GH29 and GH95) may provide an advantage to residence in the infant gut and could prove advantageous if developed into a breastfed infant delivered probiotic product.

5.7 Methods

5.7.1 Isolation and identification of *Bifidobacterium pseudocatenulatum* strains

To isolate adult-derived *B. pseudocatenulatum*, 100 mg feces were vortexed in 900 µL sterile 1X PBS, pH 7.4, serially diluted tenfold in PBS, and plated (50 µL) onto modified *Bifidobacterium* selective iodoacetate mupirocin (BSIM).[33] Plates were incubated at 37°C for 48 h anaerobically (5% CO_2, 5% H_2, and 90% N_2; Coy Laboratory Products). Colonies were streaked for three successive passages onto deMan, Rogosa, and Sharpe supplemented with 500 mg L^{-1} L-cysteine-HCl (MRSC) agar and subcultured into MRSC broth and stored at -80°C in 25% (v/v) glycerol. Additional strains of *B. pseudocatenulatum* (**Table 5.1**) were obtained from the American Type Culture Collection (ATCC), the Japanese Collection of Microorganisms (JCM), German Collection of Microorganisms and Cell Cultures (DSM) and previous isolation studies.[8,33,34] Identity of *B. pseudocatenulatum* strains were confirmed by matrix-assisted laser desorption/ionization-time of flight biotyper mass spectrometry as previously described.[33]

5.7.2 Multilocus sequence typing of *B. pseudocatenulatum* isolates

The intragenic regions of seven housekeeping genes (*clpC*, *fusA*, *gyrB*, *ileS*, *purF*, *rplB*, and *rpoB*) were selected based on previous work.[49] Primers (**Table S5.1**) were optimized using the publicly available *B. pseudocatenulatum* DSM20438 genome (Genbank Accession #AP012330). Genomic DNA was extracted with the MasterPure Gram Positive DNA Purification kit (Epicentre) and amplified on a PTC-200 Peltier Thermal Cycler (Bio-Rad). A 50 µL reaction with 1 µL extracted DNA, 1 µL of each primer (10 µM), 1 µL dNTPs, 5 µL 10X PCR buffer, 5 µL $MgCl_2$, and 0.25 µL (1.25 U) AmpliTaq Gold™ DNA polymerase (Applied Biosystems). Cycling parameters were 4 min at 95°C, 30 cycles of 95°C for 30 s, 63 - 67°C for 1 min, and 72°C for 1 min, followed by 7 min at 72°C. Amplification was confirmed by gel electrophoresis and the PCR products were purified using the QiaQuick 96 PCR purification kit (Qiagen). Sequencing was performed on an ABI 3730 Capillary Electrophoresis Genetic Analyzer using BigDye Terminator chemistries at the University of California, Davis DNA Sequencing Facility. The sequences were analyzed and aligned with CLUSTALW using BioEdit (version 7.0). Phylogenetic analysis of

concatenated sequence loci was performed (version 6.0) and a minimum evolution tree was calculated (version 7.0) using the Molecular Evolutionary Genetic Analysis software.

5.7.3 *In-vitro* consumption of human milk oligosaccharides

B. pseudocatenulatum strains (**Table 5.1**) were tested for growth in the presence of pooled HMO, purified from breast milk as described previously[50], and lactose (positive control). *B. longum* subsp. *infantis* ATCC15697 and *B. animalis* subsp. *lactis* ATCC27536 were used as positive and negative HMO growth controls, respectively. All growths were conducted anaerobically at 37°C. *Bifidobacterium* species were cultured onto MRSC agar, incubated for 48 h and subcultured into 500 µL MRSC broth. After 24 h of growth, 2% (v/v) was subcultured into 500 µL MRSC broth and incubated for 18 h. A 96-well plate containing 200 µL of modified MRS medium (mMRS)[33] supplemented with 2% (w/v) of pooled HMO or lactose per well was inoculated with 4 µL of stationary phase *Bifidobacterium* species cells. Additional inoculated wells without added carbohydrates were included as controls. All wells were covered with 50 µL of sterile mineral oil to avoid evaporation and incubated for 96 h. Optical density measurements at 600 nm (OD_{600}) using a PowerWave 340 plate reader (BioTek) were taken every 30 min, preceded by 30 sec of shaking at variable speed. After growth, cell-free supernatants were collected by centrifugation at 16,000 rcf for 1 min and stored at -80°C until identification of remaining HMO (described below). Technical triplicates of biological duplicates were performed for each bacteria and sugar combination.

A subset of the *Bifidobacterium* isolates (those able to consume 2'-FL, as well as a one that could not) were tested for growth on purified 2'-FL (Glycom) and 3'-FL (Glycom)[51] using the same methods as above.

5.7.4 *B. pseudocatenulatum* MP80 metabolite production following growth on 2'-FL

B. pseudocatenulatum MP80 was subcultured three times on MRSC broth and incubated anaerobically at 37°C for 12 h. A 5% (500 µL, v/v) inoculum was added to 10 mL of mMRS supplemented with 1% (w/v) lactose or 2'-FL. Optical density measurements were monitored in a PowerWave 340 plate reader until late log phase (OD_{600} ~0.8). Cells were pelleted by centrifugation at 3220 rcf for 3 min and washed in 10 mL 1X PBS (anaerobically conditioned) and resuspended in 15 mL mMRS supplemented

with 0.5% (w/v) lactose or 2'-FL. After 10 min of anaerobic growth, cultures were centrifuged at 3220 rcf for 3 min at 4°C. The cellular population (CFU mL^{-1}) was calculated to determine consistency between triplicates. Cell-free supernatants were filtered through a 3 kD molecular weight filter and stored at -80°C until analysis. Thawed filtrate was prepared with the addition of internal standard DSS-d6 (2,2,3,3,4,4-d6-3-(trimethylsilyl)-1-propane sulfonic acid) at a 1:10 ratio and adjusted to pH 6.8 ± 0.1 using NaOH and HCl. A 180 µL aliquot was transferred to a 3 mm Bruker NMR tube and stored at 4°C until spectral acquisition. Spectra were acquired by 1H nuclear magnetic resonance spectroscopy as previously described.[52] Fourier transformed spectra were processed in Chenomx NMR suite (version 8.4) followed by manual annotation of each metabolite.

5.7.5 *B. pseudocatenulatum* genome sequencing and comparative genomics

To whole genome sequence six isolates (SC585, MP80, JCM7040, JCM11661, L15, and GST210), 100 - 1000 ng of extracted and purified genomic DNA (described previously) was sent to the Vincent J. Coates Genomics Sequencing Laboratory at University of California Berkeley. DNA was sheared using Adaptive Focused Acoustics (Covaris) followed by library preparation using the IntegenX Apollo 324 platform with 13 rounds of amplification using Wafergen library prep kits. Single-read sequencing (50 bp) was performed using the high-throughput mode on the Illumina HiSeq2000 platform. Sequencing files were concatenated using Terminal, trimmed with a maximum of 2 ambiguous base pairs, and deleted if their quality scores were below 0.5. Remaining sequences were de-novo assembled using CLC Genomics Workbench. Subsequently, *B. pseudocatenulatum* MP80 was long-read sequenced with the Single Molecule, Real-Time platform to aid in *de novo* assembly of its entire circular genome. *B. pseudocatenulatum* MP80 was streaked onto MRSC agar incubated at 37°C anaerobically, three colonies were subcultured into 2 mL of MRSC both and incubated at 37°C anaerobically overnight. Total genomic DNA (3 x 2 mL) was extracted with the DNeasy Blood and Tissue kit including the Pretreatment for Gram-positive Bacteria (Qiagen, according to the manufacturer's instructions). Slight modifications were made, including 20 µL of 50 mg mL^{-1} lysozyme from chicken egg white and 4 U of mutanolysin were included in the enzymatic lysis buffer, followed by addition of proteinase K and RNase A (kit-provided) and incubation

for 2 min at room temperature prior to combination with the AL buffer. Total genomic DNA was eluted in 35 µL of EB and pooled (total 105 µL). Protein contamination was measured by NanoDrop™ 1000 and RNA contamination and genomic DNA shearing was evaluated by gel electrophoresis. The DNA and RNA concentration were measured using the Qubit® 2.0 Fluorometer and Qubit dsDNA BR Qubit RNA HS Assay kits; respectively (Invitrogen). Size selection of genomic DNA (at 10,000 bp) on the BluePippin system and sequencing on the PacBio Sequel system was conducted by the DNA Technologies and Expression Analysis Cores at the University of California Davis Genome Center. The genome was assembled with the filtered_subreads.fastq file using the default parameters of Canu (version 1.6).[53] *B. pseudocatenulatum* genomes were annotated and deposited in the Integrated Microbial Genome Expert Review annotation platform (GOLD Project ID: Gs0113979).

Fucosidase operon gene homologs in publicly available *B. pseudocatenulatum* genomes were identified with the PyParanoid pipeline (version 0.4.1) using default parameters.[54] Briefly, the FASTA amino acid files of 319 higher-quality genomes were chosen to generate alignments with DIAMOND (version 0.9.24).[55] Homologous proteins were identified with Markov cluster algorithm (MCL 14-137) [56] and aligned with MUSCLE (v3.8.1551).[57] Hidden Markov models of each homologous protein alignment at homology cut-off at 95% amino acid identity were created with HMMER (v. 3.2.1) and propagated to additional *Bifidobacterium* genomes. The resulting matrix of homolog presence or absence was filtered to *B. pseudocatenulatum* strains of interest. A heatmap of predicted homolog copy number was visualized with Morpheus (accessed on 7.7.2020) https://software.broadinstitute.org/morpheus/).

5.7.6 *B. pseudocatenulatum* MP80 fucosidase operon gene expression

Expression of the SBP (Ga0224696_111933), α-fucosidase GH29 (Ga0224696_111927), and α-fucosidase GH95 (Ga0224696_111926) from *B. pseudocatenulatum* MP80 and the SBP (Ga0064049_111418) and α-fucosidase GH95 (Ga0064049_111413) from *B. pseudocatenulatum* SC585 were quantified during growth on 2'-FL. Primers were designed with the Primer-BLAST tool at NCBI (**Table S5.1**). The *rnpA* housekeeping gene from *B. pseudocatenulatum* MP80 and SC585 (Ga0224696_112000 and Ga0064049_10607, respectively) was used for relative quantification (52). *B.*

pseudocatenulatum MP80 was grown on mMRS supplemented with 2% (w/v) glucose or 2'-FL in a microplate reader and cells were harvested at mid-log phase (OD_{600} 0.3 to 0.7), centrifuged at 21130 rcf and stored in RNAlater (Ambion) at -20°C. Samples were thawed on ice, centrifuged at 4°C at 21130 rcf for 2 min, washed with 1 mL RNase-free 1X PBS and recentrifuged. Samples were lysed with 250 µL of 50 mg mL^{-1} lysozyme and 120 U mutanolysin at 37°C for 20 min. Lysate was centrifuged at 4°C at 9391 rcf for 1 min, supernatant was discarded and pellets were processed with the RNAqueous™ Total RNA Isolation kit (Ambion, according to the kit's instructions) for bacterial sample preparation and RNA extraction. RNA integrity was evaluated by agarose electrophoresis (1.2% agarose gel, w/v). Subsequently, DNA was removed using the TURBO DNA-free™ kit (Ambion, according to the kit's instructions) with an extended 1 h DNase incubation. RNA was converted to total cDNA using the High-Capacity cDNA Reverse Transcription kit (Applied Biosystems, according to the kit's instructions) and stored at -20°C until use. A 20 µL reaction containing 10 µL 2X SYBR® Premix Ex Taq™ II (Tli RNase H Plus) master mix (ClonTech), 0.4 µL of each primer (10 µM, **Table S5.1**), 0.4 µL 50X ROX reference dye II and 2 µL RNA. RNA was quantified on a 7500 Fast Real-Time PCR system (Applied Biosystems) with a 20 s hold at 50°C, followed by 95°C for 10 min, 40 cycles of 95°C for 15 s and 60°C for 1 min. Delta C_T was calculated and used to determine fold-change in expression.

5.7.7 RNA-Seq screen of *B. pseudocatenulatum* MP80 transcriptome

For transcriptome screening, *B. pseudocatenulatum* MP80 was grown on basal MRS media supplemented with 1% (w/v) lactose, 2-FL or LNFP-1 in four biological replicates to understand differential expression due to varying growth substrates. Cells were grown to mid-log phase with an A_{600} of 0.6 - 0.7 and stored in RNAprotect (Qiagen Inc, Valencia). Cells were lysed with 250 µL (50 g/L) lysozyme (Sigma-Aldrich, St. Louis, MO) and 120 units of mutanolysin (Sigma-Aldrich, St. Louis, MO). RNA was extracted with the RNeasy mini kit (Qiagen Inc, Valencia) and DNase-treated twice. rRNA was depleted with the RiboMinus Transcriptome Isolation Kit, bacteria (Thermo Fisher, Waltham, MA) while the integrity of RNA was assayed using the 2100 Bioanalyzer (Agilent Technologies, Santa Clara, CA). Barcode indexed RNAseq libraries were sequenced on a NextSeq 500 (Illumina, San Diego, CA) with paired-end 75bp reads.

Sequences were processed with CLC-Bio Genomics Workbench (CLC Bio, Denmark) and reads were trimmed (maximum of 2 ambiguous base pairs) and deleted if the quality scores were below 0.5. Sequences were mapped to the *B. pseudocatenulatum* MP80 genome. RPKM values were calculated and data was log2 transformed and normalized by totals. Gene expression levels in LNFP-1 and 2-FL was compared to lactose-grown cells and statistically significant changes were analyzed using Baggerley's test with FDR p value ≤ 0.05.

5.7.8 Cloning and expression of *B. pseudocatenulatum* fucosidase operon genes

The SBP (Ga0224696_111933), α-fucosidase GH29 (Ga0224696_111927), and α-fucosidase GH95 (Ga0224696_111926) from *B. pseudocatenulatum* MP80 and the SBP (Ga0064049_111418) from *B. pseudocatenulatum* SP585 were cloned using the Champion™ pET Directional TOPO Expression kits (Invitrogen, according to kit's instructions unless noted otherwise). The SBP forward primers (listed in **Table S5.1**) start with the first nucleotide (MP80 nucleotide 88 and SC585 nucleotide 91) after the predicted signal and transmembrane domains preceded by the CACC sequence and ATG start codon. A 50 µL reaction with 1X Phusion HF buffer, 200 µM dNTPs, 0.5 µM of each primer, 100 - 150 ng genomic DNA, and 1 U Phusion DNA polymerase (New England Biolabs, Ipswich, MA). Cycling parameters are as follows; 30 s at 98°C, followed by 30 cycles of 98°C for 10 s, 64°C for 30 s, and 72°C for 45 s, with a final extension period of 5 min at 72°C. PCR amplicons were purified with QIAquick Gel Extraction kit (Qiagen) or DNA Clean and Concentrator kit (Zymo Research, Irvine, CA). Purified PCR products were cloned into the pET101 (MP80) or pET102 (SC585) dTOPO vector, transformed into One Shot® Top10 Chemically Competent *E. coli*, and plated onto LB agar containing 100 µg mL^{-1} carbenicillin. Plasmid DNA from putative transformants was isolated using the QIAprep Spin Miniprep kit (Qiagen). Clones were confirmed by PCR prior to transformation into Chemically Competent BL21star™ (DE3) One Shot® *E. coli* and plated on LB agar containing 100 µg mL^{-1} carbenicillin. Confirmed transformants were stored in 25% (v/v) glycerol at -80°C.

Inoculate 200 mL of LB broth containing 100 µg mL^{-1} carbenicillin and 1% (w/v) glucose with 4 mL overnight cultures of BL21star™ transformants and incubate at 37°C with agitation at 225 rpm. At

approximately OD_{600} = 0.6, protein expression was induced with 1 mM isopropyl-β-d-1-thiogalactopyranoside and incubated 18 to 22 h. Cells were harvested by centrifugation at 3220 rcf for 20 min at 4°C. Cell pellets were lysed in 4 mL 50 mM NaH_2PO_4, 300 mM NaCl, 10 mM imidazole, pH 8.0 containing 90 µL 50 mg mL^{-1} lysozyme and incubated for 30 min on ice. Solution was vortexed at maximum speed for 2 min, add 45 µL DNAse I solution (Roche) and 5 µL RNase A (Epicentre) and incubated for 15 min on ice. Lysates were centrifuged at 10,000 rcf for 30 min at 4°C. Supernatants were combined with Ni-NTA agarose (Qiagen) at a ratio of 4:1 and incubated on a tilt-table for 1 h at 4°C. Lysate-agarose was washed twice with 10 mL of 50 mM NaH_2PO_4, 300 mM NaCl, 20 mM imidazole, pH 8.0 in a 5 mL disposable gravity chromatography column (Qiagen). Proteins were eluted with 4 x 500 µL of 50 mM NaH_2PO_4, 300 mM NaCl, 250 mM imidazole, pH 8.0. Proteins were visualized by SDS-PAGE using a 7.5% 2X TGX Mini-PROTEAN gel (Bio-Rad). Imidazole buffer was exchanged for 1X PBS using Amicon Ultra 0.5 mL centrifugal filter units, 3 kDA cutoff (EMD Millipore). Purified proteins were stored in PBS with 25% (v/v) glycerol at -20°C.

5.7.9 *B. pseudocatenulatum* MP80 and SC585 substrate-binding protein binding specificity

An approximately 8 µL reaction, containing 10 µM substrate-binding protein and 1 µM of each HMO (**Tables S5.5 and S5.6**) was analyzed by a catch and release electrospray ionization mass spectrometry assay using a Synapt G2S ESI quadrupole-ion mobility separation TOF MS (Waters) equipped with a nanoflow electrospray ionization source with minor modifications [58]. Briefly, a capillary voltage of 1.0 kV and a cone voltage of 30 kV (in negative ion mode) was applied and the source block temperature was maintained at 60°C for electrospray ionization. Ion transmission was carried out with trap voltages of 10 − 80 V and transfer voltages of 2 to 60 V. The ion mobility separation parameters were optimized for each HMO isomer set: trap gas flow rate at 6 mL min^{-1}, the helium cell gas flow rate at 150 to 180 mL min^{-1}, the ion mobility gas flow rate at 50 to 90 mL min^{-1}, the trap direct-current bias at 50 V, the ion mobility wave velocity at 400 to 1000 m s^{-1}, and the ion mobility wave height at 15 to 40 V. For ion mobility separation, N_2 at 3.41 mbar was used. Data acquisition and processing were carried out using MassLynx (version 4.1, Waters).

5.7.10 *B. pseudocatenulatum* MP80 α-fucosidase GH29 and GH95 HMO substrate specificity

A 1.5 µL (2 mg mL^{-1}) of a reduced HMO pool was digested with 2 mg mL^{-1} of purified α-fucosidase GH29 and GH95 (described above) in 10 µL of 0.1 M NH_4 acetate buffer. Reactions were incubated at each enzyme's optimal pH, temperature and duration (data not shown) and stored at -80°C until identification of undigested HMO (described below).

5.7.11 Glycoprofiling of HMO by nano-HPLC-Chip/TOF Mass Spectrometry

Cell-free supernatants and undigested HMO were recovered, reduced, and desalted by solid-phase extraction on graphitized carbon cartridges as previously described.[8] HMO analytes were separated on a 1200 Infinity Series HPLC unit (Agilent Technologies), detected on a 6220 series TOF LC/MS unit (Agilent Technologies), and data was processed using the MassHunter Qualitative Analysis software (version B.06.01, Agilent) as previously described.[7,59,60]

DATA AVAILABILITY

The sequenced *B. pseudocatenulatum* genomes were annotated and deposited in the Integrated Microbial Genome Expert Review annotation platform (GOLD Project ID: Gs0113979). Sequenced strains located at associated IMG/JGI Analysis IDs: SC585 (Ga0064049), MP80 (Ga0224696), JCM7040 (Ga0024098), JCM11661 (Ga0064497), L15 (Ga0064499), and GST210 (Ga0064498). Additional genome accessions are provided in supplemental table 4. RNA-seq data was deposited in the NCBI GEO repository (GSE175820).

AUTHOR STATEMENTS

Funding information: This study was funded in part by UC Davis RISE program, National Institutes of Health awards AT007079 and AT008759 (D.A.M.) and the Peter J. Shields Endowed Chair in Dairy Food Science (D.A.M.).

Acknowledgements: The authors thank Dr. Juliana de Moura Bell, Dr. Joshua Cohen, and Dr. Daniela Barile for providing purified human milk oligosaccharides. The *B. pseudocatenulatum* strain L15 was kindly provided by Dr. Eva Vlková.

Author contributions: G.S. and D.A.M designed the study. G.S., J.L.H., B.E.H., and D.A.M wrote the manuscript. D.A.M secured funding for this study. G.S. conducted all experiments except as noted. J.L.H. cloned and purified *B. pseudocatenulatum* SC585's SBP. J.L.H and B.E.H. conducted qRT-PCR of bacteria grown on 2'-FL. B.E.H and S.W. performed RNA-Seq analysis. C.F.M. assembled the PacBio *B. pseudocatenulatum* MP80 genome. J.A.L, B.E.H., and C.M.S. analyzed the 2'-FL metabolite profile of *B. pseudocatenulatum* MP80. N.M.J conducted the comparative genomics analysis. E.G. and C.B.L analyzed the glycoprofiling of pooled HMO growths. A.E., L.N. and J.S.K. analyzed the binding specificity of SBP from *B. pseudocatenulatum* MP80 and SC585. All authors read, edited, and approved submission of the manuscript for publication.

5.8 References

1. Smilowitz JT, O'Sullivan A, Barile D, German JB, Lönnerdal B, Slupsky CM. The human milk metabolome reveals diverse oligosaccharide profiles. J Nutr 2013; 143:1709–18.
2. Ninonuevo MR, Park Y, Yin H, Zhang J, Ward RE, Clowers BH, German JB, Freeman SL, Killeen K, Grimm R, et al. A strategy for annotating the human milk glycome. J Agric Food Chem 2006; 54:7471–80.
3. De Leoz MLA, Kalanetra KM, Bokulich NA, Strum JS, Underwood MA, German JB, Mills DA, Lebrilla CB. Human milk glycomics and gut microbial genomics in infant feces show a correlation between human milk oligosaccharides and gut microbiota: a proof-of-concept study. J Proteome Res 2015; 14:491–502.
4. LoCascio RG, Ninonuevo MR, Freeman SL, Sela DA, Grimm R, Lebrilla CB, Mills DA, German JB. Glycoprofiling of bifidobacterial consumption of human milk oligosaccharides demonstrates strain specific, preferential consumption of small chain glycans secreted in early human lactation. J Agric Food Chem 2007; 55:8914–9.
5. Garrido D, Ruiz-Moyano S, Lemay DG, Sela DA, German JB, Mills DA. Comparative transcriptomics reveals key differences in the response to milk oligosaccharides of infant gut-associated bifidobacteria. Sci Rep 2015; 5:13517.
6. Thongaram T, Hoeflinger JL, Chow J, Miller MJ. Human milk oligosaccharide consumption by probiotic and human-associated bifidobacteria and lactobacilli. J Dairy Sci 2017; 100:7825–33.
7. Garrido D, Ruiz-Moyano S, Kirmiz N, Davis JC, Totten SM, Lemay DG, Ugalde JA, German JB, Lebrilla CB, Mills DA. A novel gene cluster allows preferential utilization of fucosylated milk oligosaccharides in Bifidobacterium longum subsp. longum SC596. Sci Rep 2016; 6:35045.
8. Ruiz-Moyano S, Totten SM, Garrido DA, Smilowitz JT, German JB, Lebrilla CB, Mills DA. Variation in consumption of human milk oligosaccharides by infant gut-associated strains of Bifidobacterium breve. Appl Environ Microbiol 2013; 79:6040–9.
9. Bunesova V, Lacroix C, Schwab C. Fucosyllactose and L-fucose utilization of infant Bifidobacterium longum and Bifidobacterium kashiwanohense. BMC Microbiol 2016; 16:248.
10. Katoh T, Ojima MN, Sakanaka M, Ashida H, Gotoh A, Katayama T. Enzymatic Adaptation of Bifidobacterium bifidum to Host Glycans, Viewed from Glycoside Hydrolyases and Carbohydrate-Binding Modules. Microorganisms 2020; 8.
11. Gotoh A, Katoh T, Sakanaka M, Ling Y, Yamada C, Asakuma S, Urashima T, Tomabechi Y, Katayama-Ikegami A, Kurihara S, et al. Sharing of human milk oligosaccharides degradants within bifidobacterial communities in faecal cultures supplemented with Bifidobacterium bifidum. Sci Rep 2018; 8:13958.
12. Turroni F, Duranti S, Milani C, Lugli GA, van Sinderen D, Ventura M. Bifidobacterium bifidum: A Key Member of the Early Human Gut Microbiota. Microorganisms 2019; 7.
13. Marcobal A, Barboza M, Sonnenburg E, Pudlo N, Martens E, Desai P. Bacteroides in the Infant Gut Consume Milk.
14. Kostopoulos I, Elzinga J, Ottman N, Klievink JT, Blijenberg B, Aalvink S, Boeren S, Mank M, Knol J, de Vos WM, et al. Akkermansia muciniphila uses human milk oligosaccharides to thrive in the early life conditions in vitro. Sci Rep 2020; 10:14330.
15. Pichler MJ, Yamada C, Shuoker B, Alvarez-Silva C, Gotoh A, Leth ML, Schoof E, Katoh T, Sakanaka M, Katayama T, et al. Butyrate producing colonic Clostridiales metabolise human milk oligosaccharides and cross feed on mucin via conserved pathways. Nat Commun 2020; 11:3285.
16. Matsuki T, Yahagi K, Mori H, Matsumoto H, Hara T, Tajima S, Ogawa E, Kodama H, Yamamoto K, Yamada T, et al. A key genetic factor for fucosyllactose utilization affects infant gut microbiota development. Nat Commun 2016; 7:11939.
17. Duar RM, Henrick BM, Casaburi G, Frese SA. Integrating the Ecosystem Services Framework to Define Dysbiosis of the Breastfed Infant Gut: The Role of B. infantis and Human Milk Oligosaccharides. Front Nutr 2020; 7:33.
18. Sela DA, Chapman J, Adeuya A, Kim JH, Chen F, Whitehead TR, Lapidus A, Rokhsar DS, Lebrilla

CB, German JB, et al. The genome sequence of Bifidobacterium longum subsp. infantis reveals adaptations for milk utilization within the infant microbiome. Proc Natl Acad Sci USA 2008; 105:18964–9.
19. James K, Motherway MO, Bottacini F, van Sinderen D. Bifidobacterium breve UCC2003 metabolises the human milk oligosaccharides lacto-N-tetraose and lacto-N-neo-tetraose through overlapping, yet distinct pathways. Sci Rep 2016; 6:38560.
20. Wada J, Ando T, Kiyohara M, Ashida H, Kitaoka M, Yamaguchi M, Kumagai H, Katayama T, Yamamoto K. Bifidobacterium bifidum lacto-N-biosidase, a critical enzyme for the degradation of human milk oligosaccharides with a type 1 structure. Appl Environ Microbiol 2008; 74:3996–4004.
21. Ashida H, Miyake A, Kiyohara M, Wada J, Yoshida E, Kumagai H, Katayama T, Yamamoto K. Two distinct alpha-L-fucosidases from Bifidobacterium bifidum are essential for the utilization of fucosylated milk oligosaccharides and glycoconjugates. Glycobiology 2009; 19:1010–7.
22. Katayama T, Sakuma A, Kimura T, Makimura Y, Hiratake J, Sakata K, Yamanoi T, Kumagai H, Yamamoto K. Molecular cloning and characterization of Bifidobacterium bifidum 1,2-alpha-L-fucosidase (AfcA), a novel inverting glycosidase (glycoside hydrolase family 95). J Bacteriol 2004; 186:4885–93.
23. Shuhaimi M, Ali AM, Saleh NM, Yazid AM. Classification of Bifidobacterium Isolates from Infant Faeces Using PCR-Based and 16S rDNA Partial Sequences Analysis Methods. Biosci Microflora 2002; 21:155–61.
24. Turroni F, Peano C, Pass DA, Foroni E, Severgnini M, Claesson MJ, Kerr C, Hourihane J, Murray D, Fuligni F, et al. Diversity of bifidobacteria within the infant gut microbiota. PLoS One 2012; 7:e36957.
25. Simeoni U, Berger B, Junick J, Blaut M, Pecquet S, Rezzonico E, Grathwohl D, Sprenger N, Brüssow H, Study Team, et al. Gut microbiota analysis reveals a marked shift to bifidobacteria by a starter infant formula containing a synbiotic of bovine milk-derived oligosaccharides and Bifidobacterium animalis subsp. lactis CNCM I-3446. Environ Microbiol 2016; 18:2185–95.
26. Yassour M, Vatanen T, Siljander H, Hämäläinen A-M, Härkönen T, Ryhänen SJ, Franzosa EA, Vlamakis H, Huttenhower C, Gevers D, et al. Natural history of the infant gut microbiome and impact of antibiotic treatment on bacterial strain diversity and stability. Sci Transl Med 2016; 8:343ra81.
27. Lawson MAE, O'Neill IJ, Kujawska M, Gowrinadh Javvadi S, Wijeyesekera A, Flegg Z, Chalklen L, Hall LJ. Breast milk-derived human milk oligosaccharides promote Bifidobacterium interactions within a single ecosystem. ISME J 2020; 14:635–48.
28. Turroni F, Foroni E, Pizzetti P, Giubellini V, Ribbera A, Merusi P, Cagnasso P, Bizzarri B, de'Angelis GL, Shanahan F, et al. Exploring the diversity of the bifidobacterial population in the human intestinal tract. Appl Environ Microbiol 2009; 75:1534–45.
29. Junick J, Blaut M. Quantification of human fecal bifidobacterium species by use of quantitative real-time PCR analysis targeting the groEL gene. Appl Environ Microbiol 2012; 78:2613–22.
30. Milani C, Mangifesta M, Mancabelli L, Lugli GA, James K, Duranti S, Turroni F, Ferrario C, Ossiprandi MC, van Sinderen D, et al. Unveiling bifidobacterial biogeography across the mammalian branch of the tree of life. ISME J 2017; 11:2834–47.
31. Yatsunenko T, Rey FE, Manary MJ, Trehan I, Dominguez-Bello MG, Contreras M, Magris M, Hidalgo G, Baldassano RN, Anokhin AP, et al. Human gut microbiome viewed across age and geography. Nature 2012; 486:222–7.
32. Odamaki T, Kato K, Sugahara H, Hashikura N, Takahashi S, Xiao J-Z, Abe F, Osawa R. Age-related changes in gut microbiota composition from newborn to centenarian: a cross-sectional study. BMC Microbiol 2016; 16:90.
33. Lewis ZT, Totten SM, Smilowitz JT, Popovic M, Parker E, Lemay DG, Van Tassell ML, Miller MJ, Jin Y-S, German JB, et al. Maternal fucosyltransferase 2 status affects the gut bifidobacterial communities of breastfed infants. Microbiome 2015; 3:13.
34. Bunešová V, Vlková E, Killer J, Rada V, Ročková Š. Identification of Bifidobacterium strains from faeces of lambs. Small Ruminant Research 2012; 105:355–60.

35. Smilowitz JT, Lemay DG, Kalanetra KM, Chin EL, Zivkovic AM, Breck MA, German JB, Mills DA, Slupsky C, Barile D. Tolerability and safety of the intake of bovine milk oligosaccharides extracted from cheese whey in healthy human adults. J Nutr Sci 2017; 6:e6.
36. Sela DA, Garrido D, Lerno L, Wu S, Tan K, Eom H-J, Joachimiak A, Lebrilla CB, Mills DA. Bifidobacterium longum subsp. infantis ATCC 15697 α-fucosidases are active on fucosylated human milk oligosaccharides. Appl Environ Microbiol 2012; 78:795–803.
37. Nishimoto M, Kitaoka M. Identification of N-acetylhexosamine 1-kinase in the complete lacto-N-biose I/galacto-N-biose metabolic pathway in Bifidobacterium longum. Appl Environ Microbiol 2007; 73:6444–9.
38. El-Hawiet A, Chen Y, Shams-Ud-Doha K, Kitova EN, Kitov PI, Bode L, Hage N, Falcone FH, Klassen JS. Screening natural libraries of human milk oligosaccharides against lectins using CaR-ESI-MS. Analyst 2018; 143:536–48.
39. El-Hawiet A, Chen Y, Shams-Ud-Doha K, Kitova EN, St-Pierre Y, Klassen JS. High-Throughput Label- and Immobilization-Free Screening of Human Milk Oligosaccharides Against Lectins. Anal Chem 2017; 89:8713–22.
40. Katayama T. Host-derived glycans serve as selected nutrients for the gut microbe: human milk oligosaccharides and bifidobacteria. Biosci Biotechnol Biochem 2016; 80:621–32.
41. Turroni F, Milani C, Duranti S, Mahony J, van Sinderen D, Ventura M. Glycan Utilization and Cross-Feeding Activities by Bifidobacteria. Trends Microbiol 2018; 26:339–50.
42. Thomson P, Medina DA, Garrido D. Human milk oligosaccharides and infant gut bifidobacteria: Molecular strategies for their utilization. Food Microbiol 2018; 75:37–46.
43. LoCascio RG, Desai P, Sela DA, Weimer B, Mills DA. Broad conservation of milk utilization genes in Bifidobacterium longum subsp. infantis as revealed by comparative genomic hybridization. Appl Environ Microbiol 2010; 76:7373–81.
44. Asakuma S, Hatakeyama E, Urashima T, Yoshida E, Katayama T, Yamamoto K, Kumagai H, Ashida H, Hirose J, Kitaoka M. Physiology of consumption of human milk oligosaccharides by infant gut-associated bifidobacteria. J Biol Chem 2011; 286:34583–92.
45. Kwak M-J, Kwon S-K, Yoon J-K, Song JY, Seo J-G, Chung MJ, Kim JF. Evolutionary architecture of the infant-adapted group of Bifidobacterium species associated with the probiotic function. Syst Appl Microbiol 2016; 39:429–39.
46. Sela DA. Bifidobacterial utilization of human milk oligosaccharides. Int J Food Microbiol 2011; 149:58–64.
47. Garrido D, Kim JH, German JB, Raybould HE, Mills DA. Oligosaccharide binding proteins from Bifidobacterium longum subsp. infantis reveal a preference for host glycans. PLoS One 2011; 6:e17315.
48. Sakanaka M, Hansen ME, Gotoh A, Katoh T, Yoshida K, Odamaki T, Yachi H, Sugiyama Y, Kurihara S, Hirose J, et al. Evolutionary adaptation in fucosyllactose uptake systems supports bifidobacteria-infant symbiosis. Sci Adv 2019; 5:eaaw7696.
49. Delétoile A, Passet V, Aires J, Chambaud I, Butel M-J, Smokvina T, Brisse S. Species delineation and clonal diversity in four Bifidobacterium species as revealed by multilocus sequencing. Res Microbiol 2010; 161:82–90.
50. Gnoth MJ, Kunz C, Kinne-Saffran E, Rudloff S. Human milk oligosaccharides are minimally digested in vitro. J Nutr 2000; 130:3014–20.
51. Zhao C, Wu Y, Yu H, Shah IM, Li Y, Zeng J, Liu B, Mills DA, Chen X. The one-pot multienzyme (OPME) synthesis of human blood group H antigens and a human milk oligosaccharide (HMO) with highly active Thermosynechococcus elongates α1-2-fucosyltransferase. Chem Commun 2016; 52:3899–902.
52. He X, Mishchuk DO, Shah J, Weimer BC, Slupsky CM. Cross-talk between E. coli strains and a human colorectal adenocarcinoma-derived cell line. Sci Rep 2013; 3:3416.
53. Koren S, Walenz BP, Berlin K, Miller JR, Bergman NH, Phillippy AM. Canu: scalable and accurate long-read assembly via adaptive k-mer weighting and repeat separation. Genome Res 2017; 27:722–

36.
54. Melnyk RA, Hossain SS, Haney CH. Convergent gain and loss of genomic islands drive lifestyle changes in plant-associated Pseudomonas. ISME J 2019; 13:1575–88.
55. Buchfink B, Xie C, Huson DH. Fast and sensitive protein alignment using DIAMOND. Nat Methods 2015; 12:59–60.
56. Enright AJ, Van Dongen S, Ouzounis CA. An efficient algorithm for large-scale detection of protein families. Nucleic Acids Res 2002; 30:1575–84.
57. Edgar RC. MUSCLE: multiple sequence alignment with high accuracy and high throughput. Nucleic Acids Res 2004; 32:1792–7.
58. El-Hawiet A, Shoemaker GK, Daneshfar R, Kitova EN, Klassen JS. Applications of a catch and release electrospray ionization mass spectrometry assay for carbohydrate library screening. Anal Chem 2012; 84:50–8.
59. Wu S, Tao N, German JB, Grimm R, Lebrilla CB. Development of an annotated library of neutral human milk oligosaccharides. J Proteome Res 2010; 9:4138–51.
60. Wu S, Grimm R, German JB, Lebrilla CB. Annotation and structural analysis of sialylated human milk oligosaccharides. J Proteome Res 2011; 10:856–68.

Strain ID[a]	Origin	Reference
SC237	Infant feces	(11)
SC564	Infant feces	(11)
SC585	Infant feces	(11)
SC665	Infant feces	(11)
SC666	Infant feces	(11)
MP80	Infant feces	(26)
MP86	Infant feces	(26)
JCM7040	Human feces	
JCM11661	Unlisted	
GST210	Adult feces	This study
L15	Lamb feces	(27)
DSM20438	Infant feces	

a: JCM = Japan Collection of Microorganisms, DSM = German Collection of Microorganisms and Cell Cultures

Table 5.1. *Bifidobacterium pseudocatenulatum* strains included in this study.

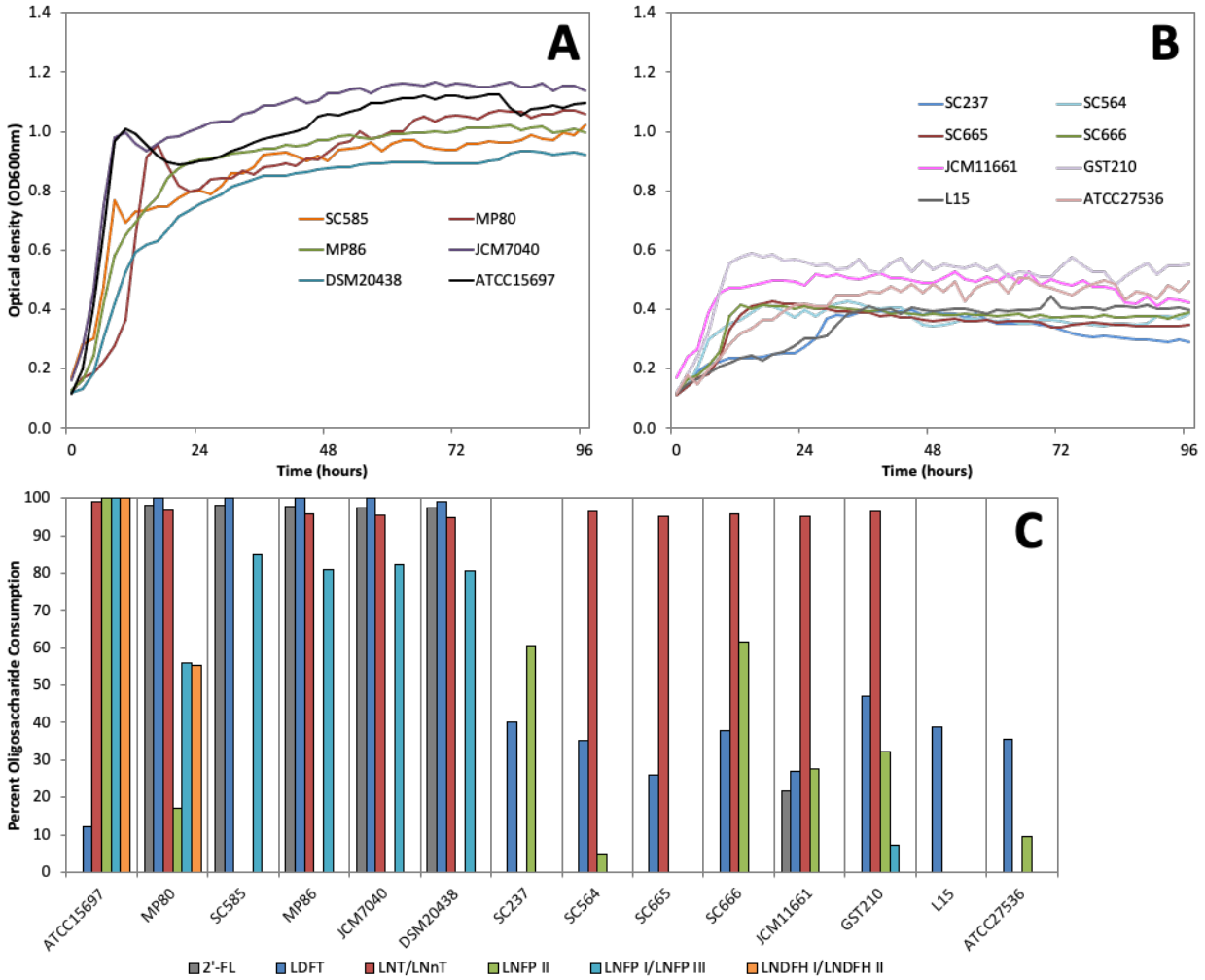

Figure 5.1. *B. pseudocatenulatum* growth and glycoprofiling on human milk oligosaccharides (HMO). *B. pseudocatenulatum* positive (A) and negative (B) isolates grown on 2% (w/v) pooled HMO. *B. longum* subsp. *infantis* ATCC15697 and *B. animalis* subsp. *lactis* ATCC27536 included as positive and negative controls, respectively. Mean optical density at 600 nm of two independent biological replicates. (C) Glycoprofiling of consumed HMO by *B. pseudocatenulatum* isolates grown on 2% (w/v) pooled HMO. Percent consumption was calculated as the difference in HMO structure abundance at 96 h relative to 0 h. Abbreviations: 2'-fucosyllactose (2'-FL), Lactodifucotetraose (LDFT), Lacto-*N*-tetraose (LNT), Lacto-*N*-neotetraose (LNnT), Lacto-*N*-fucopentaose type I, II, and III (LNFP I, II, and III), and Lacto-*N*-difucohexaose type I and II (LNDFH I and II)

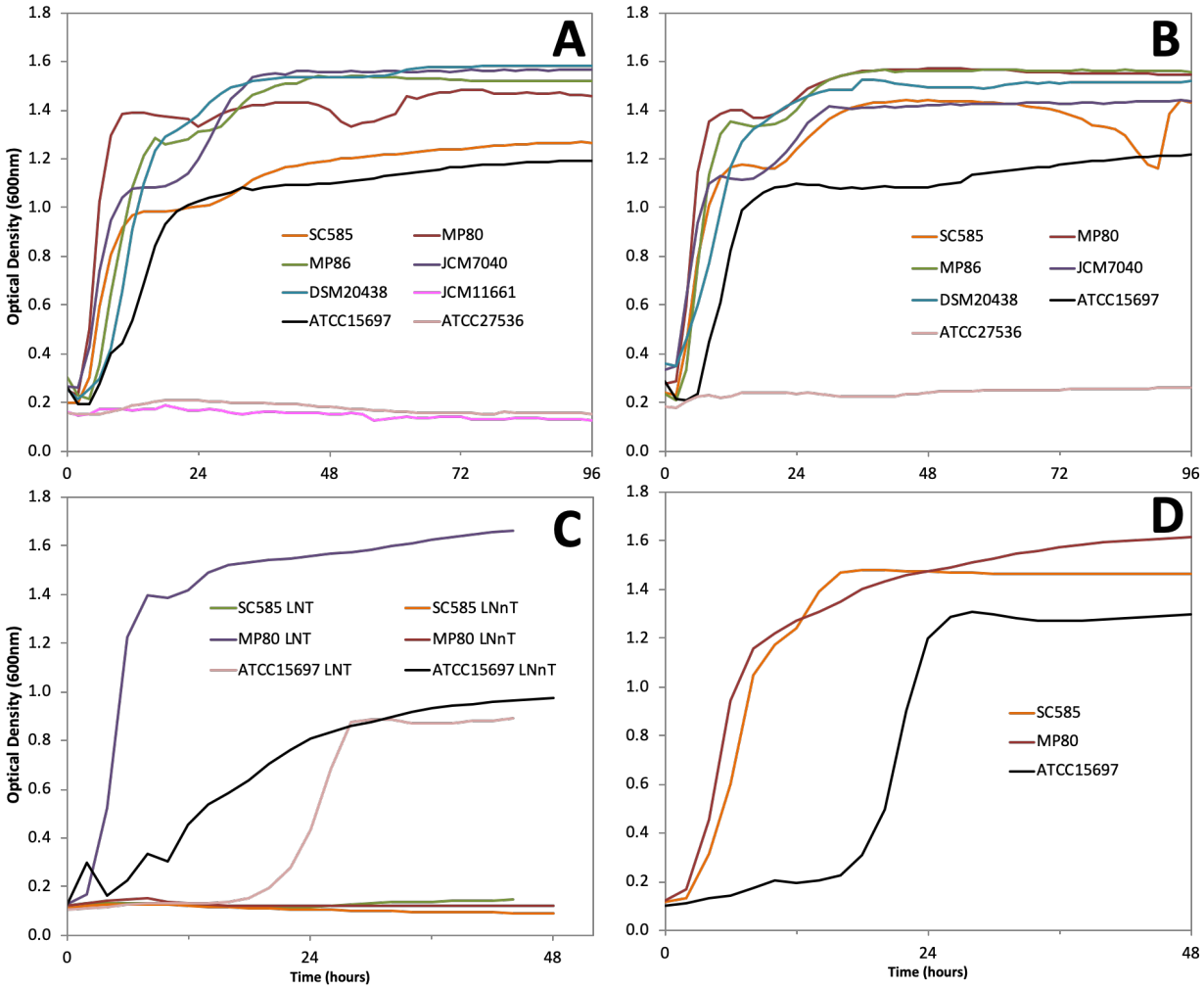

Figure 5.2. A subset of *B. pseudocatenulatum* isolates grown on 2% (w/v) 2'-fucosyllactose (A), 3'-fucosyllactose (B), Lacto-*N*-tetraose and Lacto-*N*-neotetraose (C), and Lacto-*N*-fucopentaose I (D). *B. longum* subsp. *infantis* ATCC15697 and *B. animalis* subsp. *lactis* ATCC27536 included as positive and negative controls. Mean optical density at 600 nm of two independent biological replicates.

Carbohydrate	Acetate	Lactate	Ethanol	Formate	Pyruvate	1,2-propanediol	Fucose
2'-FL	44.71 ± 1.21	19.06 ± 0.53	0.92 ± 0.02	6.20 ± 0.23	2.82 ± 0.11	4.28 ± 0.18	0.65 ± 0.01
Lactose	47.51 ± 0.20	22.79 ± 0.12	0.35 ± 0.00	0.74 ± 0.00	0.12 ± 0.00	ND	ND
p-value	0.185	0.027	<0.01	<0.01	<0.01	NA	NA

Data is presented as mean (mM) ± Standard error. 2'-FL: 2'-fucosyllactose, ND: not detected, NA: not available.

Table 5.2. Millimolar concentrations of metabolites detected in the cell-free supernatant of *B. pseudocatenulatum* MP80 grown on 1% 2'-FL versus 1% lactose.

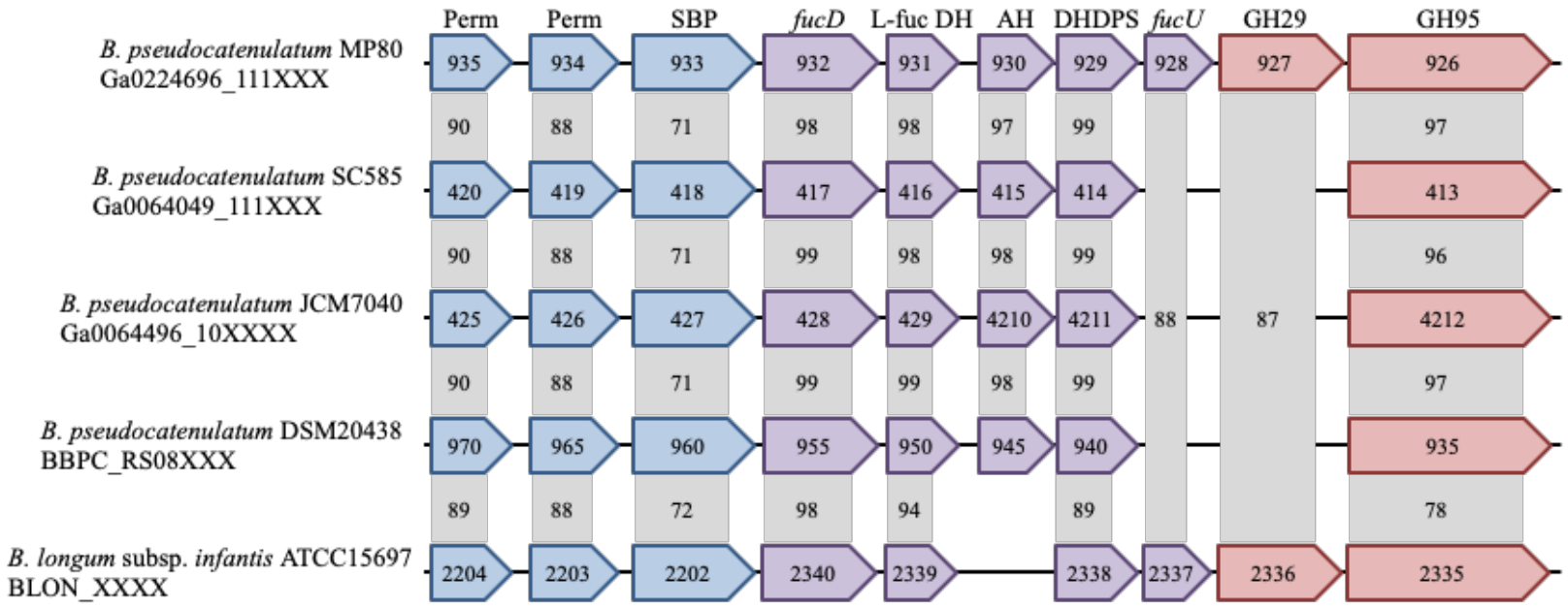

Figure 5.3. Schematic representation of the fucosylated HMO utilization cluster in *B. pseudocatenulatum* strains MP80, SC585, JCM7040, and DSM20438 (Accession # AP012330) and homologous genes in *B. longum* subsp. *infantis* ATCC15697 (Accession # CP001095). Partial gene locus tags are reported inside the arrows and gene annotations are at the top. Genes are grouped by primary function: oligosaccharide transport (blue), carbohydrate feeder pathways (purple), and glycosyl hydrolases (red). Numbers in gray boxes represent percent identity of amino acid sequences when compared to *B. pseudocatenulatum* MP80 (BLASTp from NCBI). Perm: ABC permease; SBP: substrate-binding protein; *fucD*: L-fuconate dehydratase; L-fuc DH: L-fucose dehydrogenase; AH: Amido hydrolase; DHDPS: Dihydropicolinate synthase; *fucU*: L-fucose mutarotase; GH29: α-fucosidase; GH95: α-fucosidase.

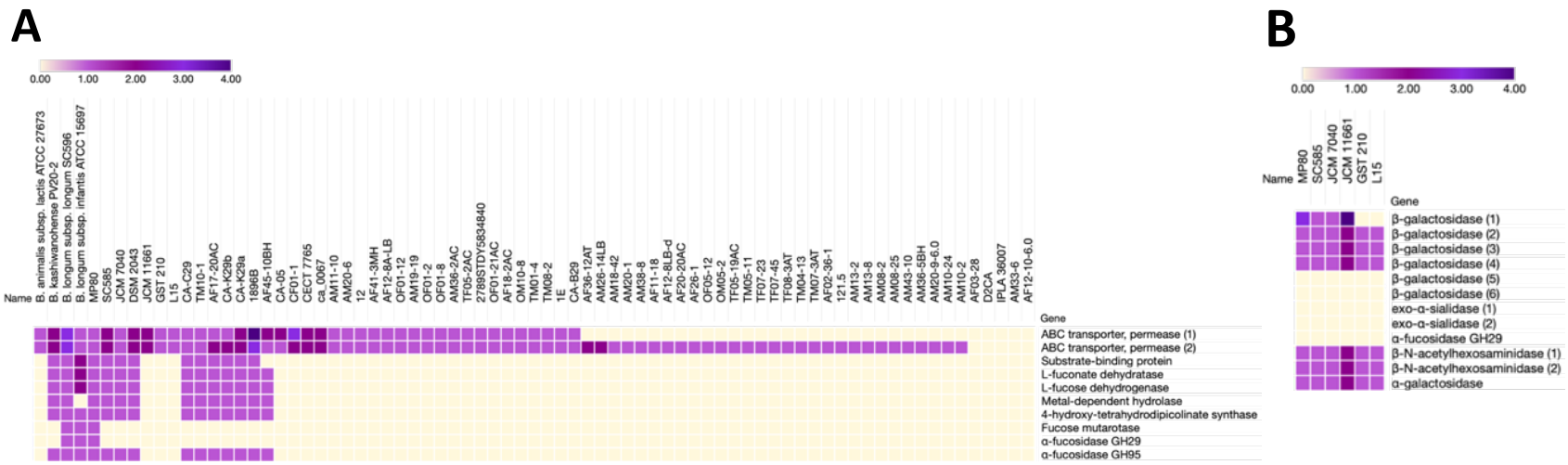

Figure 5.4. (A) Relative abundance of fucosidase operon homologs in publicly available *B. pseudocatenulatum* genomes. Color gradient represents the number of homologs of each gene predicted within the genomes depicted. Hierarchical clustering (1 - Spearman rank correlation, average linkage) was performed based on the presence or absence of homologs throughout the entire fucosidase operon. *B. animalis* subsp. *lactis* ATCC27673 (F-HMO$^+$), *B. kashiwanohense* PV20-2, *B. longum* subsp. *longum* SC596 (F-HMO$^+$) and *B. longum* subsp. *infantis* ATCC15697 (F-HMO$^+$) included for reference. *B. pseudocatenulatum* strain genome sequence accessions used are listed in supplemental table S4; (B) Additional HMO-related glycosyl hydrolases and transporters from the six *B. pseudocatenulatum* strains glycoprofiled in this work (see Figure 1 and 2). Homologs were predicted with PyParanoid (v. 0.4.1).

		Fold change during growth on substrates	
Gene ID	Annotated Function	2'-FL	LNFPI
FHMO Utilization Cluster			
2765237614	1,2-α-L-fucosidases (GH95)	**21.71**	**16.28**
2765237615	α-1,3/1,4-L-fucosidase (GH29)	**22.24**	**16.07**
2765237616	L-fucose mutarotase	**20.35**	**15.08**
2765237617	4-hydroxy-tetrahydrodipicolinate synthase	**26.74**	**21.77**
2765237618	Amido hydrolase	**42.09**	**48.53**
2765237619	L-fucose dehydrogenase	**40.28**	**51.69**
2765237620	L-fuconate dehydratase	**40.34**	**45.18**
2765237621	Solute binding protein	**30.82**	**38.22**
2765237622	ABC permease	**28.41**	**38.05**
2765237623	ABC permease	**29.60**	**41.63**
2765237623	Transcriptional regulator	**2.58**	**2.61**
LNB/GNB cluster			
2765237505	N-acetylglucosamine-6-phosphate deacetylase	1.03	**66.36**
2765237506	Glucosamine-6-phosphate deaminase	0.60	**48.50**
2765237507	β-N-acetylhexosaminidase	0.60	**21.57**
2765237508	predicted NBD/HSP70 family sugar kinase	0.51	**31.28**
2765237509	ABC permease	0.60	**12.39**
2765237510	ABC permease	0.48	**7.91**
2765237511	Type 1 HMO Solute binding protein	0.61	**2.17**
Other important HMO utilizing genes			
2765236220	β-galactosidase	0.97	**12.04**
2765237192	β-galactosidase	1.92	**6.34**
2765237343	β-galactosidase	**2.02**	1.11
2765237514	β-galactosidase	**0.67**	0.38
2765237579	β-galactosidase	1.36	**1.75**
2765237612	β-galactosidase	1.92	**2.28**
2765236421	β-N-acetylhexosaminidase	**1.97**	0.84

Table 5.3. Expression fold changes of Fucosylated HMO utilization cluster, LNB/GNB cluster and other HMO utilizing genes in *B. pseudocatenulatum* MP80 strain during growth in 2'-FL and LNFP1. The level of expression is shown as a fold change compared to the lactose control. Fold change values in bold have significant FDR p ($p \leq 0.05$).

MW	Common Name	GH29 (%)	GH95 (%)	Fucose linkage
490.19	2'-fucosyllactose	42.8	100	α(1,2)Gal
855.33	**Lacto-*N*-fucopentaose II**	**100**	**18.9**	**α(1,4)GlcNAc**
	Lacto-*N*-fucopentaose I / III	42.3	96.5	α(1,2)Gal, α(1,3)GlcNAc
1220.46	**Monofucosyl-paralacto-*N*-hexaose IV**	**90.9**	**30.3**	**α(1,3)GlcNAc**
	4120a[1]	100	-86.5	α(1,4)GlcNAc
	Monofucosyllacto-*N*-hexaose III	**100**	**6.87**	**α(1,3)GlcNAc**
	Monofucosyllacto-*N*-hexaose I	25.4	100	α(1,2)Gal
	Fucosyl-paralacto-*N*-hexaose III	**100**	**44.4**	**α(1,3)GlcNAc**
	Fucosyl-paralacto-*N*-hexaose I	4.44	100	α(1,2)Gal
1366.51	**Difucosyl-paralacto-*N*-hexose II**	**100**	**49.4**	**α(1,3)GlcNAc, α(1,4)GlcNAc**
	Difucosyllacto-*N*-hexose B	**100**	**8.80**	**α(1,3)GlcNAc, α(1,4)GlcNAc**
	Difucosyllacto-*N*-hexose A	97.5	100	α(1,2)Gal, α(1,3)GlcNAc
	Difucosyllacto-*N*-hexose C	54.6	44.9	α(1,2)Gal, α(1,4)GlcNAc
1512.57	Trifucosyllacto-*N*-hexose	100	92.5	α(1,2)Gal, α(1-3)GlcNAc, α(1,4)GlcNAc
	4320a	100	100	α(1,2)Gal, α(1-3)GlcNAc, α(1,4)GlcNAc
1585.58	5130a	71.9	66.0	α(1,3)GlcNAc
	5130b	**100**	**-22.6**	**α(1,4)GlcNAc**
	Fucosyllacto-*N*-octaose	44.7	12.1	α(1,3)GlcNAc
	5130c	38.3	100	α(1,2)Gal
1731.64	Difucosyllacto-*N*-neooctaose II	64.8	100	α(1,3)GlcNAc, α(1,3)GlcNAc
	5230a	100	100	α(1,2)Gal, α(1,3)GlcNAc
	Difucosyllacto-*N*-neooctaose I / Difucosyllacto-*N*-octaose II	83.5	89.1	α(1,3)GlcNAc, α(1,4)GlcNAc
	5230b	9.04	100	α(1,2)Gal, α(1,3)GlcNAc

[1] HMO with numerical values refer to the number of hexose (first digit), fucose (second digit) GlcNac (third digit), and *N*-acetylneuraminic acid (fourth digit). MW: molecular weight, Gal: galactose, GlcNAc: *N*-acetylglucosamine

Table 5.4. Percent digestion of fucosylated HMO by α-fucosidases (GH29 and GH95) from *B. pseudocatenulatum* MP80.

HMO	MP80	SC585
2'-fucosyllactose	●	●
3'-fucosyllactose	●	●
Difucosyllactose	◐	◐
3'-sialyl-3'-fucosyllactose	◐	◐
Lacto-*N*-fucopentaose I	◐	◐
Lacto-*N*-fucopentaose II	◐	◐
Lacto-*N*-fucopentaose III	◐	◐
Lacto-*N*-neofucopentaose V	◐	◐
Lacto-*N*-neofucopentaose	◐	◐
Lacto-*N*-difucohexaose I	◐	◐
Lacto-*N*-difucohexaose II	◐	◐
Lacto-*N*-neodifucohexaose	◐	◐

HMO	MP80	SC585
Sialyl monofucosyllacto-*N*-tetraose	○	○
Sialyl-lacto-*N*-fucopentaose V	○	○
Difucosyllacto-*N*-hexaose a	◐	○
Difucosyl-paralacto-*N*-hexaose II	◐	○
Blood group A antigen tetraose type 5	◐	◐
Blood group A antigen hexaose type 1	◐	○
A-heptasaccharide	●	○
3'-sialyl Lewis A	●	◐
Monofucosyllacto-*N*-hexaose III	●	○
Difucosyllacto-*N*-hexaose b	●	○
Difucosyl-paralacto-*N*-neohexaose	●	○

● Strong binding ○ Low/no binding

◐ Medium binding ● Not analyzed

Figure 4.5. Binding specificity of *B. pseudocatenulatum* MP80 and SC585's substrate-binding protein to fucosylated HMO.

5.9 Supplemental Information

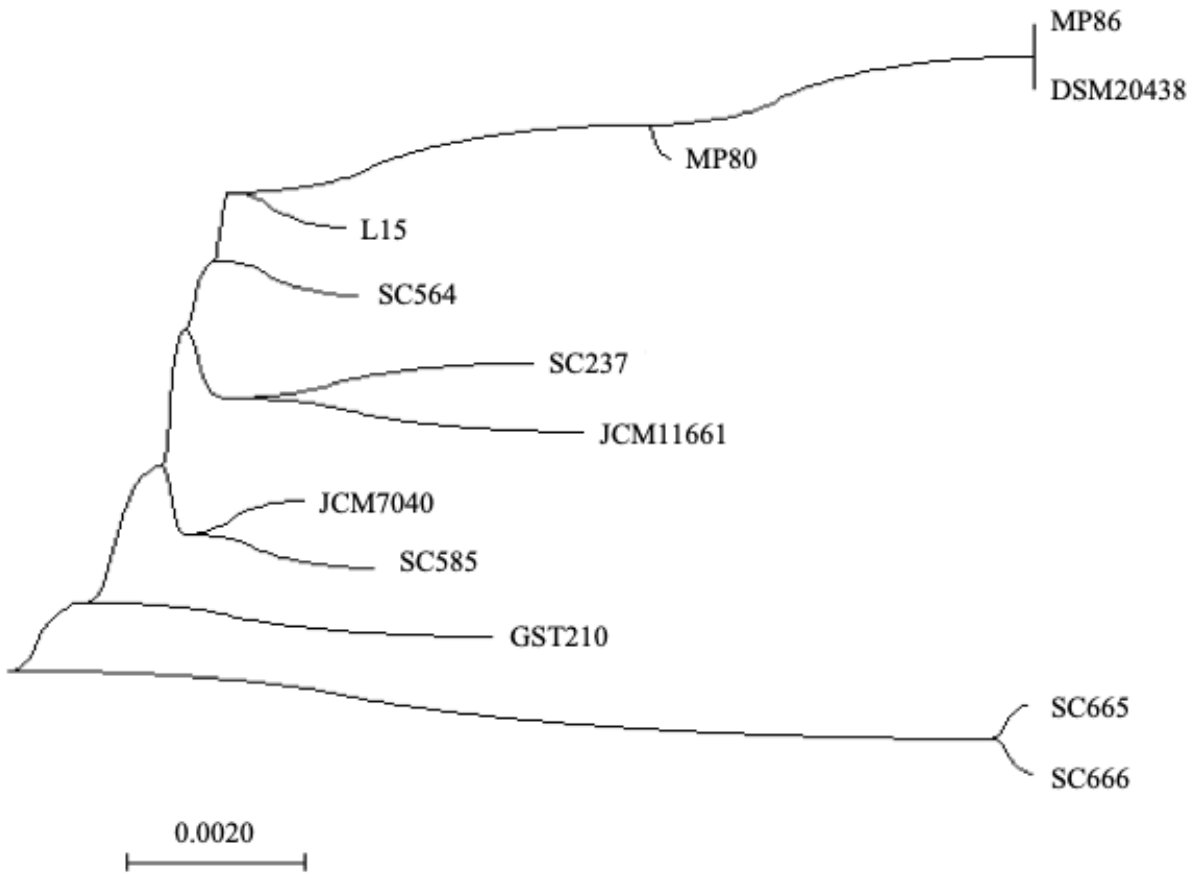

Figure S5.1. Phylogenetic relatedness of the unique *B. pseudocatenulatum* allelic profiles as determined by multilocus sequence typing. Evolutionary history was inferred using the Minimum Evolution method, followed by 1000 bootstrap replicates.

Purpose	Target		PCR Primer (5'-3')
Multilocus sequence typing[a]	*clpC*	F	GAGTACCGTAAGTACATCGAG
		R	TCCTCGTCGTCAAACAGGAAT
	purF	F	GTCGGGTAGTCGCCATTG
		R	CACTCCAATTCCGACACCGA
	gyrB	F	CATGCCGGCGGCAAGTTCG
		R	CCGAGCTTGGTCTTGGTCTG
	fusA	F	ATCGGCATCATGGCTCACATCGAT
		R	CCAGCATCGGCTGAACACCCTT
	ileS	F	CGGTATCGACATAGTCGGCG
		R	ATTCCGCGTTACCAGACCATG
	rplB	F	AGGACGGCGTGCCGGCAA
		R	GCCGTGCGGGTGATCGAC
	rpoB	F	GCATCCTCGTAGTTGTASCC
		R	GGCGAACTGATCCAGAACCA
B. pseudocatenulatum MP80 gene expression	*rnpA* (Ga0224696_112000)	F	GGTATCGCGAGAAGACATCGT
		R	ACGGCATTACGCGTCACA
	α-fucosidase GH29 (Ga0224696_111927)	F	GCTCACTTCAACCCAATGCG
		R	TTCCATAGTCAGTTCCGCCG
	α-fucosidase GH95 (Ga0224696_111926)	F	GCTTGTCCAAAGCCACGATG
		R	TCCACTGTCTGATCCGTCCA
	Substrate-binding protein (Ga0224696_111933)	F	TTCAACCGTGCTACGAACGA
		R	GCAGAATCACCGAATGCAGG
	β-galactosidase (Ga0224696_111500)	F	ACGTACAACCAGTTCACCCG
		R	ATGCGAGCACCTCAGTATCG
	β-galactosidase (Ga0224696_111924)	F	ACACCAATACCACGTTCGCA
		R	CGACCTTCTGAACGACGGTT
	β-galactosidase (Ga0224696_11522)	F	GACTACAACCCGGACCAGTG
		R	GAAATCGTACACGCCTTCGC
	β-galactosidase (Ga0224696_111652)	F	CAGCCGGAAGAAAACCGTTG
		R	TTCCGGGTGCTTTTCGTACA
B. pseudocatenulatum SC585 gene expression	*rnpA* (Ga0064049_10607)	F	GGTATCGCGAGAAGACATCGT
		R	ACGGCATTACGCGTCACA
	α-fucosidase GH95 (Ga0064049_111413)	F	TCCGTGCAAGAGGTGGAATC
		R	GCGACACGTCCCATATCAGT
	Substrate-binding protein (Ga0064049_111418)	F	TGCCGACCATTTCACCAAGT
		R	TTGCTCCATGCCTTGTCGAT
	β-galactosidase (Ga0064049_104415)	F	CGACTACGAGTCCGAATGGG
		R	GCTCGGCAATACGACCATCT
B. pseudocatenulatum SC585 gene expression	β-galactosidase (Ga0064049_10859)	F	GATCGAACTGTTGAACGCCG
		R	CGTCAAGCAGCGTAGCAATC
	β-galactosidase (Ga0064049_111411)	F	CGAATACACCGCCGATACCA
		R	TGCGATCCTGGTACGTTTCC
	β-galactosidase (Ga0064049_11171)	F	CACCAAACTGTTCCGCCAAG
		R	ATCGCCGTATCGGACTGTTC
B. pseudocatenulatum MP80 protein cloning	α-fucosidase GH29 (Ga0224696_111927		CACCATGAGCAATCCAACAAAT
			TATCCGCACCACAGCCG
	α-fucosidase GH95 (Ga0224696_111926		CACCATGAAACTCACATTCGATG
			ACGCCGGATGGTTCCCT

	Substrate-binding protein (Ga0224696_111933	CACCATGAAGGACACTAAAACTGC GTCGGCGTCGGTGGT
B. pseudocatenulatum SC585 protein cloning	Substrate-binding protein	CACCATGAGCCAGGCTAAGAGC GTCGGCGTCAGTGGTGACCT

[a] Primers were modified from Delétoile et al., 2010 for *B. pseudocatenulatum* DSM20438.
F = forward primer, R = reverse primer

Table S5.1. Oligonucleotide primers used in this study.

	2'FL	LDFT	LNT/ LNnT	LNFP II	LNFP I/ LNFP III	LNDFH I/ LNDFH II	MFLNH III/ MFLNH I	DFpLNH II	DFLNH B	DFLNH A	TFLNH
SC237	-50.97	**40.20**	-24.39	**60.45**	-29.79	-62.03	-32.65	-49.35	-34.07	-34.38	-35.78
SC564	-52.28	**35.28**	**96.42**	**4.78**	-35.83	-54.49	-45.75	-180.84	-102.09	-61.89	-93.66
SC585	**98.13**	**100.00**	-19.33	-42.01	**85.01**	-49.08	-37.62	-47.89	-28.23	-34.64	-33.05
SC665	-68.27	**25.99**	**95.29**	-89.16	-38.08	-79.63	-41.15	-233.38	-126.05	-85.21	-108.53
SC666	-48.92	**37.79**	**95.70**	**61.67**	-23.75	-58.32	-30.68	-47.58	-77.77	-49.31	-67.83
MP80	**98.07**	**100.00**	**96.68**	**17.10**	**55.96**	**55.24**	-30.88	-235.12	-78.13	-27.92	-74.32
MP86	**97.94**	**100.00**	**95.76**	-116.82	**81.09**	-78.95	-55.19	-169.11	-114.39	-31.75	-93.60
JCM7040	**97.33**	**100.00**	**95.57**	-74.52	**82.27**	-49.56	-54.60	-150.45	-94.97	-39.63	-101.08
JCM11661	**21.58**	**26.97**	**95.21**	**27.50**	-22.74	-102.34	-64.97	-85.56	-121.30	-65.04	-121.91
GST210	-22.50	**47.07**	**96.60**	**32.21**	**7.37**	-26.73	-39.67	-37.96	-50.23	-25.36	-54.90
L15	-47.61	**38.73**	-20.94	-30.40	-19.36	-52.28	-16.34	-38.93	-25.05	-36.61	-22.18
DSM20438	**97.54**	**99.24**	**94.71**	-44.71	**80.55**	-104.66	-42.73	-123.42	-109.21	-68.45	-101.22
ATCC15697	-59.87	**12.06**	**99.22**	**100.00**	**100.00**	**100.00**	**100.00**	**100.00**	**100.00**	**100.00**	**100.00**
ATCC27536	-23.23	**35.46**	-13.20	**9.65**	-23.48	-26.16	-31.60	-49.12	-20.08	-37.89	-35.40

Table S5.2. Glycoprofiling of consumed HMO by *B. pseudocatenulatum* isolates (n = 12) achieved at 96 h on 2% (w/v) pooled human milk oligosaccharides. Percent consumption was calculated as the difference in HMO structure abundance at 96 h relative to 0 h. Negative values represent lack of consumption. *B. pseudocatenulatum* strains (SC237, SC564, SC585, SC665, SC566, MP80, MP86, JCM7040, JCM11661, GST210, and L15), *B. longum* subsp. *infantis* ATCC15697, *B. animalis* subsp. *lactis* ATCC27536. HMO: 2'-fucosyllactose (2'-FL), Lactodifucotetraose (LDFT), Lacto-*N*-tetraose (LNT), Lacto-*N*-neotetraose (LNnT), Lacto-*N*-fucopentaose type I, II, and III (LNFP I, II, and III), and Lacto-*N*-difucohexaose type I and II (LNDFH I and II), Monofucosyllacto-*N*-hexaose (MFLNH I and III), Difucosyl-para-lacto-*N*-hexose type II (DFpLNH II), Difucosyllacto-*N*-hexose type B and A (DFLNH B and A), Trifucosyllacto-*N*-hexose (TFLNH).

	SC585	MP80	JCM7040	JCM11661	GST210	L15	DSM20438[a]
Whole Genome Size (bp)	2252718	2356572	2282098	2262265	2172804	2237466	2323752
Number of Contigs	124	2	131	110	111	90	1
Shortest Contig (bp)	207	37424	203	191	200	200	NA
Longest Contig (bp)	174712	2319148	181319	194473	174301	183109	2323752
Annotated Gene Count	1873	1942	1910	1963	1852	1872	1892
GC Content (%)	56.2	56.4	56.0	56.6	56.3	56.7	56.4

a: Information obtained from *B. pseudocatenulatum* DSM20438's publicly available genome (Genbank Accession: AP012330). NA: not available

Table S5.3. Summary of *B. pseudocatenulatum* genomes.

Species	Strain	Accession
B. animalis subsp. lactis	ATCC 27673	GCA_000471945.1
B. kashiwanohense	PV20-2	GCA_000800455.1
B. longum subsp. infantis	ATCC 15697	GCA_000020425.1
B. longum subsp. longum	SC596	Ga0009797
B. pseudocatenulatum	12	GCA_003952825.1
B. pseudocatenulatum	121.5	GCA_001576885.1
B. pseudocatenulatum	1896B	GCA_002075945.1
B. pseudocatenulatum	1E	GCA_002271255.1
B. pseudocatenulatum	2789STDY5834840	GCA_001405035.1
B. pseudocatenulatum	AF02-36-1	GCA_003466105.1
B. pseudocatenulatum	AF03-28	GCA_003465775.1
B. pseudocatenulatum	AF11-18	GCA_003465135.1
B. pseudocatenulatum	AF12-10-6.0	GCA_003465065.1
B. pseudocatenulatum	AF12-8A-LB	GCA_003465385.1
B. pseudocatenulatum	AF12-8LB-d	GCA_003464925.1
B. pseudocatenulatum	AF17-20AC	GCA_003460425.1
B. pseudocatenulatum	AF18-2AC	GCA_003459865.1
B. pseudocatenulatum	AF20-20AC	GCA_003459475.1
B. pseudocatenulatum	AF26-1	GCA_003458965.1
B. pseudocatenulatum	AF36-12AT	GCA_003474835.1
B. pseudocatenulatum	AF41-3MH	GCA_003474525.1
B. pseudocatenulatum	AF45-10BH	GCA_003474015.1
B. pseudocatenulatum	AM08-2	GCA_003472725.1
B. pseudocatenulatum	AM08-25	GCA_003472685.1
B. pseudocatenulatum	AM10-2	GCA_003472575.1
B. pseudocatenulatum	AM10-24	GCA_003472545.1
B. pseudocatenulatum	AM11-10	GCA_003472415.1
B. pseudocatenulatum	AM13-2	GCA_003473115.1
B. pseudocatenulatum	AM13-8	GCA_003473025.1
B. pseudocatenulatum	AM18-42	GCA_003471505.1
B. pseudocatenulatum	AM19-19	GCA_003470545.1
B. pseudocatenulatum	AM20-1	GCA_003471415.1
B. pseudocatenulatum	AM20-6	GCA_003471325.1
B. pseudocatenulatum	AM20-9-6.0	GCA_003471295.1
B. pseudocatenulatum	AM26-14LB	GCA_003470125.1
B. pseudocatenulatum	AM33-6	GCA_003468555.1
B. pseudocatenulatum	AM36-2AC	GCA_003467785.1
B. pseudocatenulatum	AM36-5BH	GCA_003467755.1

B. pseudocatenulatum	AM38-8	GCA_003467515.1
B. pseudocatenulatum	AM43-10	GCA_003467065.1
B. pseudocatenulatum	ca_0067	GCA_004167565.1
B. pseudocatenulatum	CA-05	GCA_001685965.1
B. pseudocatenulatum	CA-B29	GCA_001685985.1
B. pseudocatenulatum	CA-C29	GCA_001686005.1
B. pseudocatenulatum	CA-K29a	GCA_001686045.1
B. pseudocatenulatum	CA-K29b	GCA_001686065.1
B. pseudocatenulatum	CECT 7765	GCA_000940535.1
B. pseudocatenulatum	CF01-1	GCA_003463615.1
B. pseudocatenulatum	D2CA	Ga0009934
B. pseudocatenulatum	DSM 20438	GCA_001025215.1
B. pseudocatenulatum	GST 210	Ga0064498
B. pseudocatenulatum	IPLA 36007	GCA_000708005.1
B. pseudocatenulatum	JCM 11661	Ga0064497
B. pseudocatenulatum	JCM 7040	Ga0024098
B. pseudocatenulatum	L15	Ga0064499
B. pseudocatenulatum	MP80	Ga0224696
B. pseudocatenulatum	OF01-12	GCA_003463505.1
B. pseudocatenulatum	OF01-2	GCA_003463455.1
B. pseudocatenulatum	OF01-21AC	GCA_003463265.1
B. pseudocatenulatum	OF01-8	GCA_003463425.1
B. pseudocatenulatum	OF05-12	GCA_003439655.1
B. pseudocatenulatum	OM05-2	GCA_003438405.1
B. pseudocatenulatum	OM10-8	GCA_003438015.1
B. pseudocatenulatum	SC585	Ga0064049
B. pseudocatenulatum	TF05-19AC	GCA_003437835.1
B. pseudocatenulatum	TF05-2AC	GCA_003437825.1
B. pseudocatenulatum	TF07-23	GCA_003437155.1
B. pseudocatenulatum	TF07-45	GCA_003437075.1
B. pseudocatenulatum	TF08-3AT	GCA_003436955.1
B. pseudocatenulatum	TM01-4	GCA_003436675.1
B. pseudocatenulatum	TM04-13	GCA_003436545.1
B. pseudocatenulatum	TM05-11	GCA_003437435.1
B. pseudocatenulatum	TM07-3AT	GCA_003436315.1
B. pseudocatenulatum	TM08-2	GCA_003436105.1
B. pseudocatenulatum	TM10-1	GCA_003436025.1

Table S5.4. Genome accession numbers for strain homology analysis in Figure 4. NCBI accession numbers begin with GCA while IMG/JGI Analysis IDs begin with Ga.

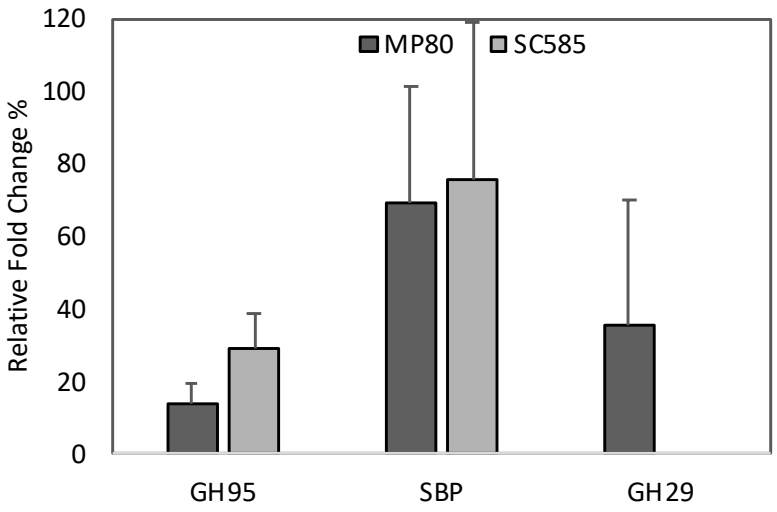

Figure S5.2. Relative expression of putative HMO utilization genes. *B. pseudocatenulatum* MP80's SBP (Ga0224696_111933), α-fucosidase GH29 (Ga0224696_111927), and α-fucosidase GH95 (Ga0224696_111926) and *B. pseudocatenulatum* SC585's SBP (Ga0064049_111418) and α-fucosidase GH95 (Ga0064049_111413) when grown on 2% 2'-fucosyllactose. Expression is in fold-change relative to growth on 2% glucose. Error bars represent standard error of fold change.

Binding level	MW (Da)	Common name	Structure
High	488.17	2'-fucosyllactose	**α-L-Fuc-(1,2)**-β-D-Gal-(1,4)-β-D-Glc
	488.17	3-fucosyllactose	β-D-Gal-(1,4)-[**α-L-Fuc-(1,3)**]-β-D-Glc
	633.21	6'-sialyllactose	α-D-Neu5Ac-(2,6)-β-D-Gal-(1,4)-β-D-Glc
	634.23	Difucosyllactose	**α-L-Fuc-(1,2)**-β-D-Gal-(1,4)-[**α-L-Fuc-(1,3)**]-β-D-Glc
	707.25	Lacto-*N*-tetraose	β-D-Gal-(1,3)-β-D-GlcNAc-(1,3)-β-D-Gal-(1,4)-β-D-Glc
	707.25	Lacto-*N*-neotetraose	β-D-Gal-(1,4)-β-D-GlcNAc-(1,3)-β-D-Gal-(1,4)-β-D-Glc
	853.31	Lacto-*N*-fucopentaose I	**α- L-Fuc-(1,2)**-β-D-Gal-(1,3)-β-D-GlcNAc-(1,3)-β-D-Gal-(1,4)-β-D-Glc
	853.31	Lacto-*N*-fucopentaose II	β-D-Gal-(1,3)-[**α-L-Fuc-(1,4)**]-β-D-GlcNAc-(1,3)-β-D-Gal-(1,4)-β-D-Glc
	853.31	Lacto-*N*-fucopentaose III	β-D-Gal-(1,4)-[**α-L-Fuc-(1,3)**]-β-D-GlcNAc-(1,3)-β-D-Gal-(1,4)-β-D-Glc
	853.31	Lacto-*N*-neofucopentaose V	β-D-Gal-(1,3)-β-D-GlcNAc-(1,3)-β-D-Gal-(1,4)-[**α-L-Fuc-(1,3)**]-β-D-Glc
	853.31	Lacto-*N*-neofucopentaose	β-D-Gal-(1,4)-β-D-GlcNAc-(1,3)-β-D-Gal-(1,4)[**α-L-Fuc-(1,3)**]-β-D-Glc
	998.34	Sialyllacto-*N*-tetraose B	α-D-Neu5Ac-(2,6)-[β-D-Gal-(1,3)]-β-D-GlcNAc-(1,3)-β-D-Gal-(1,4)- β-D-Glc
	998.34	Sialyllacto-*N*-tetraose C	α-D-Neu5Ac-(2,6)-β-D-Gal-(1,4)-β-D-GlcNAc-(1,3)-β-D-Gal-(1,4)-β-D-Glc
Medium	998.34	Sialyllacto-*N*-tetraose D	α-D-Neu5Ac-(2,3)-β-D-Gal-(1,4)-β-D-GlcNAc-(1,3)-β-D-Gal-(1,4)-β-D-Glc
	999.36	Lacto-*N*-difucohexaose I	**α-L-Fuc-(1,2)**-β-D-Gal-(1,3)-[**α-L-Fuc-(1,4)**]-β-D-GlcNAc-(1,3)-β-D-Gal-(1,4)-β-D-Glc
	999.36	Lacto-*N*-difucohexaose II	β-D-Gal-(1,3)-[**α-L-Fuc-(1,4)**]-β-D-GlcNAc-(1,3)-β-D-Gal-(1,4)-[**α-L-Fuc-(1,3)**]-β-D-Glc
	999.36	Lacto-*N*-neodifucohexaose	β-D-Gal-(1,4)-[**α-L-Fuc-(1,3)**]-β-D-GlcNAc-(1,3)-β-D-Gal-(1,4)-[**α- L-Fuc-(1,3)**]-β-D-Glc
	1072.38	Para-lacto-*N*-neohexaose	β-D-Gal-(1,4)-β-D-GlcNAc-(1,3)-β-D-Gal-(1,4)-β-D-GlcNAc-(1,3)-β-D-Gal-(1,4)-β-D-Glc
	1072.38	Lacto-*N*-neohexaose	β-D-Gal-(1,4)-β-D-GlcNAc-(1,6)-[β-D-Gal-(1,4)-β-D-GlcNAc-(1,3)]-β-D-Glc-(1,4)-Glc
	1364.50	Difucosyllacto-*N*-hexaose A	β-D-Gal-(1,4)-[**α-L-Fuc-(1,3)**]-β-D-GlcNAc-(1,6)-[**α-L-Fuc-(1,2)**-β-D-Gal-(1,3)-β-D-GlcNAc-(1,3)]-β-D-Gal-(1,4)-β-D-Glc
	1364.50	Difucosyl-para-lacto-*N*-hexaose	β-D-Gal-(1,3)-[**α-L-Fuc-(1,4)**]-β-D-GlcNAc-(1,3)-β-D-Gal-(1,4)-[**α-L-Fuc-(1,3)**]-β-D-GlcNAc-(1,3)]-β-D-Gal-(1,4)-β-D-Glc
	545.48	Lacto-*N*-triaose	β-D-GlcNAc-(1,3)-β-D-Gal(1,4)-β-D-Glc
	691.62	Blood group A antigen tetraose type 5	α-D-GalNAc-(1,3)-[**α-L-Fuc-(1,2)**]-β-D-Gal-(1,4)-β-D-Glc

	1056.96	Blood group A antigen hexaose type 1	α-D-GalNAc-(1,3)-[**α-L-Fuc-(1,2)**]-β-D-Gal-(1,3)-β-GlcNAc(1,3)-β-D-Gal(1,4)-β-D-Glc
	633.21	3'-sialyllactose	α-D-Neu5Ac-(2,3)-β-D-Gal-(1,4)-β-D-Glc
	779.27	3'-sialyl-3'-fucosyllactose	α-D-Neu5Ac-(2,3)-β-D-Gal-(1,4)-[**α-L-Fuc-(1,3)**]-β-D-Glc
Low / no binding	998.34	Sialyllacto-*N*-tetraose a	α-D-Neu5Ac-(2,3)-β-D-Gal-(1,3)-β-D-GlcNAc-(1,3)-β-D-Gal-(1,4)-β-D-Glc
	1144.40	Sialyl monofucosyllacto-*N*-tetraose	α-D-Neu5Ac-(2,3)-β-D-Gal-(1,3)-[**α-L-Fuc-(1,4)**]-β-D-GlcNAc-(1,3)-β-D-Gal-(1,4)-β-D-Glc
	1144.40	Sialyl-lacto-*N*-fucopentaose V	**α-L-Fuc-(1,2)**-β-D-Gal-(1,3)-[α-D-Neu5Ac-(2,6)]-β-D-GlcNAc-(1,3)-β-D-Gal-(1,4)-β-D-Glc
	1289.44	Disialyllacto-*N*-tetraose	α-D-Neu5Ac-(2,3)-β-D-Gal-(1,3)-[α-D-Neu5Ac-(2,6)]-β-D-GlcNAc-(1,3)-β-D-Gal-(1,4)-β-D-Glc
	1438.29	Lacto-*N*-neooctaose	β-D-Gal-(1,4)-β-D-GlcNAc-(1,3)-β-D-Gal(1,4)-β-D-GlcNAc (1,3)-β-D-Gal(1,4)-β-D-GlcNAc(1,3)-β-D-Gal(1,4)-β-D-Glc

Table S5.5: Binding of the fucosidase cluster solute-binding protein from *B. pseudocatenulatum* MP80 to various human milk oligosaccharides.

Binding level	MW (Da)	Common name	Structure
High	488.17	2'-fucosyllactose	**α-L-Fuc-(1→2)**-β-D-Gal-(1→4)-β-D-Glc
	488.17	3-fucosyllactose	β-D-Gal-(1→4)-[**α-L-Fuc-(1→3)**]-β-D-Glc
Medium	633.21	3'-sialyllactose	α-D-Neu5Ac-(2→3)-β-D-Gal-(1→4)-β-D-Glc
	633.21	6'-sialyllactose	α-D-Neu5Ac-(2→6)-β-D-Gal-(1→4)-β-D-Glc
	634.23	Difucosyllactose	**α-L-Fuc-(1→2)**-β-D-Gal-(1→4)-[**α-L-Fuc-(1→3)**]-β-D-Glc
	707.25	Lacto-*N*-tetraose	β-D-Gal-(1→3)-β-D-GlcNAc-(1→3)-β-D-Gal-(1→4)-β-D-Glc
	707.25	Lacto-*N*-neotetraose	β-D-Gal-(1→4)-β-D-GlcNAc-(1→3)-β-D-Gal-(1→4)-β-D-Glc
	779.27	3'-sialyl-3'-fucosyllactose	α-D-Neu5Ac-(2→3)-β-D-Gal-(1→4)-[**α-L-Fuc-(1→3)**]-β-D-Glc
	853.31	Lacto-*N*-fucopentaose I	**α- L-Fuc-(1→2)**-β-D-Gal-(1→3)-β-D-GlcNAc-(1→3)-β-D-Gal-(1→4)-β-D-Glc
	853.31	Lacto-*N*-fucopentaose II	β-D-Gal-(1→3)-[**α-L-Fuc-(1→4)**]-β-D-GlcNAc-(1→3)-β-D-Gal-(1→4)-β-D-Glc
	853.31	Lacto-*N*-fucopentaose III	β-D-Gal-(1→4)-[**α-L-Fuc-(1→3)**]-β-D-GlcNAc-(1→3)-β-D-Gal-(1→4)-β-D-Glc
	853.31	Lacto-*N*-neofucopentaose V	β-D-Gal-(1→3)-β-D-GlcNAc-(1→3)-β-D-Gal-(1→4)-[**α-L-Fuc-(1→3)**]-β-D-Glc
	853.31	Lacto-*N*-neofucopentaose	β-D-Gal-(1→4)-β-D-GlcNAc-(1→3)-β-D-Gal-(1→4)[**α-L-Fuc-(1→3)**]-β-D-Glc
	998.34	Sialyllacto-*N*-tetraose a	α-D-Neu5Ac-(2→3)-β-D-Gal-(1→3)-β-D-GlcNAc-(1→3)-β-D-Gal-(1→4)-β-D-Glc
	998.34	Sialyllacto-*N*-tetraose b	α-D-Neu5Ac-(2→6)-[β-D-Gal-(1→3)]-β-D-GlcNAc-(1→3)-β-D-Gal-(1→4)- β-D-Glc
	998.34	Sialyllacto-*N*-tetraose c	α-D-Neu5Ac-(2→6)-β-D-Gal-(1→4)-β-D-GlcNAc-(1→3)-β-D-Gal-(1→4)-β-D-Glc
	998.34	Sialyllacto-*N*-tetraose d	α-D-Neu5Ac-(2→3)-β-D-Gal-(1→4)-β-D-GlcNAc-(1→3)-β-D-Gal-(1→4)-β-D-Glc
	999.36	Lacto-*N*-difucohexaose I	**α-L-Fuc-(1→2)**-β-D-Gal-(1→3)-[**α-L-Fuc-(1→4)**]-β-D-GlcNAc-(1→3)-β-D-Gal-(1→4)-β-D-Glc
	999.36	Lacto-*N*-difucohexaose II	β-D-Gal-(1→3)-[**α-L-Fuc-(1→4)**]-β-D-GlcNAc-(1→3)-β-D-Gal-(1→4)-[**α-L-Fuc-(1→3)**]-β-D-Glc
	999.36	Lacto-*N*-neodifucohexaose	β-D-Gal-(1→4)-[**α-L-Fuc-(1→3)**]-β-D-GlcNAc-(1→3)-β-D-Gal-(1→4)-[**α- L-Fuc-(1→3)**]-β-D-Glc
	545.20	Lacto-*N*-triaose	β-D-GlcNAc-(1→3)-β-D-Gal(1→4)-β-D-Glc
	691.25	Blood group A antigen tetraose type 5	α-D-GalNAc-(1→3)-[**α-L-Fuc-(1→2)**]-β-D-Gal-(1→4)-β-D-Glc
	674.24	3'-sialyl-*N*-acetyllactosamine	α-D-Neu5Ac-(2→3)-β-D-Gal-(1→4)-β-D-GlcNAc

	674.24	6'-sialyl-*N*-acetyllactosamine	α-D-Neu5Ac-(2→6)-β-D-Gal-(1→4)-β-D-GlcNAc
	820.30	3'-sialyl Lewis A	α-D-Neu5Ac-(2→3)-β-D-Gal-(1→3)-[**α-L-Fuc-(1→4)**]-β-D-GlcNAc
Low/no binding	1072.38	Para Lacto-*N*-neohexaose	β-D-Gal-(1→4)-β-D-GlcNAc-(1→3)-β-D-Gal-(1→4)-β-D-GlcNAc-(1→3)-β-D-Gal-(1→4)-β-D-Glc
	1072.38	Lacto-*N*-neohexaose	β-D-Gal-(1→4)-β-D-GlcNAc-(1→6)-[β-D-Gal-(1→4)-β-D-GlcNAc-(1→3)]-β-D-Gal-(1→4)-β-D-Glc
	1144.40	Sialyl monofucosyllacto-N-tetraose	α-D-Neu5Ac-(2→3)-β-D-Gal-(1→3)-[**α-L-Fuc-(1→4)**]-β-D-GlcNAc-(1→3)-β-D-Gal-(1→4)-β-D-Glc
	1144.40	Sialyl-lacto-*N*-fucopentaose V	**α-L-Fuc-(1→2)**-β-D-Gal-(1→3)-[α-D-Neu5Ac-(2→6)]-β-D-GlcNAc-(1→3)-β-D-Gal-(1→4)-β-D-Glc
	1289.44	Disialyllacto-*N*-tetraose	α-D-Neu5Ac-(2→3)-β-D-Gal-(1→3)-[α-D-Neu5Ac-(2→6)]-β-D-GlcNAc-(1→3)-β-D-Gal-(1→4)-β-D-Glc
	1364.50	Difucosyllacto-*N*-hexaose a	β-D-Gal-(1→4)-[**α-L-Fuc-(1→3)**]-β-D-GlcNAc-(1→6)-[**α-L-Fuc-(1→2)**-β-D-Gal-(1→3)-β-D-GlcNAc-(1→3)]-β-D-Gal-(1→4)-β-D-Glc
	1364.50	Difucosyl-para-lacto-*N*-hexaose II	β-D-Gal-(1→3)-[**α-L-Fuc-(1→4)**]-β-D-GlcNAc-(1→3)-β-D-Gal-(1→4)-[**α-L-Fuc-(1→3)**]-β-D-GlcNAc-(1→3)-β-D-Gal-(1→4)-β-D-Glc
	1437.51	Lacto-*N*-neooctaose	β-D-Gal-(1→4)-β-D-GlcNAc-(1→3)-β-D-Gal(1→4)-β-D-GlcNAc (1→3)-β-D-Gal(1→4)-β-D-GlcNAc(1→3)-β-D-Gal-(1→4)-β-D-Glc
	1056.39	Blood group A antigen hexaose type 1	α-D-GalNAc-(1→3)-[**α-L-Fuc-(1→2)**]-β-D-Gal-(1→3)-β-D-GlcNAc(1→3)-β-D-Gal-(1→4)-β-D-Glc
	1202.44	A-hepta saccharide	α-D-GalNAc-(1→3)-[**α-L-Fuc-(1→2)**]-β-D-Gal-(1→3)-[**α-L-Fuc-(1→4)**]-β-D-GlcNAc(1→3)-β-D-Gal-(1→4)-β-D-Glc
	1218.44	Monofucosyllacto-N-hexaose III	β-D-Gal-(1→4)-[**α-L-Fuc-(1→3)**]-β-D-GlcNAc-(1→6)-[β-D-Gal-(1→3)-β-D-GlcNAc-(1→3)]-β-D-Gal-(1→4)-β-D-Glc
	1364.50	Difucosyllacto-*N*-hexaose b	β-D-Gal-(1→4)-[**α-L-Fuc-(1→3)**]-β-D-GlcNAc-(1→6)-[β-D-Gal-(1→3)-[**α-L-Fuc-(1→4)**]-β-D-GlcNAc-(1→3)]-β-D-Gal-(1→4)-β-D-Glc
	1364.50	Difucosyl-para-lacto-*N*-neohexaose	β-D-Gal-(1→4)-[**α-L-Fuc-(1→3)**]-β-D-GlcNAc-(1→3)-β-D-Gal-(1→4)-[**α-L-Fuc-(1→3)**]-D-GlcNAc-(1→3)]-β-D-Gal-(1→4)-β-D-Glc
	1072.38	Para Lacto-*N*-hexaose	β-D-Gal-(1→3)-β-D-GlcNAc-(1→3)-β-D-Gal-(1→4)-β-D-GlcNAc-(1→3)-β-D-Gal-(1→4)-β-D-Glc
	1510.55	Trifucosyllacto-*N*-hexaose a	β-D-Gal-(1→4)-[**α-L-Fuc-(1→3)**]-β-D-GlcNAc-(1→6)-[**α-L-Fuc-(1→2)**-β-D-Gal-(1→3)-[**α-L-Fuc-(1→4)**]-β-D-GlcNAc-(1→3)]-β-D-Gal-(1→4)-β-D-Glc

Table S6: Binding of the fucosidase cluster solute-binding protein from *B. pseudocatenulatum* SC585 to various human milk oligosaccharides.